

ELECTRON CORRELATION EFFECTS

IN H_2 AND H_3^+

AND A STUDY OF

FLUCTUATION POTENTIALS IN ATOMS

by

Jeffrey Sanders

A thesis submitted to the

UNIVERSITY OF LEICESTER

for the degree of

DOCTOR OF PHILOSOPHY

in the Faculty of Science

1988

UMI Number: U499814

All rights reserved

INFORMATION TO ALL USERS

The quality of this reproduction is dependent upon the quality of the copy submitted.

In the unlikely event that the author did not send a complete manuscript and there are missing pages, these will be noted. Also, if material had to be removed, a note will indicate the deletion.



UMI U499814

Published by ProQuest LLC 2015. Copyright in the Dissertation held by the Author.
Microform Edition © ProQuest LLC.

All rights reserved. This work is protected against
unauthorized copying under Title 17, United States Code.



ProQuest LLC
789 East Eisenhower Parkway
P.O. Box 1346
Ann Arbor, MI 48106-1346

X7S14E87S8

'We haven't the money
so we've got to think'

Lord Rutherford

ACKNOWLEDGEMENTS

I wish to express my thanks to Professors E.A. Davis and K.A. Pounds for the opportunity to work in the Physics Department at the University of Leicester.

The receipt of a Science and Engineering Research Council maintenance grant is gratefully acknowledged.

It is a pleasure to express my appreciation to Dr A. Weinmann and Dr P.K. Youngman for helpful advice and discussions throughout the course of this work.

For help in the preparation of the thesis I am indebted to Mr G.W. Sanders and Mr J.D. Wyman.

Special thanks must go to Dr K.E. Banyard, without whose advice, patience and perseverance this work would have proved impossible.

Jeffrey Sanders

CONTENTS

General Introduction	1
----------------------	---

PART I A STUDY OF ATOMIC FLUCTUATION POTENTIALS

(I.1) Introduction	12
(I.2) Investigation into the Fluctuation Potential	16
(I.3) Summary of Fluctuation Potential Investigation	34

PART II ELECTRON CORRELATION EFFECTS IN H₂ AND H₃⁺

(II.1) Introduction	37
(II.2) Molecular Electron Correlation Functions	50
.....	
(II.3) The H ₂ and H ₃ ⁺ Systems	62
(II.4) Position-Space Wavefunctions	65
(II.5) Results for H ₂ in Position-Space	77
(II.6) Discussion of H ₂ Results in Position-Space	109
(II.7) Results for H ₃ ⁺ in Position-Space	140
(II.8) Discussion of H ₃ ⁺ Results in Position-Space	157
(II.9) Summary of Position-Space Analysis	167
.....	
(II.10) Introduction to Momentum-Space	173
(II.11) Wavefunctions into Momentum-Space	177
(II.12) Results for H ₂ in Momentum-Space	190
(II.13) Discussion of H ₂ Results in Momentum-Space	226
(II.14) Results for H ₃ ⁺ in Momentum-Space	252
(II.15) Discussion of H ₃ ⁺ Results in Momentum-Space	267
(II.16) Summary of Momentum-Space Analysis	276

APPENDICES

(A1) Atomic Units	282
(A2) The Hartree Fock Technique	283
(A3) The General Theory of Natural Spin-Orbitals	293
References	309

ELECTRON CORRELATION EFFECTS
IN H_2 AND H_3^+
AND A STUDY OF
FLUCTUATION POTENTIALS IN ATOMS

by
Jeffrey Sanders

ABSTRACT

Firstly, the origin of the electron correlation problem is outlined and some approaches to its solution are discussed.

In Part I, the difference between the exact and Hartree Fock (HF) inter-electronic potentials experienced between a pair of electrons, known as the fluctuation potential, is used to investigate the effect of correlation on small atoms. They are analysed in terms of radial and angular components of correlation and the dominance of angular-based correlation for a large nuclear charge is seen.

In Part II, a new technique for examining the effects of electron correlation on molecular systems is developed. This is subsequently used to investigate the ground states of the H_2 and H_3^+ molecules in position and momentum-space.

By employing a natural orbital analysis, it was found for molecules that correlation could be examined in terms of the redistribution in electronic probability parallel to the bond (z-correlation), axially around the bond (ϕ -correlation) and perpendicular to the bond in all directions (ρ -correlation). The origins of these components were analysed mathematically and their effects on the two-particle electron density were displayed. In position-space, although z-correlation was found to be the most dominant, all types of correlation were seen to increase the mean inter-electronic separation. In momentum-space, however, ϕ and ρ -correlation acted to increase the mean inter-electronic momentum whereas z-correlation acted in opposition to this and had the effect of increasing the probability of locating both electrons travelling parallel to the bond in the same direction. This was compared with the work performed on atomic systems and the HeH^+ molecular ion.

For the electron-deficient H_3^+ ion, the investigation provided evidence to suggest that there are three distinct 'bonding regions' bent towards the centre of the molecule.

General Introduction

A description of the stationary state behaviour of electrons in atoms and molecules is given by solving the time-independent Schrödinger equation⁽¹⁾:

$$H \Psi(\underline{x}_1, \underline{x}_2, \dots, \underline{x}_N) = E \Psi(\underline{x}_1, \underline{x}_2, \dots, \underline{x}_N). \quad (I1)$$

The co-ordinate \underline{x}_i represents both the space and spin vectors of the i^{th} electron, H is the Hamiltonian, E is the energy of the state and Ψ is the wavefunction of the system. The wavefunction, from the fundamental principles of quantum mechanics, contains all the information it is possible to know about the state. For a molecule, the Born-Oppenheimer approximation⁽²⁾ may be applied; that is, since the motion of the nuclei is very much slower than the electrons, due to the difference in mass, the molecule may be represented by a frame of fixed, point-charge nuclei. By making the customary approximation of ignoring all interactions other than Coulombic forces, the Hamiltonian for a molecule consisting of N electrons and M fixed nuclei may be written as

$$H = \sum_{i=1}^N h^{\circ}(r_i) + \sum_{i>j=1}^N 1/r_{ij}, \quad (I2)$$

where the bare nuclei Hamiltonian is

$$h^{\circ}(r_i) = (-1/2) \nabla_i^2 - \sum_{A=1}^M Z_A / r_{iA}. \quad (I3)$$

The Coulombic repulsion between the i^{th} and j^{th} electrons is

given by $1/r_{ij}$, whereas Z_A/r_{iA} represents the attraction between nucleus A, of charge Z_A , and the i^{th} electron and $(-1/2)\nabla_i^2$ is the kinetic energy operator of the i^{th} electron. Unfortunately, due to the electrostatic interaction terms in the Hamiltonian, the Schrödinger equation may only be solved exactly for one-electron atoms, and for the H_2^+ molecule. For multi-electronic systems recourse must be made to approximate methods. (Atomic units have been used throughout this work and have been summarised in Appendix I.)

One of the first attempts to obtain an approximate solution to the Schrödinger equation was envisaged by Hartree⁽³⁾. This entirely intuitive approach assumed that each electron moves in a spherically averaged charge distribution of all the other electrons. Slater⁽⁴⁾ and Gaunt⁽⁵⁾ independently showed that, within this approximation, the optimum solution of the Schrödinger equation was a wavefunction in the form of a simple product of one-electron functions, ie

$$\Phi_{\text{Hartree}}(\underline{x}_1, \underline{x}_2, \dots, \underline{x}_N) = \phi_1(\underline{x}_1)\phi_2(\underline{x}_2)\dots\phi_N(\underline{x}_N). \quad (\text{I4})$$

These one-electron functions, by convention, are known as spin-orbitals and may be either atomic or molecular based. It is obvious that the main defects in this method are firstly, that the Pauli exclusion principle⁽⁶⁾ is not obeyed and secondly, that it takes no account of the indistinguishability of electrons. If the spin-orbitals are constructed to be normalised and orthogonal to each other, both problems are overcome simultaneously by arranging the orbitals in the form of a Slater determinant⁽⁷⁾. The energy

optimised wavefunction arranged in this form is known as the self-consistent field (SCF) wavefunction and may be written as

$$\phi_{\text{SCF}}(\underline{x}_1, \underline{x}_2, \dots, \underline{x}_N) = (N!)^{-1/2} \begin{vmatrix} \phi_1(\underline{x}_1) & \phi_2(\underline{x}_1) & \dots & \phi_N(\underline{x}_1) \\ \phi_1(\underline{x}_2) & \phi_2(\underline{x}_2) & \dots & \phi_N(\underline{x}_2) \\ \vdots & \vdots & \ddots & \vdots \\ \phi_1(\underline{x}_N) & \phi_2(\underline{x}_N) & \dots & \phi_N(\underline{x}_N) \end{vmatrix}, \quad (15)$$

where the factor $(N!)^{-1/2}$ simply ensures that the total wavefunction is normalised to unity. The spin-orbitals contain parameters which, by applying the variational principle⁽⁸⁾, may be adjusted to produce the most highly energy-optimised wavefunction. The form of such spin-orbitals may be chosen arbitrarily, the choice obviously being guided by any previous knowledge of approximate wavefunctions. The ideal SCF wavefunction, that is to say the wavefunction that contains the N best possible choices of energy-optimised spin-orbitals, is known as the Hartree Fock (HF) wavefunction. Most SCF wavefunctions contained in the literature are accurate and thus may be thought of as good approximations to the Hartree Fock wavefunction (for example see references 9, 10 and 11). A more complete review of the energy optimisation process, as derived by Fock⁽¹²⁾, is contained in Appendix II.

One of the principal assumptions of the Hartree Fock method is that the inter-electronic potential energy of an electron, located at some point in space, depends only upon the averaged positions of the other electrons. It therefore

follows that, even by employing the HF wavefunction, there is an inherent deficiency in describing the Coulombic electron-electron repulsion. Indeed, the Hartree Fock theory predicts that the probability of locating two electrons with anti-parallel spins at the same point in space is non-zero. Any possible improvement to the accuracy of the HF theory must introduce a 'correlation' effect between the motions of the electrons, which introduces a region around each electron largely devoid of other electrons. Correlation in this context refers to the residual error in the Hartree Fock model when describing the electron-electron Coulombic interactions.

An idea as to the extent to which the HF wavefunction of a system is in error may be obtained by evaluating the correlation energy associated with it. By exploiting the widely used definition of Löwdin⁽¹³⁾ the correlation energy may be written as

$$E_{\text{corr}} = E_{\text{exact}} - E_{\text{HF}}. \quad (16)$$

Since the Hartree Fock energy is always an upper-bound to the exact energy, the correlation energy is a negative quantity. This definition, although straightforward, has the disadvantage of being based on two quantities, neither of which can be known exactly. As an example, for the ground state of the two-electron ions, the correlation energy is approximately -0.04 a.u. which then increases proportionately with the atomic number of the system. Although this is a relatively small contribution, of the order of only a few percent of the total energy for small systems, it is

comparable in magnitude to many chemically observable properties. Such properties, for example, include the difference between spectroscopic states, binding energies and rotational barriers in molecules.

By considering the $1S$ state of the H^- ion, a Hartree Fock analysis yields an energy of about -0.48 a.u.. One would predict from this result that the ion would emit an electron to form a hydrogen atom, with the lower, and therefore more stable, energy of -0.5 a.u.. But, by including correlation in the system the exact energy becomes -0.52 a.u. and therefore the H^- ion is stable. Thus, the actual existence of the H^- ion can only be predicted by the inclusion of electron correlation.

The carbon atom, which has a ground-state energy of approximately -40 a.u. and a correlation contribution of about -0.4 a.u., provides another example of the importance of correlation. Chemical bond energies are typically of the order of -0.2 a.u. per molecule and hence cannot be calculated reliably using HF wavefunctions. It is therefore necessary, by studying the effect of correlation on atoms and molecules, to seek methods of improving the HF wavefunctions and their associated energies.

The Hartree Fock approximation represents an approximation to the description of the electron-electron interaction. Hence, electron correlation may be studied by investigating a function that represents the difference between the exact Coulombic repulsion term $1/r_{ij}$ and the

Hartree Fock equivalent. This function is known as the fluctuation potential and has considerable advantage in that the exact solution is represented rather than an approximation. The fluctuation potential was first introduced by Sinanoglu⁽¹⁴⁾ and since then little quantitative analysis has been performed on it. Part I of this thesis forms an investigation into the structure, properties and the viability of the fluctuation potential as a tool in the understanding of electron correlation.

In an historic paper of 1928, Hylleraas⁽¹⁵⁾ proposed three methods of constructing correlated wavefunctions, all of which form the basis of present day techniques. In his first method Hylleraas⁽¹⁶⁾ noted that the wavefunction for helium can be regarded as a function of r_1 , r_2 and r_{12} , that is the distances of the two electrons from the nucleus and the separation between them, respectively. He obtained extremely accurate energies for the system as correlation could be introduced explicitly into the wavefunction by the inter-electronic distance term r_{12} . Many authors (for examples see references 17-19) have employed the Hylleraas approach to create explicitly correlated wavefunctions. Particularly noteworthy is the work of Pekeris⁽²⁰⁾, who in 1958 computed a series of Hylleraas-type wavefunctions for the helium-like ions, and that of Kolos and Roothaan⁽²¹⁾, in 1960, for the hydrogen molecule. These calculations have remained virtually unsurpassed in accuracy until the present day. Unfortunately, attempts to extend these methods to systems with more than two electrons have met with very little success as elliptical co-ordinates are difficult to

construct for systems with more than two electrons⁽²²⁾.

It is possible to construct a wavefunction for a molecule directly from those of its constituent components. This technique, known as the valence bond (VB) method, is attractive as it implements, in a clear-cut way, much of the experience of chemistry. A fundamental requirement of any electronic wavefunction is antisymmetry with respect to the interchange of electrons stemming from different atoms, leading to the exchange contribution of the total energy. Physically it can be seen that this forces the wavefunctions of the participating atoms to overlap. The magnitude of the exchange energy, and consequently the strength of the covalent bond may therefore be determined broadly by the degree of non-orthogonality between the relevant orbitals. Because of the large number of iterative calculations required, until recently, interest in this approach has been fairly limited. Due to much better modern-day VB techniques^(23,24) and computer facilities, this approach is becoming more attractive and is consequently gaining in popularity^(25,26).

The third, and most widely used, method of evaluating correlated wavefunctions is that of configuration interaction (CI). The CI wavefunction is expanded as a linear combination of Slater determinants Φ , ie

$$\Psi(\underline{x}_1, \underline{x}_2, \dots, \underline{x}_N) = \sum_i c_i \Phi_i(\underline{x}_1, \underline{x}_2, \dots, \underline{x}_N). \quad (17)$$

Each of the determinants does not necessarily contain the

symmetry of the system, but they are usually grouped together to form 'configurations' which do possess this symmetry. The coefficients c_i are taken as those which minimise the total energy according to the variational principle. The major advantage of this technique is that if a complete set of configurations is used, that is an infinitely large number, the trial wavefunction Ψ will become the exact wavefunction of the system. In practice the number of configurations that can be handled conveniently is limited. However, the more configurations that are employed, the better the calculated energy becomes. The principal disadvantages of this method are firstly that, it is not obvious which configurations will be most effective in lowering the energy and secondly that, the energy convergence of a CI expansion is often extremely slow. The first problem has been overcome by arranging the CI wavefunction in natural spin-orbital form, that is rearranging the wavefunction to produce the fastest energy convergent series (see Appendix III for further details). Also, in the light of the considerable improvement in computer hardware design and modern CI analysis techniques⁽²⁷⁻²⁹⁾, many highly accurate wavefunctions for small and medium-sized atoms^(30,31) and molecules^(32,33) have been obtained. Accurate CI wavefunctions are consequently employed throughout this work as approximations to the exact wavefunction of the systems.

As all of the wavefunctions have been energy-optimised by applying the variational principle, the energies associated with them are upperbounds of the experimentally

measured exact energy. The amount of electron correlation contained in a particular wavefunction, and hence its quality, can therefore be ascertained by comparing its energy with the exact energy E_{exact} and the Hartree Fock limit E_{HF} ,

$$\% \text{corr} = (E_{\text{CW}} - E_{\text{HF}}) \times 100 / (E_{\text{exact}} - E_{\text{HF}}), \quad (18)$$

where E_{CW} is the energy of the correlated wavefunction.

The determination of the effect of electron correlation in atomic and molecular systems can be seen to be of fundamental importance when designing correlated wavefunctions and is a field of active research. In a classic paper of 1961, Coulson and Neilson⁽³⁴⁾ formulated an inter-electronic density function $f(r_{12})$ which could be evaluated at both the correlated and HF levels of accuracy. The difference between these curves $\Delta f(r_{12})$, known as the Coulomb hole, then accommodates a simple physical picture of the average extent to which electronic charge is repelled from an electron as a result of its instantaneous interaction with other electrons due to electron correlation. This approach has subsequently been developed and is the basis of present-day studies into the effects of electron correlation. Unfortunately, since there is no unique origin, this method has rarely been used profitably to investigate the very important field of correlation in molecular systems.

In Part II of this thesis a new correlation function, based upon the initial definitions of the Coulomb hole, is

developed to study the effect of electron correlation in molecules. It may be generated totally numerically and therefore has the advantage that it is independent of the type of wavefunction that is used to describe the electron distribution. It also overcomes the mathematical problems that arise when considering multi-centre systems. This function has subsequently been employed in the analysis of the effect of correlation in the H_2 and H_3^+ molecules, which represent the simplest multi-electron bi and tri-centred molecules.

PART I

A STUDY OF THE FLUCTUATION POTENTIAL

CHAPTER I.1

Introduction

The effect of electron correlation on atoms and molecules is to produce a region in space around each electron that is largely devoid of other electrons^(1.i.1). This is a consequence of the fact that, in the Hartree Fock (HF) model, each electron only experiences a potential due to the averaged effect of all the other electrons whereas an electron actually experiences a potential due to the instantaneous locations of all of the other electrons. The difference between the exact and HF potentials, which is known as the fluctuation potential, can therefore be used to measure the effect of correlation on a system. Investigations using the fluctuation potential have considerable advantage over the conventional techniques that involve correlated wavefunctions^(1.i.2) in that, as the exact potential is simply the Coulomb repulsion term r_{12}^{-1} , the total effect of correlation can be observed. Also, since only HF orbitals are employed, the necessary integrations are simple and easily evaluated.

Mathematically, the exact non-relativistic potential experienced between two electrons (defined as electron 1 and 2) is simply

$$V_{\text{Exact}}(\underline{r}_1, \underline{r}_2) = r_{12}^{-1} \quad (\text{I.1.1})$$

in atomic units (see Appendix 1 for further details). If we now confine our discussion to atoms, the potential between

electrons 1 and 2 when described by the HF energy optimised spin orbitals ϕ_α and ϕ_β may be written as

$$\begin{aligned}
 V_{\text{HF}}(\phi_\alpha(\underline{x}_1), \phi_\beta(\underline{x}_2)) &= \int \phi_\alpha^*(\underline{x}_1) r_{12}^{-1} \phi_\alpha(\underline{x}_1) d\underline{x}_1 \\
 &+ \int \phi_\beta^*(\underline{x}_2) r_{12}^{-1} \phi_\beta(\underline{x}_2) d\underline{x}_2 \\
 &- R_{\alpha\beta}(\underline{x}_1) \quad - R_{\beta\alpha}(\underline{x}_2)
 \end{aligned} \tag{I.1.2}$$

(see Appendix 2 (Equation (A2.27)) for derivation), where $R_{\alpha\beta}(\underline{x}_1)$ is an HF operator. The fluctuation potential, which will be defined here as $n(\phi_\alpha(\underline{x}_1)\phi_\beta(\underline{x}_2))$, is then simply the difference between equations (I.1.1) and (I.1.2), ie

$$\begin{aligned}
 n(\phi_\alpha(\underline{x}_1), \phi_\beta(\underline{x}_2)) &= r_{12}^{-1} - \int \phi_\alpha^*(\underline{x}_1) r_{12}^{-1} \phi_\alpha(\underline{x}_1) d\underline{x}_1 \\
 &- \int \phi_\beta^*(\underline{x}_2) r_{12}^{-1} \phi_\beta(\underline{x}_2) d\underline{x}_2 \\
 &+ R_{\alpha\beta}(\underline{x}_1) \quad + R_{\beta\alpha}(\underline{x}_2)
 \end{aligned} \tag{I.1.3}$$

The operator $R_{\alpha\beta}(\underline{x}_1)$ cannot be evaluated at a specific point in space although, for electrons possessing anti-parallel spins, ^{easily} it is zero due to spin-orthogonality properties (see Appendix 2). This brief investigation will therefore concentrate on the more important fluctuation potentials that exist in doubly occupied electronic shells where electrons possess oppositely aligned spins. In such cases the fluctuation potential may be written as

$$\begin{aligned}
n(\phi_\alpha(\underline{x}_1), \phi_\beta(\underline{x}_2)) = & r_{12}^{-1} - \int \phi_\alpha^*(\underline{x}_1) r_{12}^{-1} \phi_\alpha(\underline{x}_1) d\underline{x}_1 \\
& - \int \phi_\beta^*(\underline{x}_2) r_{12}^{-1} \phi_\beta(\underline{x}_2) d\underline{x}_2.
\end{aligned}
\tag{I.1.4}$$

This function describes the effect of correlation on the inter-electronic potential between a pair of electrons with opposing spin. For a molecule, an equivalent expression may be defined by solving the appropriate multi-centre Schrödinger equation.

The fluctuation potential $n(\phi_\alpha(\underline{x}_1), \phi_\beta(\underline{x}_2))$ is defined in exactly the same way as the 'residual fluctuation potential' of Sinanoglu^(1.i.3,4). He has also defined a related, but more complex, function which he has called the 'complete fluctuation potential',^(1.i.5). It is used extensively in the method of 'successive partial orthogonalizations',^(1.i.6-9) but is not helpful in studying correlation effects as it contains additional terms. Consequently only the $n(\phi_\alpha(\underline{x}_1), \phi_\beta(\underline{x}_2))$ function (residual fluctuation potential) will be considered further in this investigation.

For an atom possessing N -electrons there are $N(N-1)/2$ electron pairs and therefore $N(N-1)/2$ distinct fluctuation potentials which combine to produce the total correlation effect. As the shell structure in correlated electron densities is largely maintained, it has been postulated that the fluctuation potentials have a relatively short range yet this has never been investigated fully. Furthermore, since the early work performed by Sinanoglu^(1.i.8), the

fluctuation potential has received only limited attention^(1.i.10,11) and no thorough investigations have been performed into its structure, magnitude and properties. By considering two and four-electron atoms, the form, properties and ability of the fluctuation potential to describe atomic correlation effects will be investigated in this initial section of the thesis.

CHAPTER 1.2

Investigation into the Fluctuation Potential

This investigation will consist of three main parts. The first consists of investigating the form of the fluctuation potential, the second with its ability to describe the effects of electron correlation and the third with its range.

(I.2.1) Form of the Fluctuation Potential

The fluctuation potential for electrons with opposite spin $n(\phi_\alpha(\underline{x}_1)\phi_\beta(\underline{x}_2))$, as defined in Equation (I.1.4) consists of three distinct terms. The first is simply the inter-electronic Coulombic repulsion term r_{12}^{-1} and the remaining two integrals describe the HF potential. The integral

$$\int \phi_\beta(\underline{x}_2) r_{12}^{-1} \phi_\beta(\underline{x}_2) d\underline{x}_2$$

represents the potential experienced by electron 1 due to the effect of electron 2 described by spin-orbital β and, similarly

$$\int \phi_\alpha(\underline{x}_1) r_{12}^{-1} \phi_\alpha(\underline{x}_1) d\underline{x}_1$$

represents the potential experienced by electron 2 due to the effect of electron 1 whilst located in spin-orbital α . To understand the form of the fluctuation potential further,

it proves necessary to investigate the structure of one of these integrals, say, the potential experienced by electron 2 due to the the averaged effect of electron 1 when described by spin-orbital α , $v_\alpha(\underline{r}_2)$, where

$$v_\alpha(\underline{r}_2) = \int \phi_\alpha^*(\underline{x}_1) r_{12}^{-1} \phi_\alpha(\underline{x}_1) d\underline{x}_1. \quad (\text{I.2.1})$$

We may expand r_{12}^{-1} in terms of spherical harmonics^(1.ii.1) and, for s-type spin orbitals, by integrating over the spin and angular components of vector \underline{x}_1 and \underline{x}_2 , $v_\alpha(r_2)$ may be written as

$$v_\alpha(r_2) = r_2^{-1} \int_{r_1=0}^{r_2} R_\alpha^*(r_1) R_\alpha(r_1) r_1^2 dr_1 + \int_{r_1=r_2}^{\infty} R_\alpha^*(r_1) R_\alpha(r_1) r_1 dr_1 \quad (\text{I.2.2})$$

where $R_\alpha(r_1)$ is the radial component of $\phi_\alpha(\underline{x}_1)$. For s-type orbitals, the potential is spherically symmetric with respect to the nucleus. From equation (I.2.2) we see that the potential experienced at the nucleus (ie when $r_2 = 0$) will be $\langle r_1^{-1} \rangle$ for the chosen orbitals and, far from the influence of the nucleus, it will tend to r_2^{-1} . This is obviously the Coulombic potential that would be experienced due to an electron being located at the nucleus. In the intermediate regions, however, the potential will be affected by the probability distribution arising from the particular spin-orbital. As examples, the radial components of certain 1s and 2s orbital HF potentials for the four electron series have been presented in Figure (I.2.1). (The HF energy-optimised orbitals of Clementi and Roetti^(1.ii.2) have been employed in the evaluation of these functions.)

We see from Figure (I.2.1) that the range of the HF potentials is commensurate with the probability distribution appropriate to the particular orbital and the HF potentials reflect the shapes of the orbital probability distributions. The magnitude of the potentials at the nucleus, which has been shown to be equal to $\langle r_1^{-1} \rangle_{\text{HF}}$, increases with increasing values of Z. The $\langle r_1^{-1} \rangle_{\text{HF}}$ expectation values are presented in Table (I.2.1B) where, for 1s orbitals in the two, three and four electron systems considered, we may establish the relationship

$$\langle r_1^{-1} \rangle_{1s} = Z - 0.32 \quad (\text{I.2.3})$$

by simple a 'best fit line' technique. For 2s orbitals the corresponding relationship is

$$\langle r_1^{-1} \rangle_{2s} = 0.26 Z - 0.52 \quad (\text{I.2.4})$$

with an error of approximately one percent. The HF potential at the nucleus is hence directly proportional to the nuclear charge. Further, the dotted curves in Figure (I.2.1) represent the function r_2^{-1} which, as may be seen from Equation (I.2.2), is the potential associated with a system where the electrons are exceedingly close to the nucleus, and therefore the nucleus must possess a very high charge. These curves therefore represent the asymptotic limit for both the 1s and 2s HF potentials. We see from Figure (I.2.1) that the 1s orbital distributions are closer to this limit than the 2s potentials although, even for the 2s orbital, further than four atomic units away from the nucleus, r_2^{-1}

represents a good approximation to the 2s HF potential.

(I.2.2) The Effect of the Fluctuation Potential upon the
Electronic Probability Distribution

Like all two-electron functions, the fluctuation potential is dependent upon seven variables. Consequently, to be able to display this function, we must either fix or integrate over certain dimensions. In this section we investigate two such approaches.

[A] The Fluctuation Potential for a fixed location of electron 1.

By locating a test electron, electron 1 say, at a point in space, the number of variables in the fluctuation potential is reduced considerably. Not only is the number reduced by the three co-ordinates of electron 1, but, for atoms, the remaining distribution is axially symmetric with respect to the line from the nucleus to the test electron (defined as the z-axis), making the function dependent on only two variables. It may therefore be plotted, using a contour diagram, in a plane containing the nucleus and fixed electron (defined as the xz-plane).

If the location of electron 1 is fixed then the integral

$$\int \phi_{\beta}(\underline{x}_2) r_{12}^{-1} \phi_{\beta}(\underline{x}_2) d\underline{x}_2$$

is simply dependent upon the location of the test electron.

In this case, to be able to compare the form of the fluctuation potential on different systems, it is more appropriate to define the 'partial fluctuation potential' $S(\underline{r}_1, \underline{r}_2)$ for electrons with opposite spins as

$$S(\underline{r}_1, \underline{r}_2) = r_{12}^{-1} - \int \phi_{\alpha}(\underline{x}_1) r_{12}^{-1} \phi_{\alpha}(\underline{x}_1) d\underline{x}_1. \quad (I.2.5)$$

This function has the advantage that, far from the influence of the nucleus and the test electron, it will tend to zero rather than to a constant. Consequently, it has been plotted in Figures (I.2.2) and (I.2.3) for the two and four electron series, respectively. In all case the test electron has been located at a distance of $\langle r_1 \rangle$ a.u. from the nucleus and, to be able to compare surfaces, they have been scaled so that the width of each diagram corresponds to the radius that encompasses 95% of the total charge associated with the particular shell. This radius and the relevant expectation values are presented in Table (I.2.1). Also, to aid in the interpretation of the diagrams, the positive contours are represented by solid curves, the zero contour by a dotted curve and the negative contours by broken curves.

The exact inter-electronic potential r_{12}^{-1} may be thought of as that experienced between two electrons which are described by a CI wavefunction that is constructed from an infinite number of configurations. Because of this, the fluctuation potential may be analysed in terms of 'radial' and 'angular' components of correlation which have identical meaning to that employed in past investigations

into the effect of correlation on atomic systems^(1.ii.3-8).

The density associated with the roving electron will obviously be redistributed to the region of lowest potential around the nucleus . A dominance of radial correlation is therefore characterised by contours of equal potential formed by concentric spheres centred at the nucleus. This relocates the probability density associated with the roving electron either towards or away from the nucleus. In a similar way, angular correlation is identified by the equi-potential contours forming cones with their apices centred on the nucleus. A maximum will be located along the direction from the nucleus to the test electron and the minimum contour will be located on the opposite side of the nucleus. The probability of locating the roving electron on the opposite side of the nucleus to the test electron will therefore be increased irrespective of the distance of both electrons from the nucleus. However, in practice it is impossible to observe correlation effects in atomic systems which consist of either total radial or total angular correlation. Nevertheless, these models allow us to investigate the effect of correlation on atoms in terms of the relative importance of radial and angular correlation.

The partial fluctuation potentials for the K shells of some two-electron systems are presented in Figure (I.2.2). From Figure (I.2.2A) we see that, for the case of H^- , the minimum is almost centred on the nucleus. This indicates that radial correlation is most dominant and has the effect

of redistributing the probability of locating electron 2 closer to the nucleus.

By increasing the nuclear charge and passing along the two-electron series up to O^{6+} (Figures (I.2.2B)-(I.2.2H)), we see that the minimum moves away from the nucleus, the magnitudes of the surfaces increase and the zero contour changes from concave in shape to convex. This may be attributed to an increase in the relative importance of angular correlation. These observations are consistent with the work performed by Banyard and Baker^(1.ii.7,8) on the He-like series and are also characteristic of K shell correlation effects in three and four electron systems^(1.ii.5,9). The effect may be explained by realising that, as the nuclear charge is increased, the gradient of the HF electron-nuclear potential curve becomes greater. For a large nuclear charge, with a rapidly varying potential curve, it therefore becomes more energy-efficient to increase the inter-electronic separation by increasing the probability of locating the electrons on opposite sides of the nucleus rather than on a purely 'in-out' basis.

By comparing Figure (I.2.2A) with (I.2.2B) we see that the greatest change in the partial fluctuation potential surfaces is between H^- and He. This is a reflection of the instability of the H^- ion which, at the HF level, is predicted as being unstable.

Partial fluctuation potential surfaces have also been evaluated for the K shells of three and four electron ions but were found to be almost graphically indistinguishable from the two electron results. This indicates that, at the HF level, the potentials experienced between K shell electrons is almost independent of the presence of 2s electrons.

The partial fluctuation potentials for the L shells of some four-electron systems are presented in Figure (I.2.3). Like the two-electron series, we see an increase in the importance of angular correlation between Li^- and O^{6+} although for the L shell, even Li^- contains a large component of angular correlation. Due to the double maxima in the 2s-orbital probability distribution, except for Li^- , two minima are seen in the fluctuation potential surfaces. Again, the instability of the negative ion is apparent when comparing Figure (I.2.3A) with (I.2.3B).

Inter-shell fluctuation potentials obviously exist between K and L shell electrons. For electrons with opposite spins the fluctuation potentials have the same form as either the K or L shell fluctuation potentials and, for electrons with the same spin, as discussed earlier, their evaluation is complex due to the HF integral operator. Consequently, inter-shell fluctuation potentials have not been considered in this analysis

[B] Profile of the Fluctuation Potential.

It is important to investigate the effect of electron correlation on atomic systems as the position of the test electron is varied with respect to the location of the nucleus. This may be accomplished by realising that the maxima and minima of the partial fluctuation potential surfaces are located on the z-axis. Thus, if a contour diagram is constructed from the profiles of the partial fluctuation potential along the z-axis for different locations of the test electron, very little information is lost. The forms of these diagrams were found to be similar for all of the K shells and L shells considered. Consequently, as typical examples of these surfaces, only the K shell of He and the L shell of Be have been presented in Figure (I.2.4)

From Figure (I.2.4A) we see that, when one electron is located on the nucleus in He, the other electron experiences a spherically symmetric potential that is everywhere positive. Radial correlation therefore accounts for all of the correlation effect in this case and acts to redistribute the probability of locating the roving electron further from the nucleus. Once the test electron is removed from the site of the nucleus, however, a minimum develops on the surface that, when the test electron is far from the nucleus, becomes centred on the nucleus. At this point, radial correlation is once again dominant although, due to the negative region at the nucleus, it redistributes the probability of locating the roving electron closer to the nucleus.

When the test electron is at intermediate distances from the nucleus, angular correlation has an effect. The greatest effect would be expected at the same distance from the nucleus as the the test electron. For He this was found to be 0.6 a.u. from the nucleus which represents 62% of the expectation value $\langle r_1 \rangle$.

The partial fluctuation potential profiles for the L shell of Be are presented in Figure (I.2.4B). Like the K shell of He, when the test electron is located on the nucleus, the roving electron experiences a repulsive potential and hence is relocated further from the nucleus. As the test electron is moved from the nucleus, however, two minima are formed, one of which becomes coincident with the nucleus and the other tends to 1.4 a.u. from the nucleus. Thus, when the test electron is far from the nucleus, the probability of locating the roving electron at the nucleus and at 1.4 a.u. from it is increased predominantly by radial correlation. Angular correlation will have its greatest effect when the minimum is located at the same distance as the test electron from the nucleus. In this case, it occurs at about 1.8. a.u. from the nucleus.

We have therefore seen that, for both shells considered, when the test electron is close to the nucleus, radial correlation acting to redistribute the probability of locating the roving electron further from the nucleus is most dominant. As the test electron is moved further from the nucleus, the effect of radial correlation is reduced and the angular correlation component becomes greater. By

locating the test electron further from the nucleus, however, radial correlation gains in importance once more but now acts to redistribute electronic probability closer to the nucleus.

(I.2.3) the Range of the Fluctuation Potential

As discussed earlier, it has been presumed that the fluctuation potential, being the difference between two relatively long-range potentials, is itself short-ranged^(1.ii.10,11). From our analysis into the correlation effects in two and four electron atoms, however, we must conclude that this is not the case. If we allow $\langle r_1 \rangle$ to represent the average distance of the test electron from the nucleus, it can be seen immediately from Figures (I.2.2) and (I.2.3) that the fluctuation potential in both the K and L shells possesses a range of the order of the radius that contains ninety five percent of the enclosed charge. This suggest that the fluctuation potential is not short-ranged. The only exceptions to this are seen in the H^- and Li^- ions which have been shown to exhibit unusual characteristics. To support this argument, we see from Figure (I.2.4) that even when the test electron is located on the nucleus, the range of the fluctuation potential can be seen to be commensurate with the 'size' of the atomic shell.

System	$\langle r_1^{-1} \rangle_{\text{HF}}$	$\langle r_1 \rangle_{\text{HF}}$	Range of Shell
H ⁻	0.68822	2.4663	5.951
He	1.6873	0.92723	2.082
Li ⁺	2.6873	0.57237	1.238
Be ²⁺	3.6874	0.41418	0.898
B ³⁺	4.6875	0.32448	0.698
C ⁴⁺	5.6875	0.26676	0.575
N ⁵⁺	6.6875	0.22646	0.488
O ⁶⁺	7.6876	0.19675	0.389

Table (I.2.1A) The 2 Electron Series

System	$\langle r_1^{-1} \rangle_{\text{HF}}$	$\langle r_1 \rangle_{\text{HF}}$	Range of Shell
Li ⁻	K	2.6853	1.255
	L	0.24956	12.32
Be	K	3.6807	1.028
	L	0.52252	5.488
B ⁺	K	4.6746	0.805
	L	0.78015	3.598
C ²⁺	K	5.6772	0.665
	L	1.0341	2.705
N ³⁺	K	6.6757	0.568
	L	1.2866	2.175
O ⁴⁺	K	7.67429	0.472
	L	1.53910	1.582

Table (I.2.1B) The 4 Electron Series

NB (1) 'Range of Shell' is defined as that radius which encompasses 95% of the total charge associated with the shell at the HF level.

(2) Clementi and Roetti HF energy-optimised orbitals were used^(1.ii.2).

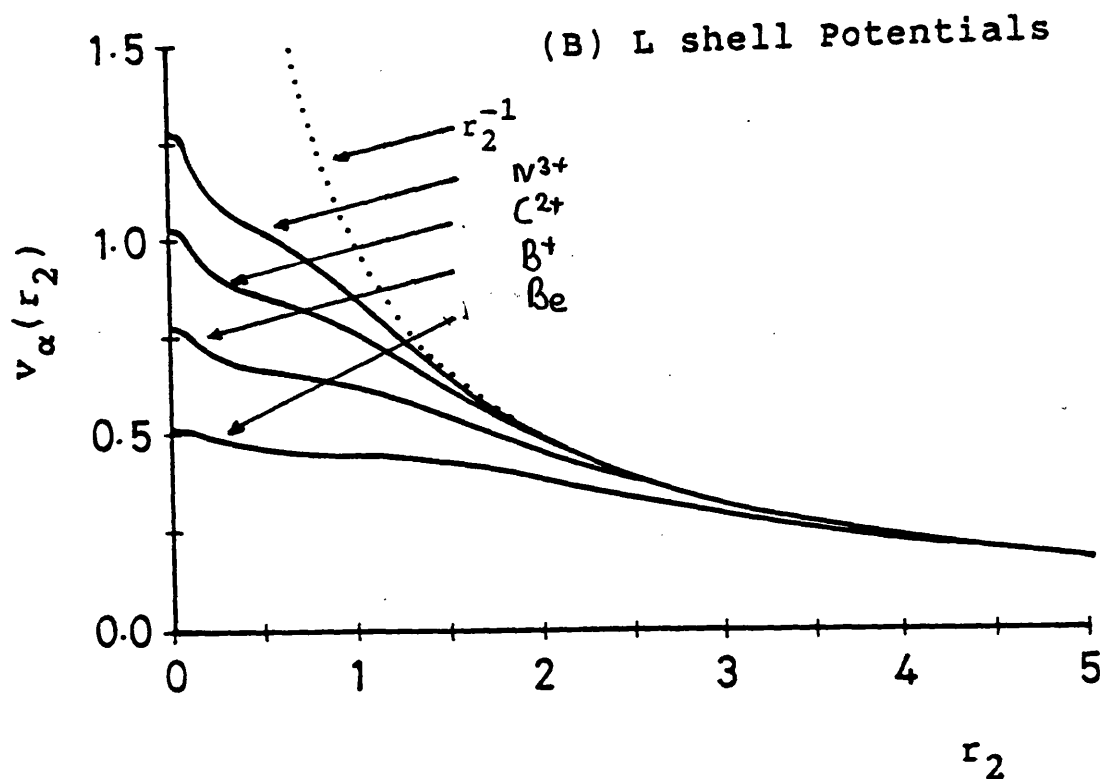
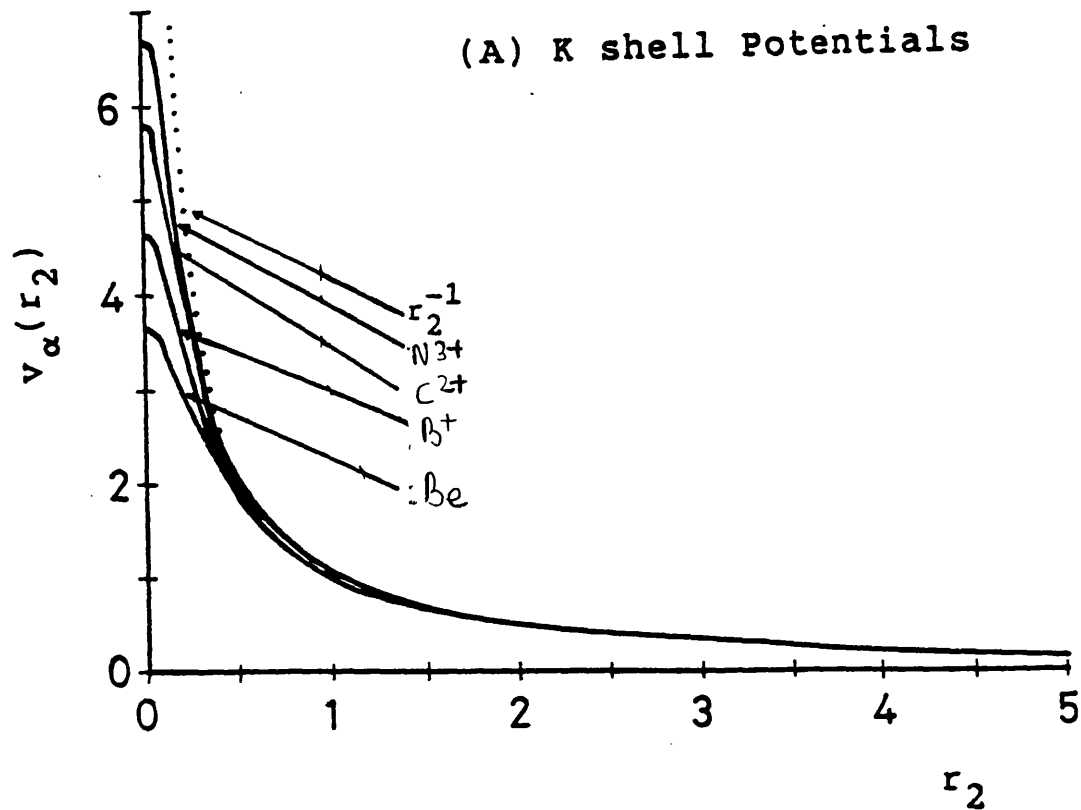
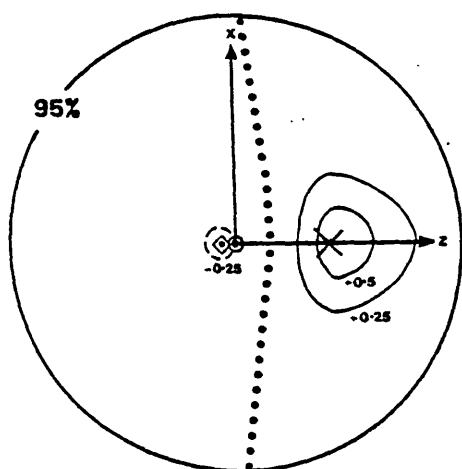
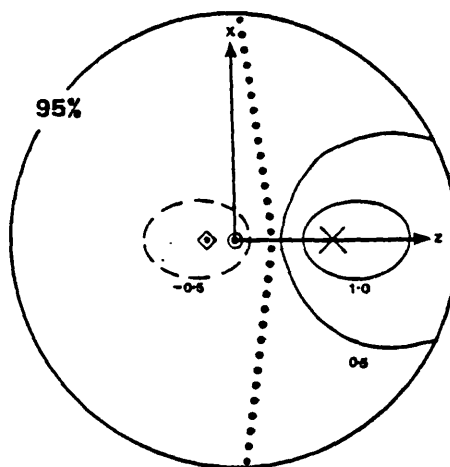


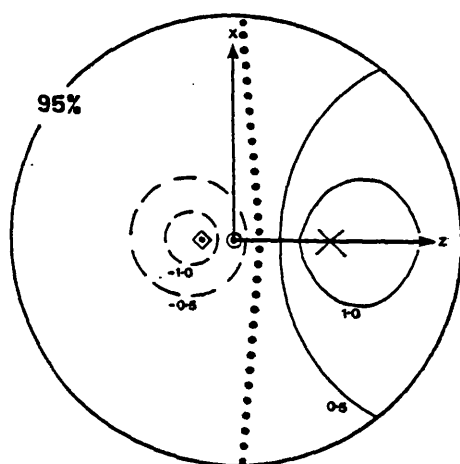
Figure (I.2.1) The radial components of the Hartree Fock inter-electronic potentials $v_\alpha(r_2)$ experienced by electron 2 due to electron 1 being located in (A) the K shell and (B) the L shell of certain four electron atoms.



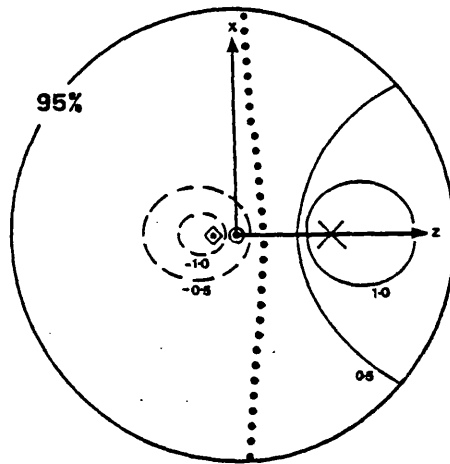
(A) H^-



(B) He



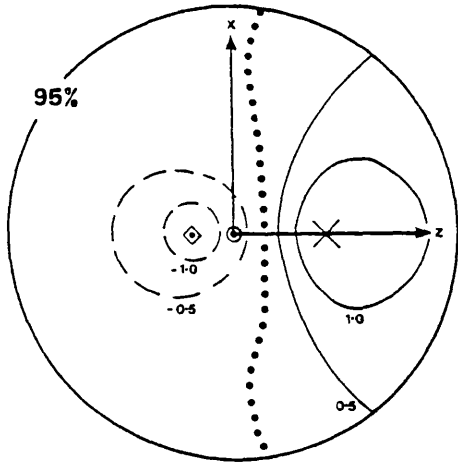
(C) Li^+



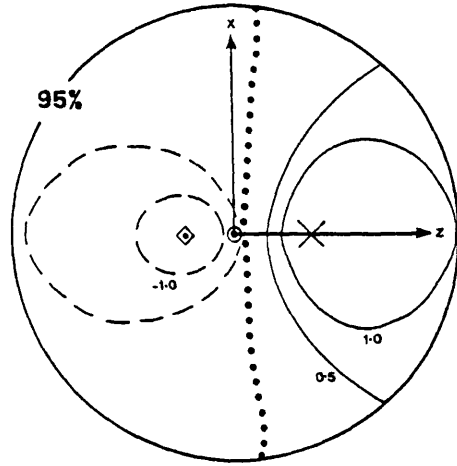
(D) Be^{2+}

⊗	Location of nucleus
x	Location of test electron
◇	Location of minimum of surface

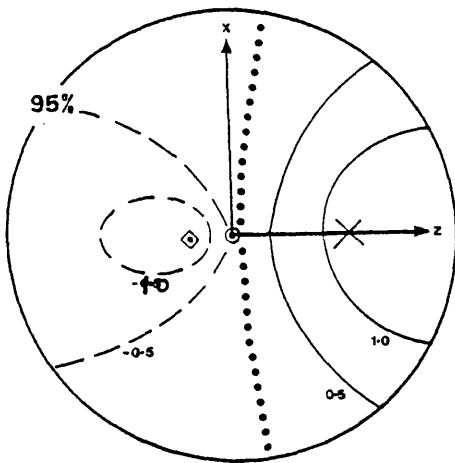
Figure (I.2.2A-D) The partial fluctuation potential surfaces for certain two electron ions scaled such that the border of each diagram corresponds to the region that contains 95% of the total charge associated with the shell (see Table (I.2.1) for values). The test electron is located at $\langle r \rangle$ in each case.



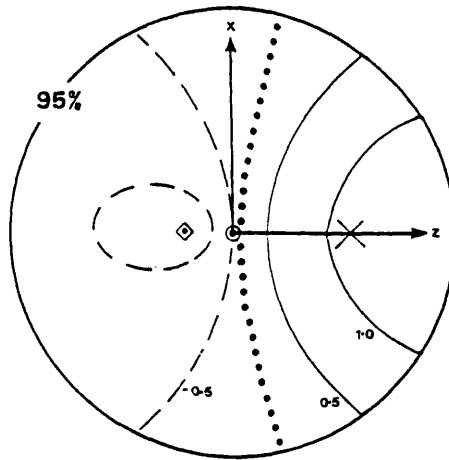
(E) B^{3+}



(F) C^{4+}



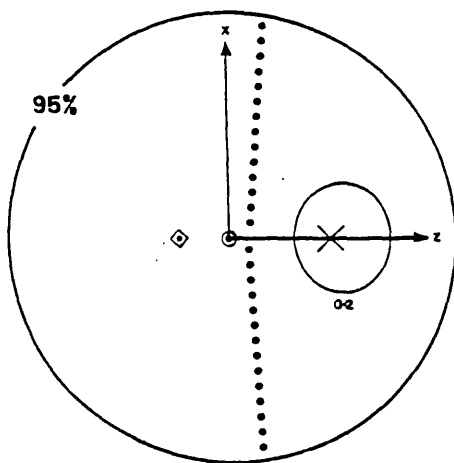
(G) N^{5+}



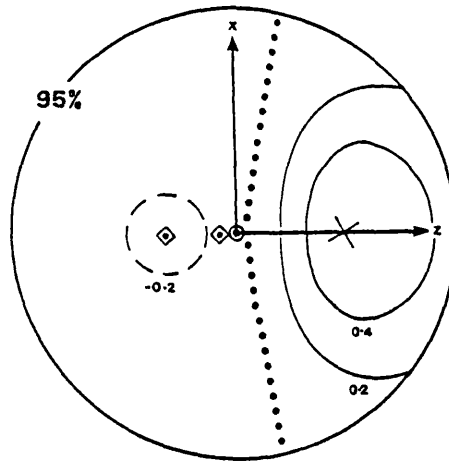
(H) O^{6+}

⊙	Location of nucleus
x	Location of test electron
◇	Location of minimum of surface

Figure (I.2.2E-H) The partial fluctuation potential surfaces for certain two electron ions scaled such that the border of each diagram corresponds to the region that contains 95% of the total charge associated with the shell (see Table (I.2.1) for values). The test electron is located at $\langle r \rangle$ in each case.



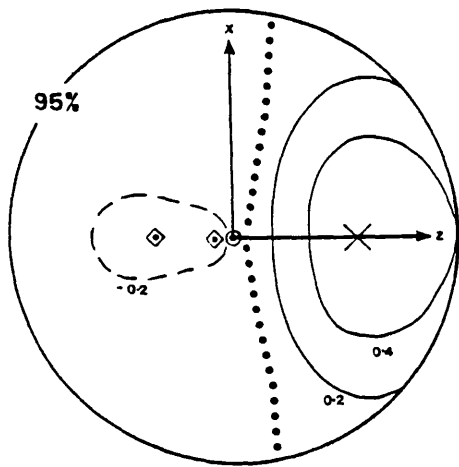
(A) Li^-



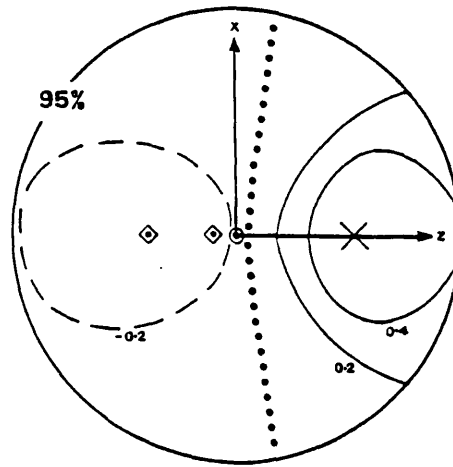
(B) Be

⊙	Location of nucleus
x	Location of test electron
◇	Location of minimum of surface

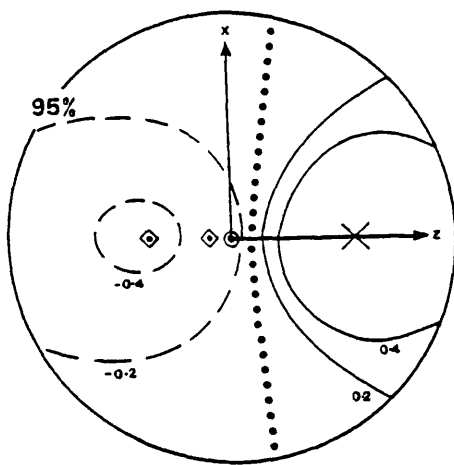
Figure (I.2.3A-B) The partial fluctuation potential surfaces for the L shells of certain four electron ions scaled such that the border of each diagram corresponds to the region that contains 95% of the total charge associated with the shell (see Table (I.2.1) for values). The test electron is located at $\langle r \rangle$ in each case.



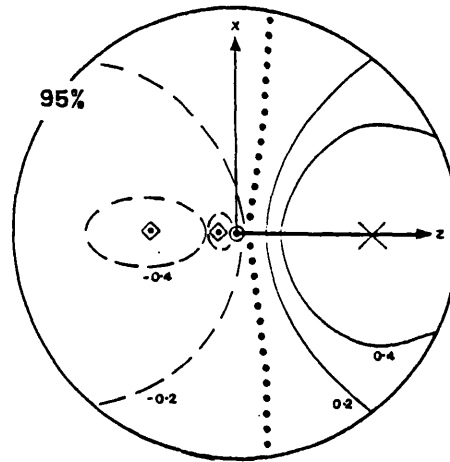
(C) B^+



(D) C^{2+}



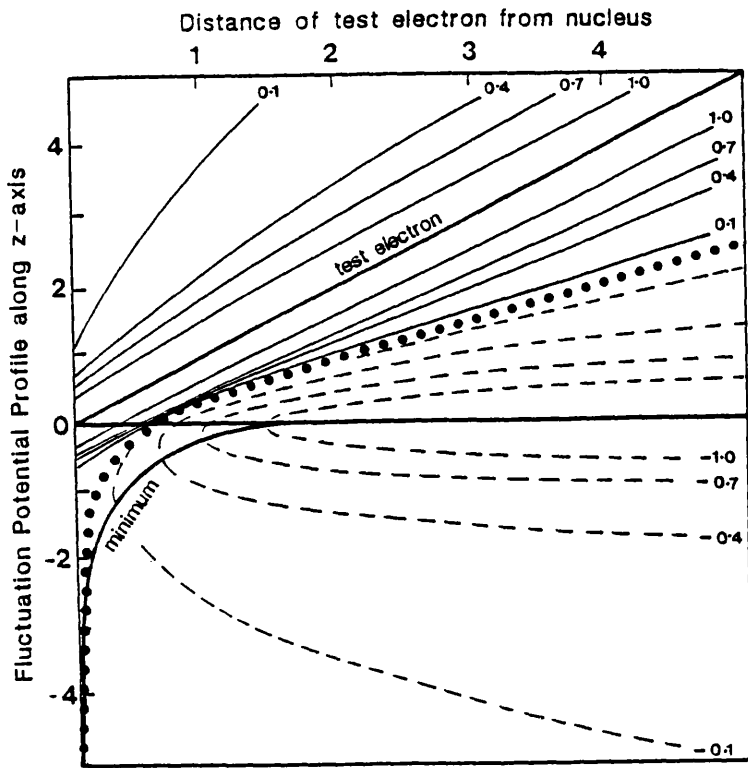
(E) N^{3+}



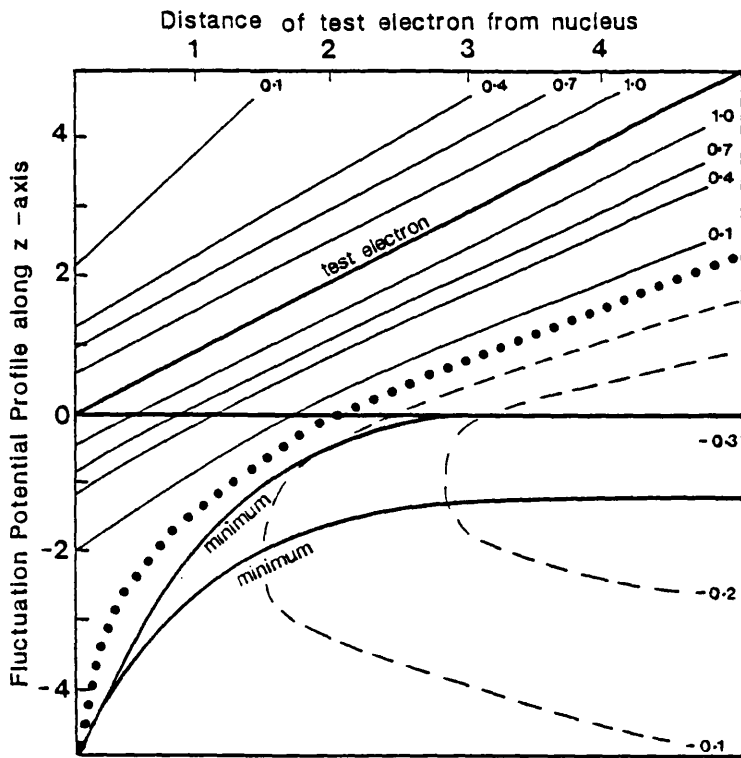
(F) O^{4+}

⊙	Location of nucleus
x	Location of test electron
◇	Location of minimum of surface

Figure (I.2.3C-F) The partial fluctuation potential surfaces for the L shells of certain four electron ions scaled such that the border of each diagram corresponds to the region that contains 95% of the total charge associated with the shell (see Table (I.2.1) for values). The test electron is located at $\langle r \rangle$ in each case.



(A) The K Shell of He



(B) The L Shell of Be

Figure (I.2.4) Fluctuation potential profiles along the z-axis with different locations of the test electron for (A) the K shell of He and (B) the L shell of Be.

CHAPTER I.3

Summary of Fluctuation Potential Investigation

The fluctuation potential, which is defined as the difference between the exact and HF potentials experienced between a pair of electrons, describes the effect of electron correlation on the inter-electronic potential. It has a considerable advantage over functions that employ correlated wavefunctions to study the effects of correlation^(1.iii.1) in that the total effect of correlation is observed. Furthermore, since only HF wavefunctions are employed in the definition of the fluctuation potential, it is relatively simple to evaluate. Unfortunately, it proves difficult to evaluate fluctuation potentials between electrons in different shells with identical spins. It has been reported, however, that these inter-shell correlation effects are relatively small and therefore unimportant compared with intra-shell effects^(1.iii.2).

By fixing the location of one of the electrons, correlation effects have been analysed in the K and L shells of certain two and four electron ions in terms of the relative composition of the radial and angular components of correlation. We have seen that, as the nuclear charge of the system is increased, the effect of angular correlation becomes most dominant. This was attributed to the fact that the angular redistribution of electron probability is preferable to radial movements in a rapidly varying

electron-nuclear potential field.

Profiles of the fluctuation potential along the axis that passes through the nucleus and the test electron were evaluated for different locations of the test electron. From this we found that, when the test electron is very close to the nucleus, radial correlation is most dominant, acting to relocate the probability density associated with the roving electron further from the nucleus. As the test electron is moved from the nucleus, the effect of angular correlation increases rapidly to reach a maximum when the fixed electron is located at about sixty percent of $\langle r_1 \rangle$ for the systems considered. However, when the test electron is far from the nucleus, and the system is almost ionised, radial correlation becomes dominant once more, this time acting to redistribute the probability of locating the other electron closer to the nucleus. These results were found to be consistent with past investigations^(1.iii.3-6).

It was discovered that the fluctuation potential is a long range function that can be used to investigate intra-shell correlation effects accurately and relatively simply. We therefore conclude that it is a valuable function that may be employed in studying the effect of electron correlation on atomic and molecular systems to obtain complementary information to that acquired from existing functions.

PART II

CORRELATION EFFECTS IN H_2 AND H_3^+

CHAPTER II.1

Introduction

The effect of electron correlation can be measured by examining how the charge density of a pair of electrons is redistributed by the inclusion of correlation to a particular system. For an N-electron system all of this information is contained in the difference between the correlated and non-correlated second-order reduced-density matrices. Hence, the correlation effect between electrons 1 and 2, say, is contained in $\Delta\Gamma_{\text{corr}}(\underline{x}'_1, \underline{x}'_2 | \underline{x}_1, \underline{x}_2)$ which, by direct analogy with the definition of correlation energy (equation I6), may be defined as

$$\Delta\Gamma_{\text{corr}}(\underline{x}'_1, \underline{x}'_2 | \underline{x}_1, \underline{x}_2) = \Gamma_{\text{CI}}(\underline{x}'_1, \underline{x}'_2 | \underline{x}_1, \underline{x}_2) - \Gamma_{\text{HF}}(\underline{x}'_1, \underline{x}'_2 | \underline{x}_1, \underline{x}_2). \quad (\text{II.1.1})$$

The second-order reduced-density matrix^(2.i.1) associated with a general, normalised wavefunction ψ , which may be correlated or non-correlated, is given by

$$\Gamma(\underline{x}'_1, \underline{x}'_2 | \underline{x}_1, \underline{x}_2) = N(N-1)/2 \int \psi^*(\underline{x}'_1, \underline{x}'_2, \dots, \underline{x}'_N) \psi(\underline{x}_1, \underline{x}_2, \dots, \underline{x}_N) d\underline{x}_3 d\underline{x}_4 \dots d\underline{x}_N, \quad (\text{II.1.2})$$

which, by convention, is normalised to the number of electron pairs within the system. The notation implies that integrations should be performed over the space and spin co-ordinates of all electrons except for electron 1 and 2. The primes indicate that when evaluating the expectation value of some operator, \underline{x}'_1 is put equal to \underline{x}_1 after the

operation has been performed and consequently the operator acts only upon the unprimed co-ordinates. Using the method of successive partial orthogonalisations first proposed by Sinanoglu^(2.i.2), the correlated wavefunction may be expanded into electron cluster form. This allows the second-order density to be partitioned approximately into its pair-wise components; the uncorrelated wavefunction, on the other other hand may be partitioned exactly, thus

$$\Delta\Gamma_{\text{corr}}(\underline{x}'_1, \underline{x}'_2 | \underline{x}_1, \underline{x}_2) = \sum_{i>j=1}^N \Delta\Gamma_{ij}(\underline{x}'_1, \underline{x}'_2 | \underline{x}_1, \underline{x}_2). \quad (\text{II.1.3})$$

The i and j values label occupied spin-orbitals and hence permits the effect of correlation to be observed in 'intra' and 'inter-electronic shells',^(2.i.3-5).

Unfortunately, since $\Delta\Gamma_{\text{corr}}$ is a function of six variables, it is extremely complex to study. Most approaches of analysing the effect of correlation have found ways of reducing the number of these variables, either by integrating over, or fixing some of them. Information is always lost by doing this, but by examining, for example, a radial based function in tandem with an angular function, an overall view of the effects of correlation may be constructed. Molecular-based correlation functions are further complicated since, to gain specific information about the redistribution of the electrons with respect to the nuclear framework, they must also envelop the 'symmetry' of the molecule.

The first attempt to study the effect of correlation in

single-centre systems was by Coulson and Neilson^(2.i.6). As correlation represents an improvement to the description of the electron-electron interaction, they noted the importance of evaluating the change in probability of finding two electrons with a separation of $r_{12} = |\underline{r}_1 - \underline{r}_2|$. This difference function, known as the Coulomb hole, may be defined as

$$\Delta f(r_{12}) = \int \Delta \Gamma_{\text{corr}}(\underline{x}'_1, \underline{x}'_2 | \underline{x}_1, \underline{x}_2) d\sigma_1 d\sigma_2 d\underline{r}_1 d\underline{r}_2 / dr_{12}, \quad (\text{II.1.4})$$

where the integrations are performed over all variables except for any reference to r_{12} . It therefore follows that

$$\int \Delta f(r_{12}) dr_{12} = 0, \quad (\text{II.1.5})$$

which simply states that no electronic charge is lost or gained, merely redistributed around the system. Since 1961, at least two other definitions of the Coulomb hole have been proposed. Gilbert^(2.i.7) has suggested that $\Delta f(r_{12})$ should be weighted by a factor of r_{12}^{-1} , thereby providing a better indication of the relationship between the correlation energy and the size of the Coulomb hole. Tatewaki and Tanaka^(2.i.8), on the other hand, claim that $\Delta f(r_{12}) r_{12}^{-2}$ is a more appropriate quantity for investigation since the resulting hole is a measure of the change in electron probability per unit volume. Neither of these two alternative definitions appears to have found much favour, possibly due to the fact that both lack some of the conceptual simplicity of the original suggestion.

In direct analogy to the definition of $\Delta f(r_{12})$ by Coulson and Neilson it is possible to define an 'angular' hole as

$$\Delta P(\gamma) = \int \Delta \Gamma_{\text{corr}}(\underline{x}'_1, \underline{x}'_2 | \underline{x}_1, \underline{x}_2) d\underline{\sigma}_1 d\underline{\sigma}_2 d\underline{r}_1 d\underline{r}_2 / d\gamma. \quad (\text{II.1.6})$$

In this case the integration has been performed over all variables except for γ , the inter-electronic angle with respect to the nucleus as the origin. These functions have been employed with some success to both the ground states of several atoms^(2.i.9-14) as well as to a few excited states^(2.i.15-17). With molecules, however, misleading information may be obtained due to their lower order symmetry. For example, with H_2 there is a high probability of discovering both electrons close to either of the nuclei with a separation of 1.4 a.u. as well as them being close to the same nucleus. This will distort and complicate the Coulomb hole curve. Also, there is the added difficulty of having no natural choice of origin to define the inter-electronic angle when evaluating $\Delta P(\gamma)$. Even with these difficulties certain molecular systems have been studied^(2.i.18,19) and an overall view of the probability redistributions has been successfully obtained.

The Coulomb hole functions produce a description of the total correlation effects in atoms but much of the information has been integrated out. For example, it is of considerable interest to investigate how correlation varies as one of the electrons, electron 1 say, moves with respect to the nucleus. Consequently, the partial Coulomb hole $\Delta g(r_{12}, r_1)$ may be defined as

$$\Delta g(r_{12}, r_1) = \int \Delta \Gamma_{\text{corr}}(\underline{x}'_1, \underline{x}'_2 | \underline{x}_1, \underline{x}_2) d\underline{\sigma}_1 d\underline{\sigma}_2 d\underline{r}_1 d\underline{r}_2 / dr_{12} dr_1. \quad (\text{II.1.7})$$

The partial Coulomb hole represents the probability redistribution due to the instantaneous location of electron 1 at a distance r_1 from the nucleus due to correlation. It therefore follows that

$$\Delta f(r_{12}) = \int \Delta g(r_{12}, r_1) dr_1. \quad (\text{II.1.8})$$

Selected partial Coulomb hole curves for certain values of r_1 were employed first by Boyd and Coulson^(2.i.15) to study the correlation effects in the 2^3S and 2^1S states of helium. Since then Banyard and his co-workers have developed full surfaces in isometric projection of $\Delta g(r_{12}, r_1)$ and employed them widely to investigate the effects of correlation in the two^(2.i.20), three^(2.i.17) and four^(2.i.12,14) electron systems for both ground and excited states^(2.i.16,18). Inter and intra shell correlation effects have also been analysed, as well as the effect of 'radial' and 'angular' based correlation types.

Obviously it is possible to introduce an angular partial Coulomb hole $\Delta g(r_{12}, r_1, \alpha_{12})$ which may be defined such that

$$\Delta g(r_{12}, r_1) = \int \Delta g(r_{12}, r_1, \alpha_{12}) d\alpha_{12}.$$

Banyard^(2.i.20), Tatum^(2.i.21) and Moiseyev^(2.i.22) have chosen α_{12} to represent the inter-electronic angle with respect to the nucleus, however Boyd and Ugalde^(2.i.23) have chosen it to be the angle between the nucleus, electron

1 and electron 2. This has the advantage that the angular features of the correlation may be investigated from the point of view of the reference electron rather than the nucleus. Both definitions of the angle may be used, however, to study the angular aspects of the partial Coulomb hole. It must be emphasised that techniques of studying the effect of electron correlation in atoms, other than those outlined in this brief discussion, are possible. The work of Lennard-Jones and Pople^(2.i.24) and Berry and co-workers^(2.i.25,26) is of particular note.

In recent years considerable progress has been made in the experimental determination of X-ray, photon, and electron-scattering profiles^(2.i.27) and these reflect the nature of the momentum distribution of the target electrons. In order to evaluate accurately momentum distributions it is therefore desirable to understand the effects and consequences of electron correlation in momentum-space. To study correlation in this important complementary space Banyard and Reed^(2.i.28) have formulated the 'Coulomb shift' $\Delta f(p_{12})$ by employing momentum-space wavefunctions in equation (II.1.4) and hence obtaining

$$\Delta f(p_{12}) = \int \Gamma_{\text{corr}}(\underline{q}'_1, \underline{q}'_2 | \underline{q}_1, \underline{q}_2) d\underline{\sigma}_1 d\underline{\sigma}_2 d\underline{p}_1 d\underline{p}_2 / dp_{12}. \quad (\text{II.1.9})$$

The vector \underline{q}_1 represents both the momentum and spin-vectors of electron 1, whereas \underline{p}_1 and $\underline{\sigma}_1$ represent the individual momentum and spin-vectors, respectively. Using this approach it is also possible to derive momentum-space partial Coulomb shifts and the other momentum-space functions using the

same technique as used in position-space. The momentum-space correlation functions are known as 'shifts' rather than 'holes' as it was found that $\Delta f(p_{12})$ usually possesses more than one major minimum or maximum, thus making it difficult to define a 'hole'.

Coulomb shift functions have consequently been used to investigate the effect of electron correlation in momentum-space on the ground and excited states of certain atoms and molecules^(2.i.28-31). Comparison between momentum and position-space correlation effects have then been observed. For example, 'radial' and 'angular' correlation effects reinforce each other in position-space yet oppose each other in momentum-space. It is also worthwhile to study correlation for certain small molecules using conventional Coulomb shifts as their momentum density distributions are single-centred and hence the point $p=0$ represents a unique origin^(2.i.18).

Because of the problems in utilising both the position and momentum-space correlation functions to describe molecular systems, in general, methods must be devised to evaluate molecular Coulomb holes which embody the 'symmetry' of molecules yet are practicable in their evaluation. One such technique involves the use of intracule and extracule density functions.

Using the notation proposed first by Eddington^(2.i.32), Coleman^(2.i.33) defined the extracule and intracule functions, for identical particles, to be

$$\underline{R}_{12} = (\underline{r}_1 + \underline{r}_2)/2 \quad (\text{II.1.10})$$

and

$$\underline{r}_{12} = \underline{r}_1 - \underline{r}_2 \quad (\text{II.1.11})$$

respectively. From equations (II.1.10) and (II.1.11), \underline{r}_1 and \underline{r}_2 may then be expressed as

$$\underline{r}_1 = \underline{R}_{12} + \underline{r}_{12}/2 \quad (\text{II.1.12})$$

and

$$\underline{r}_2 = \underline{R}_{12} - \underline{r}_{12}/2 \quad (\text{II.1.13})$$

and, by simply inserting these definitions into equation (II.1.2) and integrating over spin-variables, the second-order reduced-density space matrix may be rewritten as

$$\Gamma(\underline{R}'_{12}, \underline{r}'_{12} | \underline{R}_{12}, \underline{r}_{12}) = \int \Gamma(\underline{x}'_1, \underline{x}'_2 | \underline{x}_1, \underline{x}_2) d\underline{\sigma}_1 d\underline{\sigma}_2 \quad (\text{II.1.14})$$

since the Jacobian of the transformation is unity. The extracule density is therefore defined by

$$E(\underline{R}_{12}) = \int \Gamma(\underline{R}'_{12}, \underline{r}'_{12} | \underline{R}_{12}, \underline{r}_{12}) d\underline{r}_{12} \quad (\text{II.1.15})$$

and the intracule density by

$$I(\underline{r}_{12}) = \int \Gamma(\underline{R}'_{12}, \underline{r}'_{12} | \underline{R}_{12}, \underline{r}_{12}) d\underline{R}_{12}. \quad (\text{II.1.16})$$

These functions inherit the normalisations of the Γ matrix, that is being equal to the number of electron pairs in the system, consequently

$$\int E(\underline{R}_{12}) d\underline{R}_{12} = \int I(\underline{r}_{12}) d\underline{r}_{12} = N(N-1)/2 \quad (\text{II.1.17})$$

where the integration limits are chosen to be appropriate to the co-ordinate system used.

The extracule density is the probability density function of the centre of mass of an electron pair. It can be seen that $E(\underline{R}_{12})d\underline{R}_{12}$ represents the number of electron pairs contained within the volume element $d\underline{R}_{12}$ at some point \underline{R}_{12} . As $E(\underline{R}_{12})$ contains information about the location of electron pairs it is of interest to chemists. It is also possible to define an extracule Coulomb hole as

$$\Delta E(\underline{R}_{12}) = E_{\text{CI}}(\underline{R}_{12}) - E_{\text{HF}}(\underline{R}_{12}) \quad (\text{II.1.18})$$

which obviously represents the redistribution of the centre of mass of the electron pair due to correlation. Extracule density functions have been evaluated for the ground states of the lightest elements^(2.i.34) but attempts to interpret the information contained within them have met with limited success.

As the intracule density represents the probability density function with respect to the inter-electronic displacement, it is much more important in the study of electron correlation effects. The intracule Coulomb hole may be written as

$$\Delta I(\underline{r}_{12}) = I_{\text{CI}}(\underline{r}_{12}) - I_{\text{HF}}(\underline{r}_{12}). \quad (\text{II.1.19})$$

Obviously $\Delta I(\underline{r}_{12})$ is a function in three dimensional space and hence ways must be found to reduce the number of

dimensions further to simplify the presentation of the function. The Coulomb hole of Coulson and Neilson can be seen to be a specific example of the intracule Coulomb hole where angular integration has been performed to fabricate a function that is only dependent upon the inter-electronic distance rather than the vector displacement.

Lester and Krauss^(2.i.35) were the first to try to develop an intracule Coulomb hole to describe the effect of correlation in molecules. They simply evaluated the intracule density for selected orientations of the electron pair relative to the nuclear frame, thus allowing them to investigate electron correlation in the equilateral and linear conformations of the H_3^+ molecule. Unfortunately the results obtained by Lester and Krauss must be considered as unreliable due to the poor quality of the wavefunctions used by them (the magnitude of the energy of their CI wavefunction is less than the accepted present-day HF limit^(2.i.36)).

Thakkar and Smith^(2.i.7) have studied a spherically averaged intracule Coulomb hole $\Delta h(r_{12})$. This is of the same form as that of Tatewaki and Tanaka^(2.i.8) and, of course, this is related to the Coulson and Neilson Coulomb hole by

$$\Delta f(r_{12}) = 4\pi r_{12}^2 \Delta h(r_{12}). \quad (\text{II.1.20})$$

Although this function exhibits all of the problems associated with the conventional Coulomb hole when applied to molecules, it has the advantage that it reveals the short-range correlation effects that have been masked in

$\Delta f(r_{12})$ by the volume element $4\pi r_{12}^2$. In the same vein Sharma and Thakkar^(2.i.19) have also created a 'cylindrical' intracule Coulomb hole in an attempt to encapsulate the symmetry of axially symmetrical molecules. Yet another approach has been to evaluate the intracule density in a particular molecular plane^(2.i.19,38). Studies have been performed successfully on H_2 and N_2 and the effect of the electrons being near the same or different nuclei may be observed indirectly. Unfortunately, although a detailed picture may be obtained by subsequently generating the planar intracule Coulomb hole, for the example of H_2 , the nuclear reference point is lost, thus making it difficult to analyse.

From this brief discussion it may be seen that many techniques have been developed for examining the intracule Coulomb hole for molecules (a review of the intracule and extracule density methods may be seen elsewhere^(2.i.39)). None of these functions, however, give any information about the redistribution in electron probability with respect to the actual framework of the molecule. As this represents the most logical and important reference frame available, functions that could describe the effect of electron correlation with respect to this frame would be of great interest. In the light of this, two independent attempts to include the nuclear frame will be discussed.

By simply integrating over the dimensions of particle 2, the one-particle density function $\rho(\underline{r}_1)$ may be obtained, that is

$$\rho(\underline{r}_1) = \int \Gamma(\underline{x}'_1, \underline{x}'_2 | \underline{x}_1, \underline{x}_2) d\underline{\sigma}_1 d\underline{x}_2. \quad (\text{II.1.21})$$

The difference between a correlated and non-correlated one-particle density has been employed by Duben and Lowe^(2.i.40) as a measure of the effect of electron correlation in the H_3^+ molecule. As the nuclear sites may still be located they were able to evaluate one-particle density profiles along particular lines through the molecule. They made certain conclusions concerning electron correlation in the molecule, and in addition, they compared the efficiencies of certain CI wavefunctions to incorporate electron correlation.

For axially symmetric molecules, by integrating either longitudinally or transversely and locating electron 1 at a certain point in space, Doggett^(2.i.41,42) has formulated the transverse and longitudinal correlation holes. The molecule is set to lie along the z-axis, hence the longitudinal hole is given by

$$\Delta L(\underline{r}_2, z_1) = \int_{\rho=0}^{\infty} \int_{\phi=0}^{\pi} \Delta \Gamma_{\text{corr}}(\underline{x}'_1, \underline{x}'_2 | \underline{x}_1, \underline{x}_2) d\underline{\sigma}_1 d\underline{\sigma}_2 d\phi_2 \rho_2 d\rho_2 \quad (\text{II.1.22})$$

whereas the transverse correlation hole is

$$\Delta T(\underline{r}_2, \rho_1) = \int_{z=-\infty}^{\infty} \int_{\phi=0}^{\pi} \Delta \Gamma_{\text{corr}}(\underline{x}'_1, \underline{x}'_2 | \underline{x}_1, \underline{x}_2) d\underline{\sigma}_1 d\underline{\sigma}_2 d\phi_2 dz_2. \quad (\text{II.1.23})$$

The longitudinal correlation hole consequently represents the change in probability of finding electron 2 at some distance z_2 , irrespective of ρ_2 and ϕ_2 , due to the

instantaneous location of electron 1 at \underline{r}_1 . In a similar way, the transverse hole represents the change in probability of finding electron 2 at a distance ρ_2 from the z-axis as a result of locating electron 1 at \underline{r}_1 . These functions are able to utilise the axis of the molecule as an origin and thus can reflect the axial symmetry of the system. When viewed together they give a detailed account of the effect of correlation. Obviously, however, they are restricted to linear molecules.

Unfortunately there are no functions to date for describing the effect of correlation that can reflect the symmetry of any general molecule but still maintain explicit reference to the nuclear framework. The purpose of this work has therefore been to develop logically functions that have this ability. They must augment existing definitions yet be general enough to allow the effect of correlation in any molecule to be investigated. Any of the many accurate correlated wavefunctions that already exist should thus be usable in the generation of these functions and hence their definition should be independent of the type or size of the basis set of the wavefunction employed.

CHAPTER II.2

Molecular Electron Correlation Functions

It is possible to investigate the effects of electron correlation by using both one and two-electron functions. Only general information may be acquired from the one-particle density though since the effect of one of the electrons has been averaged out over all space. Consequently, to gain specific information about the charge relocation due to correlation, two-particle density functions must be employed. Molecular correlation functions are further complicated by the need to maintain reference to the location of the nuclei, and also to incorporate the symmetry of the molecule. This allows the charge redistribution due to the effect of electron correlation to be investigated with respect to the arrangement of the nuclei, this being the most important, logical and easily analysed reference frame available.

All of the information concerning the relative distribution of a pair of electrons, electron 1 and 2 say, is contained in the second-order reduced-density matrix (see equation (II.1.2)). Since, in this analysis, no operators will act upon the matrix, the 'dash' notation may be omitted. Also, to form a purely spatial function, the spin vectors of electron 1 and 2 may be integrated out, allowing it to be written in the form

$$\Gamma(\underline{r}_1, \underline{r}_2) = N(N-1)/2 \int \psi^*(\underline{x}_1, \underline{x}_2, \dots, \underline{x}_N) \psi(\underline{x}_1, \underline{x}_2, \dots, \underline{x}_N) d\underline{\sigma}_1 d\underline{\sigma}_2 \\ d\underline{x}_3 d\underline{x}_4 \dots d\underline{x}_N. \quad (\text{II.2.1})$$

This function has been the mathematical foundation of many past analyses of correlation effects and will be employed in this work.

Following Banyard and Reed^(2.ii.1), by employing momentum-space wavefunctions in equation (II.2.1), it is possible to define momentum-space equivalents of the position-space correlation functions by using exactly the same derivation processes. This analysis will therefore be restricted to position-space, apart from stating the formal definitions of the most important momentum-space correlation functions.

(II.2.1) The One-Particle Density Functions

The one-particle density function $\rho(\underline{r}_1)$ represents the probability of locating electron 1 at some point defined by \underline{r}_1 , when the influence of electron 2 has been integrated over all space, and hence it may be expressed as

$$\rho(\underline{r}_1) = \int \Gamma(\underline{r}_1, \underline{r}_2) d\underline{r}_2. \quad (\text{II.2.2})$$

The vector \underline{r}_1 may be expressed in terms of the three cartesian co-ordinates x_1 , y_1 and z_1 . Thus, by fixing one of these variables, it is possible to define a one-particle density surface that reflects the symmetry of the molecule. The volume under this surface is not normalised but is equal

to the probability of locating electron 1 somewhere within the chosen molecular plane.

In keeping with previous definitions, electron correlation may be studied by examining the difference between the correlated and Hartree Fock one-particle densities, ie

$$\Delta\rho(\underline{r}_1) = \rho(\underline{r}_1)_{CI} - \rho(\underline{r}_1)_{HF}. \quad (\text{II.2.3})$$

$\Delta\rho(\underline{r}_1)$ represents the change in probability of locating electron 1 at a point defined by the vector \underline{r}_1 , when the influence of electron 2 has been averaged over all space. The volume under the Δ -surface is, in general, non-zero and is a measure of the amount of charge brought into the plane due to correlation. The momentum-space Δ -one-particle planar density $\Delta\rho(\underline{p}_1)$ represents the change in probability of locating electron 1, with momentum \underline{p}_1 , when the effect of the momentum associated with electron 2 has been averaged over all space.

Since $\Delta\rho(\underline{r}_1)$ is a function of \underline{r}_1 , the positions of the nuclei may be located with respect to the origin of \underline{r}_1 , whereas if it were purely a function of vector \underline{r}_{12} , the inter-electronic displacement, this obviously could not occur. Its use is limited, however, to measure only an averaged correlation effect due to the integration that has been performed. One-particle density functions therefore form only a small portion of the investigation into correlation effects. For a more detailed analysis recourse must be made to the two-particle density functions.

(II.2.2) The Two-Particle Density Functions

Even by restricting the analysis to one particular plane, the two-particle density is still a function of four variables and consequently is difficult to analyse. In a similar way to the derivation of the partial Coulomb hole, by fixing the position of one of the electrons, electron 1 say, with respect to the nuclear frame we have defined a new function; the partial planar two-particle density. This is only a function of two variables, and hence may be represented on a contour diagram. It also has the added advantage that, because no integration has been performed apart from in the generation of $\Gamma(\underline{r}_1, \underline{r}_2)$, it may be generated numerically for any wavefunction, thus enabling any molecule to be studied.

Since correlation represents an improvement to the description of the electron-electron interaction, it is important to study the location of the roving electron, electron 2, with respect to the position of the fixed electron. The partial planar density $V(\underline{r}_{12}, \underline{r}_1)$, for a fixed value of \underline{r}_1 , is given by

$$V(\underline{r}_{12}, \underline{r}_1) = \Gamma(\underline{r}_1, \underline{r}_{12}) r_{12} \quad (\text{II.2.4})$$

where \underline{r}_{12} , which is restricted to be a function of two dimensions, is expressed as

$$\underline{r}_{12} = \underline{r}_1 - \underline{r}_2 \quad (\text{II.2.5})$$

The inclusion of the multiplying factor r_{12} in equation (II.2.4) enables $V(\underline{r}_{12}, \underline{r}_1)$ to be interpreted as the probability of discovering the roving electron at a position located by the vector \underline{r}_{12} , relative to the fixed electron, and simultaneously finding the fixed electron at a point defined by \underline{r}_1 , relative to the nuclear frame. Again the volume under the surface is not normalised, but in this instance it is equal to the probability of finding the fixed electron at the point defined by \underline{r}_1 whilst the roving electron is located somewhere within the chosen plane.

The redistribution in probability due to correlation is then given by the difference between the correlated (CI) partial planar density and the equivalent Hartree Fock density,

$$\Delta V(\underline{r}_{12}, \underline{r}_1) = V(\underline{r}_{12}, \underline{r}_1)_{CI} - V(\underline{r}_{12}, \underline{r}_1)_{HF}. \quad (\text{II.2.6})$$

The volume under the $\Delta V(\underline{r}_{12}, \underline{r}_1)$ surface represents both the probability of discovering electron 2 in the chosen plane and also electron 1 being located at the point defined by \underline{r}_1 . A particular point on the Δ -partial planar surface consequently is a measure of both the increase in the probability of locating the roving electron at a point defined by \underline{r}_{12} , relative to \underline{r}_1 , and also the fixed electron being located at a point defined by \underline{r}_1 due to correlation. Similarly, a point on the momentum-space density surface $\Delta V(\underline{p}_{12}, \underline{p}_1)$ represents the change in probability of locating electron 2 with momentum \underline{p}_{12} , relative to \underline{p}_1 , and electron 1 possessing a momentum of \underline{p}_1 due to correlation.

Although $\Delta V(\underline{r}_{12}, \underline{r}_1)$ is technically a function of \underline{r}_{12} , since \underline{r}_{12} is defined with respect to the vector \underline{r}_1 , which is itself defined with respect to a known origin, the nuclear sites may still be identified. This surface is therefore of fundamental importance in the investigation of electron correlation in molecules as it contains all of the information necessary to describe the redistribution in probability with respect to the fixed electron and the molecular frame in the plane.

As \underline{r}_{12} is constrained to be a function of only two dimensions, it may be expressed, relative to the location of the fixed electron, using the co-ordinates r_{12} and ϵ , where r_{12} represents the distance between the two electrons and ϵ is an angular co-ordinate. Since, in general, no natural choice of origin exists, ϵ cannot be defined with respect to the molecular frame. It is therefore defined as the angle subtended in an anti-clockwise direction, between the axis with highest symmetry and the vector \underline{r}_{12} . This has the advantage that ϵ defines the same direction for any fixed electron position in a particular plane or in any plane parallel to it. An example of this can be seen in Figure (II.5.3B) for the xz -plane of the H_2 molecule in position-space. Here the axis of highest symmetry is obviously the z -axis, and thus ϵ is defined as the angle between a line parallel to this axis and the line connecting the roving electron to the fixed electron. The ranges of the co-ordinates are

$$0 \leq r_{12} \leq \infty$$

and

(II.2.7)

$$0 \leq \varepsilon \leq 2\pi.$$

Although $\Delta V(r_{12}, \varepsilon, \underline{r}_1)$ contains a full account of the effect of electron correlation in the plane, it must be shown on a rather complicated contour diagram. In an attempt to derive simpler functions, it is possible to integrate either over the angular or radial co-ordinates of $\Delta V(r_{12}, \varepsilon, \underline{r}_1)$ to produce either a radial or an angular partial planar Coulomb hole. Consequently, we have defined two more functions: (a) The radial partial planar Coulomb hole which is given by

$$\Delta S(r_{12}) = \int_{\varepsilon=0}^{2\pi} \Delta V(r_{12}, \varepsilon, \underline{r}_1) d\varepsilon. \quad (\text{II.2.8})$$

(b) The angular partial planar Coulomb hole, which is defined as

$$\Delta U(\varepsilon) = \int_{r_{12}=0}^{\infty} \Delta V(r_{12}, \varepsilon, \underline{r}_1) dr_{12}. \quad (\text{II.2.9})$$

The reference to the fixed electron position, \underline{r}_1 , has been implied in the definitions of $\Delta S(r_{12})$ and $\Delta U(\varepsilon)$. The areas defined by these functions are the same and equal to the volume under the Δ -partial planar surface, thus

$$\int_{r_{12}=0}^{\infty} \Delta S(r_{12}) dr_{12} = \int_{\varepsilon=0}^{2\pi} \Delta U(\varepsilon) d\varepsilon = \int_{r_{12}=0}^{\infty} \int_{\varepsilon=0}^{2\pi} \Delta V(r_{12}, \varepsilon) dr_{12} d\varepsilon. \quad (\text{II.2.10})$$

Formally, the radial partial planar Coulomb hole represents

the simultaneous change in probability of finding electron 2, the roving electron, at a distance r_{12} from electron 1, and of finding electron 1 at the point specified by \underline{r}_1 . The angular partial planar Coulomb hole represents the change in probability of finding the electron 2 along a direction specified by the angle ϵ , relative to the location of electron 1, and, at the same time, the change in probability of discovering electron 1 at the point specified by \underline{r}_1 . Although explicit reference to the nuclei is partially lost in these functions, they may be employed together to gain an insight into the overall effect of correlation in the plane. The $\Delta S(r_{12})$ and $\Delta U(\epsilon)$ curves may also be used to make simple comparisons between the quality of different wavefunctions when describing correlation effects.

In keeping with past work, the momentum-space Coulomb holes are known as Coulomb shifts. Consequently, a point on the momentum-space partial planar Coulomb shift $\Delta S(p_{12})$ is a measure of both the change in probability of discovering electron 2, with a momentum of p_{12} , relative to the momentum p_1 of electron 1, and also of discovering electron 1 with momentum p_1 . The momentum-space angular partial planar Coulomb shift $\Delta U(\epsilon)$ is similarly defined as the increase in probability of discovering electron 2 with a momentum in the ϵ direction and also finding electron 1 with a momentum of p_1 .

These partial planar Coulomb holes and shifts are defined in the same manner as the conventional partial

Coulomb holes derived by Boyd and Coulson^(2.ii.2), and developed and used extensively by Banyard and his co-workers^(2.ii.3-5). We may also examine 'inter' and 'intra' electronic shell correlation effects by using the shell partitioning technique as developed first by Banyard and Mashat^(2.ii.6) from the work of Sinanoglu^(2.ii.7). By making a sensible choice of fixed electron position and molecular plane, the effect of electron correlation may be studied extensively in any molecule by employing a combination of $\Delta V(r_{12}, \epsilon)$, $\Delta S(r_{12})$ and $\Delta U(\epsilon)$ and the momentum-space equivalents. These functions form the basis of the subsequent investigation into the effect of electron correlation in position and momentum-space on the H_2 and H_3^+ molecules.

The definitions of the three most widely used functions in each space are summarised overleaf.

Definition of the Position-Space Correlation Functions

The Δ -Partial Planar Density $\Delta V(r_{12}, \varepsilon, \underline{r}_1)$

A point on the surface represents both the change in probability of locating the roving electron at this point and simultaneously the change in probability of finding the fixed electron located by the vector \underline{r}_1 with respect to a predefined origin, due to the effect of correlation.

The Radial Partial Planar Coulomb Hole

A point on the $\Delta S(r_{12})$ curve is a measure of the change in probability of locating the roving electron at a distance r_{12} away from the fixed electron in the chosen plane and also of locating the fixed electron at the point defined by \underline{r}_1 , with respect to a predefined origin, due to the effect of electron correlation.

The Angular Partial Planar Coulomb Hole

A point on the $\Delta U(\varepsilon)$ curve represents the change in probability of locating the roving electron along a direction defined by ε , relative to the fixed electron, and also of locating the fixed electron at the point specified by \underline{r}_1 , with respect to a predefined origin, due to the effect of electron correlation.

Definition of the Momentum-Space Correlation Functions

The Δ -Partial Planar Density $\Delta V(p_{12}, \epsilon, p_1)$

A point on the surface represents the change in probability of locating electron 2 with a momentum specified by p_{12} and ϵ , relative to p_1 , and of discovering electron 1 with a momentum of p_1 , due to the effect of electron correlation.

The Radial Partial Planar Coulomb Shift

A point on the $\Delta S(p_{12})$ curve represents the change in probability of locating electron 2 with a momentum of p_{12} , relative to p_1 , the momentum of electron 1, and also of finding electron 1 with a momentum of p_1 , due to the effect of correlation.

The Angular Partial Planar Coulomb Shift

A point on the $\Delta U(\epsilon)$ curve in momentum-space represents the change in probability of locating electron 2 with a momentum along a direction given by ϵ , relative to p_1 , the momentum of electron 1, and also of discovering electron 1 with a momentum of p_1 , due to the effect of electron correlation.

POSITION-SPACE ANALYSIS OF H_2 AND H_3^+

CHAPTER II.3

The H_2 and H_3^+ Systems

The H_2 and H_3^+ molecules have been chosen to test the viability of the partial planar technique mainly because they represent the simplest stable, multi-electron, diatomic and polyatomic molecules available. Due to the diatomic nature of the H_2 molecule, it is also possible to categorise the main correlation-types for such molecules. The H_3^+ molecular-ion, on the other hand, is more complicated to study than the H_2 molecule since the axial symmetry has been lost and thus it proves to be an ideal example to test the partial planar theory on a general system.

From the early pioneering work of Heitler and London^(2.iii.1) and James and Coolidge^(2.iii.2), H_2 has been recognised as the natural bridge between the quantum mechanical study of atoms and molecules. It is consequently disturbing to discover that, whilst experimental and theoretical results for small atoms have a history of excellent agreement with each other, major discrepancies occur in the case of H_2 ^(2.iii.3-5). For example, only in recent years has the Compton profile of H_2 been ^{calculated} accurately using highly correlated wavefunctions and been found to be consistent with experimental results^(2.iii.6,7). This was only achieved by employing wavefunctions that contain a high degree of electron correlation and describe the rotational and vibrational effects of the molecule^(2.iii.8,9) well. By investigating the effects of

correlation on H_2 it should be possible to create shorter wavefunctions, that are obviously easier to manipulate, without losing the high degree of accuracy that is necessary in such calculations.

In 1912 Thomson^(2.iii.10) discovered the existence of the H_3^+ ion in electrical discharges in gaseous hydrogen. It is produced whenever an H_2 molecule is in collision with an H_2^+ molecular-ion. Initial experiments were concerned with evaluating bending and stretching modes^(2.iii.11) and scattering cross sections^(2.iii.12,13). Surprisingly, it was not until 1978 that experimental evidence was produced by Gaillard and his co-workers^(2.iii.14) to confirm the earlier theoretical prediction of Christoffersen^(2.iii.15) that H_3^+ is arranged in an equilateral triangle conformation. We also note that the infrared spectrum of H_3^+ and D_3^+ was only discovered^(2.iii.16,17) in 1980 (an improved analysis has recently been performed^(2.iii.18)) and the microwave spectrum^(2.iii.19) in 1985.

Current theoretical and experimental interest in the H_3^+ molecular-ion is still quite high due to its possible role in thermonuclear devices^(2.iii.20), its suggested effect upon the thermodynamic behaviour of certain metals^(2.iii.21) and its postulated astrophysical significance as a participant in ion-molecular reactions^(2.iii.22,23). A precise knowledge of electron correlation effects in this system would be extremely useful in order to obtain more accurate theoretical results in these fields.

As discussed in Chapter (II.2), some attempts have been made to study the effects of electron correlation in H_3^+ by either considering the difference between the correlated and non-correlated one-particle densities^(2.iii.24) or directional Coulomb holes^(2.iii.25). The results, however, have proved difficult to analyse and consequently provided little information. It would therefore seem appropriate to attempt to obtain a more detailed, but easily analysed, account of the correlation effects in H_3^+ .

In addition to studying the correlation effects in H_2 and H_3^+ to test the viability of the partial planar technique, useful information may also be gained from this work that is essential in order to evaluate more precise theoretical results.

Chapter II.4

Position-Space Wavefunctions

As discussed earlier, electron correlation is usually studied by approximating the exact non-relativistic wavefunction by a highly correlated Configuration Interaction (CI) wavefunction and the Hartree Fock (HF) wavefunction by an accurate Self-Consistent Field (SCF) wavefunction (see Appendix II for a more complete discussion of Hartree Fock theory). There are no constraints on the types of basis functions that can be used in wavefunctions to generate partial planar Coulomb density surfaces but, since it is intended to extend this analysis into momentum-space, wavefunctions containing explicit reference to the inter-electronic distance cannot be used.

(II.4.1) The H₂ Molecule

A wide variety of wavefunctions have been evaluated at both CI and SCF levels of accuracy for the hydrogen molecule^(2.iv.1-6). The best available wavefunction was found to be that of Kolos and Roothaan^(2.iv.7). This is a fifty-four term wavefunction written in confocal ellipsoidal co-ordinates (also termed prolate spheroidal co-ordinates) but unfortunately also containing the inter-electronic distance r_{12} . Using a method devised by Davidson^(2.iv.8), Davidson and Jones^(2.iv.9) have transformed the Kolos and Roothaan wavefunction into natural orbital (NO)

form^(2.iv.10) (see Appendix III). By curtailing the wavefunction to incorporate only the first ten natural orbitals and renormalising, 97% of the correlation energy can still be accounted for, this being better than any of the other available wavefunctions. The natural orbital form of the wavefunction is again written in confocal ellipsoidal co-ordinates but has the advantage that there is now no dependence on the inter-electronic distance, hence alleviating the problem associated with converting it into momentum-space.

The Davidson and Jones^(2.iv.9) wavefunction can be written in position-space as

$$\Psi(\underline{r}_1, \underline{r}_2) = \sum_{i=1}^{10} \mu_i \begin{cases} \chi_i^*(\underline{r}_1) \chi_i(\underline{r}_2) & \text{if } m = 0 \\ \chi_i^*(\underline{r}_1) \chi_i(\underline{r}_2) + \chi_i(\underline{r}_1) \chi_i^*(\underline{r}_2) & \text{if } m \neq 0 \end{cases} \quad (\text{II.4.1})$$

where the natural orbitals $\chi_i(\underline{r})$ are of the form

$$\chi_i(\underline{r}) = (2/R)^{3/2} (2\pi)^{-1/2} \sum_{k=1}^{15} c_k \xi^{nk} \eta^{jk} (\xi^2 - 1)^{mi/2} (1 - \eta^2)^{mi/2} \exp(im_i \phi) \exp(-\alpha \xi). \quad (\text{II.4.2})$$

The quantum numbers n , j and m are given by Davidson and Jones, the exponent α was fixed by them to be 0.995 for all orbitals and the bondlength R was chosen to be the near-equilibrium value of 1.4 a.u.. The co-ordinates are defined in Figure (II.4.1) such that

$$\begin{aligned} \xi &= (r_A + r_B)/2 \\ \eta &= (r_A - r_B)/2 \end{aligned} \quad (\text{II.4.3})$$

and ϕ is the conventional azimuthal angle.

A property of expressing the wavefunction in natural orbital form is that the configurations are arranged to produce the fastest energy convergent series^(2.iv.11), consequently electron correlation is introduced in the most rapid and logical manner. The ground state of the molecule is of $1 \sum_g^+$ symmetry, hence the wavefunction must also be symmetrical under all transformations of the $D_{\infty h}$ group. By employing the Davidson technique^(2.iv.8), all matrix elements that are functions of basis orbitals of different symmetry type vanish, thus allowing Davidson and Jones to compute each symmetry type separately.

It can be seen, from Table (II.4.1) that the first natural orbital is by far the most dominant term in the expansion and, by using it alone, the energy obtained is virtually at the Hartree Fock limit. Using the wavefunction expansion devised by Sinanoglu^(2.iv.13), Davidson and Jones explain that the first natural orbital may be considered as being equivalent to the Hartree Fock wavefunction to within the second order of a perturbation expansion. Also, Schwartz and Schaad^(2.iv.4) have devised an SCF wavefunction that yields an energy of -1.3342 a.u., which is further from the Hartree Fock limit than the first natural orbital of the Davidson and Jones wavefunction. For these reasons, and to eliminate any possible basis-set dependency, the first natural orbital has been used in this analysis as a reliable approximation to the Hartree Fock wavefunction.

The second, third and fourth natural orbitals have occupation numbers of the same order of magnitude (see Table

(II.4.1)) and should therefore be considered together. The second natural orbital is of σ_u symmetry and therefore correlation is introduced in a direction parallel to the bond. The third, however, being of π_u symmetry, brings in electron correlation angularly around the bond. The fourth natural orbital, which has σ_g symmetry, then incorporates electron correlation in directions perpendicular to the bond axis. From these observations it can be seen that, for axially symmetric molecules, electron correlation may be partitioned along the three orthogonal directions of the cylindrical co-ordinate system. This is similar to the more symmetrical atomic case where, using natural orbital expansions of wavefunctions, electron correlation has been classified as either radial or angular^(2.iv.14-15). Thus, if the Davidson and Jones wavefunction were curtailed to use only the first two natural orbitals and renormalised to unity, the effect of z-correlation alone could be incorporated into the wavefunction. In a similar way, by using the first three, then first four natural orbitals, ϕ then ρ -correlation types are introduced into the wavefunction. It is interesting to note that the wavefunction curtailed to embody the first four natural orbitals, and therefore including the cumulative effects of z, ϕ and ρ -correlation, can account for 89% of the correlation energy.

The remaining six natural orbitals only account for 8% of the correlation energy and have very much smaller, but similar in magnitude, occupation numbers. The symmetries of these orbitals represent the six possibilities of coupling

the three major types of correlation together. Consequently they may be considered as second order corrections to the wavefunction and will be included in the wavefunction collectively.

In summary, therefore, we see that the natural orbital form of the wavefunction has the advantage in that it allows us to investigate the effects of different types of correlation. The first natural orbital can also be used as an accurate approximation to the Hartree Fock wavefunction. Moreover the whole wavefunction can be transformed into momentum-space where a corresponding examination may be undertaken.

(II.4.2) The H_3^+ Molecule

Both single^(2.iv.16-19) and multi-centre^(2.iv.20-27) electronic wavefunctions have been evaluated for the equilateral triangle conformation of the H_3^+ molecule. The lowest energy CI wavefunction available was found to be that of Salmon and Poshusta^(2.iv.26). It has a fixed nuclear separation of 1.65 a.u. and a total non-relativistic energy of -1.34335 a.u.. Thus, if the value for the exact energy is taken as -1.34470 a.u.^(2.iv.20) and the Hartree Fock limit as -1.30007 a.u. the Salmon and Poshusta wavefunction incorporates 97% of the total correlation energy. The wavefunction consists of the linear combination of fifteen configurations in the form of Singer polynomials^(2.iv.2), hence

$$\Psi(\underline{r}_1, \underline{r}_2) = \sum_{i=1}^{15} c_i [1 + P_{12}] [\Sigma T] \phi_i(\underline{r}_1, \underline{r}_2) \quad (\text{II.4.4})$$

where the Singer polynomial $\phi_i(\underline{r}_1, \underline{r}_2)$ is of the form

$$\phi_i(\underline{r}_1, \underline{r}_2) = \exp \left[-a_i (\underline{r}_1 - \underline{S}_{1i})^2 - 2g_i (\underline{r}_1 - \underline{S}_{1i}) \cdot (\underline{r}_2 - \underline{S}_{2i}) - b_i (\underline{r}_2 - \underline{S}_{2i})^2 \right]. \quad (\text{II.4.5})$$

The constants c_i , a_i , g_i and b_i together with the vectors \underline{S}_{1i} and \underline{S}_{2i} have been given by Salmon and Poshusta^(2.iv.26). The vectors \underline{S}_{1i} and \underline{S}_{2i} locate Gaussian-type expansion centres and are constrained to be in the plane of the molecule. The operator P_{12} is simply the permutation operator and therefore represents an interchange of electron labels whereas ΣT represents a summation over all twelve elements of the D_{3h} symmetry group. Fortunately, since the expansion centres are all contained within the plane of the molecule, it is sufficient to sum over the six elements of the C_{3v} sub-group. Consequently, all of the centres of the Singer polynomials must undergo a three-fold rotation about the centre of the molecule and then all of these generated points are reflected in the xz -plane (a reflection in the xy -plane, the plane of the molecule, does not occur with C_{3v} symmetry). The co-ordinate system used to describe H_3^+ is shown in Figure (II.4.2). Thus, after these operations have been performed, the Salmon and Poshusta wavefunction actually consists of the combination of one hundred and eighty independent Singer polynomials.

To avoid any possible basis-set dependency arising in the analysis, the SCF wavefunction was chosen to be also in Gaussian form. The best SCF wavefunction available for equilateral H_3^+ was that of Schwartz and Schaad^(2.iv.27). It is constructed from the product of two one-electron molecular orbitals, each one consisting of a linear combination of fifteen unnormalised 1s floating Gaussian type orbitals (GTO). The Schwartz and Schaad wavefunction may therefore be written as

$$\Phi_{\text{SCF}}(\underline{r}_1, \underline{r}_2) = \Phi^*(\underline{r}_1)\Phi(\underline{r}_2) \quad (\text{II.4.6})$$

with the molecular orbital $\Phi(\underline{r})$ given by

$$\Phi(\underline{r}) = \sum_{i=1}^5 c_i \left[\phi_i^A(\underline{r}) + \phi_i^B(\underline{r}) + \phi_i^C(\underline{r}) \right]. \quad (\text{II.4.7})$$

The three nuclei are labelled A, B and C and thus, for example, the symbol $\phi_i^A(\underline{r})$ represents an unnormalised 1s GTO, with exponent a_i , centred at a distance d_i from nucleus A along a line extending from it towards the centre of the molecule. The advantage of this is that, although the molecular orbitals are built up from fifteen basis functions, Schwartz and Schaad have only been required to optimise five independent sets of parameters.

Unfortunately the Schwartz and Schaad wavefunction has been energy-optimised at a fixed nuclear separation of 1.6405 a.u. whereas the separation for the Salmon and Poshusta wavefunction was 1.65 a.u.. For this reason it was decided to extend the inter-nuclear separation of the

Schwartz and Schaad wavefunction to 1.65 a.u.. This was performed, firstly by keeping the distance d_i the same fraction of the nuclear separation, resulting in the transform

$$d_i^{(1.65)} = d_i^{(1.6405)} \times (1.65/1.6405). \quad (\text{II.4.8})$$

The exponents of the orbitals, on the other hand, were transformed to maintain the full width at half the maximum height of the orbitals as the same fraction of the nuclear separation to give

$$a_i^{(1.65)} = a_i^{(1.6405)} \times (1.6405/1.65)^2. \quad (\text{II.4.9})$$

By utilising the standard computer package Gaussian 82^(2.iv.29), the linear expansion coefficients of the extended bondlength wavefunction were energy reoptimised and the parameters obtained are shown in Table (II.4.2). The total energy associated with this wavefunction is -1.29906 a.u., which is not significantly different from the energy of -1.29955 a.u. that is obtained from the original Schwartz and Schaad wavefunction. The extended Schwartz and Schaad wavefunction has therefore been used, in this analysis, as an accurate approximation towards the Hartree Fock wavefunction for H_3^+ at a bondlength of 1.65 a.u..

N_i (a)	μ_i of configuration added (b)	sym. con. (c)	Total Energy (a.u.)	%correlation (d)	type of corr.
1	0.991058	σ_g	-1.133467	-0.3870	
2	-0.099473	σ_u	-1.151939	44.86	z
3	-0.065109	π_u	-1.162811	71.49	ϕ
4	-0.054810	σ_g	-1.169884	88.82	ρ
5	-0.011845	π_g	-1.170660	90.72	{ $\phi\rho$ }
6	-0.009967	σ_g	-1.171185	92.01	{zz}
7	-0.009745	σ_u	-1.171691	93.25	{ ρz }
8	-0.009723	δ_g	-1.172178	94.44	{ $\phi\phi$ }
9	-0.009362	π_u	-1.172742	95.82	{ ϕz }
10	-0.006552	σ_g	-1.173032	96.53	{ $\rho\rho$ }
HF		σ_g	-1.133625	0.00	
Exp			-1.174475 ^(e)	100.00	

(a) N_i is the number of configurations employed in the wavefunction.

(b) μ_i has been defined in equation (II.4.1) and also $\mu_i^2 = n_i$, where n_i is the occupation number of the configuration.

(c) Symmetry of configuration added.

(d) %correlation has been defined with respect to the Hartree Fock limit as

$$\%corr = (E_i - E_{HF}) \times 100 / (E_{exp} - E_{HF}).$$

(e) see reference (2.iv.1).

Table 3 (II.4.1) Occupation numbers and correlation energies of the Davidson and Jones wavefunction for H_2 at a fixed bondlength of 1.4 a.u..

i	c_i	a_i	d_i
1	0.038021	0.221479	0.246439
2	0.112565	0.735221	0.165356
3	0.085695	2.66357	0.059684
4	0.055738	11.90808	0.007181
5	0.029452	82.47117	0.000102

Nuclear Energy	=	1.818182 a.u.
Electronic Energy	=	-3.118088 a.u.
Total Energy	=	-1.299906 a.u.
$-V/T$ (virial theorem)	=	2.0060

Table (II.4.2) The coefficients of the extended Schwartz and Schaad wavefunction for H_3^+ as defined by equation (II.4.7).

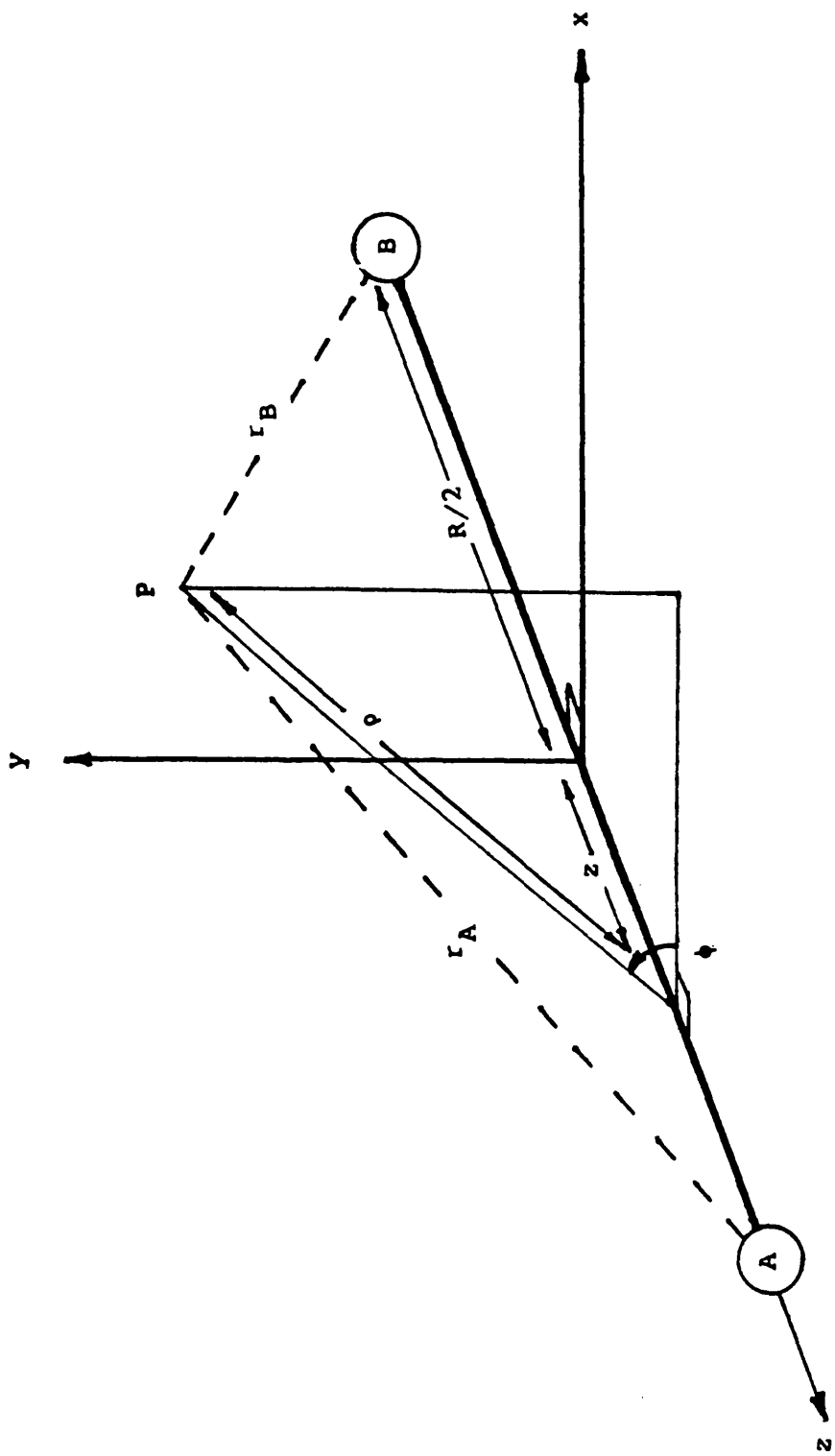


Figure (II.4.1) The co-ordinate system used in the analysis of correlation effects in the H_2 molecule. The bond length R is 1.4 a.u. and the molecule is aligned to coincide with the z -axis.

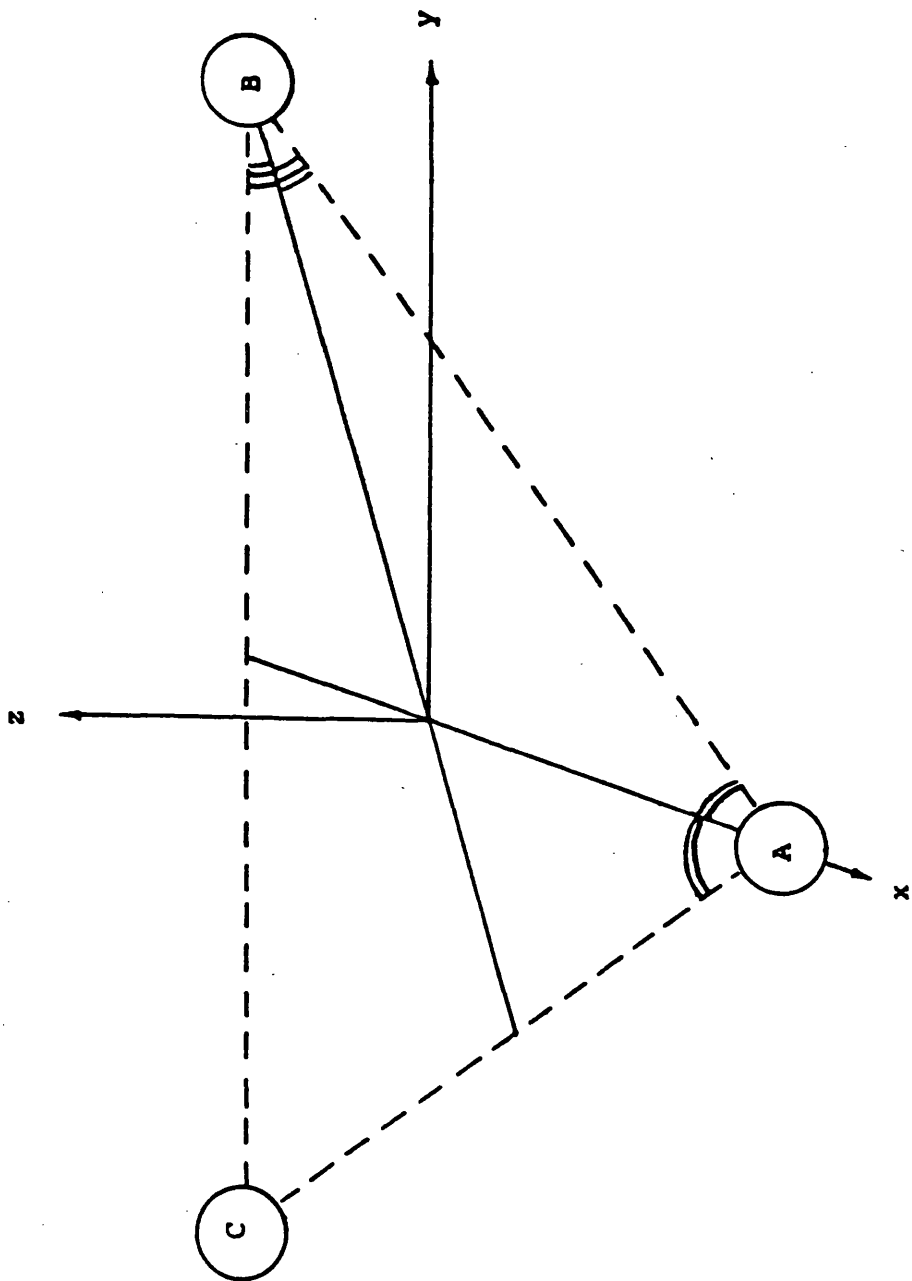


Figure (II.4.2) The co-ordinate system used in the analysis of correlation effects in the H_3^+ molecular-ion. The distance between two nuclei is 1.65 a.u. and the x-axis passes through nucleus A and bisects the line r_{CB} .

CHAPTER II.5

Results for H₂ in Position-Space

The Davidson and Jones^(2.v.1) ten natural orbital approximation of the Kolos and Roothaan^(2.v.2) wavefunction has been used in the generation of the subsequent results. Also, to highlight the axially symmetric nature of the hydrogen molecule, standard cylindrical co-ordinates have been employed in this analysis with the z-axis defined to lie along the bond direction (see Figure (II.4.1)). The first natural orbital in the Davidson and Jones wavefunction has been used to represent the Hartree Fock limit. By curtailing the wavefunction to encompass only the sum of the first two, three, four and finally the full ten natural configurations and then renormalising to unity, the effect of introducing z , ϕ , ρ and second-order correlation may be observed respectively. In the diagrams that follow, the abbreviations 1NO, 2NO, 3NO, 4NO and 10NO obviously refer to the number of natural orbitals employed in the renormalised wavefunction.

As discussed earlier, the results may be divided into one and two-particle density functions, with the two-particle density functions forming the main section of the investigation. For both types of planar function it is important to present the HF densities as well as the Δ -densities in order to gain insight into the relative importance of correlation at a particular point in space.

Both types of function are therefore shown. To accentuate the geometry of each surface, certain contours are chosen from the following sets:

Hartree Fock Surface Contours

1	0.0001	6	0.02
2	0.0005	7	0.03
3	0.0025	8	0.04
4	0.0075	9	0.10
5	0.010	10	0.15

Δ -Surface Contours

1	-0.0050	15	0.0001
2	-0.0040	16	0.0002
3	-0.0030	17	0.0003
4	-0.0025	18	0.0005
5	-0.0020	19	0.0007
6	-0.0015	20	0.0009
7	-0.0011	21	0.0011
8	-0.0009	22	0.0015
9	-0.0007	23	0.0020
10	-0.0005	24	0.0025
11	-0.0003	25	0.0030
12	-0.0002	26	0.0040
13	-0.0001	27	0.0050
14	0.0000	28	0.0060

Also, on the contour diagrams the negative contours are represented by broken curves, positive contours by full curves and the zero contour by a dotted curve. It must be emphasised, however, that not all of the possible contours are represented on each surface, merely a selection that are chosen to highlight the geometry of the distribution. The following abbreviations are also used:

- x = position of fixed electron, located relative to the nuclear frame
- ⊙ = position of nucleus.

This analysis has been performed at the, generally accepted, equilibrium bond length of 1.4 a.u. The full width of the surfaces is 8 a.u., thus, on the smaller surface views, 9 millimetres corresponds to 1 a.u. and on the larger surface, (Figure (II.5.1)), 1 a.u. is 18 millimetres.

(II.5.1) The One-Particle Density Results

The obvious plane to choose in order to highlight the symmetry of the H₂ molecule is the plane containing the two nuclei, defined as the xz-plane. From this, any other one-particle density plane may be generated since, due to the axially symmetric nature of the molecule, contours in perpendicular planes to this would simply form concentric circles about the bond axis. The following results are therefore concerned only with the xz-plane:

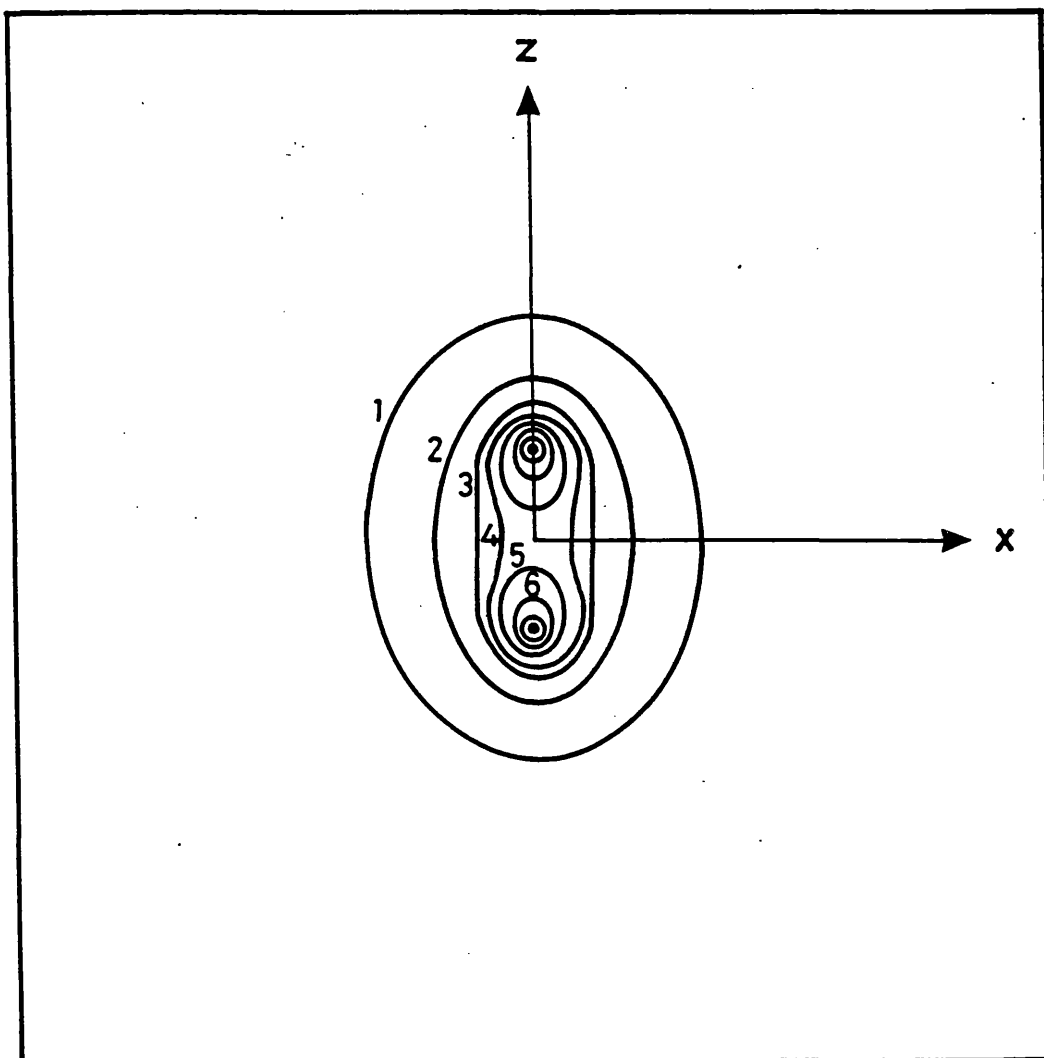
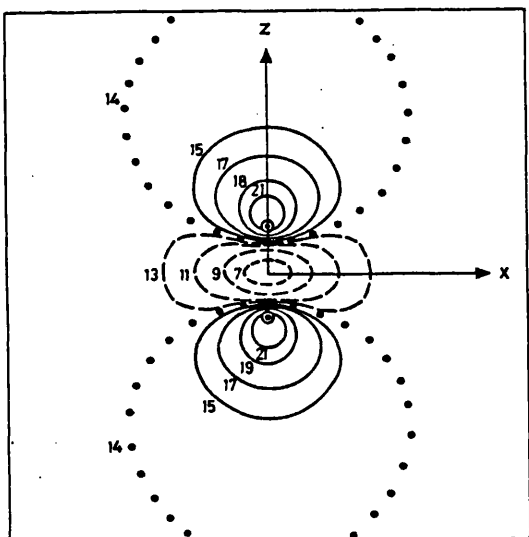
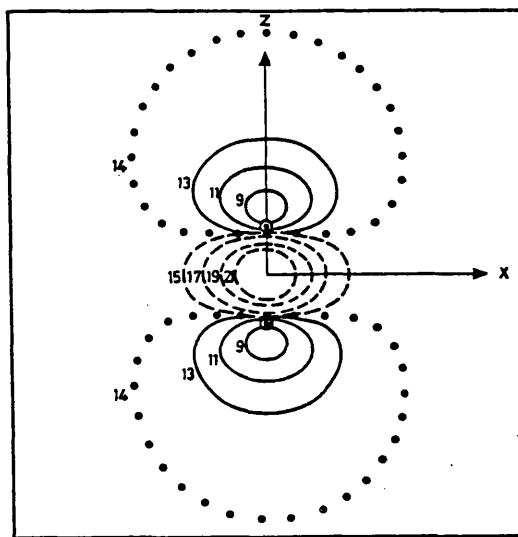


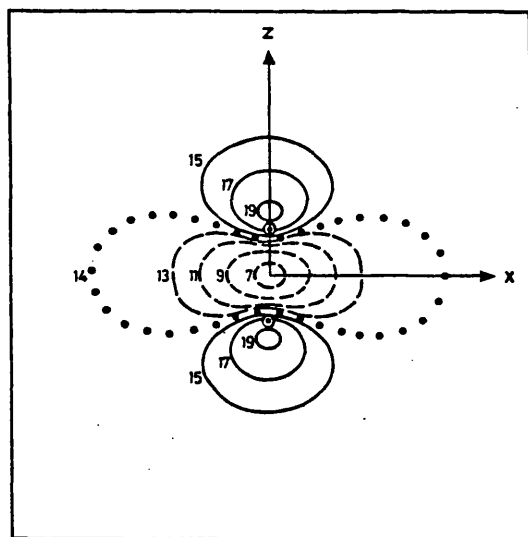
Figure (II.5.1) The H_2 position-space HF one-particle density, $\rho(\underline{r}_1)$, in the xz-plane with $y = 0$.



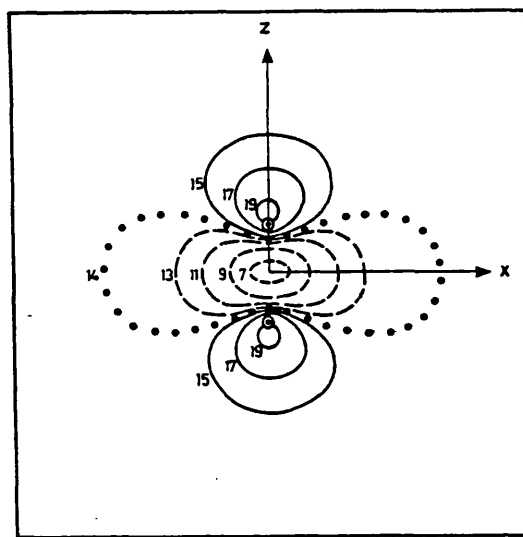
(A) 2NO - 1NO
z - correlation



(B) 3NO - 1NO
(z + φ) - correlation



(C) 4NO - 1NO
(z + φ + ρ) - correlation



(D) 10NO - 1NO
(z + φ + ρ + 2nd order)
- correlation

Figure (II.5.2) The position-space Δ -one-particle densities, $\Delta\rho(\underline{r}_1)$, in the xz -plane with $y = 0$.

(II.5.2) The Two-Particle Density Results

When examining two-particle density functions, both the plane to be studied and the fixed electron position must be chosen. The fixed electron is located with respect to the nuclear frame, hence the first logical choice of fixed electron position is mid way between the two nuclei (position [I]). The second choice, position [II], is then on a nucleus and, to examine the effect of electron correlation when an electron is behind the nucleus, position [III] is chosen to be a half bondlength (0.7 a.u.) past the nucleus. These three fixed electron positions still maintain the axial symmetry of the system and therefore the logical choice of plane of investigation is the plane containing both nuclei, chosen to be the xz-plane. These results are presented in Figures (II.5.4-11). A perpendicular plane of investigation to this would simply result in Δ -partial planar density surfaces constructed from concentric contours which could easily be generated from the xz-plane. The xy-plane results for positions [I], [II] and [III] therefore have been omitted from this analysis.

Obviously ϕ -correlation can have no effect for the above, axially symmetric, cases and consequently certain off-axis fixed electron positions should be studied. Position [IV] is defined as being a half bondlength, in a perpendicular direction to the bond, away from the mid bond position. In exactly the same manner, position [V] is chosen to be at a half bondlength off-axis from position [II], the nucleus, and position [VI] is the same distance from

position [III]. Figures (II.5.12-19) represent the results obtained by examining the xz-plane. Since the axial symmetry is lost in these cases, the xy-plane must also be considered in order to build up a complete view of the effect of correlation; these results are displayed in Figures (II.5.20-27). The fixed electron positions have been summarised in Figure (II.5.3A) and it should be noted that this choice of positions and planes, because of reflection and rotational symmetry, represents a view of the most important regions of the charge distribution in the H₂ molecule.

When examining fixed electron positions in the plane containing the nuclei (xz-plane), ϵ is defined as the angle between a line parallel to the z-axis and the vector \underline{r}_{12} in an anticlockwise direction (see Figure (II.5.3B)). This has the advantage that $U(\epsilon)$ for the first three positions needs only to be generated for half of the range as it is symmetrical about $\epsilon = 180^\circ$. Similarly, due to the mirror symmetry in the xz-plane, by defining ϵ with respect to the x-axis, only ϵ up to 180° needs to be considered when generating $U(\epsilon)$ in the xy-plane (see Figure (II.5.3C)).

The following results therefore represent a survey of the partial planar density functions:

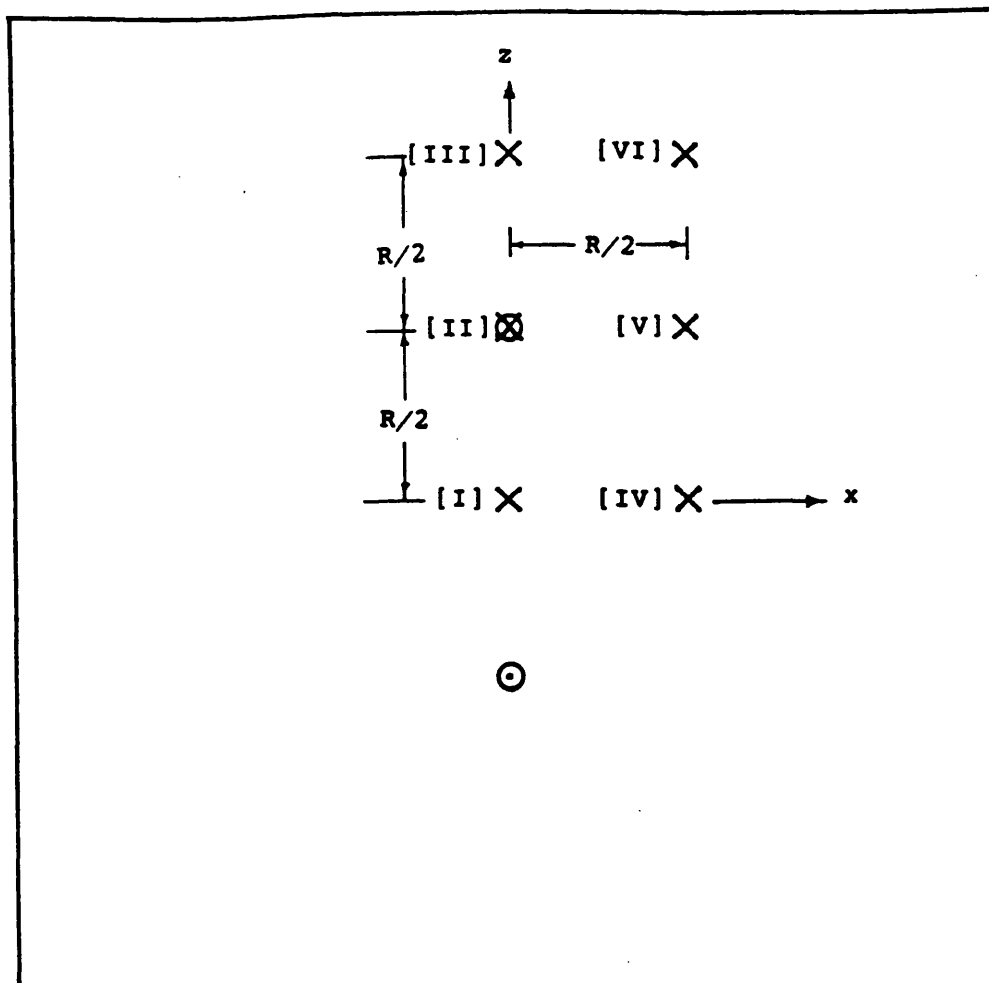


Figure (II.5.3A) The locations of the chosen fixed electron positions of the partial planar distribution functions for hydrogen in position-space. The equilibrium bond length, R , is 1.4 a.u..

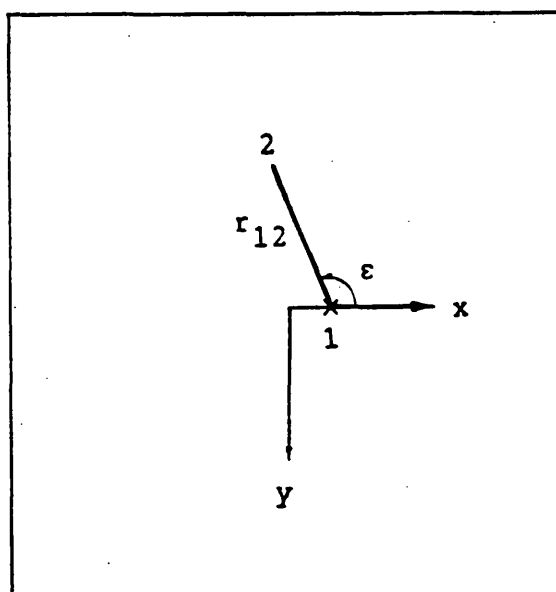
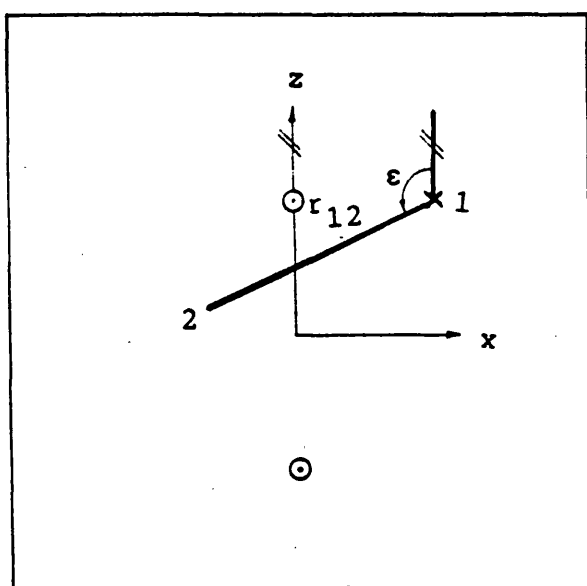
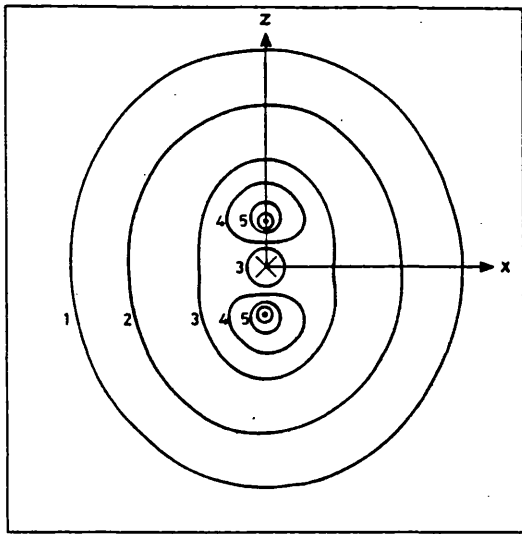
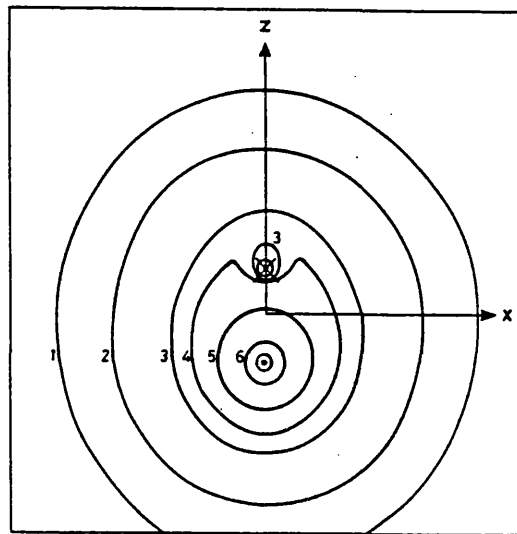


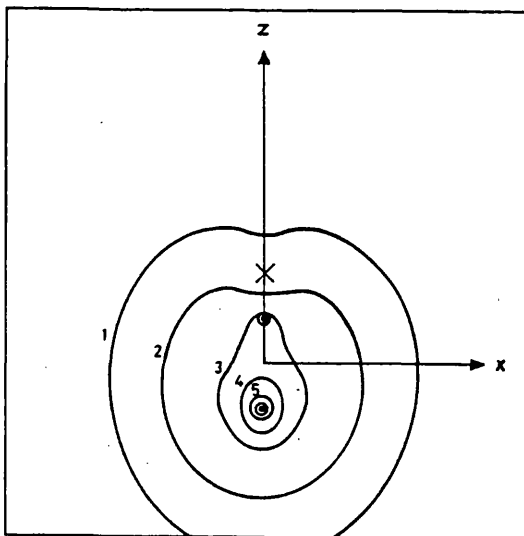
Figure (II.5.3B) & Figure (II.5.3C) The definition of the angle ϵ and the distance r_{12} when analysing correlation effects in (a) the xz -plane or (b) the xy -plane.



(A) Position [I]



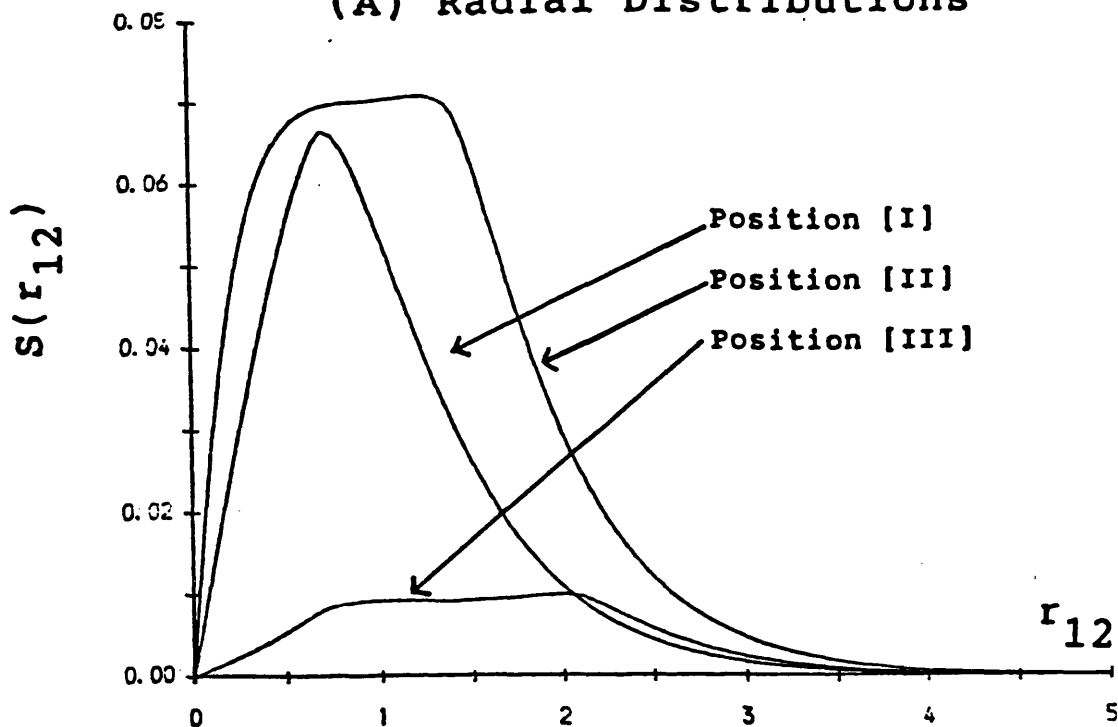
(B) Position [II]



(C) Position [III]

Figure (II.5.4) The Hartree Fock $V(\underline{r}_2, \underline{r}_1)$ distribution functions for positions [I], [II] and [III] in the xz -plane with $y = 0$.

(A) Radial Distributions



(B) Angular Distributions

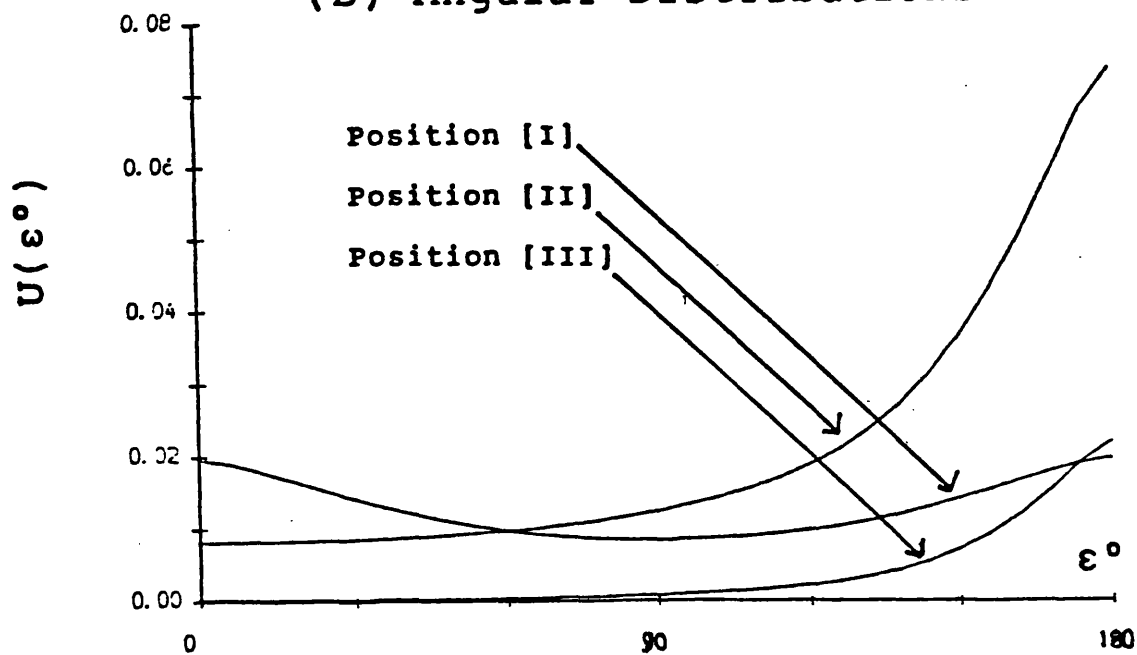
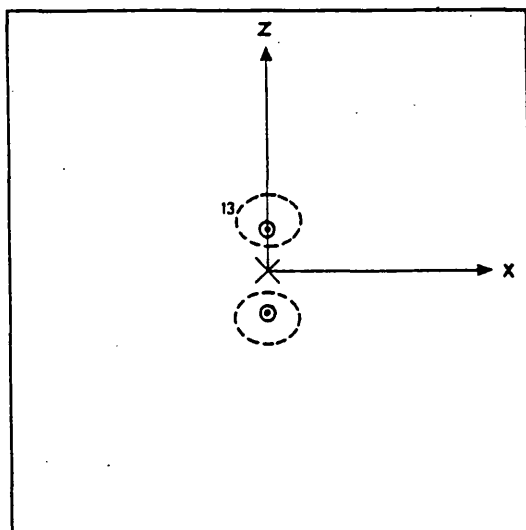
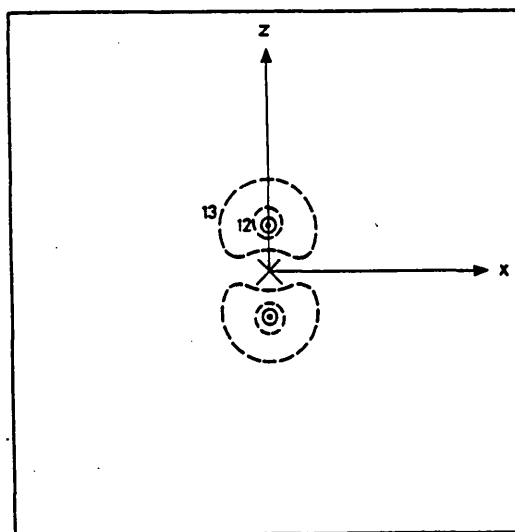


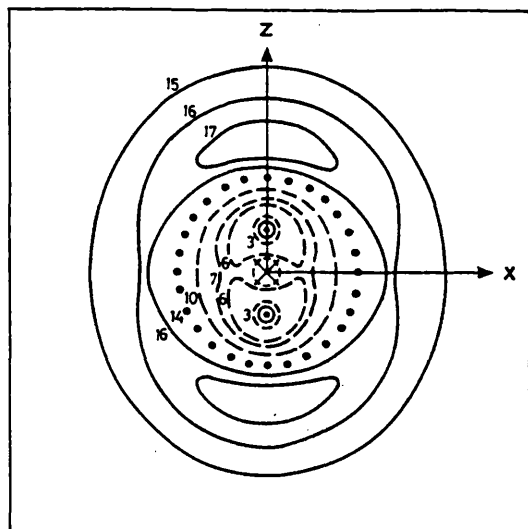
Figure (II.5.5) HF partial planar distribution functions for H_2 , with electron 1 fixed at positions [I], [II] and [III] (see Fig.(II.5.3)) and electron 2 moving in the xz plane, were obtained by appropriate integration of Fig.(II.5.4).



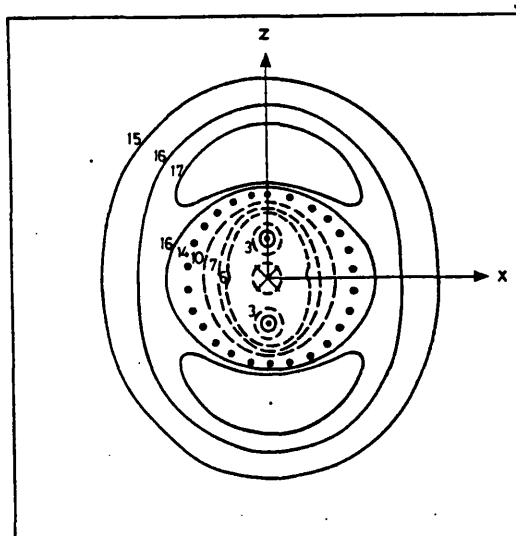
(A) 2NO - 1NO
z - correlation



(B) 3NO - 1NO
(z + ϕ) - correlation



(C) 4NO - 1NO
(z + ϕ + ρ) - correlation



(D) 10NO - 1NO
(z + ϕ + ρ + 2nd order)
- correlation

Figure (II.5.6) The partial planar Δ -surfaces, $\Delta V(\underline{r}_{12}, \underline{r}_1)$, for fixed electron position [I] (see Figure (II.5.3A) for the definition), with the roving electron located in the xz-plane with $y = 0$.

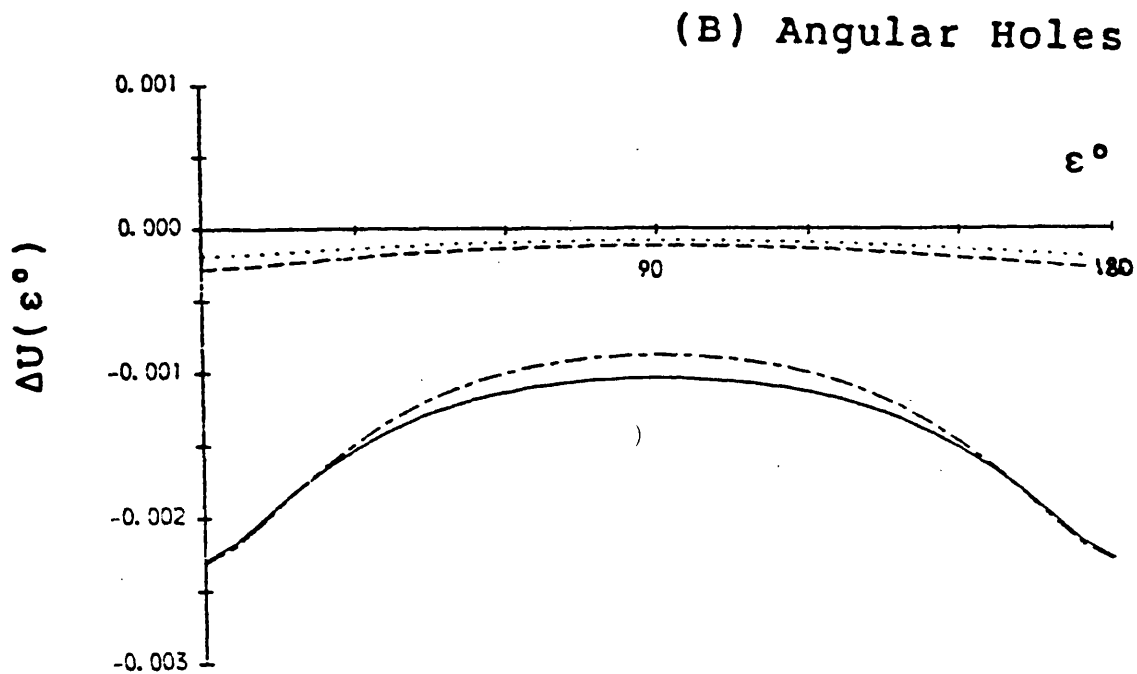
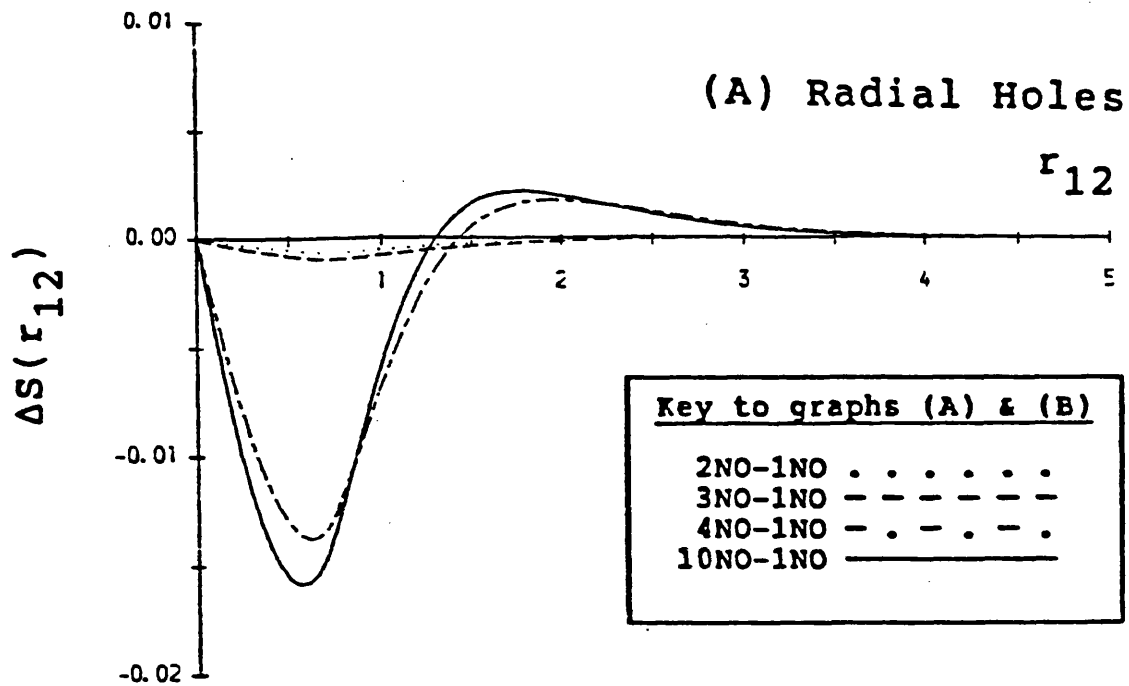
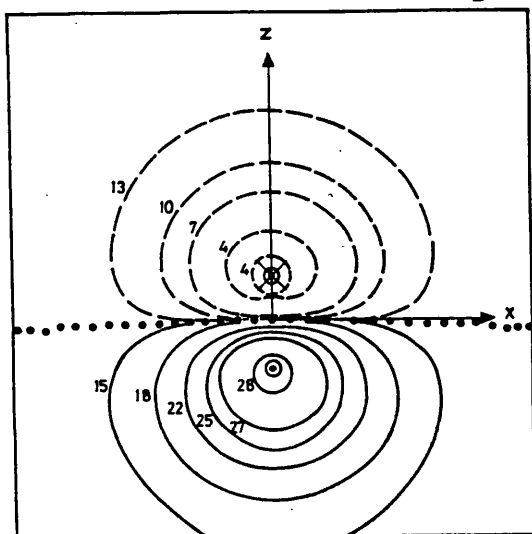
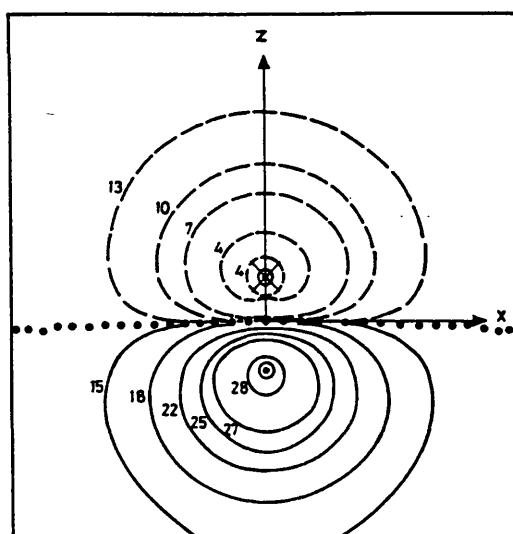


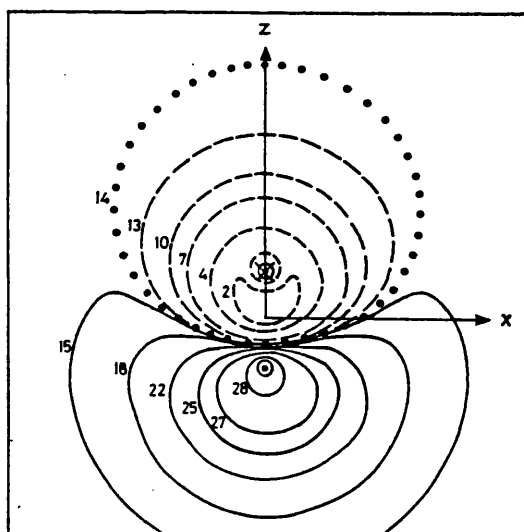
Figure (II.5.7) Partial planar Coulomb holes for H_2 , with electron 1 fixed at position [I] (see Fig.(II.5.3)) and electron 2 moving in the xz plane, were obtained by appropriate integration of Fig.(II.5.6).



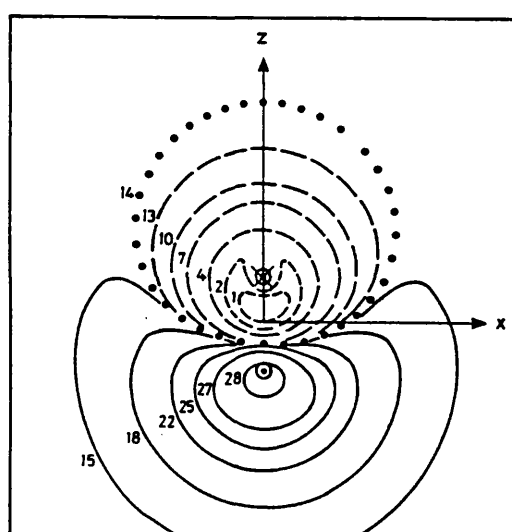
(A) 2NO - 1NO
z - correlation



(B) 3NO - 1NO
(z + ϕ) - correlation

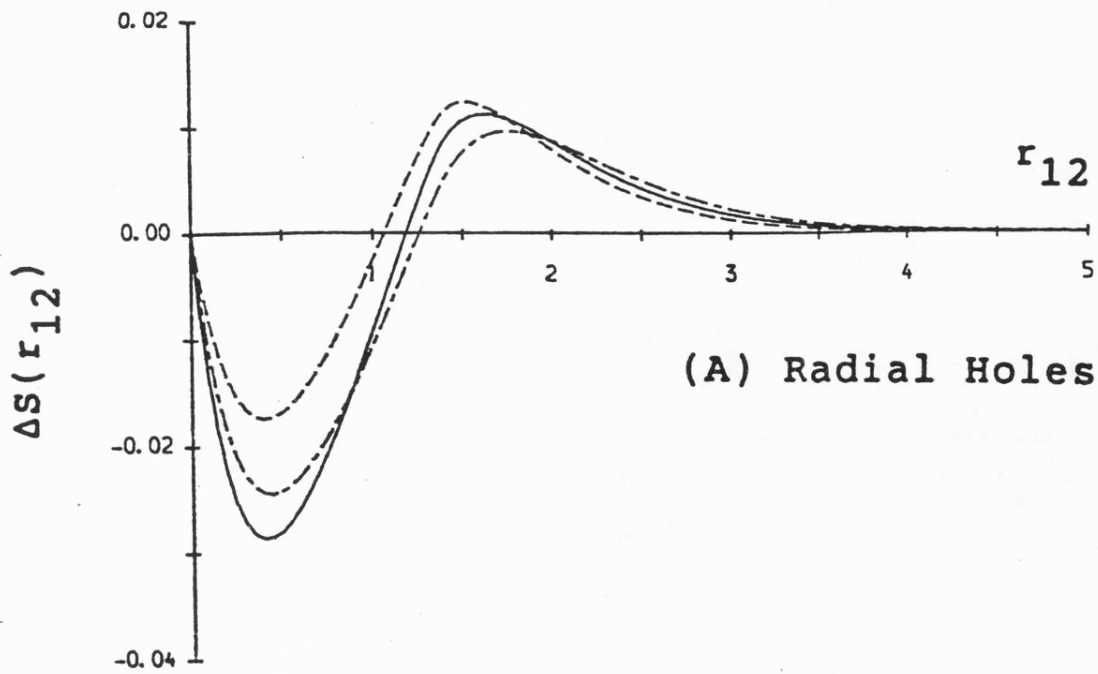


(C) 4NO - 1NO
(z + ϕ + ρ) - correlation



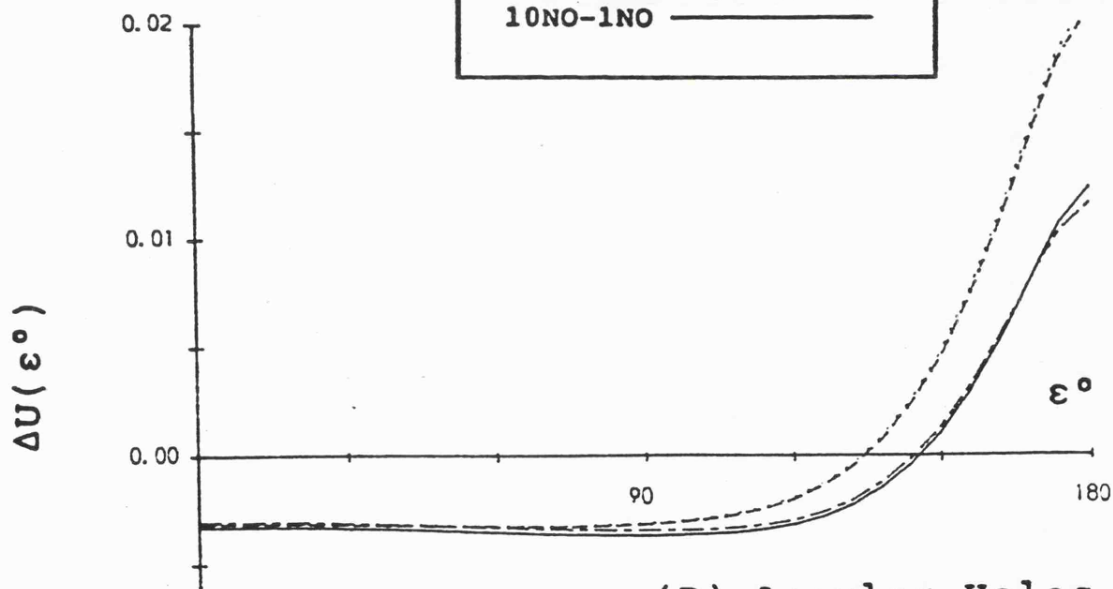
(D) 10NO - 1NO
(z + ϕ + ρ + 2nd order)
- correlation

Figure (II.5.8) The partial planar Δ -surfaces, $\Delta V(\underline{r}_{12}, \underline{r}_1)$, for fixed electron position [II] (see Figure (II.5.3A) for the definition), with the roving electron located in the xz -plane with $y = 0$.



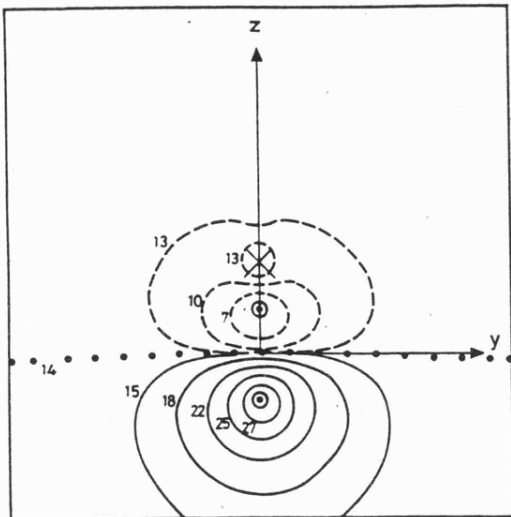
(A) Radial Holes

Key to graphs (A) & (B)	
2NO-1NO
3NO-1NO	-----
4NO-1NO	- . - . - .
10NO-1NO	—————

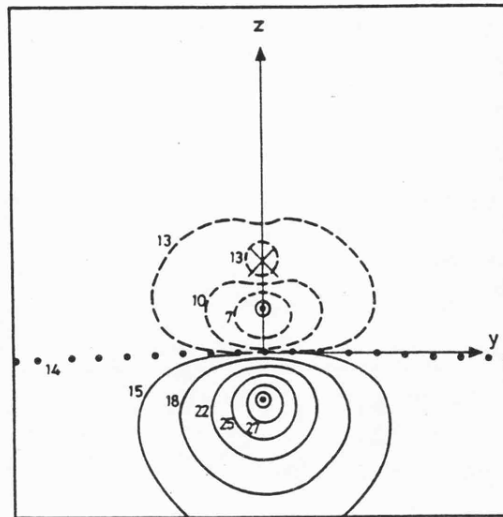


(B) Angular Holes

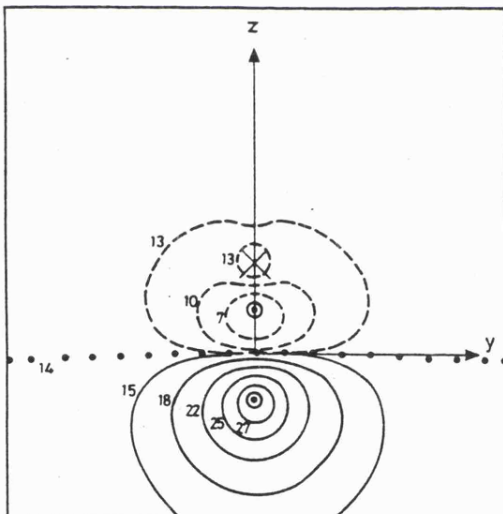
Figure (II.5.9) Partial planar Coulomb holes for H_2 , with electron 1 fixed at position [II] (see Fig.(II.5.3)) and electron 2 moving in the xz plane, were obtained by appropriate integration of Fig.(II.5.8).



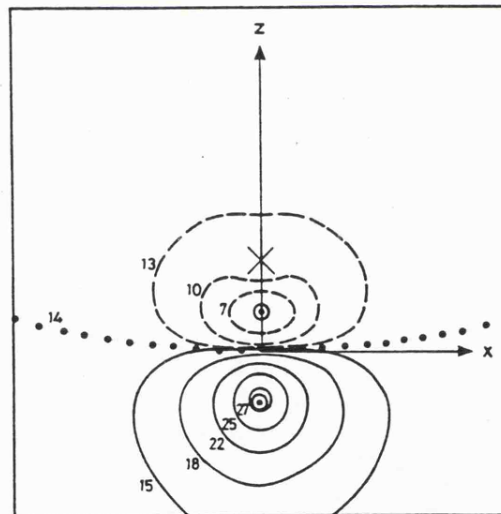
(A) 2NO - 1NO
z - correlation



(B) 3NO - 1NO
(z + ϕ) - correlation

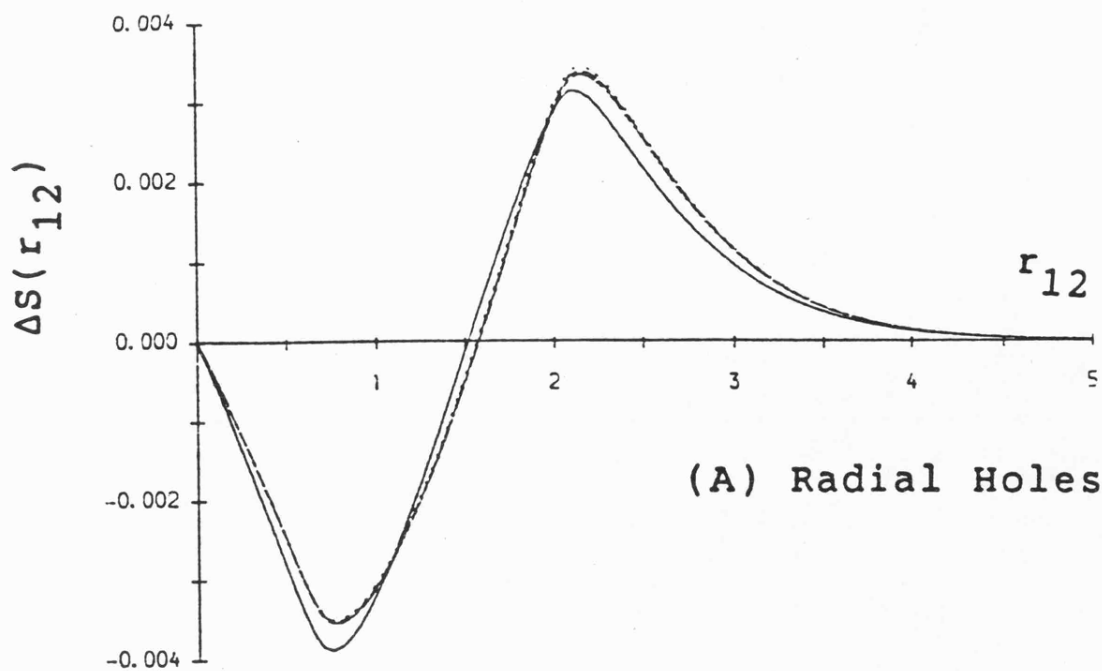


(C) 4NO - 1NO
(z + ϕ + ρ) - correlation



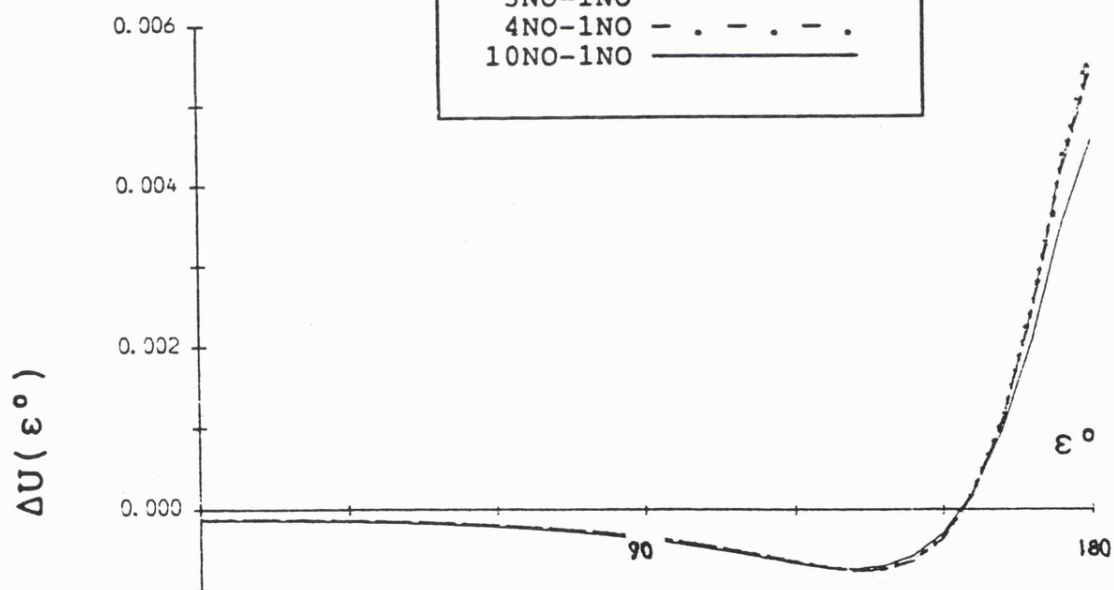
(D) 10NO - 1NO
(z + ϕ + ρ + 2nd order)
- correlation

Figure (II.5.10) The partial planar Δ -surfaces, $\Delta V(\underline{r}_{12}, \underline{r}_1)$, for fixed electron position [III] (see Figure (II.5.3A) for the definition), with the roving electron located in the xz-plane with $y = 0$.



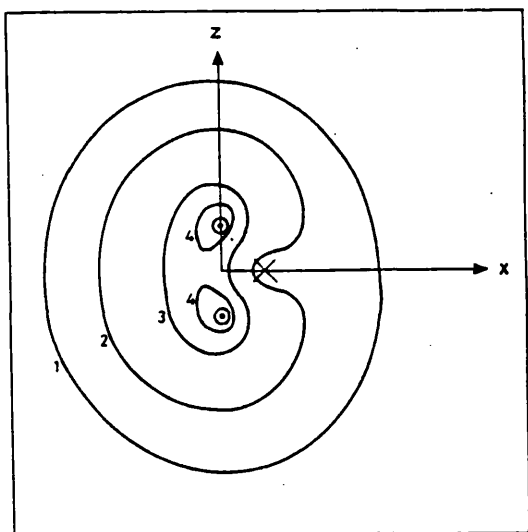
(A) Radial Holes

Key to graphs (A) & (B)	
2NO-1NO
3NO-1NO	-----
4NO-1NO	- . - . - .
10NO-1NO	—————

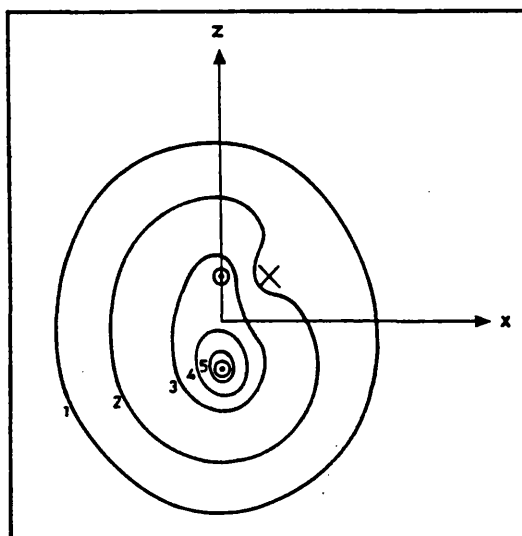


(B) Angular Holes

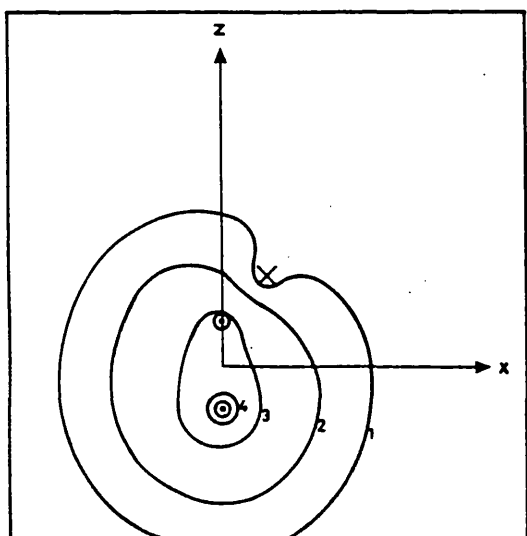
Figure (II.5.11) Partial planar Coulomb holes for H_2 , with electron 1 fixed at position [III] (see Fig.(II.5.3)) and electron 2 moving in the xz plane, were obtained by appropriate integration of Fig.(II.5.10)



(A) Position [IV]



(B) Position [V]



(C) Position [VI]

Figure (II.5.12) The Hartree Fock $V(\underline{r}_{12}, \underline{r}_1)$ distribution functions for positions [IV], [V] and [VI] in the xz -plane with $y = 0$.

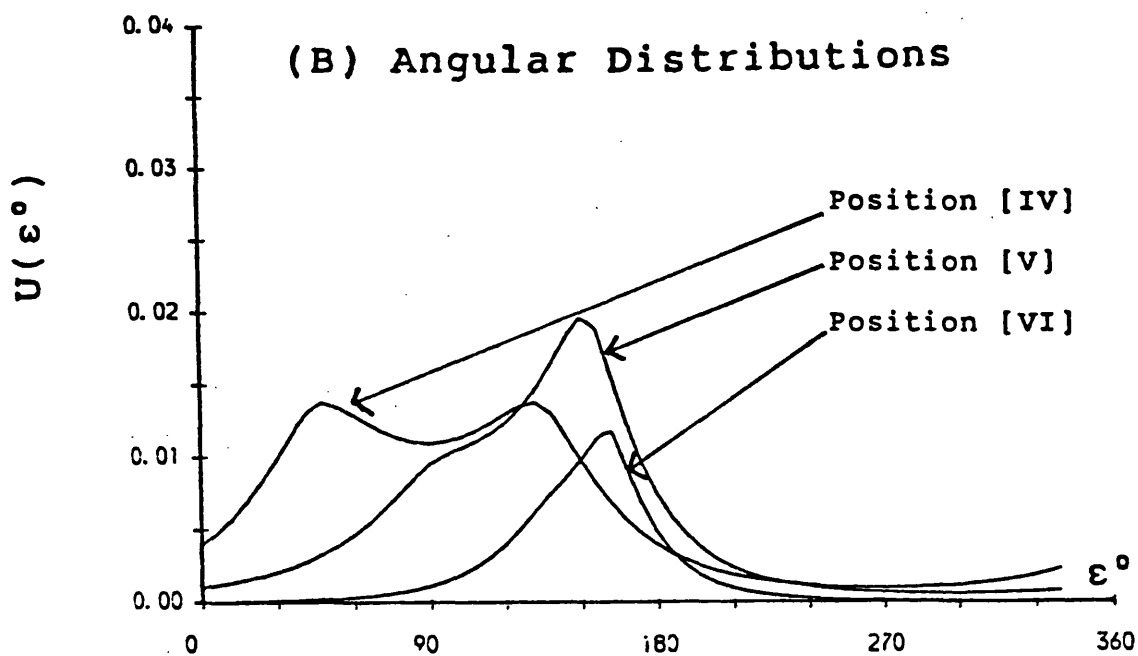
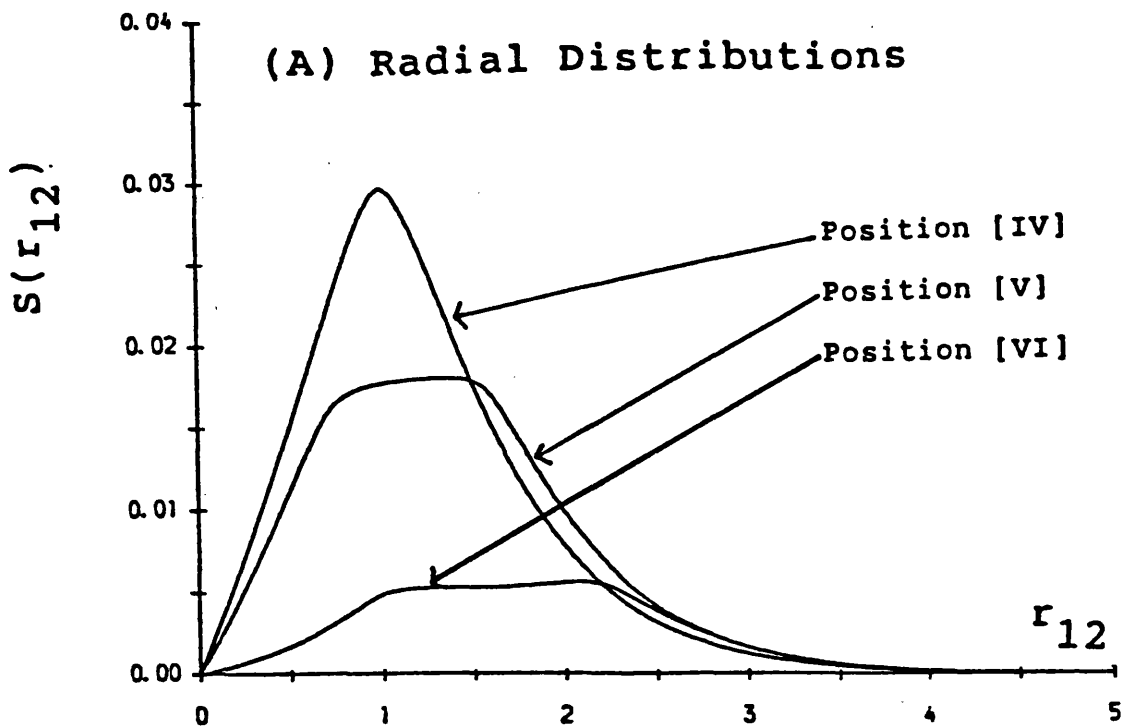
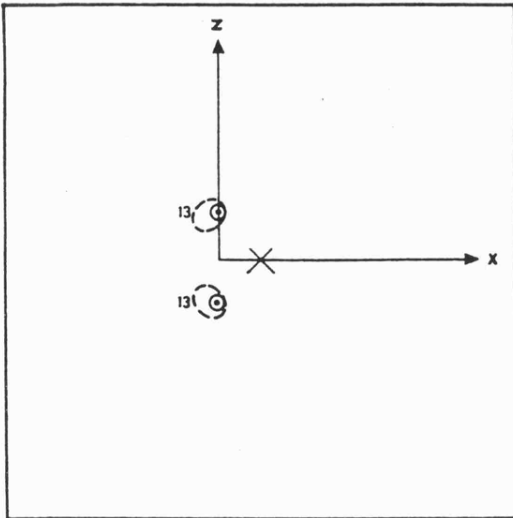
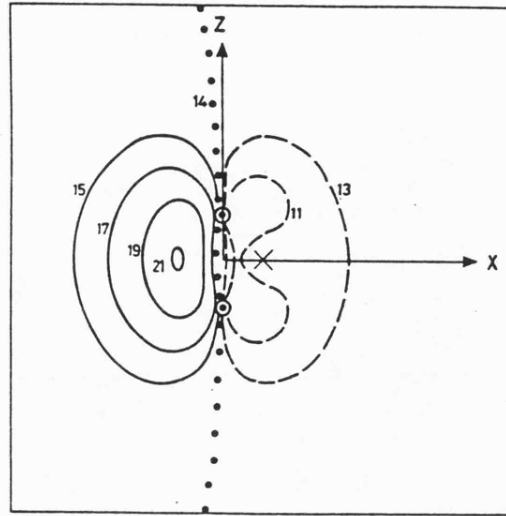


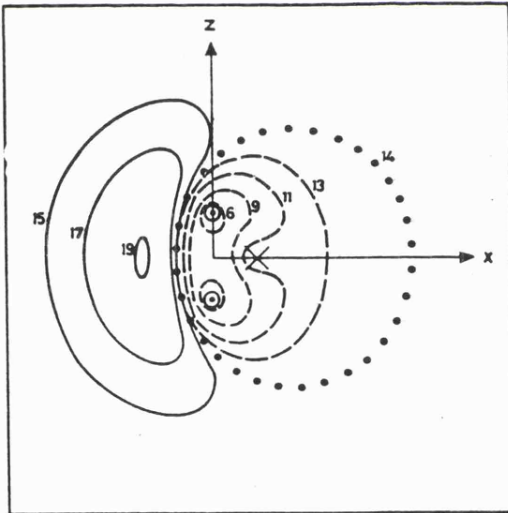
Figure (II.5.13) HF partial planar distribution functions for H_2^+ with electron 1 fixed at positions [IV], [V] and [VI] (see Fig.(II.5.3)) and electron 2 moving in the xz plane, were obtained by appropriate integration of Fig.(II.5.12).



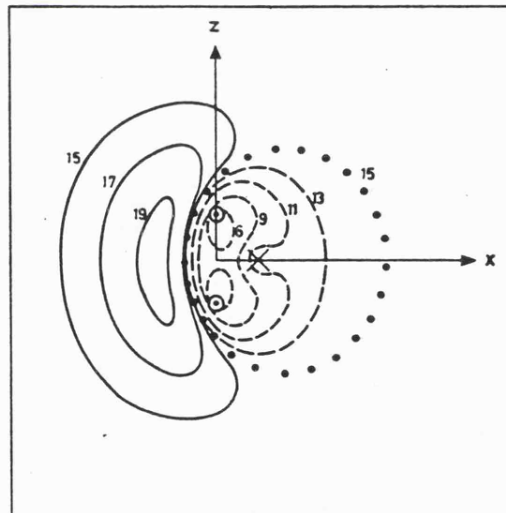
(A) 2NO - 1NO
z - correlation



(B) 3NO - 1NO
(z + ϕ) - correlation

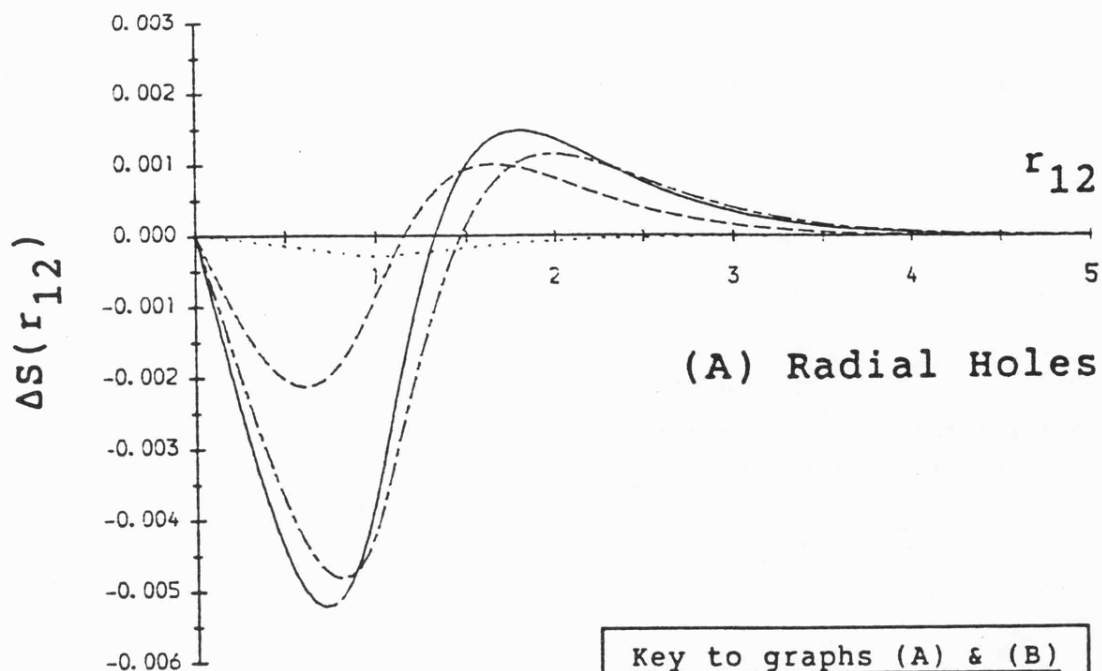


(C) 4NO - 1NO
(z + ϕ + ρ) - correlation



(D) 10NO - 1NO
(z + ϕ + ρ + 2nd order)
- correlation

Figure (II.5.14) The partial planar Δ -surfaces, $\Delta V(\underline{r}_{12}, \underline{r}_1)$, for fixed electron position [IV] (see Figure (II.5.3A) for the definition), with the roving electron located in the xz -plane with $y = 0$.



Key to graphs (A) & (B)	
2NO-1NO
3NO-1NO	-----
4NO-1NO	- . - . - .
10NO-1NO	—————

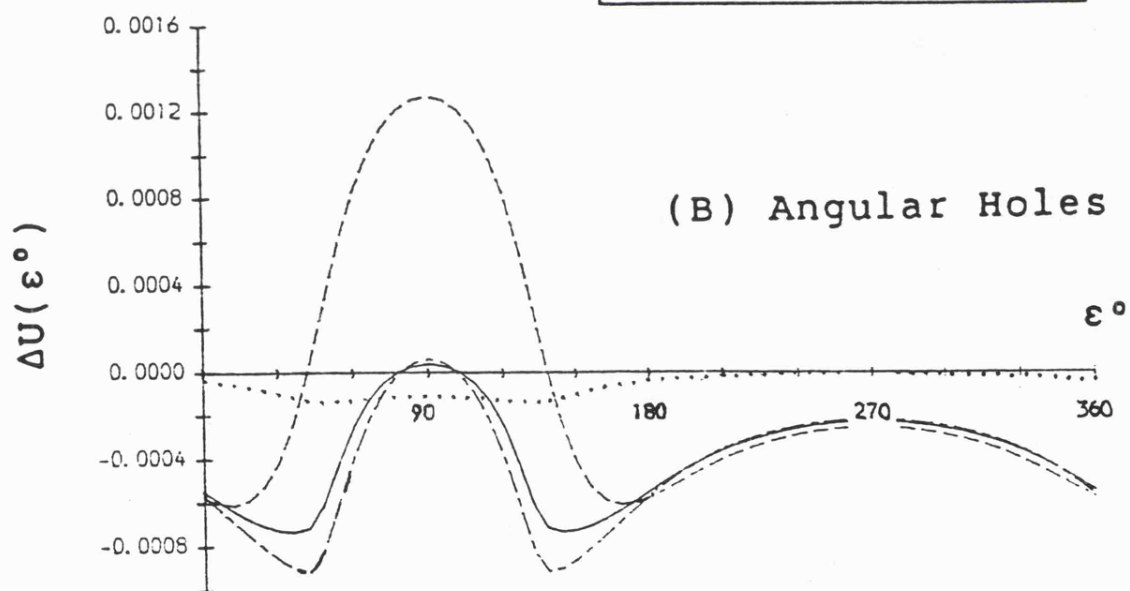
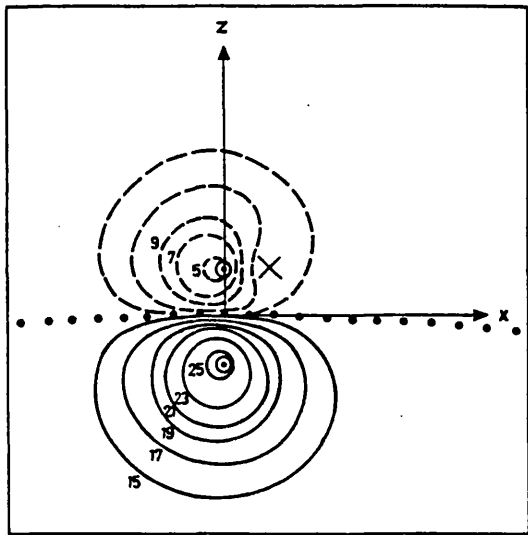
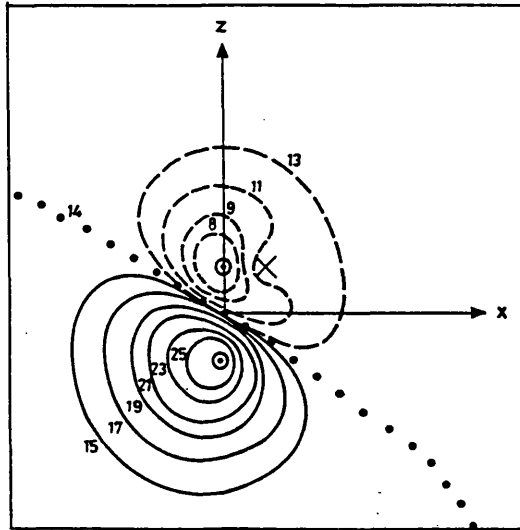


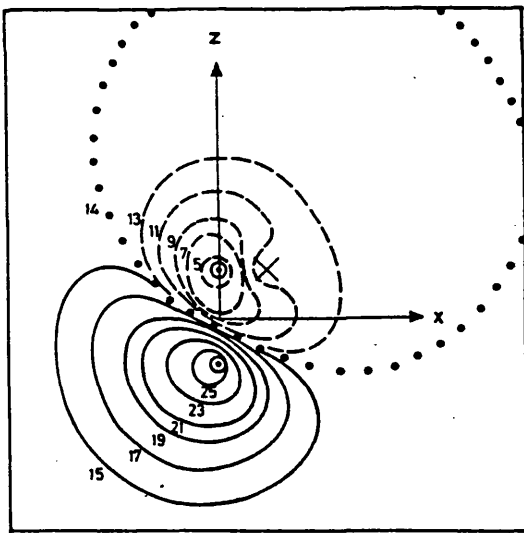
Figure (II.5.15) Partial planar Coulomb holes for H_2 , with electron 1 fixed at position [IV] (see Fig.(II.5.3))² and electron 2 moving in the xz plane, were obtained by appropriate integration of Fig.(II. 5.14).



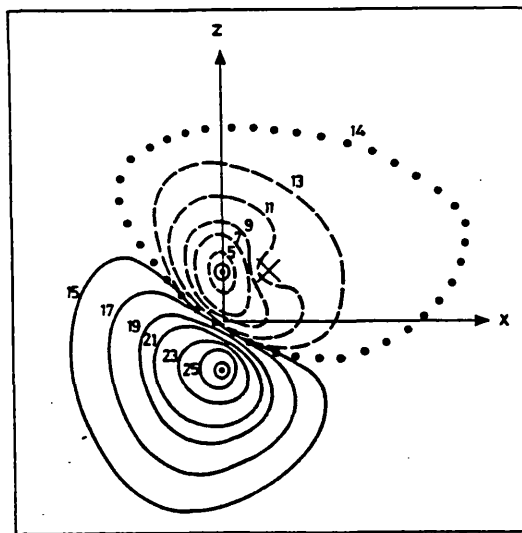
(A) 2NO - 1NO
z - correlation



(B) 3NO - 1NO
(z + ϕ) - correlation

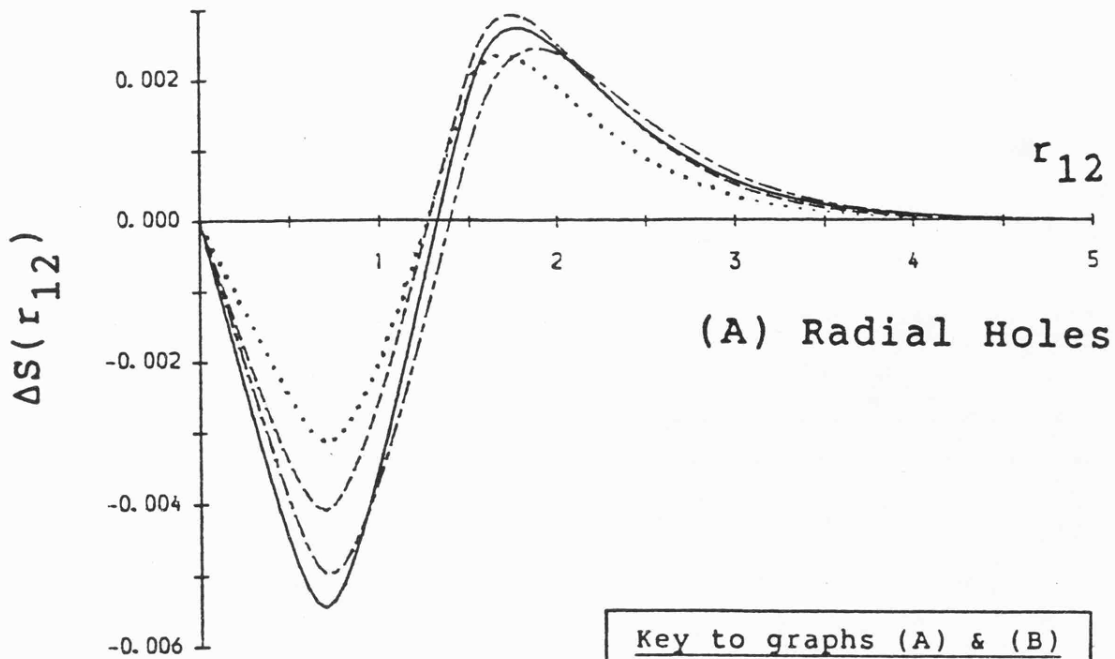


(C) 4NO - 1NO
(z + ϕ + ρ) - correlation



(D) 10NO - 1NO
(z + ϕ + ρ + 2nd order)
- correlation

Figure (II.5.16) The partial planar Δ -surfaces, $\Delta V(\underline{r}_{12}, \underline{r}_1)$, for fixed electron position [V] (see Figure (II.5.3A) for the definition), with the roving electron located in the xz -plane with $y = 0$.



Key to graphs (A) & (B)	
2NO-1NO
3NO-1NO	-----
4NO-1NO	- . - . - .
10NO-1NO	—————

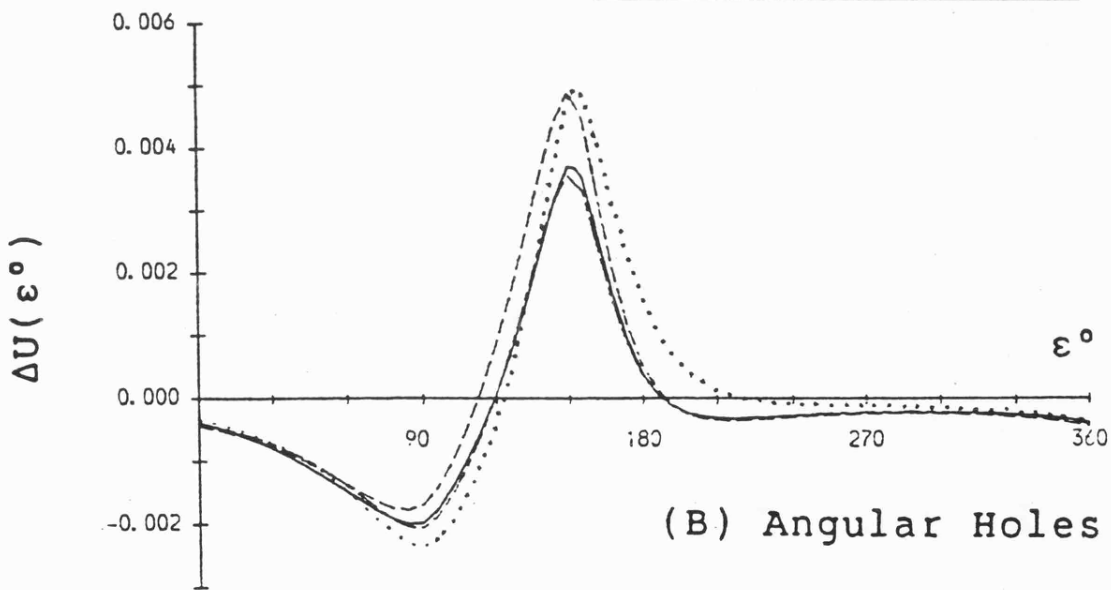
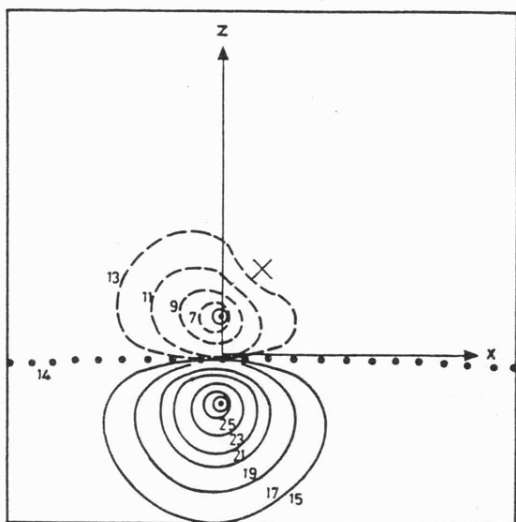
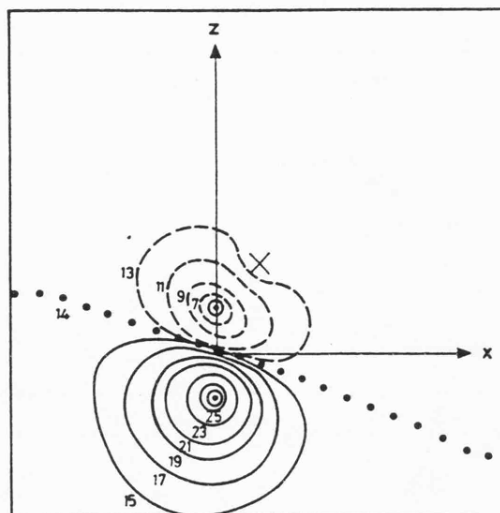


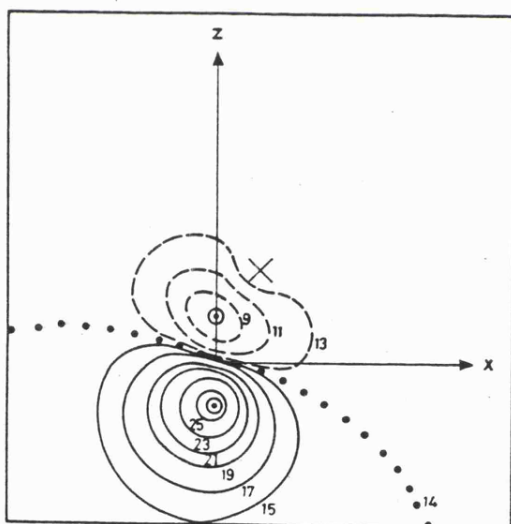
Figure (II.5.17) Partial planar Coulomb holes for H_2 , with electron 1 fixed at position $[V]$ (see Fig.(II.5.3))² and electron 2 moving in the xz plane, were obtained by appropriate integration of Fig.(II.5.16).



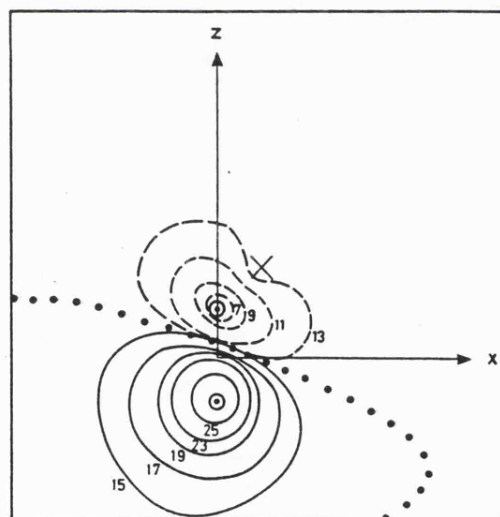
(A) 2NO - 1NO
z - correlation



(B) 3NO - 1NO
(z + ϕ) - correlation

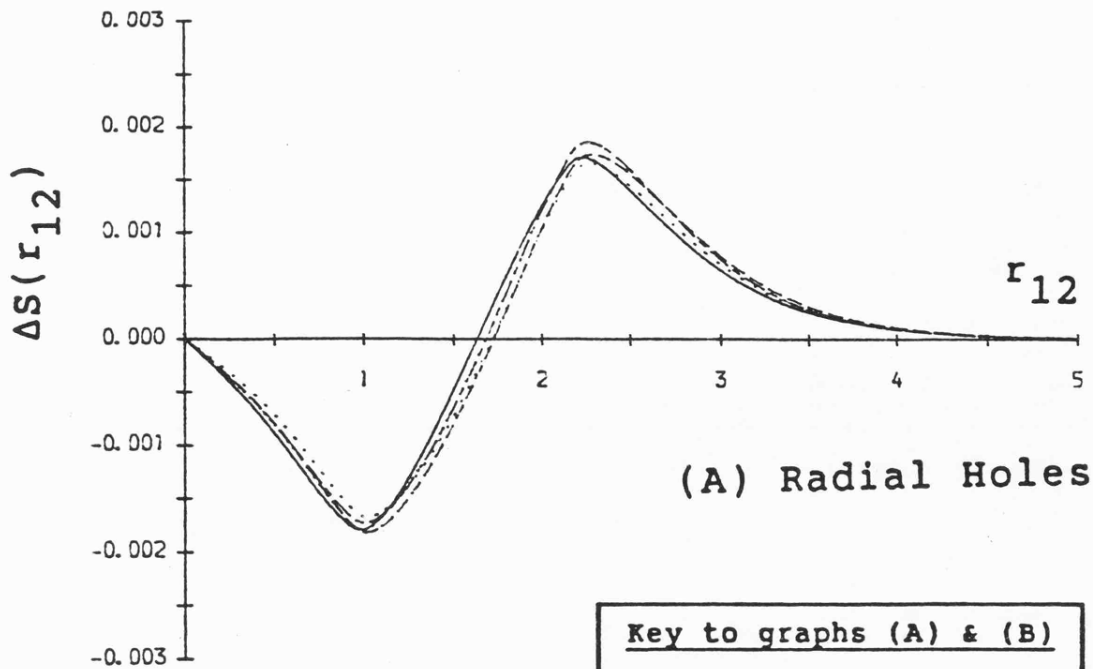


(C) 4NO - 1NO
(z + ϕ + ρ) - correlation



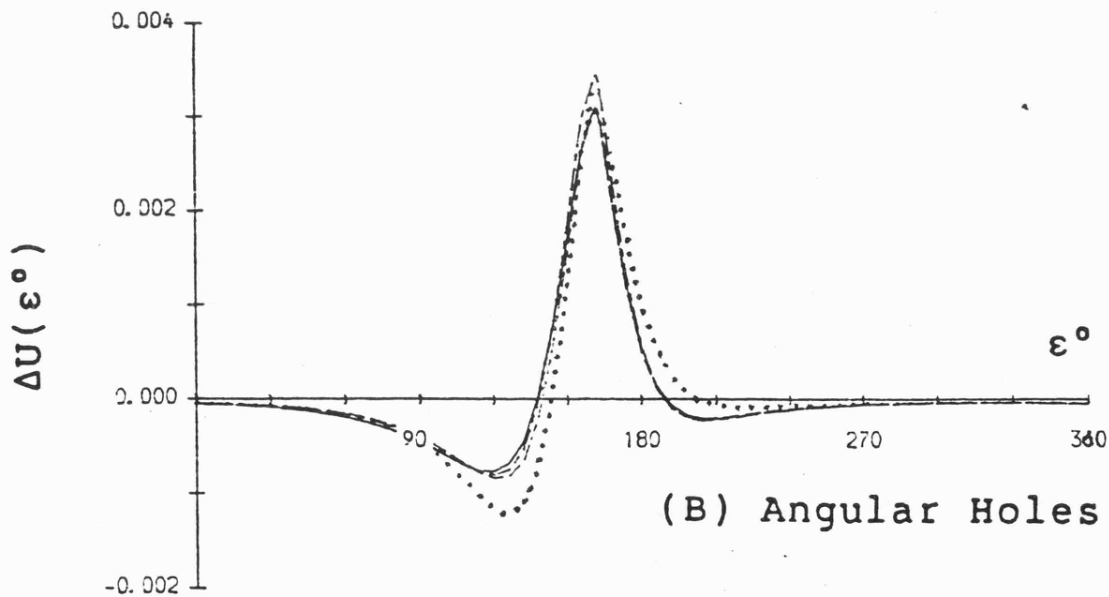
(D) 10NO - 1NO
(z + ϕ + ρ + 2nd order)
- correlation

Figure (II.5.18) The partial planar Δ -surfaces, $\Delta V(\underline{r}_{12}, \underline{r}_1)$, for fixed electron position [VI] (see Figure (II.5.3A) for the definition), with the roving electron located in the xz -plane with $y = 0$.



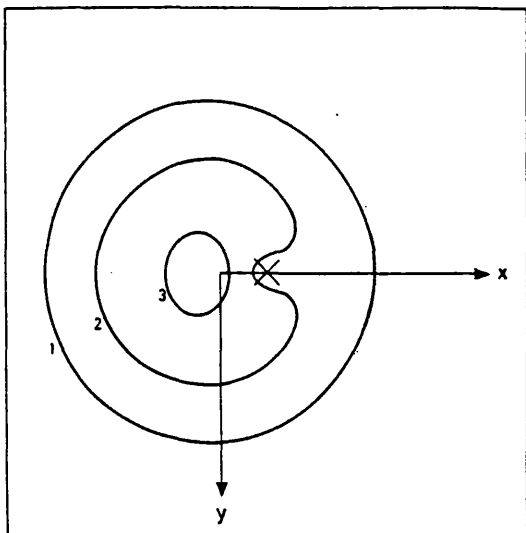
(A) Radial Holes

Key to graphs (A) & (B)	
2NO-1NO
3NO-1NO	-----
4NO-1NO	- . - . - .
10NO-1NO	—————

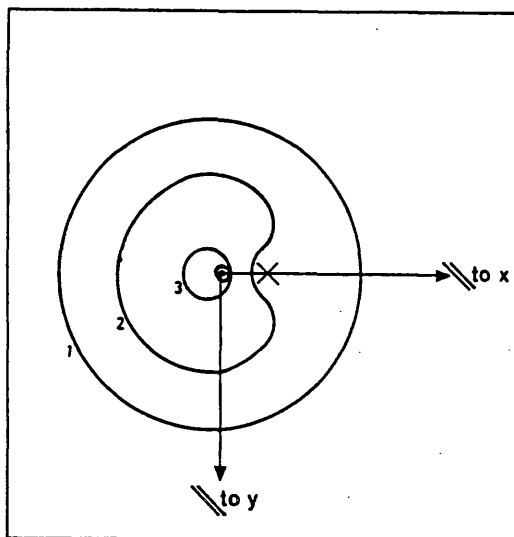


(B) Angular Holes

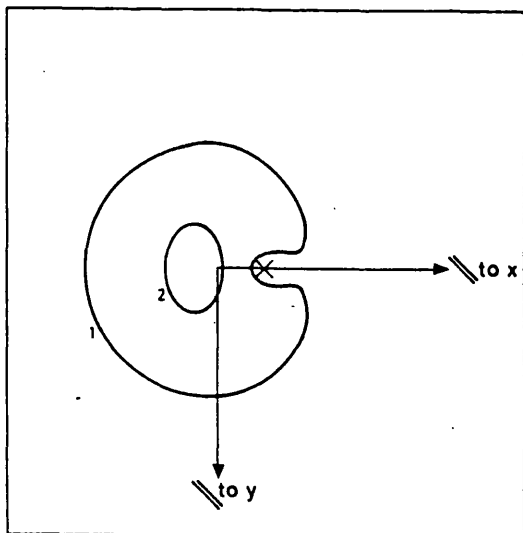
Figure (II.5.19) Partial planar Coulomb holes for H_2 , with electron 1 fixed at position [VI] (see Fig.(II.5.3))² and electron 2 moving in the xz plane, were obtained by appropriate integration of Fig.(II.5.18).



(A) Position [IV]



(B) Position [V]



(C) Position [VI]

Figure (II.5.20) The Hartree Fock $V(\underline{r}_2, \underline{r}_1)$ distribution functions for positions [IV], [V] and [VI] in the xy -plane with $z = 0$.

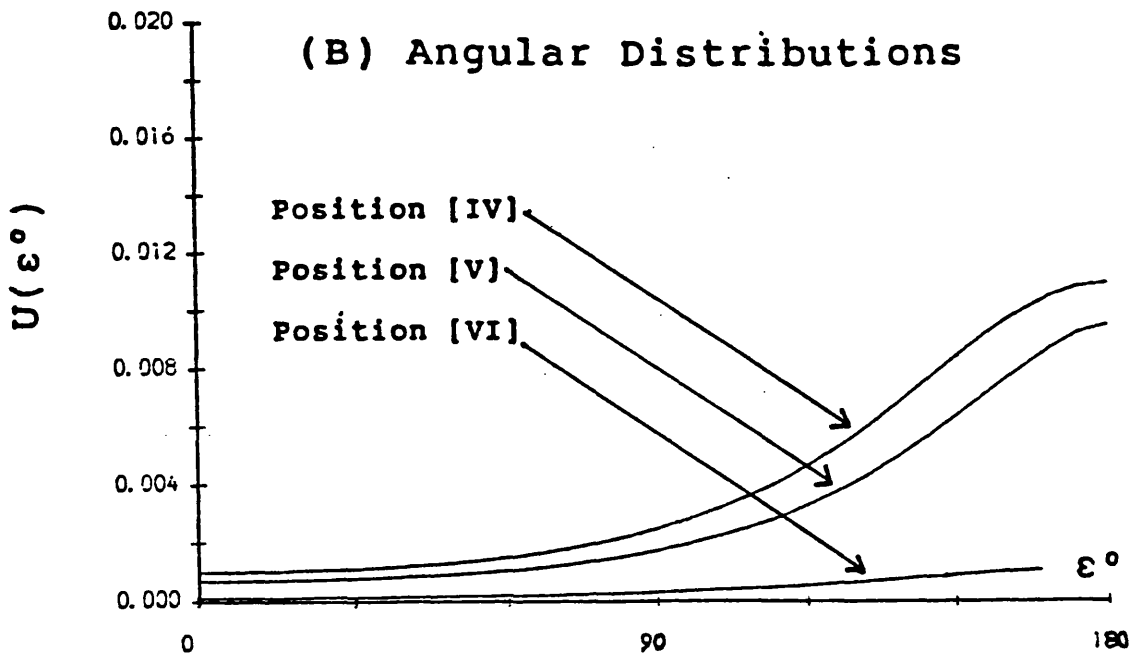
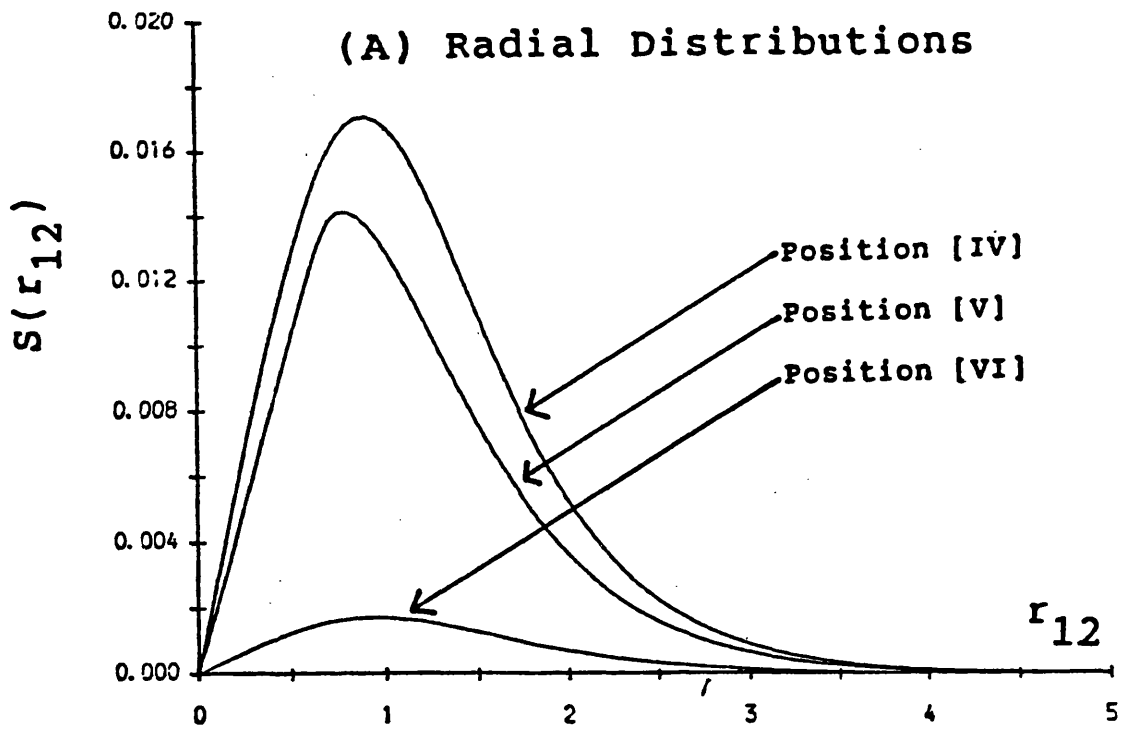
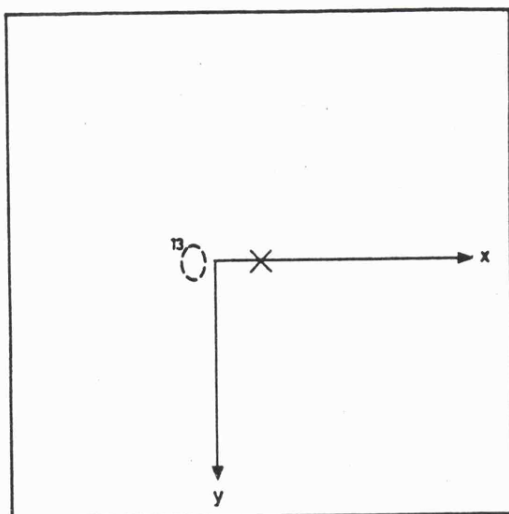
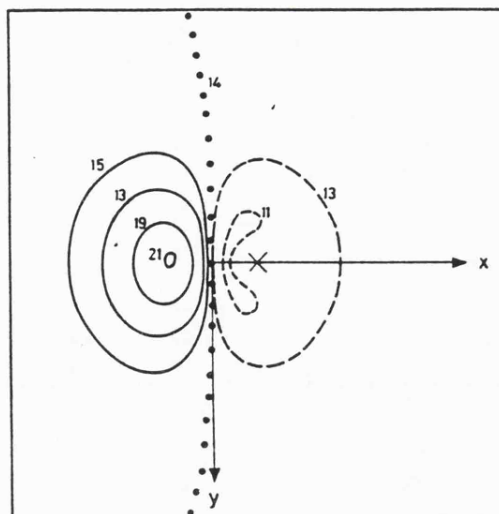


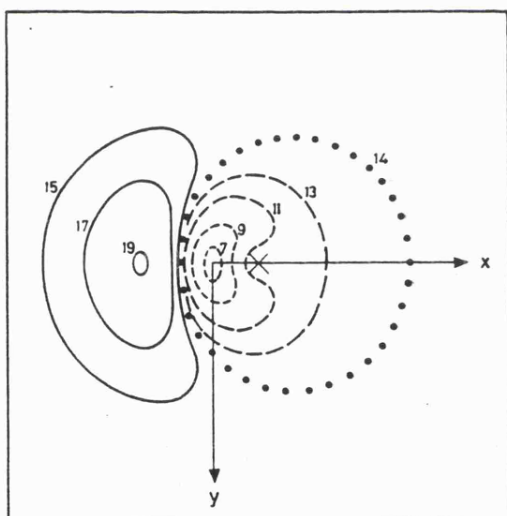
Figure (II.5.21) HF partial planar distribution functions for H_2 , with electron 1 fixed at positions [IV], [V] and [VI] (see Fig.(II.5.3)) and electron 2 moving in the xy plane, were obtained by appropriate integration of Fig.(II.5.20).



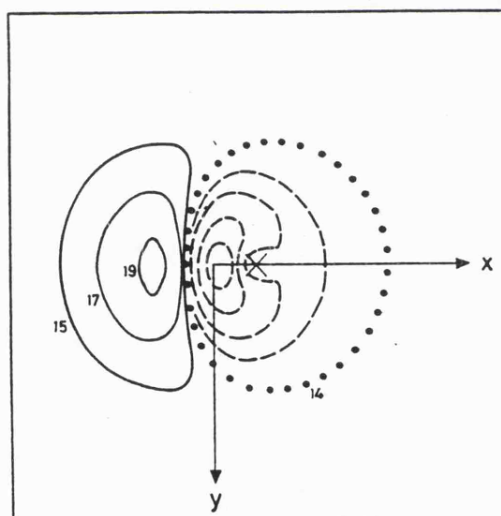
(A) 2NO - 1NO
z - correlation



(B) 3NO - 1NO
(z + ϕ) - correlation



(C) 4NO - 1NO
(z + ϕ + ρ) - correlation



(D) 10NO - 1NO
(z + ϕ + ρ + 2nd order)
- correlation

Figure (II.5.22) The partial planar Δ -surfaces, $\Delta V(\underline{r}_{12}, \underline{r}_1)$, for fixed electron position [IV] (see Figure (II.5.3A) for the definition), with the roving electron located in the xy-plane with $z = 0$.

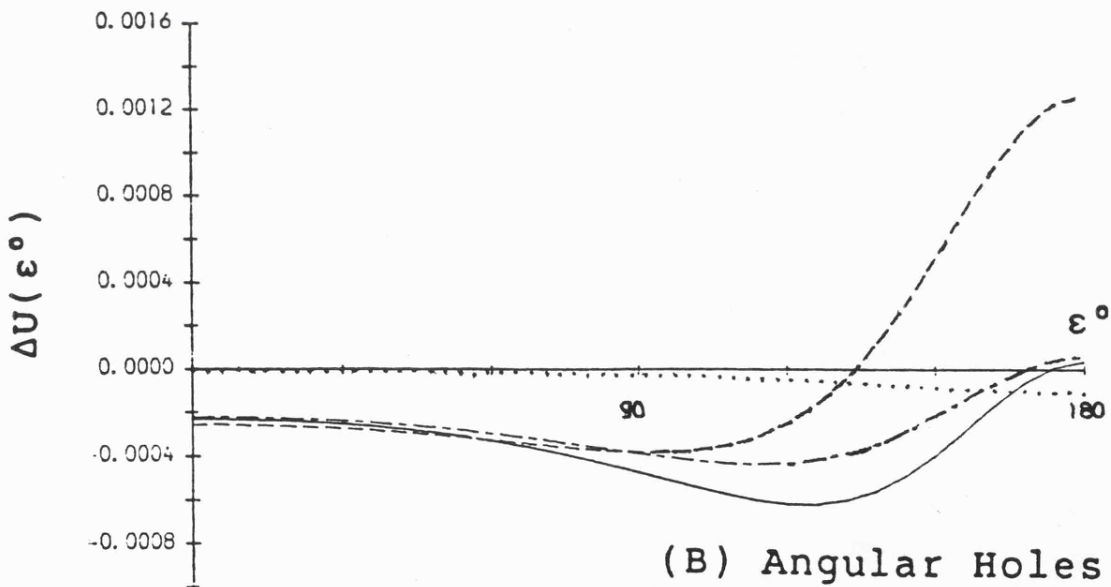
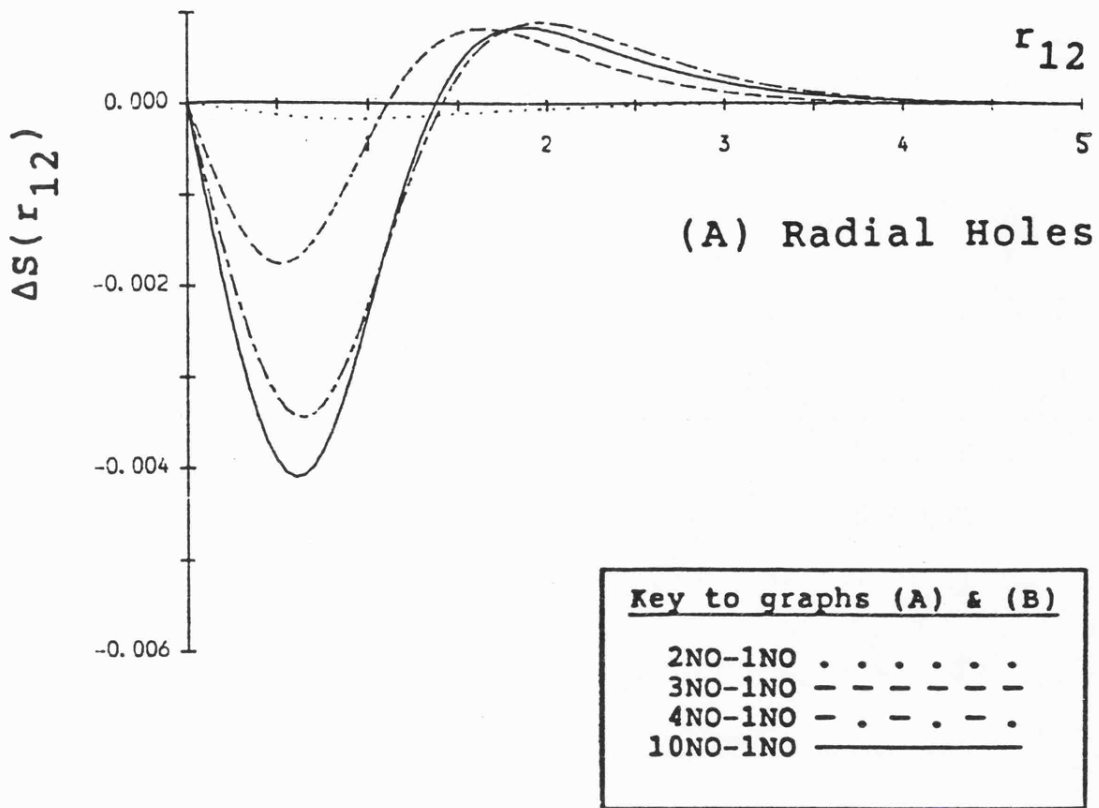
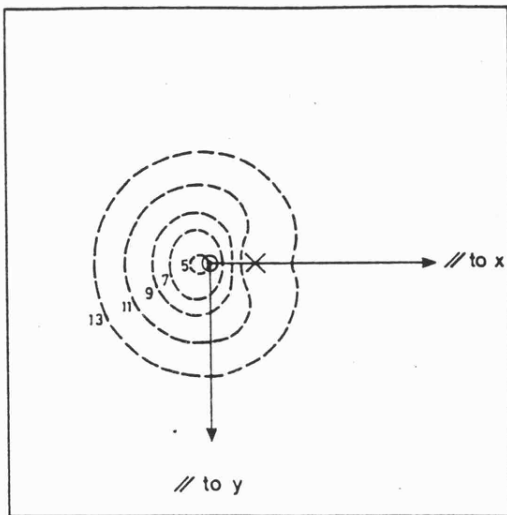
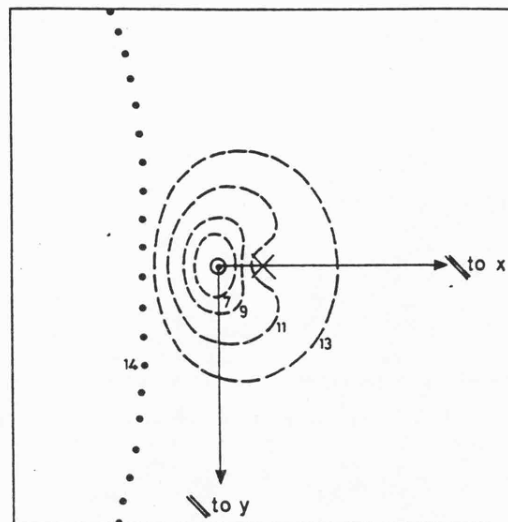


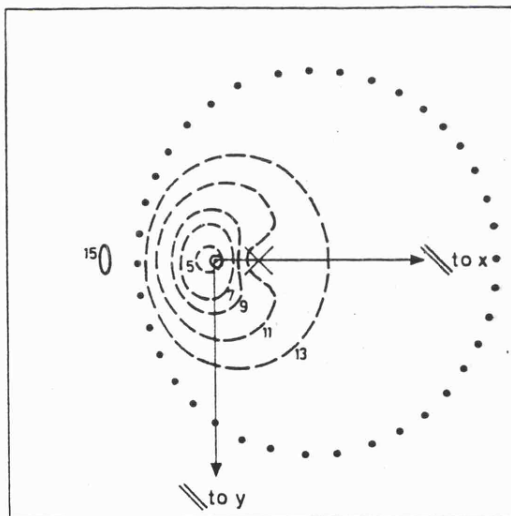
Figure (II.5.23) Partial planar Coulomb holes for H_2 , with electron 1 fixed at position [IV] (see Fig.(II.5.3))² and electron 2 moving in the xy plane, were obtained by appropriate integration of Fig.(II.5.22).



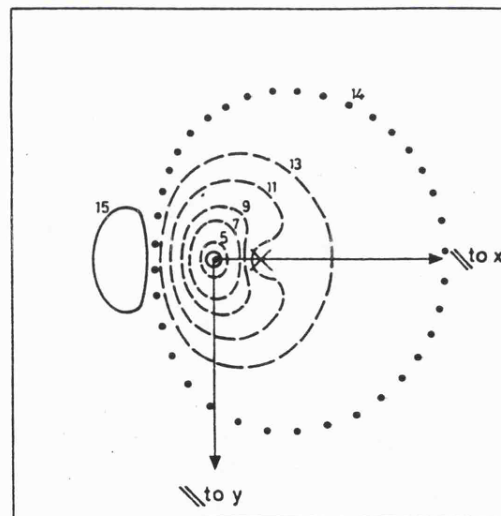
(A) 2NO - 1NO
z - correlation



(B) 3NO - 1NO
(z + φ) - correlation

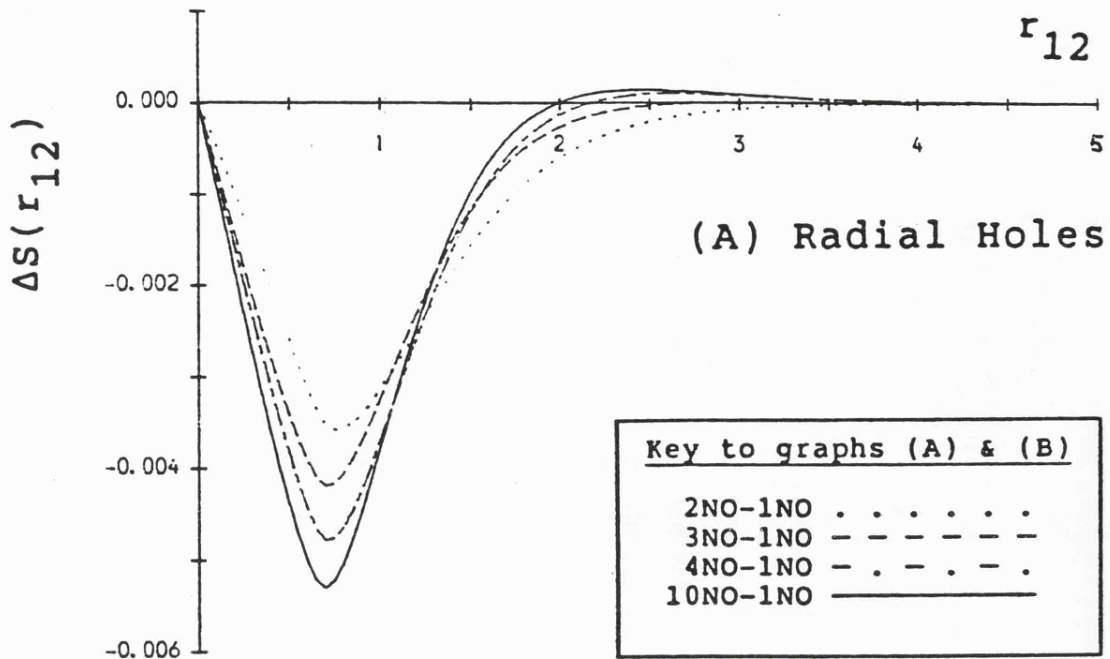


(C) 4NO - 1NO
(z + φ + ρ) - correlation



(D) 10NO - 1NO
(z + φ + ρ + 2nd order)
- correlation

Figure (II.5.24) The partial planar Δ -surfaces, $\Delta V(\underline{r}_{12}, \underline{r}_1)$, for fixed electron position [V] (see Figure (II.5.3A) for the definition), with the roving electron located in the xy -plane with $z = 0$.



(B) Angular Holes

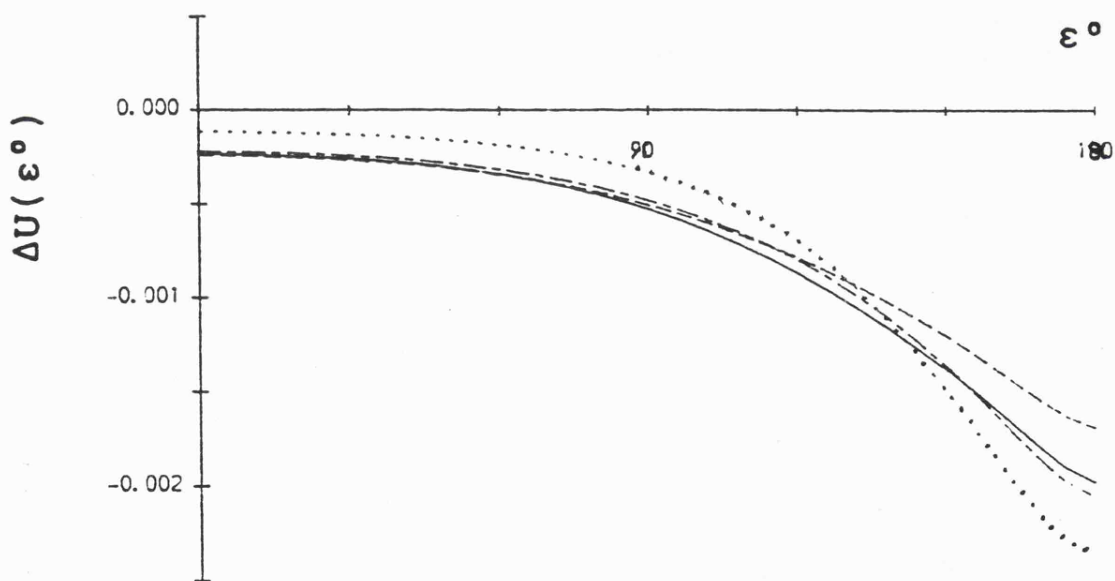
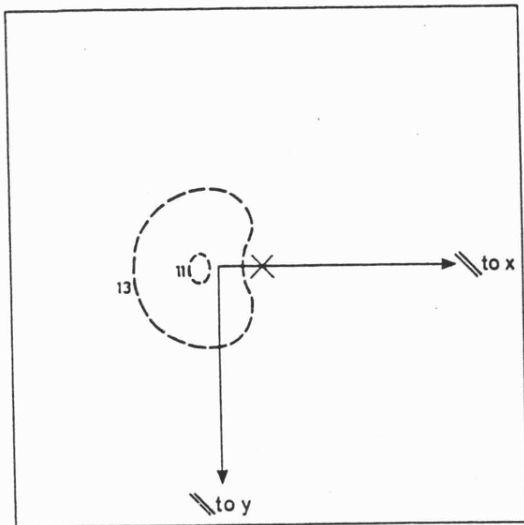
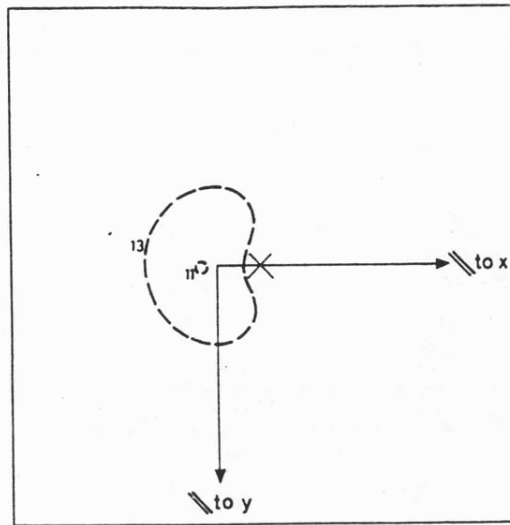


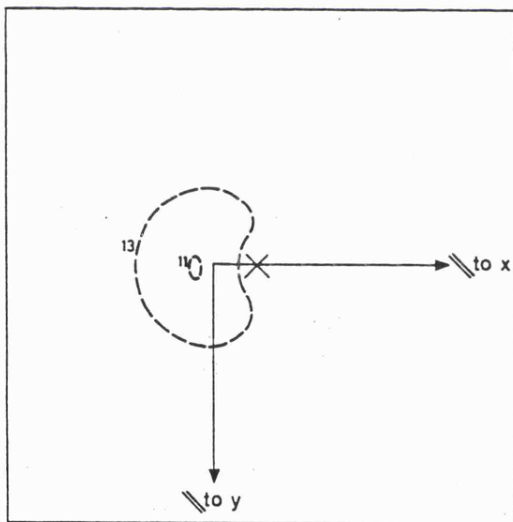
Figure (II.5.25) Partial planar Coulomb holes for H_2 , with electron 1 fixed at position [V] (see Fig.(II.5.3))² and electron 2 moving in the xy plane, were obtained by appropriate integration of Fig.(II.5.24).



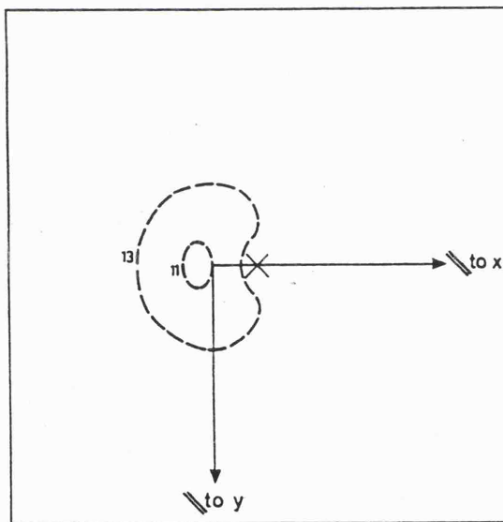
(A) 2NO - 1NO
z - correlation



(B) 3NO - 1NO
(z + φ) - correlation



(C) 4NO - 1NO
(z + φ + ρ) - correlation



(D) 10NO - 1NO
(z + φ + ρ + 2nd order)
- correlation

Figure (II.5.26) The partial planar Δ -surfaces, $\Delta V(\underline{r}_{12}, \underline{r}_1)$, for fixed electron position [VI] (see Figure (II.5.3A) for the definition), with the roving electron located in the xy-plane with $z = 0$.

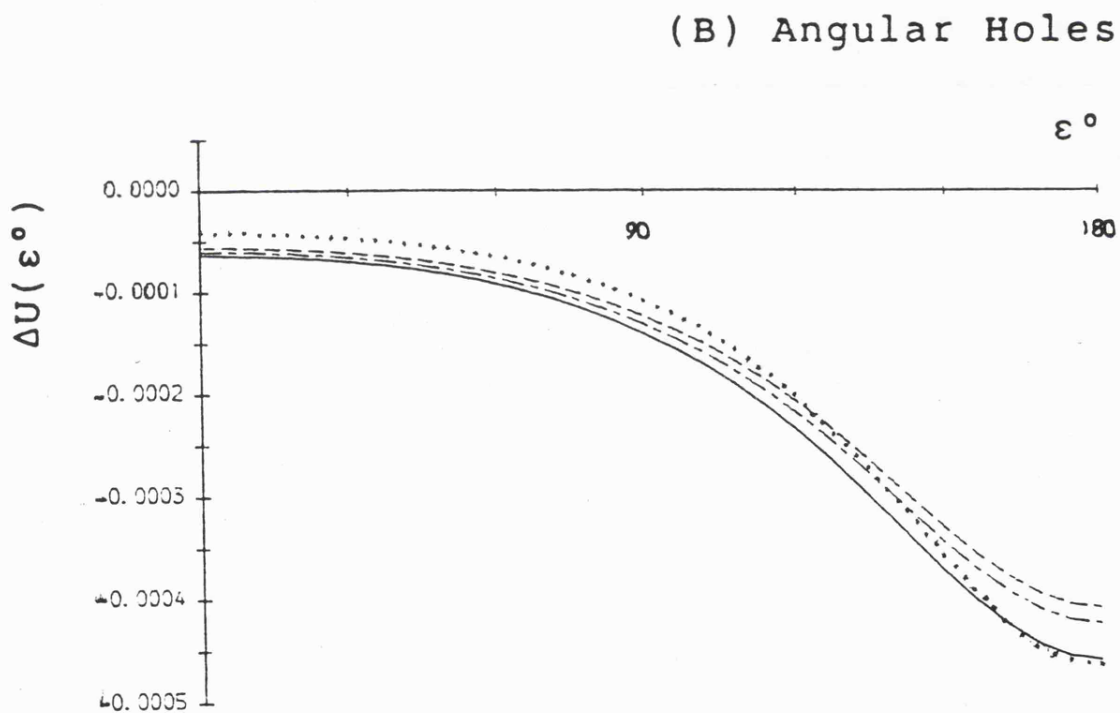
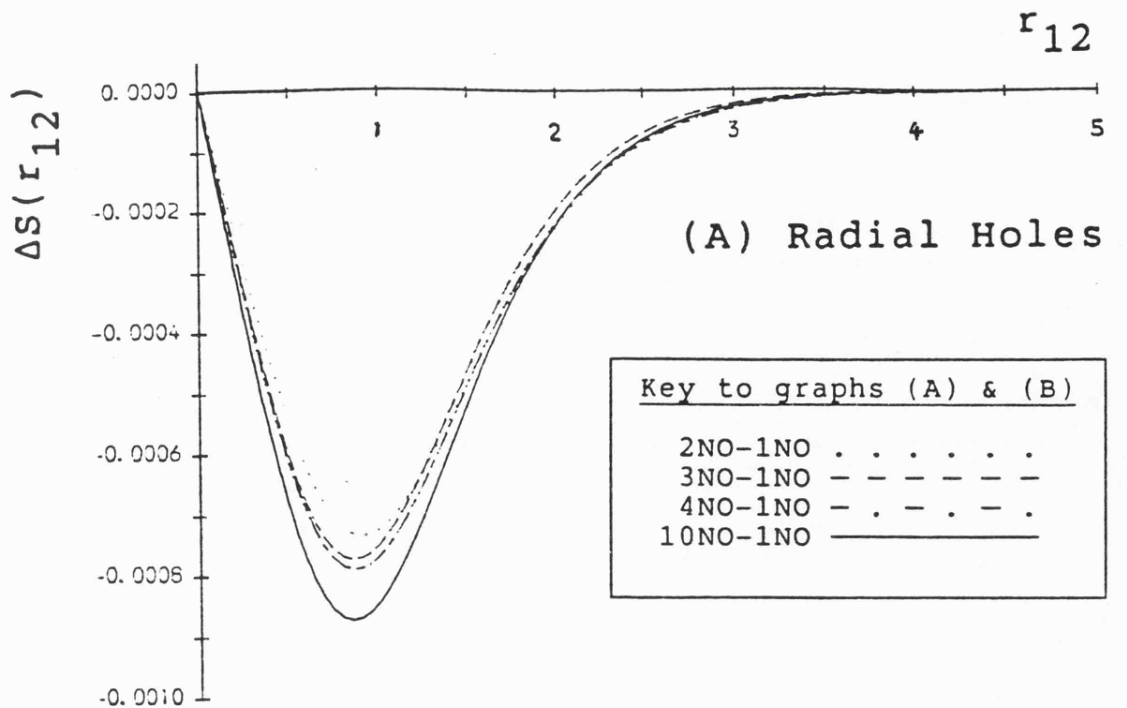


Figure (II.5.27) Partial planar Coulomb holes for H_2 , with electron 1 fixed at position [VI] (see Fig.(II.5.3)) and electron 2 moving in the xy plane, were obtained by appropriate integration of Fig.(II.5.26).

CHAPTER II.6

Discussion of H₂ Results in Position-Space

(II.6.1) The One-Particle Density Analysis

In order to discuss the effects of correlation, it will be useful to consider first the one-particle distribution of electrons as described by the Hartree Fock (HF) wavefunction in the plane containing the nuclei (xz-plane). In this way, a theoretical 'model' of the system at the uncorrelated level may be constructed, and then the changes which occur in that model as a result of introducing electron correlation may be analysed. As anticipated, the HF one-particle density surface, shown in Figure (II.5.1), possesses two distinct maxima, each associated with the location of a nucleus. From these maxima the electron probability decays and at large distances from the nuclei ellipsoidal contours may be observed.

The effect of electron correlation on these surfaces, $\Delta\rho(\underline{r}_1)$, is shown in Figure (II.5.2). It can be seen that they have a complex structure and have a range of the same order as the HF density. To be able to understand the structure of these diagrams, however, it is first necessary to investigate the mathematics of the functions.

As the Davidson and Jones wavefunction^(2.vi.1) is constructed from ten orthonormal natural orbitals, the one-particle density for the wavefunction, curtailed to

employ the first M natural configurations, $\rho_M(\underline{r}_1)$, may be written simply as

$$\rho_M(\underline{r}_1) = \sum_{i=1}^M A_M \mu_i^2 \chi_i^*(\underline{r}_1) \chi_i(\underline{r}_1) \quad (\text{II.6.1})$$

where A_M , the renormalisation constant, is defined as

$$A_M = 1 / \sum_{i=1}^M \mu_i^2. \quad (\text{II.6.2})$$

As all of the terms in A_M are positive, then

$$A_{M-1} > A_M > A_{M+1}. \quad (\text{II.6.3})$$

The Δ -one-particle density $\Delta\rho_M(\underline{r}_1)$ connected with the M -natural orbital wavefunction may be written in the form

$$\begin{aligned} \Delta\rho_M(\underline{r}_1) &= \sum_{i=1}^M A_M \mu_i^2 \chi_i^*(\underline{r}_1) \chi_i(\underline{r}_1) - A_1 \mu_1^2 \chi_1^*(\underline{r}_1) \chi_1(\underline{r}_1) \\ &= \sum_{i=2}^M A_M \mu_i^2 \chi_i^*(\underline{r}_1) \chi_i(\underline{r}_1) - (A_1 - A_M) \mu_1^2 \chi_1^*(\underline{r}_1) \chi_1(\underline{r}_1). \end{aligned} \quad (\text{II.6.4})$$

Since $(A_1 - A_M)$ is positive, $\Delta\rho_M(\underline{r}_1)$ may be considered as the sum of contributions from the correlating orbitals, from which a portion of the HF density is subtracted due to the renormalisation of the wavefunction. Electron correlation in the one-particle density is therefore due to the redistribution in electronic probability from the HF model into the correlating orbitals. Thus, by utilising equation (II.6.4), it is possible to express $\Delta\rho_M(\underline{r}_1)$ for $M = 2, 3, 4$ and 10 as

$$\Delta\rho_2(\underline{r}_1) = 0.009974 \chi_2^*(\underline{r}_1)\chi_2(\underline{r}_1) - 0.009974 \chi_1^*(\underline{r}_1)\chi_1(\underline{r}_1) \quad (\text{II.6.5})$$

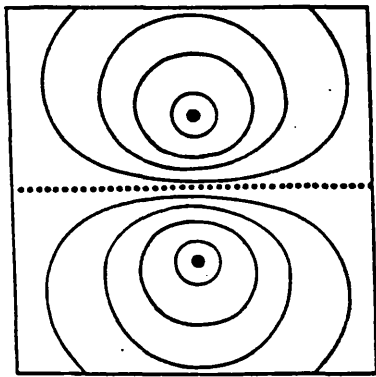
$$\Delta\rho_3(\underline{r}_1) = 0.009931 \chi_2^*(\underline{r}_1)\chi_2(\underline{r}_1) + 0.004255 \chi_3^*(\underline{r}_1)\chi_3(\underline{r}_1) - 0.014186 \chi_1^*(\underline{r}_1)\chi_1(\underline{r}_1) \quad (\text{II.6.6})$$

$$\Delta\rho_4(\underline{r}_1) = 0.009902 \chi_2^*(\underline{r}_1)\chi_2(\underline{r}_1) + 0.004242 \chi_3^*(\underline{r}_1)\chi_3(\underline{r}_1) + 0.003006 \chi_4^*(\underline{r}_1)\chi_4(\underline{r}_1) - 0.017150 \chi_1^*(\underline{r}_1)\chi_1(\underline{r}_1) \quad (\text{II.6.7})$$

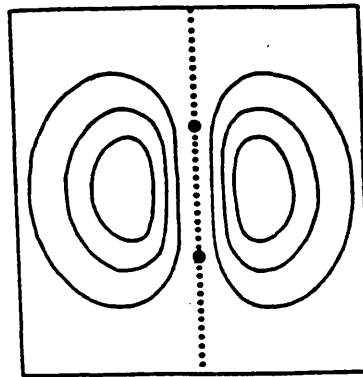
$$\Delta\rho_{10}(\underline{r}_1) = 0.009902 \chi_2^*(\underline{r}_1)\chi_2(\underline{r}_1) + 0.004242 \chi_3^*(\underline{r}_1)\chi_3(\underline{r}_1) + 0.003002 \chi_4^*(\underline{r}_1)\chi_4(\underline{r}_1) + 0.000670 \chi_{5-10}^*(\underline{r}_1)\chi_{5-10}(\underline{r}_1) - 0.017804 \chi_1^*(\underline{r}_1)\chi_1(\underline{r}_1). \quad (\text{II.6.8})$$

The notation $\chi_{5-10}^*(\underline{r}_1)\chi_{5-10}(\underline{r}_1)$ refers the cumulative effect of the last six natural, which, as discussed earlier, only contribute to a second-order correlation effect in the wavefunction.

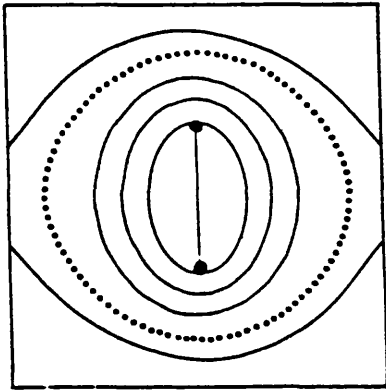
Before proceeding further with the discussion it is useful to sketch the shape of the one-particle density functions associated with each of the main natural orbitals separately. The density from the first natural orbital has already been presented in Figure (II.5.1) and need not be considered further. The second natural orbital produces the one particle density shown in Figure (II.6.1A). Due to the axial symmetry of the system the zero contour, as usual represented by a dotted line, actually defines a plane of zero influence which is a perpendicular bisector of the



(A) $\chi_2(\underline{r}_1)\chi_2(\underline{r}_1)$



(B) $\chi_3(\underline{r}_1)\chi_3(\underline{r}_1)$



(C) $\chi_4(\underline{r}_1)\chi_4(\underline{r}_1)$

Figure (II.6.1) Sketches of the $\chi_i(\underline{r}_1)\chi_i(\underline{r}_1)$ probability surfaces for $2 \leq i \leq 4$ where $\chi_i(\underline{r}_1)$ has been defined in equation (II.4.2). The surfaces are viewed in the xz -plane and are aligned in the z -direction.

molecular axis. Maxima then occur at the sites of the nuclei. The third natural orbital one-particle density is shown in Figure (II.6.1B). In this case the zero contour defines a line passing along the z-axis with a torroid of maximum probability enclosing the molecule. The zero contour for the fourth natural orbital is ellipsoidal in shape with a ridge of maximum probability along the bond axis.

We can now investigate the Δ -one-particle density surfaces. The second natural configuration has the greatest effect upon the correlation energy and is responsible for introducing a 'left-right' correlation effect. Due to the alignment of the molecule with respect to the co-ordinate system we have defined this to be z-correlation. An examination of equation (II.6.5) discloses that 0.9974% of the probability associated with electron 1 is transferred from the HF description of the molecule to the second natural orbital one-particle density. Figure (II.5.2A) may therefore be generated by mentally subtracting the HF one-particle density surface from the z-correlating natural orbital surface. Since most of the charge associated with the second natural orbital is located at the nuclei, this region remains positive. But, in the mid bond region the HF density is greater, making the surface negative. The influence of the Hartree Fock density on the second natural orbital density is therefore to split the zero contour to generate two ellipsoids around each of the nuclei and form the region of largest negative effect in the centre of the bond. Consequently, z-correlation has the effect of moving charge from the mid bond region to the region slightly

behind each of the nuclei in the one-particle density approximation.

By including the third natural orbital in the wavefunction ϕ -correlation is introduced into the Δ -one-particle density surface. Equation (II.6.6) reveals that 1.14186% of the total charge is moved from the HF description into the z and ϕ -correlating orbitals collectively. Virtually no difference is observed in the amount of charge moved into the second natural orbital, thus an extra 0.4255% of the charge is transferred into the third natural orbital from the HF orbital. To construct Figure (II.5.2B) $\chi_3^*(\underline{r}_1)\chi_3(\underline{r}_1)$ may therefore be added to Figure (II.5.2A) and then extra HF density is subtracted to compensate. As the ϕ -correlating density has no effect along the z -axis, the electronic probability is reduced in this region due to the influence of the HF probability which is obviously non-zero, causing the magnitude of the maxima at the nuclear sites to be diminished slightly. Charge is built up, though, in the regions at the side of the molecule, consequently contracting the region covered by the negative contours and 'flattening' out of the zero contours. It is impossible to interpret classically the effect of ϕ -correlation in an axially symmetric one-particle density, hence the resulting diagrams can only represent a generalised result.

Equation (II.6.7) demonstrates that 0.3002% of the charge is move into the fourth natural orbital. Also, since once again the occupation numbers of the other electrons remain almost unchanged, Figure (II.5.2C) may be generated by adding $\chi_4^*(\underline{r}_1)\chi_4(\underline{r}_1)$ to Figure (II.5.2B) and subtracting additional charge associated with the HF orbital. Davidson and Jones^(2.vi.1) have defined the correlation introduced by the fourth natural orbital to be 'in-out' correlation. In view of the co-ordinate system used we have defined this to be ρ -correlation. Contrary to the effect of z-correlation, ρ -correlation actually increases the charge in the mid bond region and slightly decreases the charge in the vicinity of the nuclei. This causes the zero contours to join up and form an enclosed region of negative charge in the centre of the molecule.

The remaining six natural orbitals have a negligible effect on the one-particle density and in fact, from equation (II.6.8), it can be seen that only 0.0670% of the total charge is associated with all of them, this being only about 4% of the total redistributed charge. Through close scrutiny of Figure (II.5.2D) it appears that these orbitals only slightly contract the range of the contours. Nevertheless, since Figure (II.5.2D) represents the redistribution in density due to the full Davidson and Jones wavefunction, it is very important as it represents the most accurate view of the overall effect of electron correlation on the one-particle density of the H_2 molecule.

The main global feature to note is that correlation is responsible for transferring electronic probability from the mid bond region to just behind the nuclei. Similar observations have also been made in one-particle density studies of the HeH^+ ^(2.vi.2) and LiH ^(2.vi.3) molecules. It is also particularly pleasing to note that these results are in accordance with the second-order perturbation analysis performed by Grimaldi on the nitrogen^(2.vi.4) and carbon monoxide^(2.vi.5) molecules.

By employing a similar argument as that used by Ruedenberg in diatomic hydrides^(2.iv.6) and water^(2.vi.7), it can be seen that the kinetic energy of the electrons will increase as they are brought closer to the nuclei and hence experience a larger electro-nuclear attractive force. For a molecule in equilibrium, though, the potential energy must compensate within the virial theorem^(2.vi.8), that is

$$\text{potential energy} / \text{kinetic energy} = -2. \quad (\text{II.6.9})$$

If the kinetic energy increases by say an amount ΔE , due to correlation, then the potential energy must decrease by $2\Delta E$ to compensate. The sum of the kinetic and potential energies will therefore be lower, producing a more stable system, by the amount ΔE .

It is also interesting to note that, when each of the correlating orbitals is included in the Davidson and Jones wavefunction, a certain amount of charge is transferred into them. This quantity then remains virtually unchanged when

subsequent orbitals are introduced into the wavefunction. As commented upon by Shull^(2.vi.9), this is a common feature of natural orbital expansions where the occupation numbers are essentially independent of the type or size of the basis set used. It seems that electronic probability is transferred into each of these orbitals to a predefined level which is almost independent of the presence of the other correlating orbitals. Also, since correlation is introduced into the one-particle density by moving charge from the HF description into doubly occupied correlating orbitals, only a very 'general' picture of the effects of correlation may be observed.

One-particle density surfaces are useful in discussing the effects of correlation on H_2 , and we have seen how correlation increases the stability of the system. However, it has also been noted that only an averaged view of electron correlation can be seen due to the influence of one of the electrons being integrated over all space.

(II.6.2) The Two-Particle Density Analysis

[A] Form of Position-Space Functions

An accurate view of the effects of correlation may only be obtained by considering two-electron distribution functions^(2.vi.10,11); these results consequently represent a realistic interpretation of how electron probability is redistributed due to electron correlation. Before the characteristics of the surfaces and curves can be discussed, the mathematical form of the partial planar distribution

functions should be investigated.

Since no integration has been performed in the generation of the partial planar density, it is mathematically more complex than the one-particle density function. For the Davidson and Jones wavefunction^(2.vi.1) curtailed to embody only the first M natural configurations with electron 1 fixed at a point specified by \underline{r}_1 , the partial planar density surface $V_M(\underline{r}_{12}, \underline{r}_1)$ may be defined as

$$V_M(\underline{r}_{12}, \underline{r}_1) = \sum_{i,j=1}^M A_M^{\mu_i \mu_j} r_{12} [i]^*(\underline{r}_1, \underline{r}_2) [j](\underline{r}_1, \underline{r}_2), \quad (\text{II.6.10})$$

where $[i](\underline{r}_1, \underline{r}_2)$ represents the i^{th} configuration. The renormalisation constant A_M is given in equation (II.6.2) and obviously

$$\underline{r}_{12} = \underline{r}_1 - \underline{r}_2. \quad (\text{II.6.11})$$

By a simple rearrangement of equation (II.6.10), $V_M(\underline{r}_{12}, \underline{r}_1)$ may be rewritten as

$$V_M(\underline{r}_{12}, \underline{r}_1) = \sum_{i>j=1}^M A_M^{\mu_i \mu_j} r_{12} \left([i]^*(\underline{r}_1, \underline{r}_2) [j](\underline{r}_1, \underline{r}_2) + [i](\underline{r}_1, \underline{r}_2) [j]^*(\underline{r}_1, \underline{r}_2) \right) + \sum_{i=1}^M A_M^{\mu_i^2} r_{12} [i]^*(\underline{r}_1, \underline{r}_2) [i](\underline{r}_1, \underline{r}_2). \quad (\text{II.6.12})$$

Since this analysis is performed in the xz -plane, where all of the configurations are real, $V_M(\underline{r}_{12}, \underline{r}_1)$ may be simplified to

$$\begin{aligned}
V_M(\underline{r}_{12}, \underline{r}_1) &= \sum_{i>j=1}^M A_M \mu_i \mu_j r_{12}^2 [i](\underline{r}_1, \underline{r}_2) [j](\underline{r}_1, \underline{r}_2) \\
&+ \sum_{i=1}^M A_M \mu_i^2 r_{12} [i]^2(\underline{r}_1, \underline{r}_2). \quad (\text{II.6.13})
\end{aligned}$$

Thus $\Delta V_M(\underline{r}_{12}, \underline{r}_1)$, the effect of electron correlation on the partial planar density surface, will be

$$\begin{aligned}
\Delta V_M(\underline{r}_{12}, \underline{r}_1) &= \sum_{i>j=1}^M A_M \mu_i \mu_j r_{12}^2 [i](\underline{r}_1, \underline{r}_2) [j](\underline{r}_1, \underline{r}_2) \\
&+ \sum_{i=2}^M A_M \mu_i^2 r_{12} [i]^2(\underline{r}_1, \underline{r}_2) \\
&- (A_1 - A_M) r_{12} \mu_1^2 [1]^2(\underline{r}_1, \underline{r}_2). \quad (\text{II.6.14})
\end{aligned}$$

Immediately it can be seen that the last two terms in the Δ -partial planar density $\Delta V_M(\underline{r}_{12}, \underline{r}_1)$ are similar in form to the Δ -one particle density $\Delta \rho_M(\underline{r}_1)$ which, as discussed earlier, only introduces an averaged correlation effect. The two-particle density functions, however, contain additional off diagonal terms; it is these that must be responsible for introducing correlation with explicit reference to the position of the fixed electron. We may write $\Delta V_M(\underline{r}_{12}, \underline{r}_1)$ as

$$\begin{aligned}
\Delta V_M(\underline{r}_{12}, \underline{r}_1) &= \sum_{i>j=1}^M a_{ij}^2 r_{12} [i](\underline{r}_1, \underline{r}_2) [j](\underline{r}_1, \underline{r}_2) \\
&+ \sum_{i=1}^M a_{ij} r_{12} [i]^2(\underline{r}_1, \underline{r}_2) \quad (\text{II.6.15})
\end{aligned}$$

where, by definition,

$$a_{ij} = \mu_i \mu_j A_M \quad (\text{II.6.16})$$

for all values of i and j except for a_{11} when

$$a_{11} = -(A_1 - A_M) \mu_1^2. \quad (\text{II.6.17})$$

The importance of each term in equation (II.6.15) may therefore be obtained by the appropriate value of a_{ij} . Values of a_{ij} for the main correlating orbitals, ie $M = 2, 3$ and 4 are presented below:

Table (II.6.1) values of a_{ij} when $M=2$

	i \longrightarrow		
j		1	2
	1	-0.009974	-0.099369
↓	2		0.009974

Table (II.6.2) values of a_{ij} when $M=3$

	i \longrightarrow			
j		1	2	3
	1	-0.01486	-0.098467	-0.064765
↓	2		0.009931	0.006500
	3			0.004255

Table (II.6.3) values of a_{ij} when $M=4$

	i \longrightarrow				
j		1	2	3	4
	1	-0.017150	-0.098649	-0.064570	-0.054356
↓	2		0.009902	0.006481	0.005456
	3			0.004242	0.003571
	4				0.003006

The values of a_{ij} are virtually independent of the size of the basis set employed and the diagonal elements in a_{ij} are the same coefficients as obtained in the Δ -one-particle density analysis. This allows us to analyse separately the effects of z , ϕ and ρ -correlation as the magnitude of, for example, z -correlation will be almost identical in all four surfaces. The other main feature is that the magnitudes of the a_{i1} terms, although negative, are at least a factor of ten bigger than the other values of a_{ij} . These terms must therefore be responsible for introducing the main correlation effects. This means that the term $i = 1, j = 2$ will bring z -correlation into the system, $i = 1, j = 3$ will introduce ϕ -correlation and $i = 1, j = 4$ will introduce ρ -correlation. Before proceeding further, however, we will investigate the form of the products of the natural configurations, paying particular attention to the product of the first natural configuration with the others.

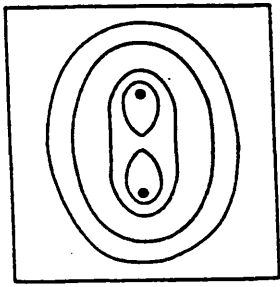
If the m_i and m_j magnetic quantum numbers in the Davidson and Jones wavefunction are both zero, which occurs in most configurations, then

$$[i1](\underline{r}_1, \underline{r}_2)[j1](\underline{r}_1, \underline{r}_2) = \chi_i(\underline{r}_1)\chi_j(\underline{r}_1)\chi_i(\underline{r}_2)\chi_j(\underline{r}_2). \quad (\text{II.6.18})$$

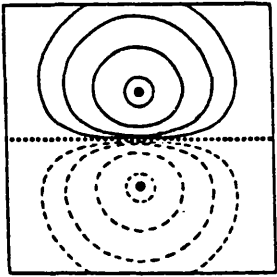
In cases when m_i and m_j are non-zero, the product of the configurations must be expressed as the linear combination of such products of natural orbitals. Thus, for electron 1 located at \underline{r}_1 , $\chi_i(\underline{r}_1)\chi_j(\underline{r}_1)$ is a constant which multiplies the probability surface $\chi_i(\underline{r}_2)\chi_j(\underline{r}_2)$ of electron 2 for $m_i=0$; for non-zero m_i and m_j a linear combination of these terms

is obtained. The surfaces $\chi_i(\underline{r})\chi_j(\underline{r})$ are therefore extremely useful as they may be used, not only to investigate the shape of the distribution of electron 2, but also to evaluate the probability of locating electron 1 at \underline{r}_1 . Consequently they have been sketched in Figure (II.6.2) using the conventional notation of a full curve to represent positive contours, broken curves for negative contours and a dotted curve to represent the zero contour. These surfaces may now be used in the analysis of the characteristic effects of the three main types of correlation in the Δ -partial planar surface.

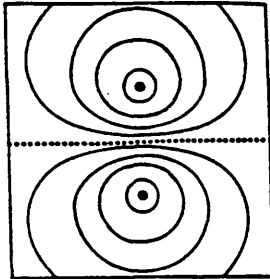
When $M=2$, only z -correlation is introduced into the wavefunction. As the coefficient a_{12} is by far the largest, it is the term $a_{12}^2 r_{12} \chi_1(\underline{r}_1)\chi_2(\underline{r}_1)\chi_1(\underline{r}_2)\chi_2(\underline{r}_2)$ that is responsible for introducing the main z -correlation effect. Figure (II.6.2) shows that the $\chi_1(\underline{r})\chi_2(\underline{r})$ surface has a maximum associated with one nucleus and a minimum, of the same magnitude but of opposite sign, at the site of the other nucleus with the zero contour perpendicularly bisecting the bond-axis. Suppose now that the fixed electron is located on the positive side of the zero contour. If the roving electron is also on the positive side then the total contribution to the Δ -surface will be negative due to the sign of a_{12} ; although, once the electron moves into the negative region of $\chi_1(\underline{r})\chi_2(\underline{r})$ the total contribution will then be positive. A similar argument may be applied when the fixed electron is located on the negative side of $\chi_1(\underline{r})\chi_2(\underline{r})$ to obtain corresponding results. This term therefore has the effect of increasing the probability of locating the roving



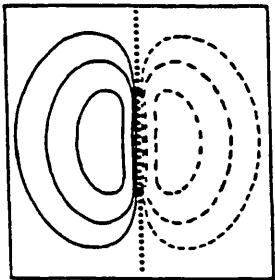
$$\chi_1(\underline{r})\chi_1(\underline{r})$$



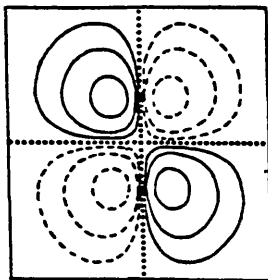
$$\chi_1(\underline{r})\chi_2(\underline{r})$$



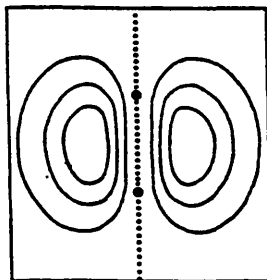
$$\chi_2(\underline{r})\chi_2(\underline{r})$$



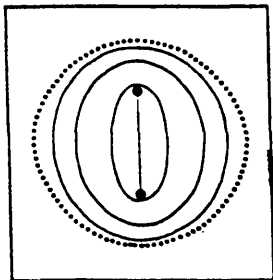
$$\chi_1(\underline{r})\chi_3(\underline{r})$$



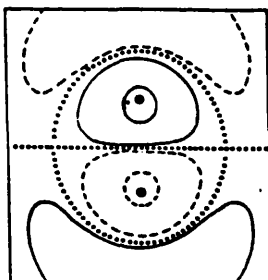
$$\chi_2(\underline{r})\chi_3(\underline{r})$$



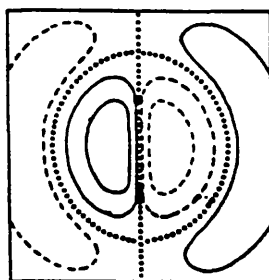
$$\chi_3(\underline{r})\chi_3(\underline{r})$$



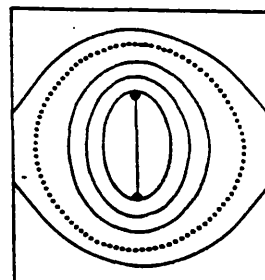
$$\chi_1(\underline{r})\chi_4(\underline{r})$$



$$\chi_2(\underline{r})\chi_4(\underline{r})$$



$$\chi_3(\underline{r})\chi_4(\underline{r})$$



$$\chi_4(\underline{r})\chi_4(\underline{r})$$

Figure (II.6.2) Sketches of the $\chi_i(\underline{r})\chi_j(\underline{r})$ probability surfaces for $1 \leq i, j \leq 4$ where $\chi_i(\underline{r})$ has been defined in equation (II.4.2). The surfaces are viewed in the xz -plane and are aligned in the z -direction.

electron in the vicinity of the nucleus that is furthest from the fixed electron and decreasing the probability of locating the roving electron near to the closest nucleus. As the r_{12} term can have no effect on the zero contour it remains bisecting the bond, irrespective of the location of the fixed electron.

The remaining two diagonal terms only account for 5% of the total effect and thus only introduce minor perturbations to this picture. The term $a_{22}r_{12}x_2^2(\underline{r}_1)x_2^2(\underline{r}_2)$ simply adds probability to the regions around both nuclei and $a_{11}r_{12}x_1^2(\underline{r}_1)x_1^2(\underline{r}_2)$, due to a_{11} being negative, reduces the probability over the entire surface. This has the effect of causing a slight bending of the zero contour towards the region of positive probability. It is interesting to note that if the fixed electron is located on a locus that is equidistant from each of the nuclei, the only non-zero contribution will be from the $i = 1, j = 1$ term. Since this is due only to the renormalisation of the wavefunction, we may conclude that z-correlation can have no effect along this line. The effect of z-correlation, however, will increase in magnitude as the fixed electron is located closer to one particular nucleus.

When $M=3$, ϕ -correlation is introduced into the wavefunction and, from past experience, we would expect that the main correlation effect would be described by the function $2a_{13}r_{12} [1](\underline{r}_1, \underline{r}_2)[3](\underline{r}_1, \underline{r}_2)$. If this analysis is followed through in detail it can be seen that this function consists of the sum of two terms. The first is of the form

$2a_{13}r_{12}\chi_1(\underline{r}_1)\chi_3(\underline{r}_1)\chi_1(\underline{r}_2)\chi_3(\underline{r}_2)$ and as a consequence $\chi_1(\underline{r})\chi_3(\underline{r})$ is shown in Figure (II.6.2). It possesses a zero contour which forms a plane of zero influence perpendicular to the x-axis and therefore passes through the z-axis. An elongated maximum may be observed at one side of the molecular-axis and a minimum, of equal magnitude, at the other. The second term is of the same form as this except that it is centred in the yz-plane and therefore the xz-plane corresponds to its nodal plane and need not be considered in this analysis.

Applying the same argument used to investigate z-correlation, we see that ϕ -correlation decreases the probability of locating the roving electron on the same side of the bond as the fixed electron and increases the probability of discovering it on the opposite side. As expected, ϕ -correlation can have no effect when the fixed electron is located on the major axis of the molecule but, when the other terms are included $a_{11}r_{12}\chi_1^2(\underline{r}_1)\chi_1^2(\underline{r}_2)$, it will once again cause the zero contour to bend towards the positive region of the surface. The remaining terms have a negligible effect on the surface and are not considered.

ρ -correlation is introduced mainly by the term $2a_{14}r_{12}\chi_1(\underline{r}_1)\chi_4(\underline{r}_1)\chi_1(\underline{r}_2)\chi_4(\underline{r}_2)$. The $\chi_1(\underline{r})\chi_4(\underline{r})$ surface consists of a ridge of maximum probability along the entire length of the bond, an elliptically shaped zero contour and a negative region at larger distances from the molecule. Thus, if electron 1 is located in the same region of $\chi_1(\underline{r})\chi_4(\underline{r})$ as electron 2, the total contribution to the

electronic probability will be negative whereas, if they are in different regions, the contribution will be positive. It follows that ρ -correlation acts to redistribute the probability of finding the roving electron to distances further from the bond in all directions if the fixed electron is within the positive region of $\chi_1(\underline{r})\chi_4(\underline{r})$. Although, once the fixed electron is located further from the nuclei, in the negative region of $\chi_1(\underline{r})\chi_4(\underline{r})$, it becomes energetically more feasible to move the roving electron closer to the nuclear frame.

In short, the main contributions to the Δ -partial planar surfaces originate from the product of the first natural configuration with the correlating configurations and all other terms have only a very small effect. This enables simple 'classical' characteristics of the main types of correlation to be envisaged and the individual Δ -partial planar surfaces to be analysed in terms of their relative compositions of z , ϕ and ρ -correlation.

[B] Test Electron fixed on Molecular Axis

The first three fixed electron positions to be considered are located on the z -axis. To create a basis from which the correlation effects may be applied, the HF Δ -partial planar distribution functions are shown in Figure (II.5.4). These surfaces possess maxima in probability in the vicinity of the nuclei and zero at the position of the fixed electron due to the effect of r_{12} . The appropriate radial and angular distribution functions are also displayed in Figure (II.5.5). Whilst the effect of the nuclei may be seen to a

certain extent the relative magnitude of each of the distributions is particularly apparent.

The effect of correlation in position [I] is unusual because, due to the fixed electron being located in the mid bond position, both the z and ϕ -correlation components may have no effect. This can be observed in Figures (II.5.6A) and (II.5.6B) since both surfaces are very shallow and negative with the imprint of the $a_{11}r_{12}\chi_1^2(\underline{r}_1)\chi_1^2(\underline{r}_2)$ renormalisation term clearly visible. The minima in Figure (II.5.6B) are deeper than the minima in Figure (II.5.6A) by a factor of $a_{11}(M=3)/a_{11}(M=2) \approx 1.5$. The inclusion of ρ -correlation in Figure (II.5.6C) has a dramatic effect on the Δ -surface. As predicted, charge associated with electron 2 is removed from around the nuclei to regions further away, in particular behind each of the nuclei and also a characteristic ellipse shaped zero contour may be seen. As demonstrated in Figure (II.5.6D), only minor changes are introduced by the inclusion of the remaining six natural configurations. Thus, when one of the electrons is fixed instantaneously at position [I], the total correlation effect is due almost entirely to ρ -correlation. This is emphasised by examining the partial planar Coulomb holes shown in Figure (II.5.7). The first two radial and angular Coulomb holes are small and negative but a relatively large contribution is introduced by the fourth natural configuration.

Since this example retains the axial symmetry of the H_2 molecule, it may be thought that the area contained within

the $\Delta S(r_{12})$ and $\Delta U(\epsilon)$ curves should be zero as this, by definition, represents the probability of locating the electrons in the chosen plane. This is not the case. The partial planar holes are functions of the positions of two electrons and hence the change in probability of locating the fixed electron at position [I] must also be taken into account.

The fixed electron is located on the site of a nucleus in position [II] and, as demonstrated by the one-particle analysis, this represents the most likely position of electron 1. Figure (II.5.8A) shows that z-correlation has a relatively large effect on the Δ -surface. As predicted, the zero contour almost bisects the bond and a slight bending towards the region of positive probability due to the $a_{11}r_{12}x_1^2(\underline{r}_1)x_1^2(\underline{r}_2)$ term can be seen. This highlights how unimportant these minor terms are. Apart from this effect, the probability of discovering the roving electron near to the nucleus on which the fixed electron is located is reduced but is increased in the vicinity of the other nucleus.

There is very little difference between Figure (II.5.8A) and Figure (II.5.8B) indicating that ϕ -correlation has no effect. The inclusion of ρ -correlation however does have a marked effect on the Δ -surface. The probability of discovering the roving electron near to the fixed electron is reduced and a minimum is observed on the bond axis. The zero contour becomes ellipsoidal in form and encloses the region of negative probability.

The remaining configurations, as demonstrated in Figure (II.5.8D), have the effect of slightly contracting the area covered by the contours and also increasing the depth of the minimum. From the partial planar Coulomb holes in Figure (II.5.9) the relative magnitude of each of the types of electron correlation may be observed. For example, the difference in the curves between employing two and three natural configurations is almost graphically indistinguishable, demonstrating that ϕ -correlation has no effect. The curves generated from the wavefunction curtailed to encompass only two configurations, on the other hand, are relatively large which indicates the importance of z -correlation. These curves nevertheless represent averaged views and some information is lost. For instance, the generation of the minimum on the bond axis in Figure (II.5.8C) cannot be observed as it is masked by the much larger magnitude of the maximum.

Position [III] is defined by the fixed electron being located at a half bond length (0.7 a.u.) behind the nucleus on the z -axis. We observe from Figure (II.5.10A) that the probability of discovering the roving electron near to the closest nucleus to the fixed electron is diminished but it is increased around the furthest nucleus. ϕ -correlation has no effect, as shown in Figure (II.5.10B) whilst Figure (II.5.10C) demonstrates that the effect of ρ -correlation is also very much reduced.

Interestingly, the last six natural configurations introduce small ρ -correlation characteristics. Since the zero contour remains virtually at the same position in these diagrams we may conclude that z-correlation is by far the most dominant contribution to the total effect. This is also demonstrated by the partial planar Coulomb holes (shown in Figure (II.5.11)) as they all are almost identical. The increase in the importance of z-correlation may be explained by realising that, as the fixed electron is located at greater distances from the nuclei, the electron-electron repulsion effect, which is responsible for introducing correlation, will act increasingly only in the z-direction. However, when the fixed electron is located at extremely large distances from the nuclei, where the distance between the nuclei is negligible compared to the distance from the nuclear frame to the fixed electron, the fixed electron will experience only one nuclear force. In this case, the correlation effect will be identical to the correlation redistribution in the united atom of H_2 , helium, and consequently ρ -correlation will dominate.

It is also possible to study surfaces that are perpendicular to the xz-plane for position [I], [II], and [III], however, they would be axially symmetric and hence could be generated from the Δ -surfaces in the xz-plane. The axial symmetry would also cause the $\Delta S(r_{12})$ curves to be simply 2π times the axial profile of the Δ -surfaces and the $U(\epsilon)$ curves to be horizontal lines.

[C] Test Electron Fixed off Molecular Axis

Positions [IV], [V] and [VI] do not possess axial symmetry and consequently the study of the Δ -partial planar surfaces in the xy-plane is worthwhile. In addition, due to the lower-order symmetry, the angular partial planar holes in the xz-plane, for these fixed electron positions, must be extended to the full range for ϵ of $0 \rightarrow 2\pi$ in order to encapsulate the full angular redistribution in probability.

To aid this discussion, the correlation effects observed in the xz-plane will be discussed concurrently with the xy-plane results. The xz-plane HF partial planar distributions are displayed in Figure (II.5.12) and the xy-plane functions are shown in Figure (II.5.20). The surfaces are perpendicular views of the same probability distribution resulting in their contours being coincident along the common line of intersection, in this case, the x-axis.

Position [IV] is located by the fixed electron being situated at a half bond length (0.7 a.u.) from the mid bond position on the x-axis. Since this position is still on the plane that bisects the bond, again z-correlation has no direct effect. The minima observed in Figure (II.5.14A), like position [I], are due simply to the renormalisation of the wavefunction and Figure (II.5.22A) is a perpendicular view of this. The minima are moved slightly away from the nuclei due to the effect of the r_{12} term.

This is the first fixed electron position for which

ϕ -correlation has a relatively large effect on the Δ -surface. From Figures (II.5.14B) and (II.5.22B) we see that the probability of locating the roving electron on the same side of the molecule as the fixed electron is reduced but it is increased on the other side. Two minima are generated rather than one single minimum as the surface is fixed to be zero at the position of electron 1. As the fixed electron is located at further distances from the nuclei on the x-axis, though, one would expect that they would become one. In both the xz and xy-planes, as predicted, the zero contour is seen to bend towards the region of positive probability due to the renormalisation of the wavefunction when the ϕ -correlating configuration is introduced. Subsequently, ρ -correlation causes the probability to be reduced in the neighbourhood of the nuclei and the zero contour to form into an ellipse that encloses the region of negative probability. From these observations we see that the total electron correlation effect is due to a large contribution of both ϕ and ρ -correlation. The corresponding partial planar Coulomb holes shown in Figure (II.5.15) and (II.5.23) clearly illustrate this point as, contrary to most of the holes already discussed, all of the curves are discernible from each other. It is important to note that ϕ -correlation has a greater effect on the angular planar holes than the radial holes. In Figure (II.5.15B) it can be seen that ϕ -correlation overcompensates in the redistribution of probability and creates a large maximum when $\epsilon = 90^\circ$ (ie along a direction towards the mid bond position). This may also be observed in the xy-plane by examining Figure (II.5.23B). This illustrates the need for

studying both radial and angular based Coulomb holes in tandem to gain a complete insight into the total effect of electron correlation.

When the fixed electron is located at the side of a nucleus, as in position [V], z-correlation once again contributes a large effect to the Δ -surfaces (see Figure (II.5.16A)). Even though the fixed electron is located in an asymmetric position, it is pleasing to observe the standard z-correlation effects. The equivalent surface in the xy-plane is not so interesting as only a cross-sectional view of the minimum at the site of the nucleus may be seen. This lack of detail is expected when attempting to measure a movement in the z-direction by examining the xy-plane. The introduction of ϕ -correlation in Figure (II.5.16B) causes the zero contour to still curve towards the positive region on the surface although, in this example, it is inclined at approximately fifty degrees to the bond axis. From this it could be inferred that the total electronic correlation effect consists of almost fifty percent contributions from each type of correlation. The introduction of ρ -correlation complicates this picture as the characteristic ellipse shaped zero contour is observed in Figure (II.5.16C) and also (II.5.24C). The size of the ellipse is relatively large, indicating that the effect of ρ -correlation is small and thus the fixed electron must be approaching the zero contour on the $\chi_1(\underline{r})\chi_4(\underline{r})$ surface (see Figure (II.6.2) for further details). The remaining configurations have the effect of contracting the area covered by the zero contour, however, from Figure (II.5.16D) we observe that the symmetry

of the ellipse is lost.

The effect of z-correlation on position [VI] (shown in Figure(II.5.18A)) is surprisingly similar to position [III] (see Figure (II.5.10A)). Again, when ϕ -correlation is introduced, the zero contour becomes inclined to the bond axis. In this case though it is very much larger, indicating that the contribution from z-correlation is greater than in position [V]. The importance of z-correlation may be illustrated by examining the Δ -surfaces in the xy-plane (Figure (II.5.26)). All four of the surfaces are negative and exhibit the general shape of the z-correlation surface first seen in Figure (II.5.24A). Figures (II.5.19A) and (II.5.27A) show that z-correlation accounts for almost all of the radial Coulomb holes though the angular holes once more highlight the small but appreciable effect of ϕ -correlation. The inclusion of ρ -correlation in this example, although it has a relatively small effect, is of considerable interest as the zero contour clearly curves to the region of positive probability rather than, as in all the previous Δ -surface, to the negative. From this it must be concluded that the fixed electron is located in the negative region of the $\chi_1(\underline{r})\chi_4(\underline{r})$ surface. In this region ρ -correlation acts to increase the electron probability in the bond region. To test this hypothesis $\chi_1(\underline{r})\chi_4(\underline{r})$ was evaluated at position [VI] and this was found to be the case.

[D] Summary

In summary, we have observed that the three major types of correlation, namely z , ϕ and ρ , are responsible for introducing almost all of the electron correlation and combine in various ways depending upon the location of the fixed electron. In particular, the terms

$$2a_{12}r_{12}X_1(\underline{r}_1)X_2(\underline{r}_1)X_1(\underline{r}_2)X_2(\underline{r}_2),$$

$$2a_{13}r_{12}X_1(\underline{r}_1)X_3(\underline{r}_1)X_1(\underline{r}_2)X_3(\underline{r}_2) \text{ and}$$

$$2a_{14}r_{12}X_1(\underline{r}_1)X_4(\underline{r}_1)X_1(\underline{r}_2)X_4(\underline{r}_2)$$

introduce over ninety percent of the z , ϕ and ρ -correlation, respectively. Since the location of electron 1 has been fixed, it is the constant $2a_{12}X_1(\underline{r}_1)X_2(\underline{r}_1)$, that gives a measure of the importance of z -correlation and the probability surface $X_1(\underline{r}_2)X_2(\underline{r}_2)$ that actually describes the distribution of electron 2. Hence, if it is assumed that all of the correlation is introduced by these three terms, the percentage contribution from each of the correlation-types, for a specific location of the test electron defined by \underline{r}_1 , may be expressed as

$$\% \text{age } z\text{-corr} = |2a_{12} X_1(\underline{r}_1)X_2(\underline{r}_1)| \times T \quad (\text{II.6.19})$$

$$\% \text{age } \phi\text{-corr} = |2a_{13} X_1(\underline{r}_1)X_3(\underline{r}_1)| \times T \quad (\text{II.6.20})$$

$$\% \text{age } \rho\text{-corr} = |2a_{14} X_1(\underline{r}_1)X_4(\underline{r}_1)| \times T \quad (\text{II.6.21})$$

where

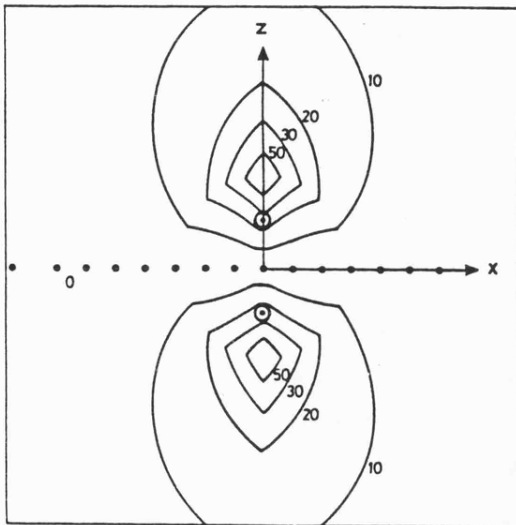
$$T = 1/(|2a_{12} X_1(\underline{r}_1)X_2(\underline{r}_1)| + |2a_{13} X_1(\underline{r}_1)X_3(\underline{r}_1)| + |2a_{14} X_1(\underline{r}_1)X_4(\underline{r}_1)|) \quad (\text{II.6.22})$$

Since these relationships are true for all values of \underline{r}_1 , they may be represented by contour diagrams in chosen planes (see Figure (II.6.3) for the xz -plane of H_2). Formally these

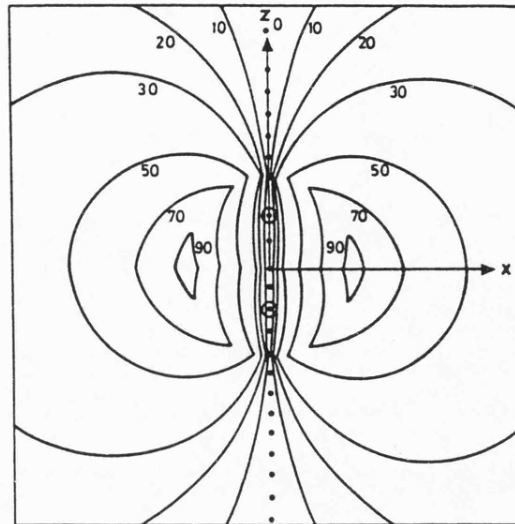
surfaces represent the percentage contributions from the main correlation types that are imparted upon electron 2, whilst travelling in the plane containing electron 1 and the two nuclei, due to the instantaneous location of electron 1 at r_1 .

The surface representing the contribution from z-correlation is given in Figure (II.6.3A)). Since z-correlation has the effect of transferring electron probability from the vicinity of the closest nucleus to electron 1 to the furthest, it can have no effect along the plane that is equidistant from each of the nuclei. However, as electron 1 is located closer to the nuclei, the relative contribution from z-correlation increases towards maxima behind each of the nuclei. Within the adopted approximation, the maxima are located at the intersection of the zero contours from the ϕ and ρ -percentage contribution surfaces' (see Figure (II.6.3B) and (II.6.3C)) and consequently at these points z-correlation is responsible for the entire correlation effect. Bearing in mind that z-correlation is the most dominant correlation-type, it may appear at first sight puzzling that the area where it possess a sizeable influence is relatively small. We must remember, though, that this area is a region of high probability and therefore z-correlation has the capacity to move a large amount of charge between the nuclei which has a large bearing upon the correlation energy.

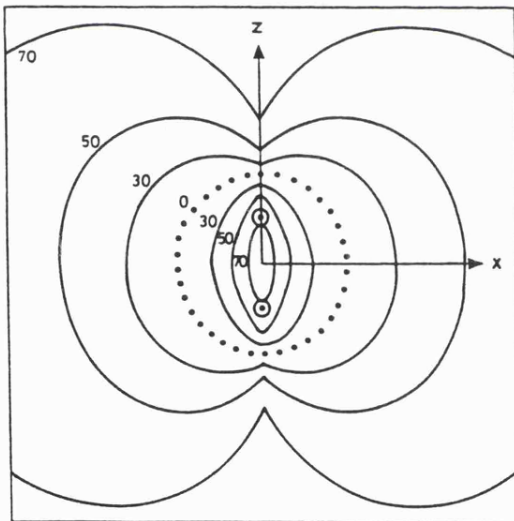
From Figure (II.6.3B) we see that the influence of ϕ -correlation increases rapidly as electron 1 is located at



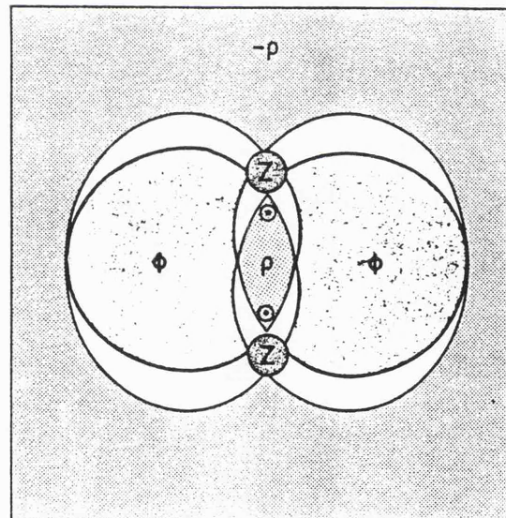
(A) Percentage z-correlation



(B) percentage ϕ -correlation



(C) percentage ρ -correlation



(D) regions where each correlation-type is most important

Figure (II.6.3) The percentage contributions from z , ϕ and ρ -correlation to the total correlation effect in the xz -plane using Equations (II.6.19-21) and also the regions where each correlation-type accounts for more than fifty percent of the total effect.

further distances from the bond axis to reach a maximum of one hundred percent at the intersection of the zero contours from the z and ρ -percentage contribution surfaces. Since this maximum lies almost 1.5 a.u. from the bond, the probability density is relatively small when compared to the on-axis density, and hence the contribution from ϕ -correlation to the total contribution is less important than the z -correlation contribution.

Close to the molecular frame, ρ -correlation has the effect of redistributing electron probability to regions further from the molecule. Indeed, as shown in Figure (II.6.3C), this type of ρ -correlation is responsible for all of the correlation when electron 1 is located in the mid bond position. As the effect of z and ϕ -correlation increase to their maximum levels, the effect of ρ -correlation diminishes until an elliptical zero contour is obtained. Far from the molecule, however, the effect of ρ -correlation once again becomes dominant, but now the movement in probability is towards the molecular axis. The probability density is tiny for large r_1 and consequently this region is unimportant physically. Nevertheless, it is pleasing to note that the contours become radial in nature at these large distances and hence, tend towards the redistribution one would expect to observe in the He atom. The effect of ρ -correlation is therefore the most complex as it is responsible for relocating probability in two opposing directions depending upon the location of electron 1.

The important regions of each of the correlation-types,

defined by contributing over fifty percent of the total correlation effect, are presented in Figure (II.6.3D) from which it can be seen that only over a relatively small area of the surface there is no dominant correlation-type.

CHAPTER II.7

Results for H_3^+ in Position-Space

For the purposes of this analysis, the correlated and non-correlated electron distributions for the equilateral triangle conformation of the H_3^+ molecule have been evaluated from the Salmon and Poshusta^(2.vii.1) and the Schwartz and Schaad^(2.vii.2) wavefunctions, respectively. Both wave functions are written in Cartesian co-ordinates, with their origins fixed at the centre of the triangle formed by the nuclei. As seen in Figure (II.4.2), the x-axis has been defined to bisect nucleus A, the y-axis to be parallel to the line BC and the z-axis to be perpendicular to the plane of the molecule. For convenience, we have used this co-ordinate system for the analysis of correlation effects since, by fixing one of the co-ordinates, it is relatively simple to define a plane that is either parallel or perpendicular to the molecule.

The contours used in these surface views have been chosen from the same set as was employed in H_2 (see Chapter (II.5) for further details). The negative contours are still represented by broken curves, the positive contours by full curves and the zero contour by a dotted curve. In addition, the definitions

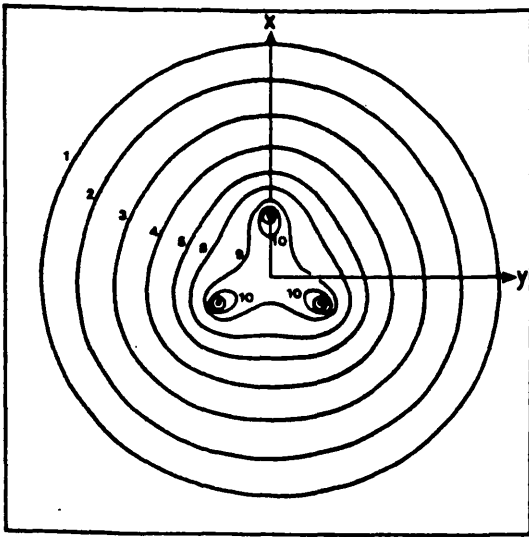
x = position of fixed electron which is located
relative to the nuclear frame

⊙ = position of nucleus

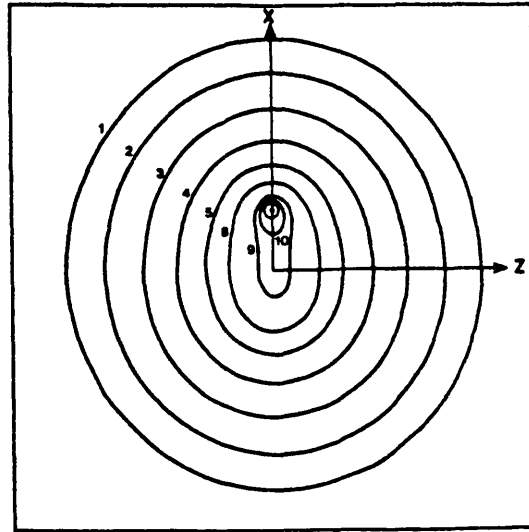
have been used. This analysis has been performed at the near equilibrium nuclear separation of 1.65 a.u.. The full width of the surfaces is 8 a.u. and consequently 9 millimetres corresponds to 1 a.u..

(II.7.1) The One-Particle Density Results

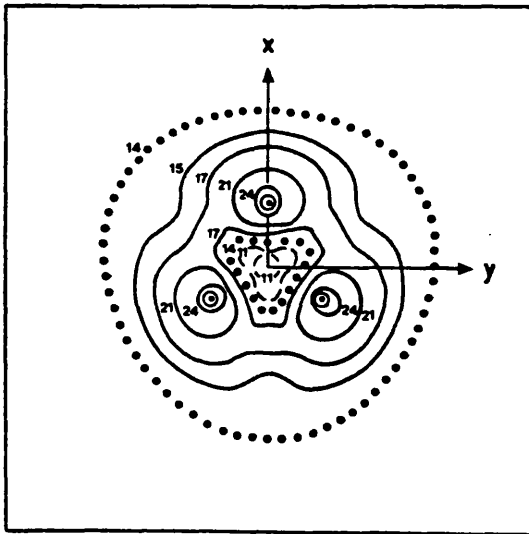
The one-particle density distribution $\rho(\underline{r}_1)$ and the difference in the one-particle density due to electron correlation $\Delta\rho(\underline{r}_1)$ have been evaluated in both the xy and xz-planes. Due to the three fold symmetry of the molecule, a comprehensive view of the electron probability distribution in the molecule may be built up from these planes.



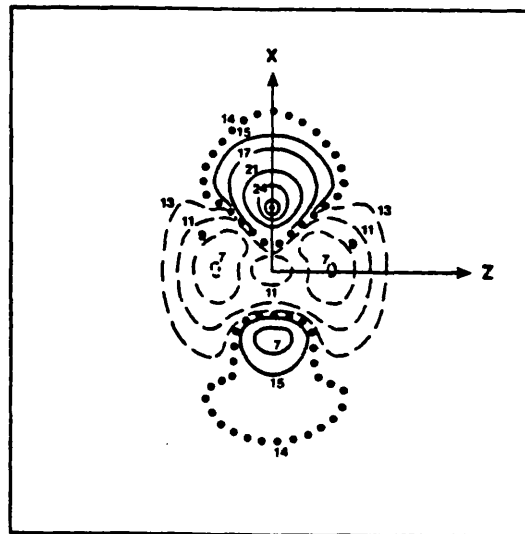
(A) $\rho(\underline{r}_1)$
xy-plane ($z = 0$)



(B) $\rho(\underline{r}_1)$
xz-plane ($y = 0$)



(C) $\Delta\rho(\underline{r}_1)$
xy-plane ($z = 0$)



(D) $\Delta\rho(\underline{r}_1)$
xz-plane ($y = 0$)

Figure (II.7.1) The one-particle density and Δ -one-particle density for H_3^+ in the xy-plane (with $z = 0$) and the xz-plane (with $y = 0$).

(II.7.2) The Two-Particle Density Results

Like the one-particle density, the Hartree Fock $V(\underline{r}_{12}, r_2)$ functions and the partial planar distribution surfaces $\Delta V(\underline{r}_{12}, \underline{r}_1)$ have been evaluated in both the xy and xz-planes. Consequently, the fixed electron positions have been chosen to lie on the x-axis and are summarised in Figure (II.7.2A). By fixing the distance between successive electron positions to be 0.4763 a.u. (ie $1.65/(2\sqrt{3})$ a.u.), position [A] may be used to investigate the effects of correlation outside of the nuclear framework. Position [B] is then located midway between two nuclei in the classical bonding region, position [C] is at the centre of the molecule and position [D] is midway between the centre of the molecule and a nucleus. The fixed electron is located on a nucleus in position [E] and position [F] is once again outside of the nuclear frame, this time near to a single nucleus. By evaluating the $V(\underline{r}_{12}, \underline{r}_1)$ and $\Delta V(\underline{r}_{12}, \underline{r}_1)$ surfaces for these fixed electron locations and chosen planes an extensive view of the effect of electron correlation on the H_3^+ molecule may be gained.

For reasons of space, both the HF distribution functions and partial planar Coulomb holes for both planes have been presented on the same graphs. It is also noted that, to enable comparisons to be made between curves from different fixed electron locations, the same scale has been used for all six positions. We have defined ϵ as the angle subtended between the x-axis and the vector \underline{r}_{12} in an anti-clockwise direction. Hence, due to the symmetry of the system, $U(\epsilon)$ and $\Delta U(\epsilon)$ have only been presented for $0^\circ \leq \epsilon \leq 180^\circ$.

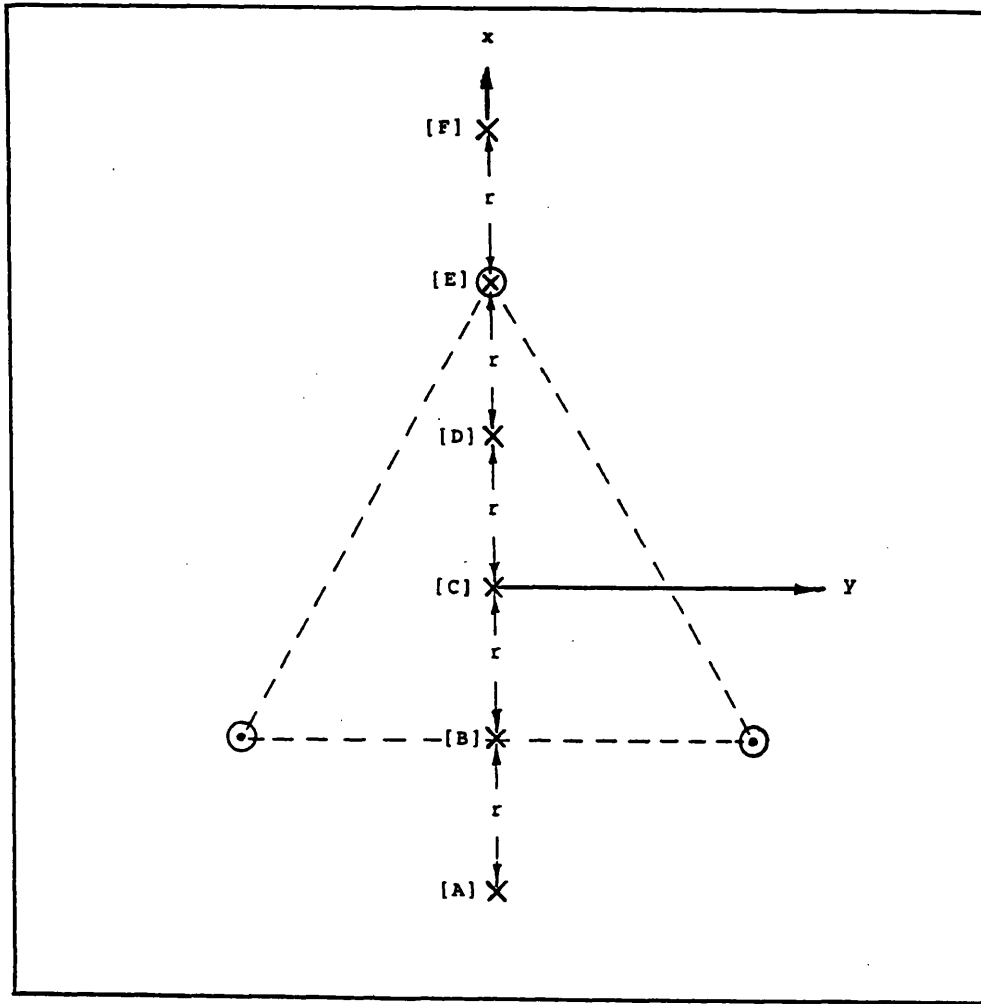


Figure (II.7.2A) The locations of the chosen fixed electron positions of the partial planar distribution functions for H_3^+ in position-space. The equilibrium nuclear separation, R , is 1.65 a.u. and the constant, r , has been chosen so that $r = R/2\sqrt{3} = 0.48$ a.u..

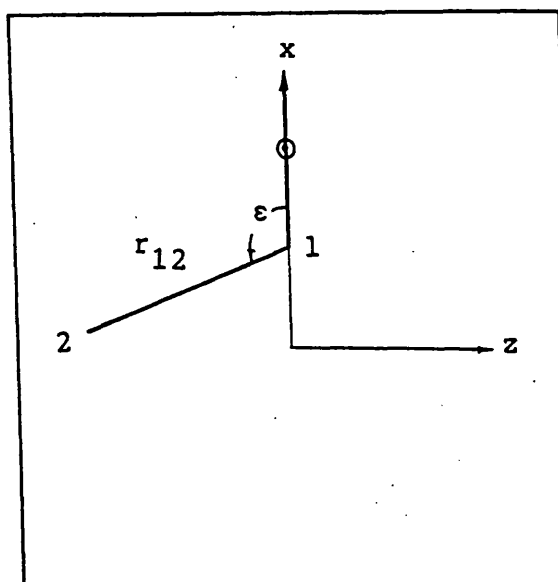
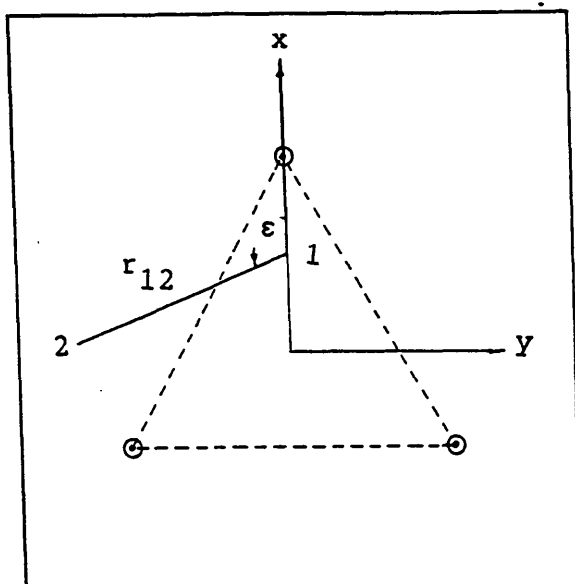
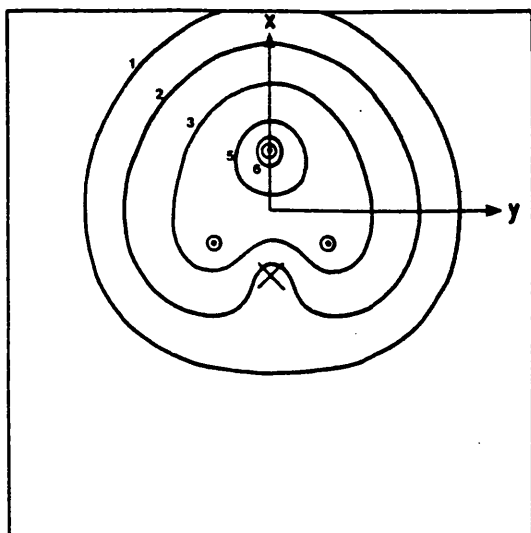
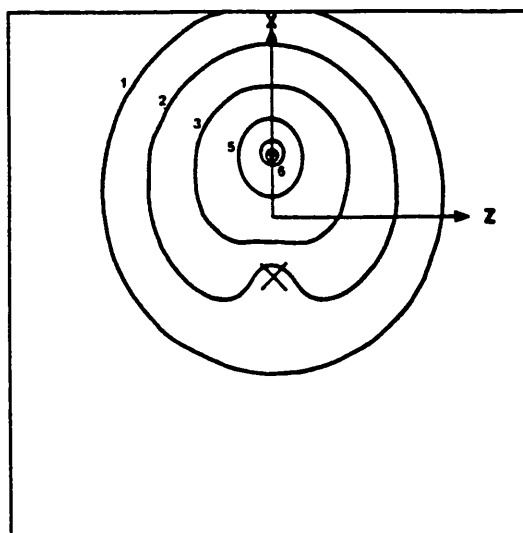


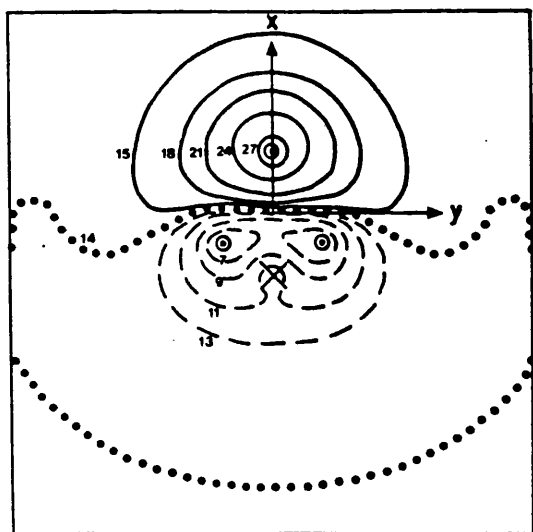
Figure (II.7.2B) & Figure (II.7.2C) The definition of the angle ϵ and the distance r_{12} when analysing correlation effects in (B) the xy -plane (C) the xz -plane.



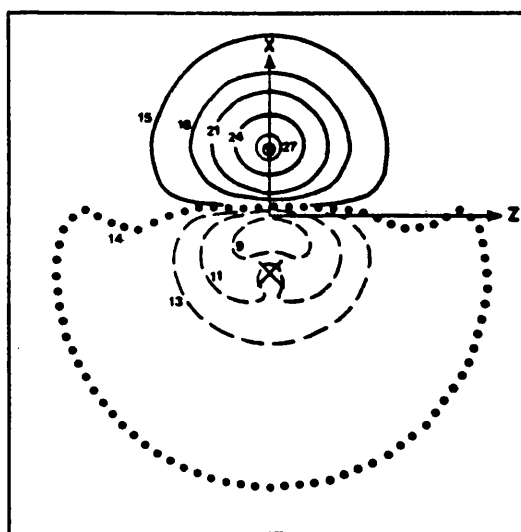
(A) $V(\underline{r}_{12}, \underline{r}_1)$
xy-plane ($z = 0$)



(B) $V(\underline{r}_{12}, \underline{r}_1)$
xz-plane ($y = 0$)



(C) $\Delta V(\underline{r}_{12}, \underline{r}_1)$
xy-plane ($z = 0$)



(D) $\Delta V(\underline{r}_{12}, \underline{r}_1)$
xz-plane ($y = 0$)

Figure (II.7.3) The Hartree Fock $V(\underline{r}_{12}, \underline{r}_1)$ surfaces and the $\Delta V(\underline{r}_{12}, \underline{r}_1)$ surfaces for fixed electron position [A] (see Figure (II.7.2A) for the definition).

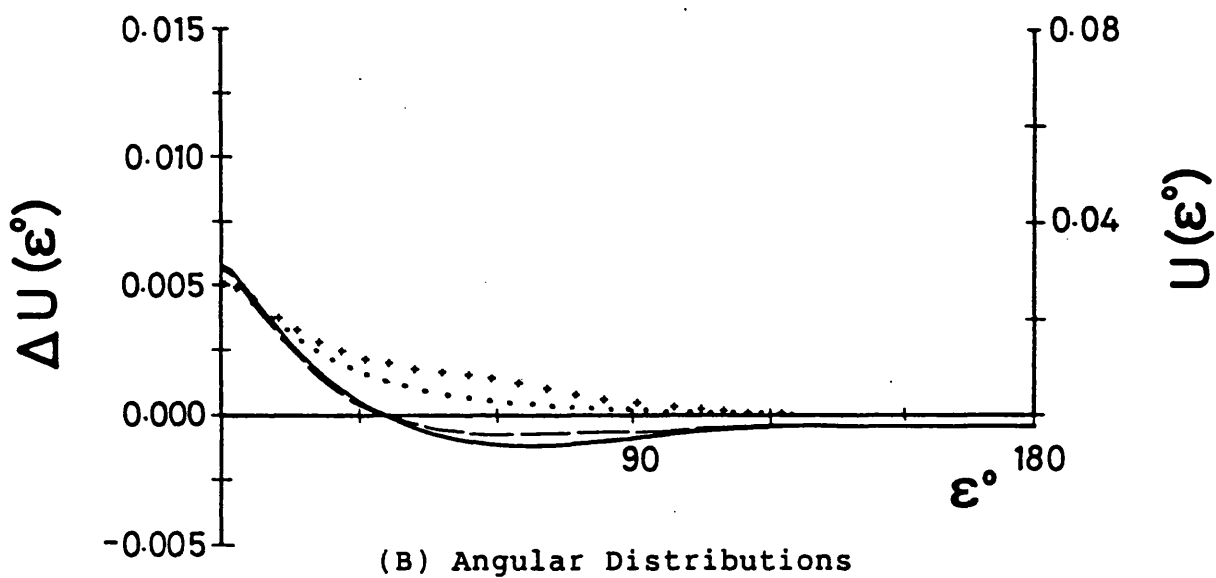
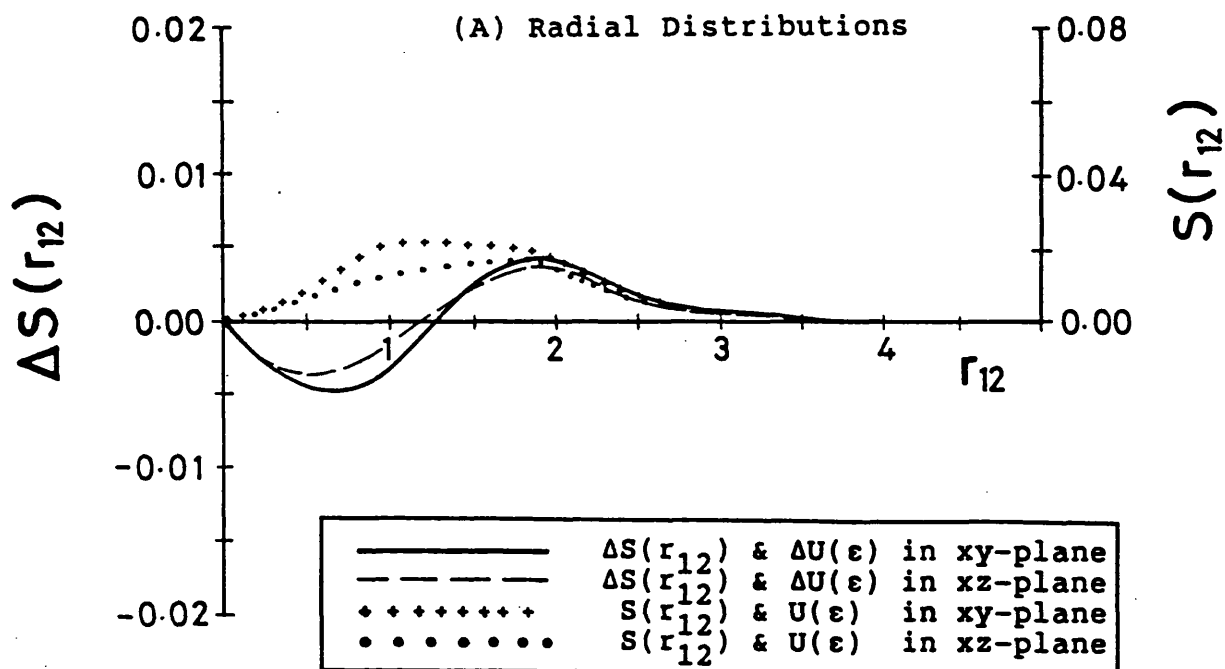
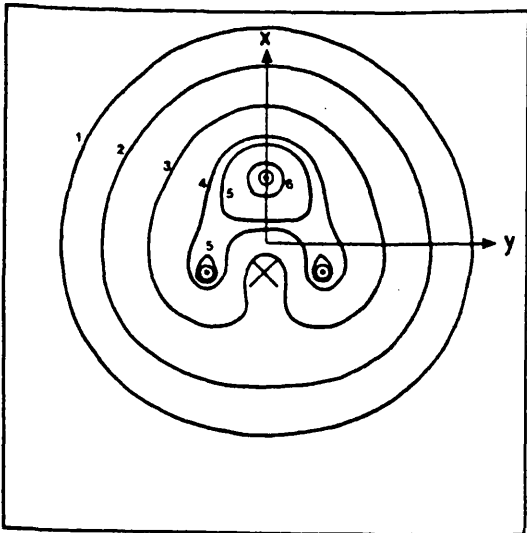
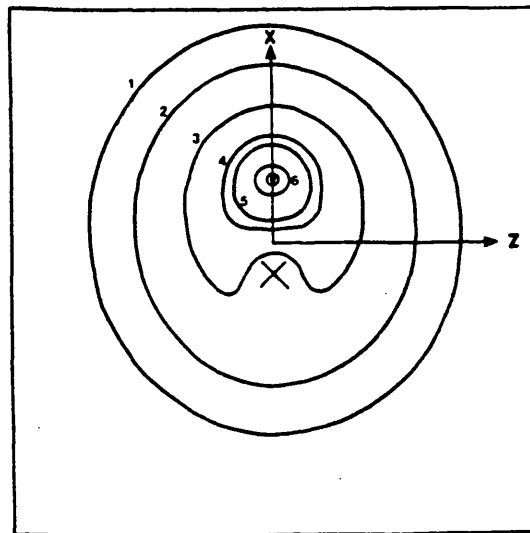


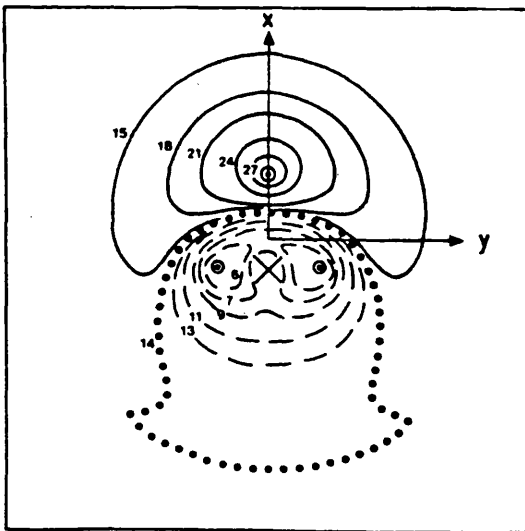
Figure (II.7.4) Partial planar Coulomb holes and distribution functions for H_3^+ , with electron 1 located at position [A] (see Figure (II.7.2A) for definition) and electron 2 moving either in the xy-plane or the xz-plane.



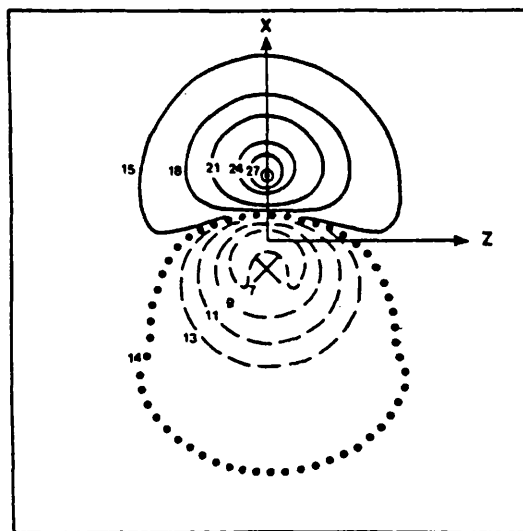
(A) $V(\underline{r}_{12}, \underline{r}_1)$
xy-plane ($z = 0$)



(B) $V(\underline{r}_{12}, \underline{r}_1)$
xz-plane ($y = 0$)



(C) $\Delta V(\underline{r}_{12}, \underline{r}_1)$
xy-plane ($z = 0$)



(D) $\Delta V(\underline{r}_{12}, \underline{r}_1)$
xz-plane ($y = 0$)

Figure (II.7.5) The Hartree Fock $V(\underline{r}_{12}, \underline{r}_1)$ surfaces and the $\Delta V(\underline{r}_{12}, \underline{r}_1)$ surfaces for fixed electron position [B] (see Figure (II.7.2A) for the definition).

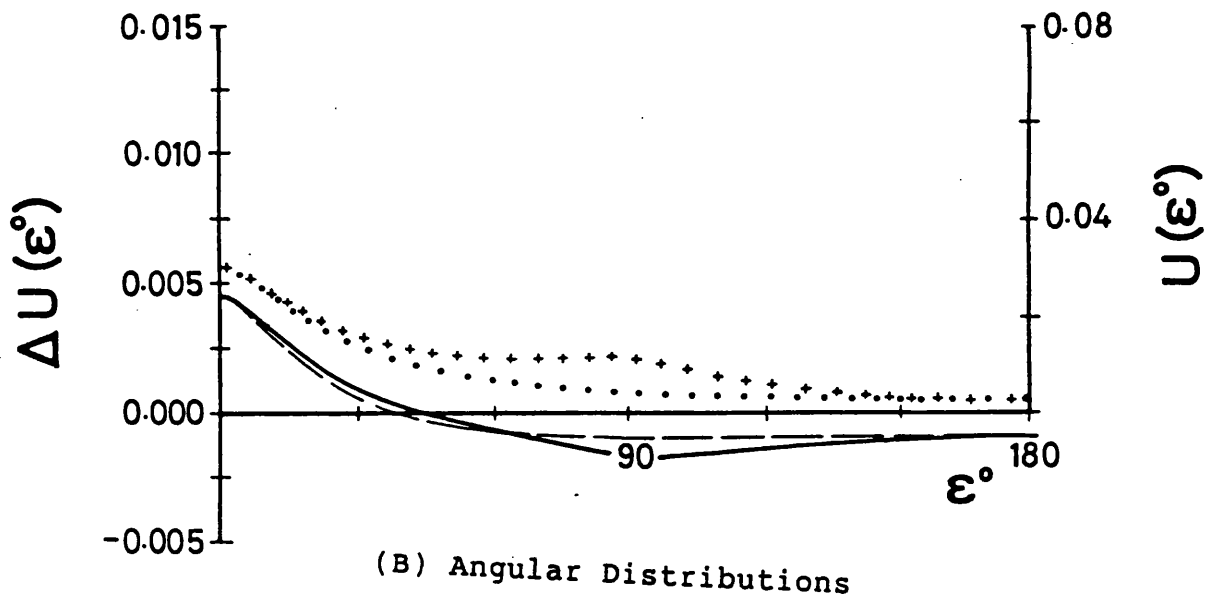
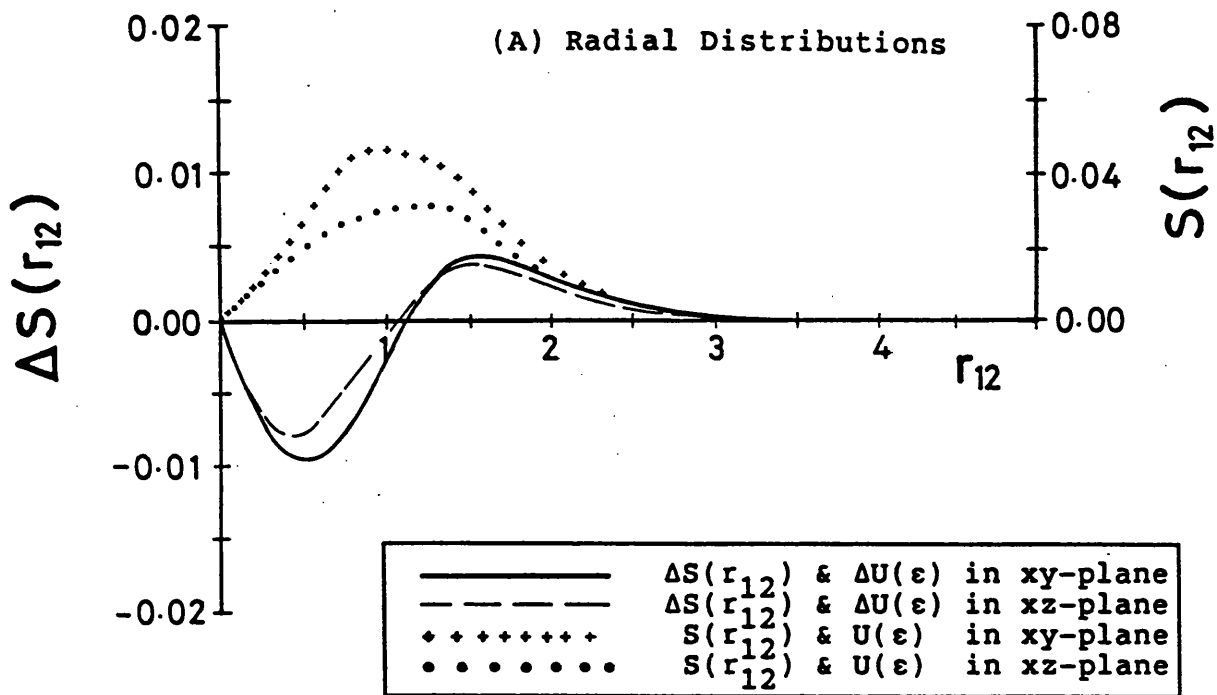
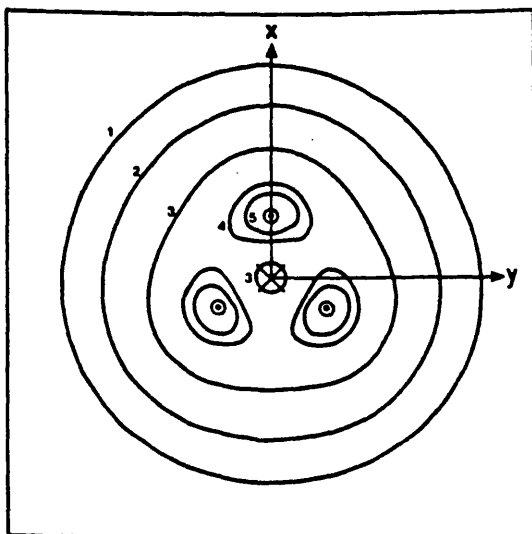
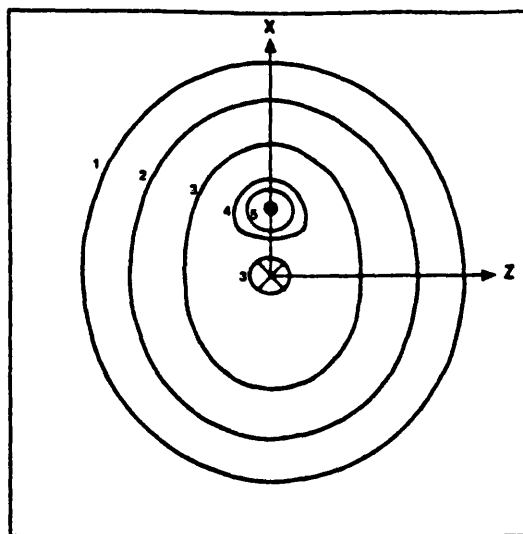


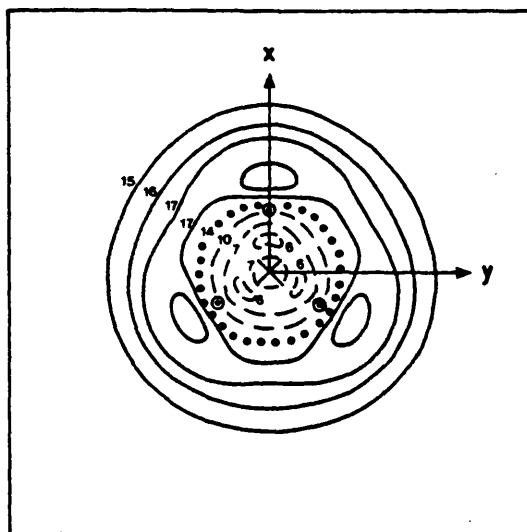
Figure (II.7.6) Partial planar Coulomb holes and distribution functions for H_3^+ , with electron 1 located at position [B] (see Figure (II.7.2A) for definition) and electron 2 moving either in the xy-plane or the xz-plane.



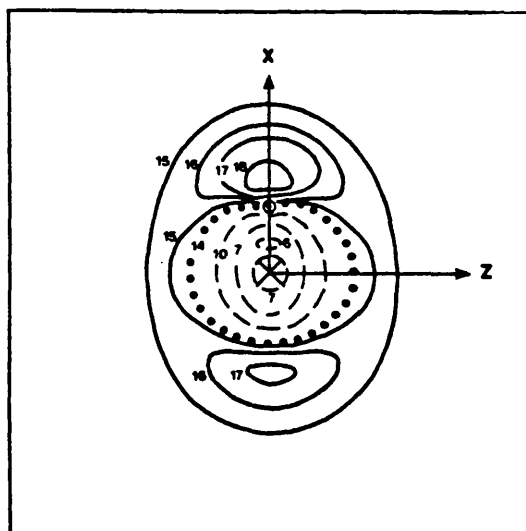
(A) $V(\underline{r}_{12}, \underline{r}_1)$
xy-plane ($z = 0$)



(B) $V(\underline{r}_{12}, \underline{r}_1)$
xz-plane ($y = 0$)



(C) $\Delta V(\underline{r}_{12}, \underline{r}_1)$
xy-plane ($z = 0$)



(D) $\Delta V(\underline{r}_{12}, \underline{r}_1)$
xz-plane ($y = 0$)

Figure (II.7.7) The Hartree Fock $V(\underline{r}_{12}, \underline{r}_1)$ surfaces and the $\Delta V(\underline{r}_{12}, \underline{r}_1)$ surfaces for fixed electron position [C] (see Figure (II.7.2A) for the definition).

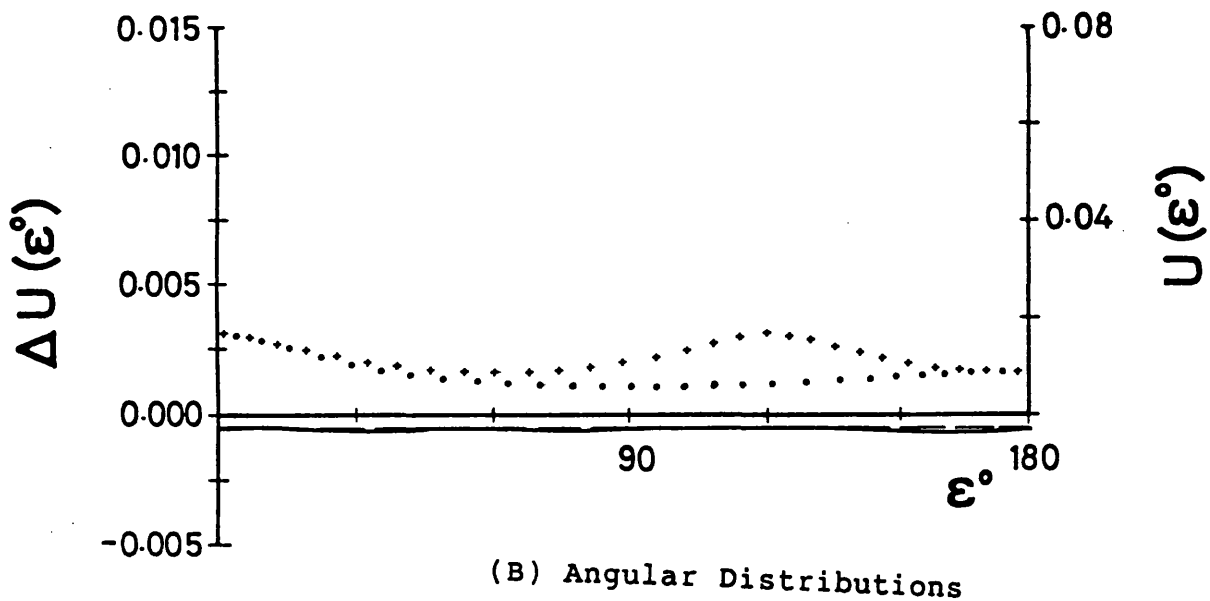
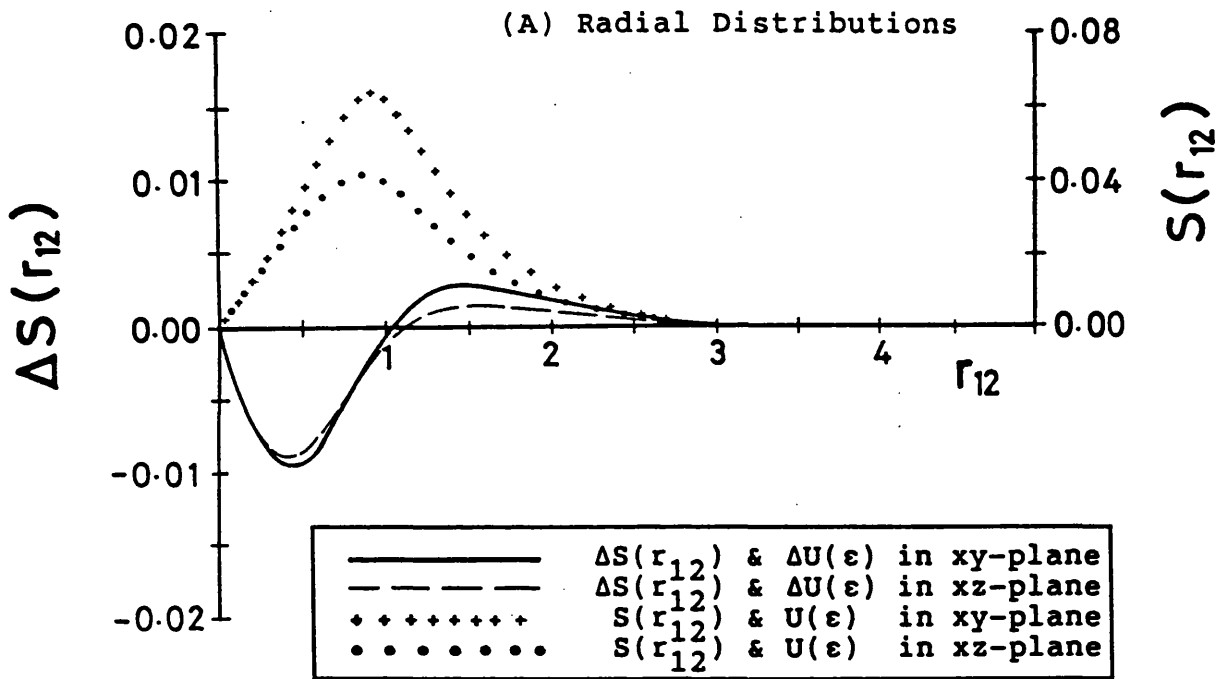
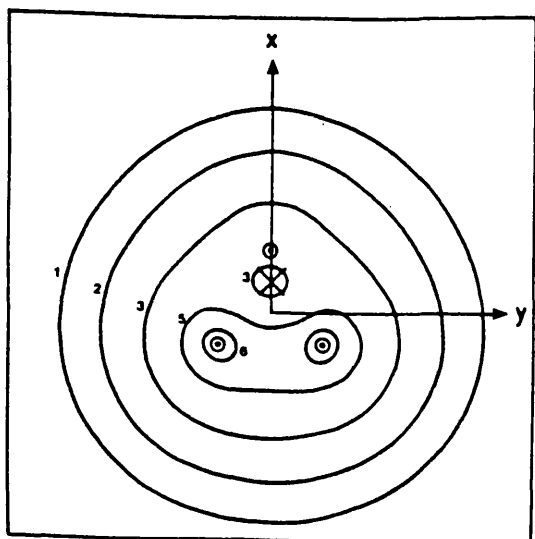
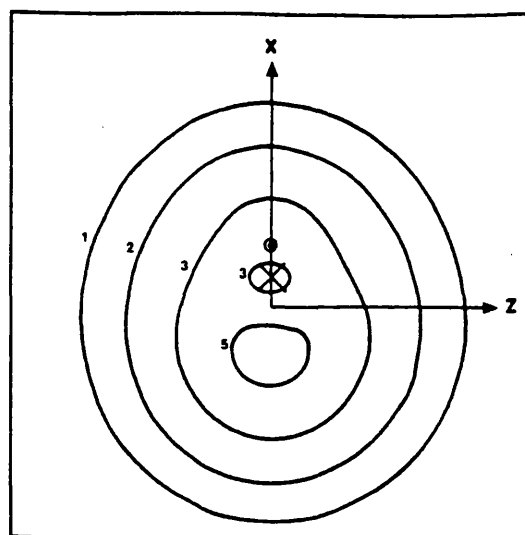


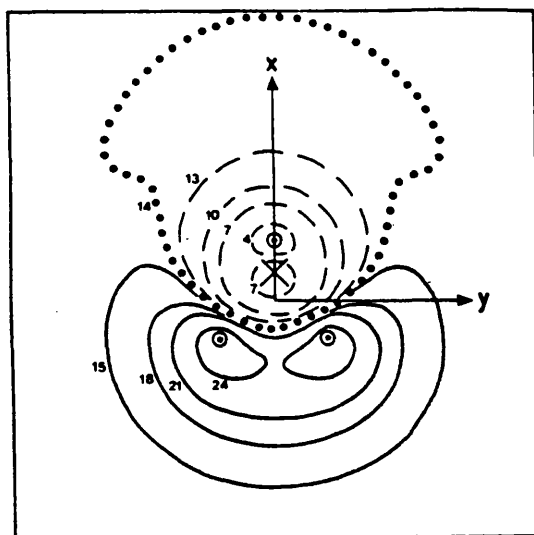
Figure (II.7.8) Partial planar Coulomb holes and distribution functions for H_3^+ , with electron 1 located at position [C] (see Figure (II.7.2A) for definition) and electron 2 moving either in the xy-plane or the xz-plane.



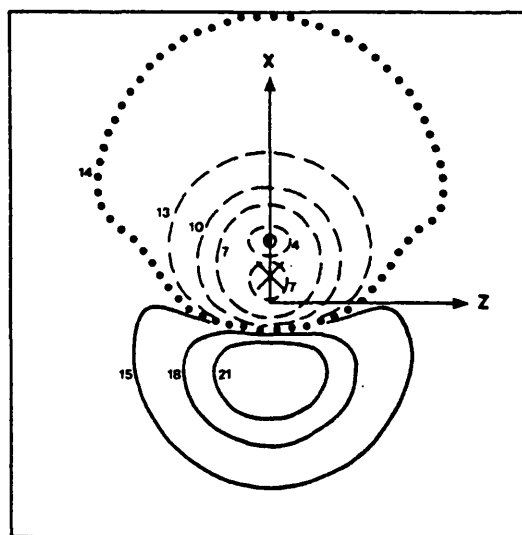
(A) $V(\underline{r}_{12}, \underline{r}_1)$
xy-plane ($z = 0$)



(B) $V(\underline{r}_{12}, \underline{r}_1)$
xz-plane ($y = 0$)



(C) $\Delta V(\underline{r}_{12}, \underline{r}_1)$
xy-plane ($z = 0$)



(D) $\Delta V(\underline{r}_{12}, \underline{r}_1)$
xz-plane ($y = 0$)

Figure (II.7.9) The Hartree Fock $V(\underline{r}_{12}, \underline{r}_1)$ surfaces and the $\Delta V(\underline{r}_{12}, \underline{r}_1)$ surfaces for fixed electron position [D] (see Figure (II.7.2A) for the definition).

(A) Radial Distributions

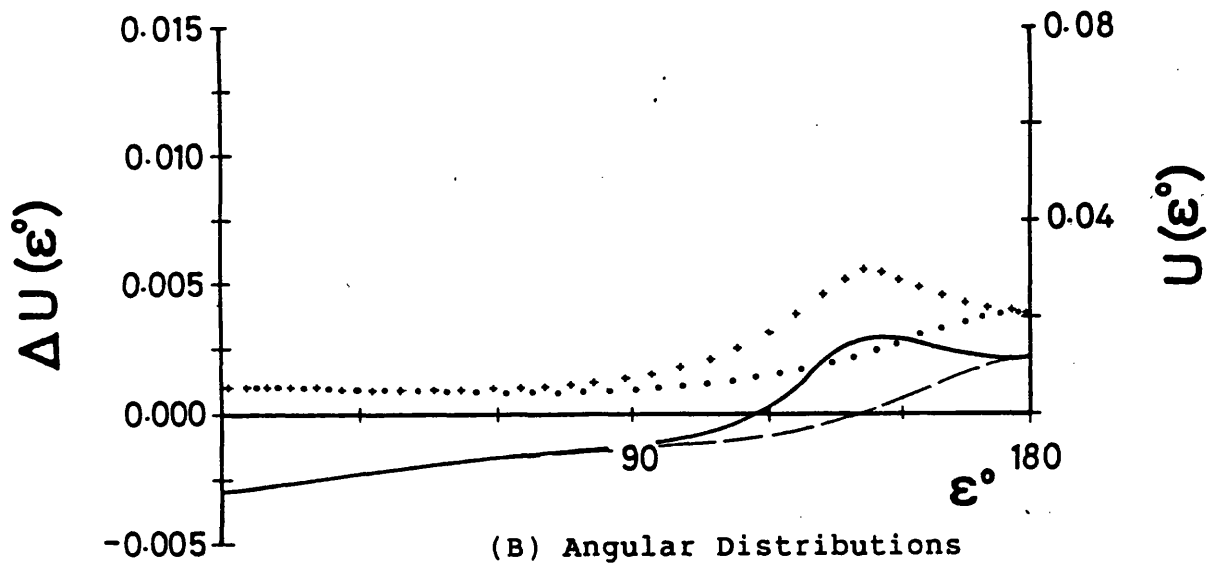
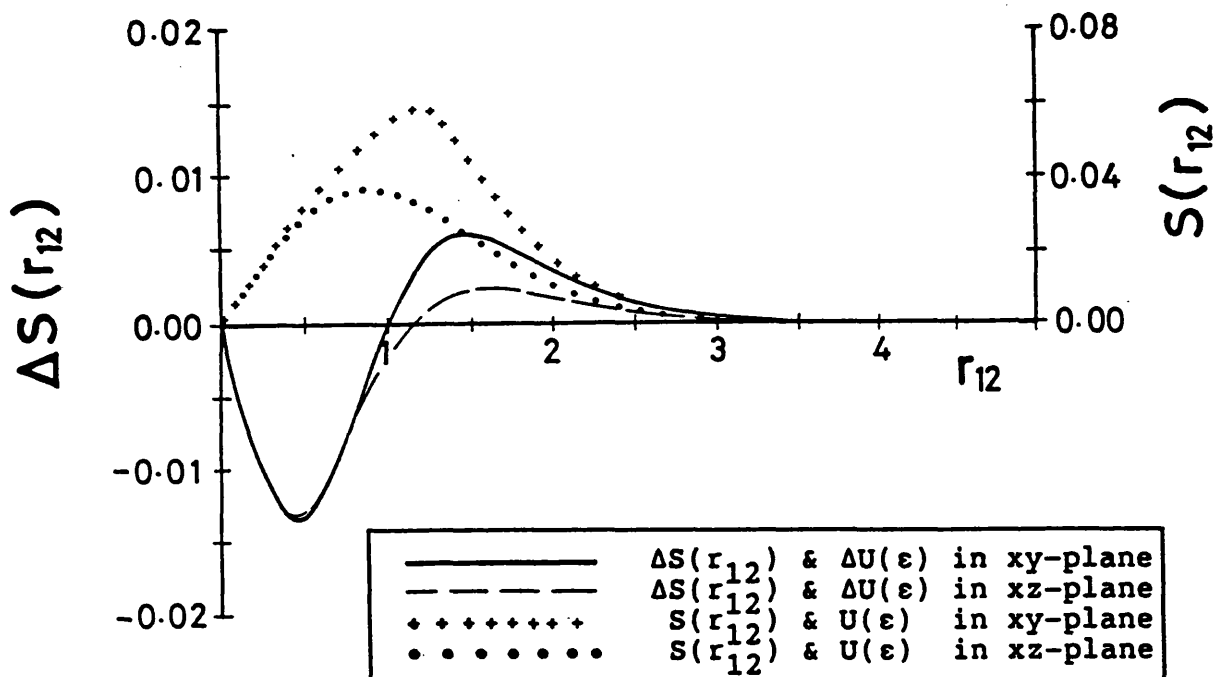
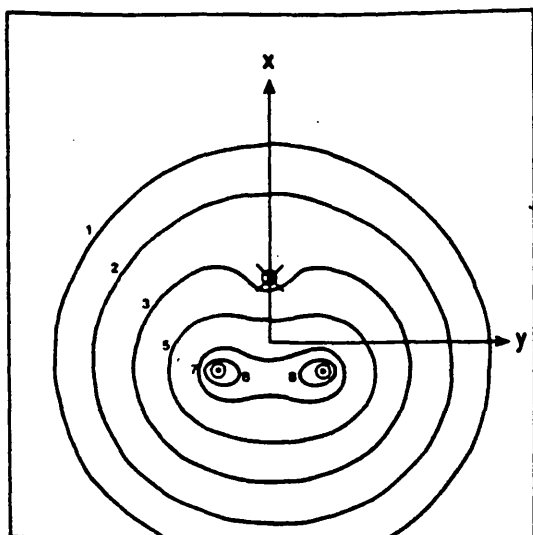
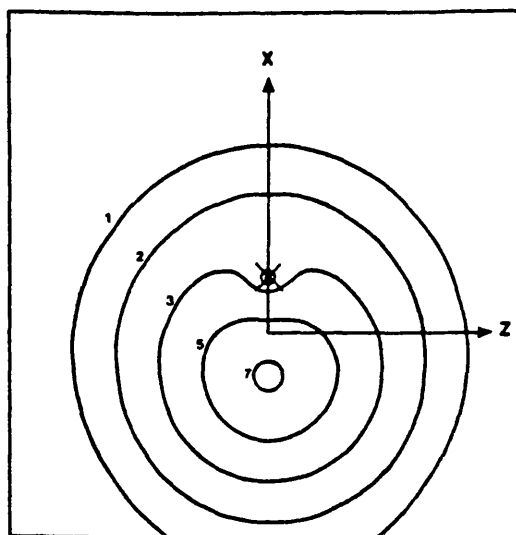


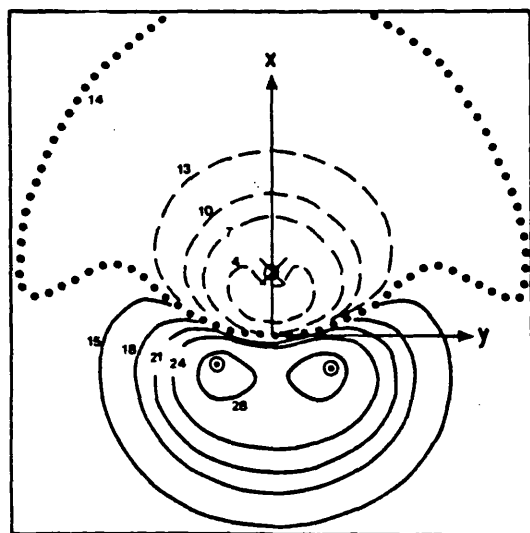
Figure (II.7.10) Partial planar Coulomb holes and distribution functions for H_3^+ , with electron 1 located at position [D] (see Figure (II.7.2A) for definition) and electron 2 moving either in the xy-plane or the xz-plane.



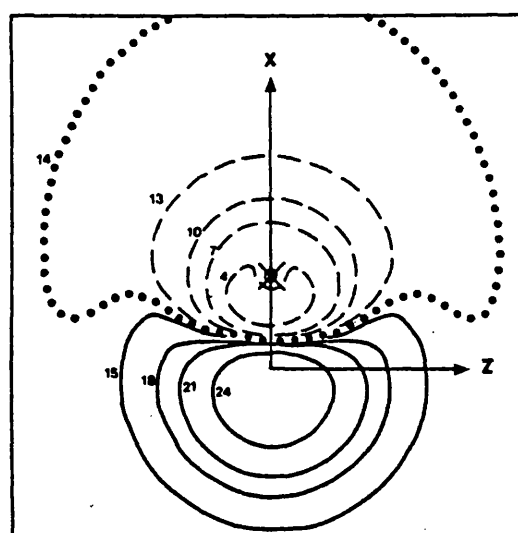
(A) $V(\underline{r}_{12}, \underline{r}_1)$
xy-plane ($z = 0$)



(B) $V(\underline{r}_{12}, \underline{r}_1)$
xz-plane ($y = 0$)



(C) $\Delta V(\underline{r}_{12}, \underline{r}_1)$
xy-plane ($z = 0$)



(D) $\Delta V(\underline{r}_{12}, \underline{r}_1)$
xz-plane ($y = 0$)

Figure (II.7.11) The Hartree Fock $V(\underline{r}_{12}, \underline{r}_1)$ surfaces and the $\Delta V(\underline{r}_{12}, \underline{r}_1)$ surfaces for fixed electron position [E] (see Figure (II.7.2A) for the definition).

(A) Radial Distributions

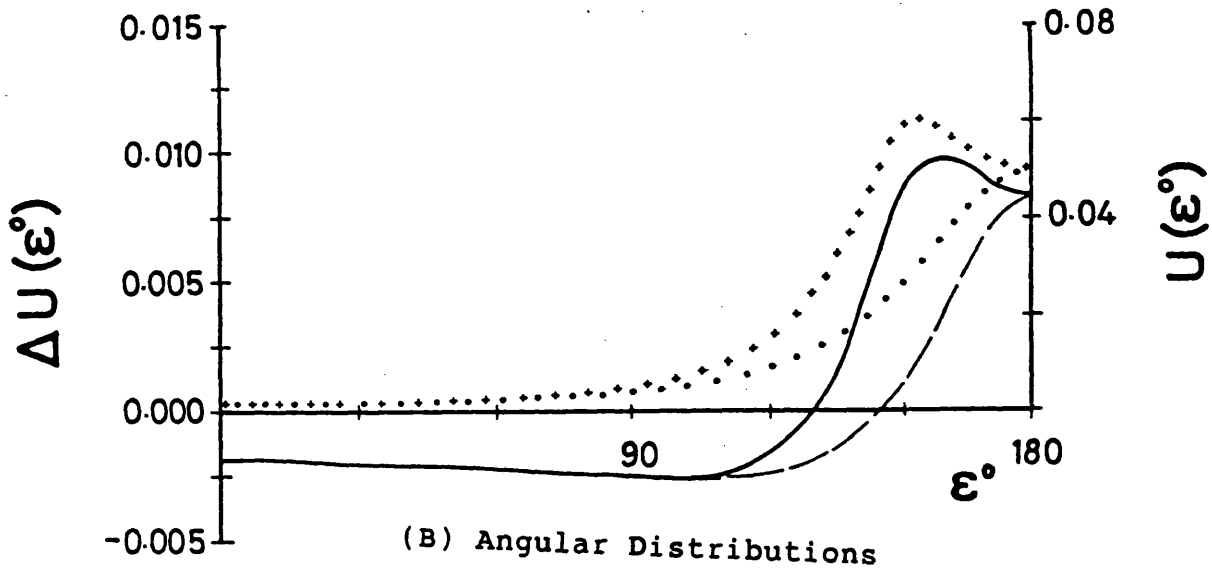
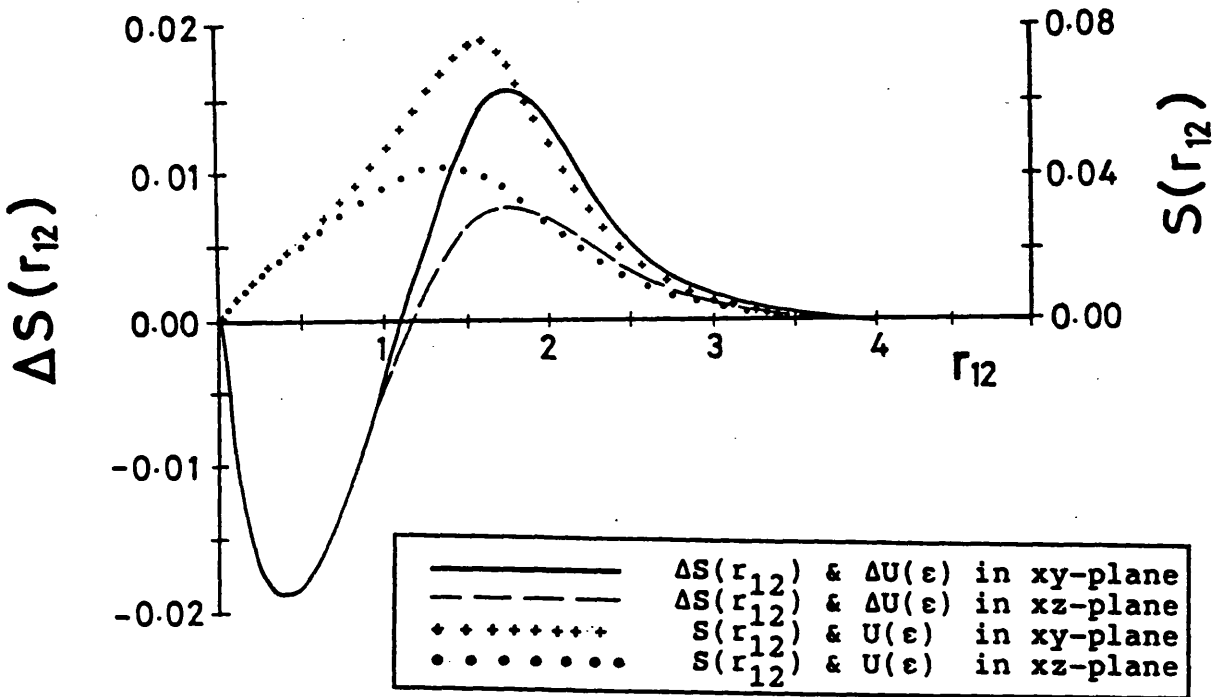
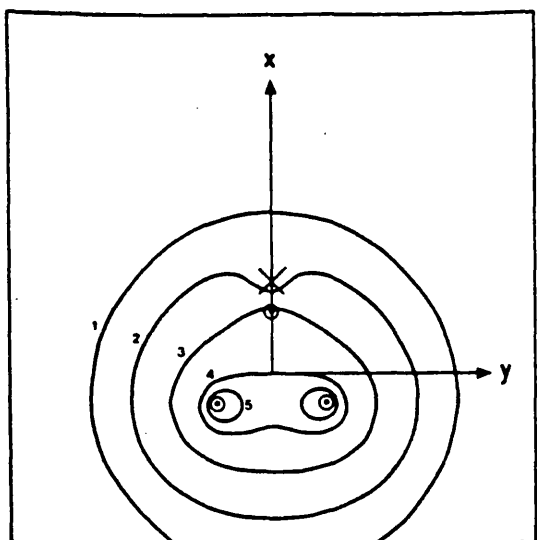
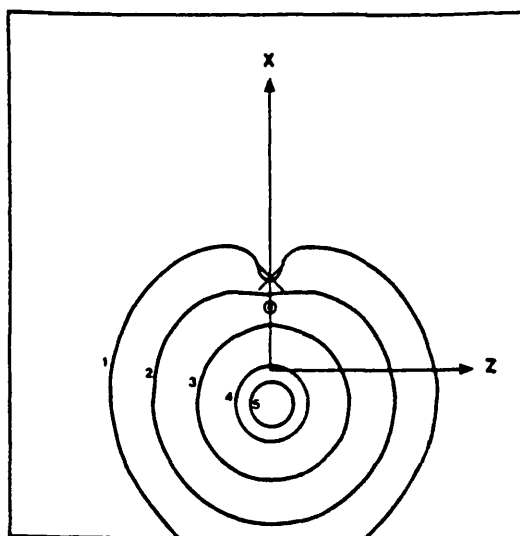


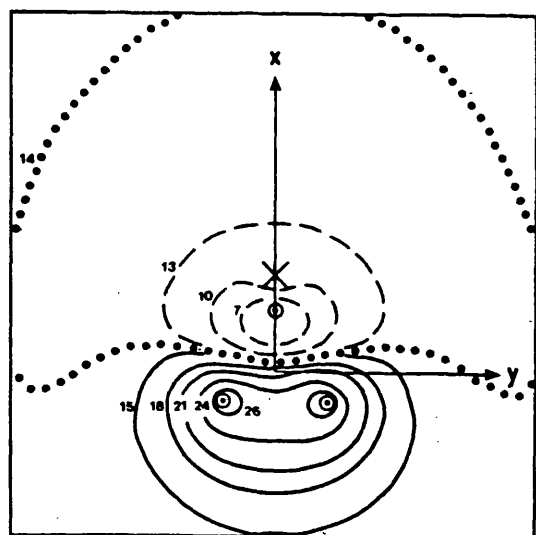
Figure (II.7.12) Partial planar Coulomb holes and distribution functions for H_3^+ , with electron 1 located at position [E] (see Figure (II.7.2A) for definition) and electron 2 moving either in the xy-plane or the xz-plane.



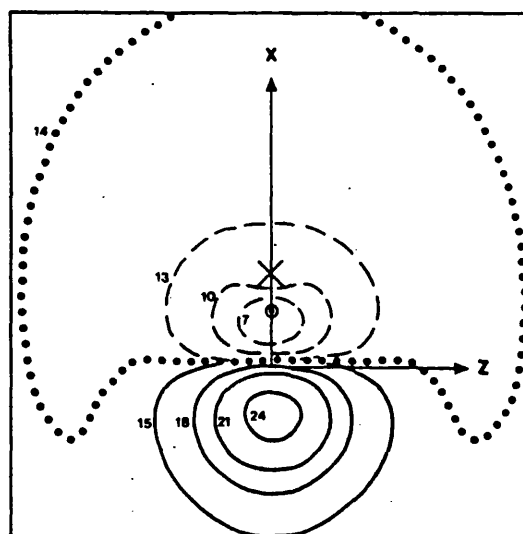
(A) $V(\underline{r}_{12}, \underline{r}_1)$
xy-plane ($z = 0$)



(B) $V(\underline{r}_{12}, \underline{r}_1)$
xz-plane ($y = 0$)



(C) $\Delta V(\underline{r}_{12}, \underline{r}_1)$
xy-plane ($z = 0$)



(D) $\Delta V(\underline{r}_{12}, \underline{r}_1)$
xz-plane ($y = 0$)

Figure (II.7.13) The Hartree Fock $V(\underline{r}_{12}, \underline{r}_1)$ surfaces and the $\Delta V(\underline{r}_{12}, \underline{r}_1)$ surfaces for fixed electron position [F] (see Figure (II.7.2A) for the definition).

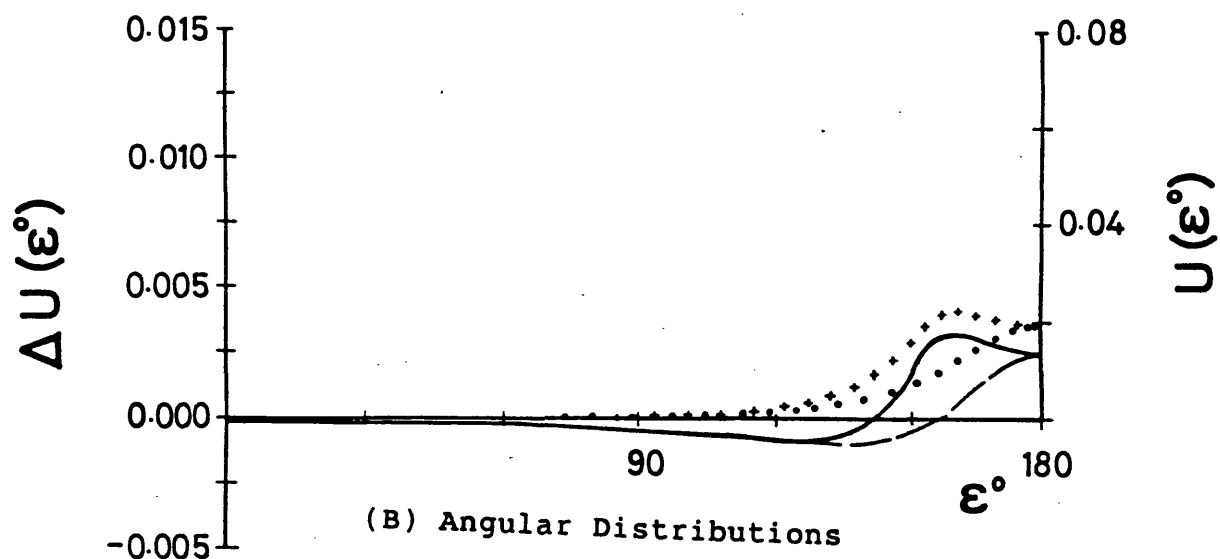
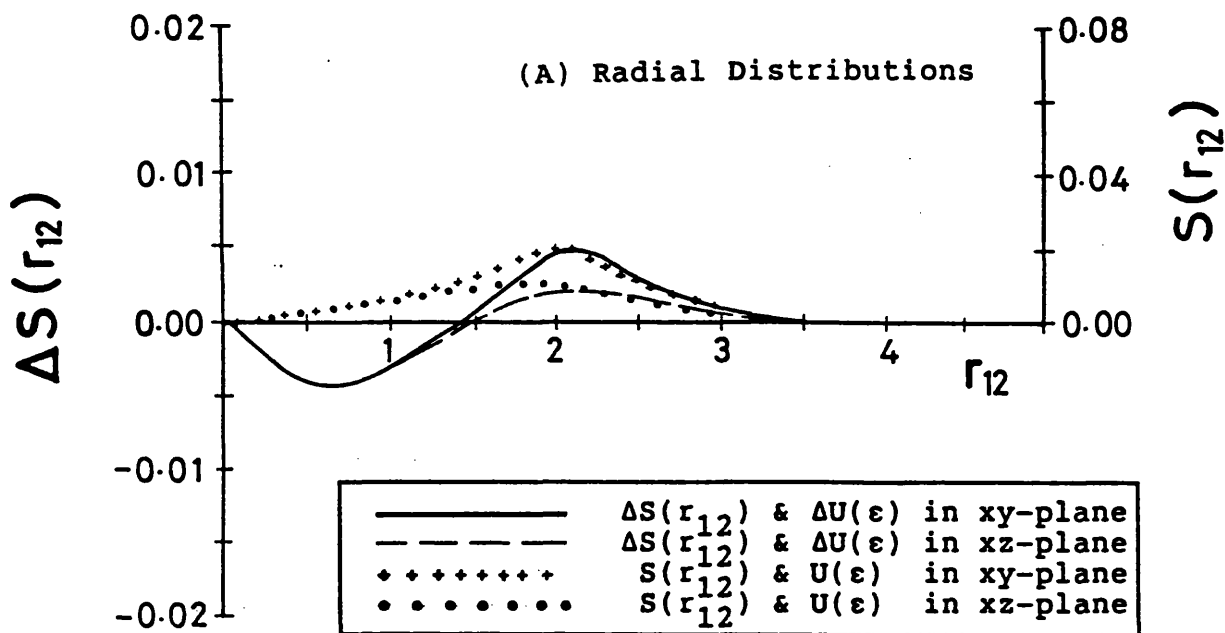


Figure (II.7.14) Partial planar Coulomb holes and distribution functions for H_3^+ , with electron 1 located at position [F] (see Figure (II.7.2A) for definition) and electron 2 moving either in the xy-plane or the xz-plane.

CHAPTER II.8

Discussion of H_3^+ Results in Position-Space

Since H_3^+ consists of three atoms yet only two electrons to bind them together, it is the simplest example of an electron-deficient system. Surprisingly, this type of bond is extremely strong, the binding energy of H_3^+ being almost twice that of H_2 (2.viii.1). An investigation into the effects of electron correlation on this system would therefore be very interesting as it could disclose information concerning electron-deficient systems. Consequently, this analysis has been performed with the H_3^+ molecule in its most stable nuclear conformation of an equilateral triangle with a nuclear separation of 1.65 a.u..

(II.8.1) The One-Particle Density Analysis

The HF one-particle density $\rho(\underline{r}_1)$ has been presented for the xy-plane ($z = 0$), the plane containing the molecule, and the xz-plane in Figures (II.7.1A) and (II.7.1B), respectively. Maxima of probability are associated with the sites of the nuclei, however, there is no build up of probability between them that would be characteristic of a 'normal' two-electron bond. Instead it appears that probability is drawn towards the centre of the triangle formed by the nuclei to create one central bond. By evaluating profiles of one-particle density functions in

specified directions, Duben and Lowe^(2.viii.2) have observed this effect and noted that it is typical of electron deficient bonding.

The effect of electron correlation on the HF one-particle density, given by $\Delta\rho(\underline{r}_1)$, is presented in Figures (II.7.1C) and (II.7.1D). At first sight the redistributions appear to be complex but the overall effect is to increase the the probability of discovering the electrons nearer to the nuclei. This property was seen earlier for the H_2 molecule, and similar accounts have been reported for many other systems (for example HeH^+ (2.viii.3), N_2 (2.viii.4) and CO (2.viii.5)). These authors have also noted that electron probability has been transferred from the regions where bonds have been formed.

Returning to H_3^+ , it is apparent that electron probability is reduced in two distinct regions within the molecule. From Figure (II.7.1C), three small minima may be observed near to the centre of the molecule, each of which may be associated with a particular 'bonding region'. From this, it seems that there are three distinct, but only partially occupied, σ -type 'bonds' which, due to the electron deficient nature of the system, are bent towards the centre of the molecule^(2.viii.6).

The second area from which probability is transferred may be seen from Figure (II.7.1D) to be above and below the molecular plane. The minima are much deeper than in the other region and, by considering the three-fold symmetry of

the molecule, we may observe that they actually form volumes of reduced probabilities above and below the plane of the molecule. This is a consequence of the fact that, since the Schwartz and Schaad HF wavefunction is constructed from floating 1s Gaussian orbitals located along the principal axes only, in attempting to describe the bonding accurately, it has been forced to overcompensate in the amount of charge located in these regions. This effect would be very much less well pronounced if a numerical HF wavefunction had been employed. Nevertheless, this emphasises the need to include configurations constructed from 2p STO or GTO orbitals with their nodal planes centred in the plane of the molecule in the correlated wavefunction.

(II.8.2) The Two-Particle Density Analysis

Like the one-particle density surfaces, the partial planar distribution functions have been evaluated in both the xy-plane (the plane containing the molecule) and the xz-plane (perpendicular to the molecule). The six chosen fixed electron locations, defined by [A] - [F], lie on the x-axis and are equidistant from each other (see Figure (II.7.2A) for the location of these points).

The HF $V(\underline{r}_2, \underline{r}_1)$ surfaces for the xy-plane and xz-plane have been presented in Figures (II.7.3A) and (II.7.3B), respectively for location [A]. There are two regions of high probability associated with the two closest nuclei but a much larger maximum in the vicinity of the furthest nucleus.

Thus, as would be expected, when electron 1 is located closer to two of the nuclei, the probability of locating electron 2 around the other nucleus is greater. By comparing the areas covered by the contours in both planes, it is also possible to build a three dimensional model of the shape of the electron probability distribution.

The effect of electron correlation on position [A] is shown in Figures (II.7.3C) and (II.7.3D). Electron probability has been transferred from the region near to the closest nuclei and between them to the vicinity of the furthest nucleus. The shape of the zero contour is also particularly interesting as it defines the locus where correlation has no effect. From Figure (II.7.3C) we see that it bisects the x-axis very close to the centre of the molecule and then, at larger distances from the molecule, it forms an unusual 'butterfly wing-shape'. This feature is also present in the xy-plane but much less pronounced, indicating that the two closest nuclei are at least partially responsible for the effect. The distribution at the 'edge' of the wings may be interpreted as being due to the effect of correlation redistributing probability between the nuclei whereas the shape near to the molecule is due mainly to radial correlation effects.

The $S(r_{12})$, $U(\epsilon)$, $\Delta S(r_{12})$ and $\Delta U(\epsilon)$ curves for the xy and xz-planes are all displayed in Figure (II.7.4). The first maximum of the $S(r_{12})$ curve in the xy-plane corresponds to the distance that the two nearest nuclei are away from the fixed electron and the inflection may be

attributed to the furthest nucleus. The xz-plane curve is very similar to the xy-plane except that the influence of the two nearest nuclei is less pronounced. This may also be illustrated in Figure (II.7.4B) by examining the $U(\epsilon)$ curve. The maximum at $\epsilon = 0^\circ$ is a result of the nucleus on the x-axis and the maximum at $\epsilon \approx 60^\circ$, which is missing in the xz-plane curve, to one of the other nuclei since the third nucleus would be located at $\epsilon \approx 300^\circ$. Apart from the maxima at $\epsilon = 0^\circ$ in the $\Delta U(\epsilon)$ curves, it is impossible to identify the location of the nuclei from the shapes of the partial planar Coulomb holes alone. It is interesting to note that, except for the slightly greater magnitude in the xy-plane, correlation has a very similar effect in both planes.

The fixed electron is located mid way between two nuclei in position [B] and the HF planar distribution surfaces are shown in Figures (II.7.5A) and (II.7.5B) for the xy and xz-planes, respectively. Again, from Figures (II.7.5C) and (II.7.5D), we see that correlation has the effect of removing electron probability from the centre of the molecule and near to each of the closest nuclei and of building it up around the furthest nucleus. The range of the correlation effect in the y-direction is very much reduced, however, due to the partial cancelling out of the effect of the fixed electron by the nuclei. The zero contour still exhibits the usual 'butterfly-wing' shape in the xy-plane although, in this case, it is bent very much further back due to the closer proximity of the nuclei and, in the confines of the nuclear triangle, it is more curved. This increase in curvature is associated with an increase in the

importance of radially-based correlation.

The geometry of the molecule is highlighted by the $S(r_{12})$ and $U(\epsilon)$ curves (see Figure (II.7.6)). Slightly misleading information may be derived from the $S(r_{12})$ curve in the xy -plane as the maximum is again due to the combined effect of two nuclei, each contributing half of the total effect. Electron correlation then simply transfers electron probability from the closest nuclei to the furthest.

Position [C] is located by electron 1 being fixed to be in the centre of the triangle formed by the nuclei. It is therefore reasonable that the partial planar distribution surface, shown in Figure (II.7.7A), should consist of three identical maxima at the sites of each of the nuclei. Figure (II.7.7B) illustrates that there is no ridge of probability between the nuclei that could be associated with conventional bonding in the same way as the one particle density function.

The effect of correlation on this fixed electron position proves to be very interesting. Firstly we note that the zero contour is contained within the molecular frame and the nuclei lie almost upon it. By examining Figure (II.7.7C) and (II.7.7D) we see that the zero contour forms a slightly distorted sphere. Correlation has the effect of transferring electron probability from within the nuclear triangle, and in particular in front of each of the nuclei, to distances further from the molecule, especially directly behind the nuclei. Hence, almost all of the correlation

effect is 'radially' based. This is illustrated further by examining the angular holes shown in Figure (II.7.8B). These curves almost form horizontal lines, demonstrating that the redistribution is almost spherically symmetric.

In position [D], the fixed electron is located closer to the single nucleus than the two off-axis nuclei. We see, therefore, in Figure (II.7.9C), that correlation has the effect of shifting probability from the closest nuclei to the two nuclei further away. The characteristic 'butterfly wing' shaped zero contour reappears in this diagram, except that it now is bent in the other direction. Close to the nuclei, the zero contour is curved which suggests that a large amount of correlation is still due to movement in a radial manner.

The fixed electron is located on the site of a nucleus in position [E]. From Figures (II.7.11A) and (II.7.11B) it may be seen that away from the immediate vicinity of the fixed electron the HF partial planar distribution function is almost axially symmetric with respect to the line joining the other nuclei. Here too, correlation has the effect of redistributing electron probability from just in front of the fixed electron to the vicinity of the other two nuclei. The zero contour is more flat than in position [C], indicating that, like H_2 , a greater contribution to the total correlation effect is due to movement in the x-direction (obviously, because of the different orientation of the axis, this is z-correlation in H_2).

The final fixed electron location, position [F], is again outside the triangle and a very large reduction in the probability distribution may be observed (see Figures (II.7.13A) and (II.7.13B)). In this location electron correlation transfers probability from the closest nucleus to the furthest nuclei but this time the zero contour is almost straight when inside the nuclear triangle. This suggests that almost all of the correlation effect is due to movement in the x-direction. Although the wing-shape of the zero contour is pronounced, we note that this is the first fixed electron position where the shape is more exaggerated in the xz-plane than in the plane of the molecule.

In summary we see that, as the fixed electron is moved from position [A] to [F] the effect of correlation in the x-direction decreases and in-out (radial) correlation compensates until it accounts for all of the correlation effect at the centre of the molecule. By drawing closer to a nucleus again the relative contribution of correlation in the x-direction increases again. From the work performed on H_2 , however, we would expect that, by moving further from the molecule, the relative effect of radial based correlation would become dominant once more but would now redistribute electron probability in directions towards the centre of the molecule.

If the fixed electron locations are rotated by 120° and 240° about the centre of the molecule to coincide with the other two principal axes identical results would be obtained. Consequently, we note firstly the importance of

redistributing probability between the centre of the molecule and each of the nuclei. This is similar to z-correlation in H_2 except, of course, that there are now three nuclei and the function must be antisymmetric with respect to each of them. From the results we can see that this type of correlation is the most important.

Correlation may also be analysed in terms of a radially based component. In view of the symmetry of the molecule, it is more logical to define this type of correlation as being perpendicular to each of the principal axes in all directions and may be introduced by including configurations of σ_g symmetry. This is similar to ρ -correlation (defined in the H_2 work) but superimposed in three directions.

Finally, an angular component of correlation is necessary that consists of independent rotations about the three principal axes. This effect cannot be observed in the chosen fixed electron positions since they all lie upon a principal axis and possess a high level of symmetry. This angular effect may be used to transfer electron probability to a region below the molecule when electron 1 is located above it.

Functions of these three forms could be used to incorporate the major amount of electron correlation in the system although, to improve the energy of the wavefunction further, second order correlation effects must be considered. Like H_2 , there are six independent second-order functions and each would possess the symmetry that is

associated with the product of two of the main correlation types with each other.

The analysis demonstrates the importance of including configurations constructed firstly from 2p orbitals fixed on the nuclei and pointing towards the centre of the nuclear triangle to describe correlation effects between the nuclei. Furthermore, configurations consisting of s-based orbitals that are located on the principal axes are needed to introduce radial-based correlation. Finally, configurations constructed from 2p orbitals with their nodal planes centred in the plane of the molecule are important to introduce correlation effects above and below the plane of the molecule.

CHAPTER II.9

Summary of Position-Space Analysis

The effects of electron correlation have been analysed in the ground states of the H_2 and H_3^+ molecules in terms of both one and two-electron probability distributions by employing the planar techniques described in Chapter (II.2)

The natural orbital^(2.ix.1) arrangement of the Kolos and Roothaan^(2.ix.2) wavefunction by Davidson and Jones^(2.ix.3) was used to describe the electron distribution in the H_2 molecule. By writing the wavefunction in this way, it has been possible to compute densities from natural orbitals for each symmetry type separately. The first natural orbital, which has by far the greatest effect, was shown to be an accurate approximation to the HF wavefunction. The second natural orbital is of σ_u symmetry with respect to the centre of the bond and was therefore responsible for introducing correlation by redistributing electronic charge between the nuclei in directions parallel to the molecular axis. Due to the alignment of the molecule with respect to the co-ordinate system, this has been defined as z-correlation. In a similar way, the third natural orbital, which possesses π_u symmetry with respect to the bond, introduced correlation by allowing electron probability to be redistributed axially around the bond and consequently has been defined as ϕ -correlation. The fourth natural orbital, which possesses σ_g symmetry, is responsible for introducing correlation in

all directions perpendicular to the bond and hence has been defined as ρ -correlation. The remaining six natural orbitals taken together were found to contribute only about eight percent of the correlation energy and, by examining the symmetries of these orbitals, it was observed that they represented second order effects to the first three main correlation types. Thus, they were seen to play only a minor role in introducing correlation effects.

In a similar way to that in which atomic correlation effects were analysed in terms of 'radial' and 'angular' correlation^(2.ixi.4), the effect of electron correlation on H_2 was analysed with respect to the relative composition of z , ϕ and ρ -correlation. A similar type of analysis to this could be used to investigate the effects of correlation on individual bonds in multi-bonded molecules.

(II.9.1) The One-Particle Density

The HF one-particle density surface $\rho(\underline{r}_1)$ and the difference due to correlation $\Delta\rho(\underline{r}_1)$ were evaluated in the plane containing the nuclei for both molecules and also perpendicular to the molecule for H_3^+ . The effects of z , ϕ and ρ -correlation were observed for H_2 although, without explicit reference to the other electron, only a very general view of the effects of correlation could be observed.

We found that electron correlation has the effect of transferring electronic probability from the regions where bonding occurs to the vicinity of the nuclei for both molecules. This was seen to be consistent with observations made on other systems^(2.ix.5,6) and indicates that the HF description of the molecule overcompensates in the amount of charge redistributed into the bonding region in molecular formation. Consequently, evidence of a conventional σ bond could be seen in the H_2 molecule whereas, in H_3^+ , σ -type bonds were seen to bend towards the centre of the nuclear triangle due to the electron deficient nature of the system (obviously these are only partial occupied). In the case of H_3^+ , however, much greater amounts of electron probability were also removed from regions above and below the plane of the molecule. This is a result of the fact that, since the HF wavefunction for H_3^+ is constructed from 1s GTO's located along the principal axes, by attempting to describe accurately the bond formation in the plane of the molecule, it has been forced to overcompensate in the amount of charge located in these regions. This emphasised the importance of including configurations that are constructed from 2p-type STO or GTO orbitals with their nodal planes corresponding to the plane of the molecule in the correlated wavefunction.

(II.9.2) The Two-Particle Density

The partial planar distribution functions $V(\underline{r}_{12}, \underline{r}_1)$ and the difference in the function due to correlation $\Delta V(\underline{r}_{12}, \underline{r}_1)$ as defined in Chapter (II.2) were used to obtain a realistic

interpretation of the effects of electron correlation on H_2 and H_3^+ .

Approximately ninety percent of the total effect of correlation on the H_2 molecule was found to be due to the product of the HF wavefunction with the z , ϕ and ρ -correlating configurations, respectively. These three terms were then analysed mathematically and simple pictorial views of each of the different types of correlation were obtained.

It was seen that, when the test electron was in the centre of the molecule, the greatest contribution was from ρ -correlation redistributing electronic probability away from the molecule. When the test electron was located closer to one particular nucleus, however, the z -correlation component became more dominant and when it was located to the side of the molecule, ϕ -correlation had a greater effect. At extremely large distances from the molecule, though, the importance of ρ -correlation became greatest once more, this time redistributing electronic probability towards the nuclei. In general, however, at regions of large electronic probability, z -correlation characteristics were seen to dominate the partial planar distributions, indicating the importance of orbitals possessing σ_u symmetry when describing conventional σ -bonds.

The test electron was fixed on a principal axis in the investigation of the effects of correlation on the H_3^+ molecule. The importance of 'radial-based' correlation (σ_g

symmetry) could be easily seen when the test electron was located at the centre of the molecule. Once it was moved closer to one nucleus, however, the predominant correlation movement very rapidly became in a direction from the closest nucleus to the furthest. Unfortunately, due to the high degree of symmetry in the chosen locations of the test electron, 'angular-based' correlation, although present in the correlated description of the H_3^+ molecule, could not be seen.

The radial and angular partial planar Coulomb holes which are generated by either angular or radial integration of the relevant Δ -partial planar distribution surfaces proved to be less useful than the full surfaces. Nevertheless, they were relatively simple to evaluate once the surface had been computed and enabled comparisons to be made between different Δ -surfaces. For example, from the radial holes, the effect of correlation upon the mean inter-electronic separation and the magnitude of the effect of correlation could be easily seen.

In summary, the partial planar distribution surface technique has been successful in describing the position-space correlation effects on the H_2 and H_3^+ molecules. The most important types of symmetry in the correlated description of the molecules and the regions where bonding occurs were observed. Furthermore, rudimentary principles concerning the effect of electron correlation in multi-centred systems have also been discovered which, in future, could be applied easily to more complex molecules.

MOMENTUM-SPACE ANALYSIS OF H_2 AND H_3^+

CHAPTER II.10

Introduction to Momentum-Space

The primary effort in quantum mechanical calculations is directed towards the determination of the appropriate wavefunction for a given system. Usually such functions are defined with respect to the positions of the constituent particles in the system but this is by no means unique. For instance, given an N-electron atom or molecule, it is equally possible to discuss the behaviour of the electrons in terms of their momenta. More formally, we may consider the system wavefunction, not in position-space, but in momentum-space^(2.x.1). Recently, a number of studies have shown that, as well as being able to provide valuable new information about certain chemical properties such as bond formation and scattering profiles, momentum-space calculations also contribute additional insight into the effect of electron correlation on the system.

From the early pioneering work of Eve^(2.x.2), Bragg^(2.x.3) and Gray^(2.x.4) more than three-quarters of a century ago, the historical development of this subject has been rather disjointed and has been summarised in an excellent review by Stuewer and Cooper^(2.x.5). Much of the work associated with momentum-space has been concerned with evaluating accurate Compton profiles as this is a means by which experimental and theoretical work may be compared. Within the impulse approximation^(2.x.6) it is possible to

show that, for an isotropic system, the Compton profile $J(q)$ is

$$J(q) = \frac{1}{2} \int_{p=q}^{\infty} [I(p)/p] dp \quad (\text{II.10.1})$$

where q is the projection of the electronic momentum along the scattering vector (see for example references (2.x.7) and (2.x.8)). We may express $I(p)$ as

$$I(p) = \int_{\theta=0}^{\pi} \int_{\phi=0}^{2\pi} \rho(\underline{p}) p^2 \sin\theta d\theta d\phi \quad (\text{II.10.2})$$

and $\rho(\underline{r})$ represents the one-particle density. However, Dirac^(2.x.1) has shown that position and momentum-space orbitals are Fourier transforms of each other. Thus by examining equation (II.10.3) it may be seen that $\rho(\underline{p})$ is simply the momentum-space one-particle density and hence $I(p)$ is the radial momentum distribution. By employing accurate momentum-space wavefunctions, however, it is possible to evaluate Compton profiles directly.

Additional information concerning the effect of electron correlation may also be acquired through momentum-space studies. As mentioned briefly in Chapter (II.1), Banyard and Reed^(2.x.9) discovered that, relative to the HF description, radial-based correlation increases the probability of a large momentum separation $p_{12} = |\underline{p}_1 - \underline{p}_2|$ and decreases the

occurrence of smaller values of p_{12} . However, they also found that the effect of introducing angular-based configurations is to produce, on average, an enhanced alignment between the momentum vectors p_1 and p_2 . They concluded, therefore, that radial and angular based correlation effects for atoms with $1s$ symmetry act in opposition to each other. It is interesting to compare this with position-space calculations where both radial and angular correlation effects seek to increase the inter-electronic separation and thus augment each other. A comparative analysis of the effects of the z , ϕ and ρ -correlation for the hydrogen molecule in momentum and position-space would consequently prove intriguing.

In this chapter it is also useful to discuss the physical interpretation of momentum-space. For example, although a high momentum corresponds to a large kinetic energy and therefore to an electron very close to a nucleus, the site of a nucleus can not be specifically located in momentum-space. Also, for the case of homonuclear molecules, the momentum distributions are single-centred since the momentum of an electron associated with each of the nuclei is identical. The origin in momentum-space, that is when $p=0$, corresponds to an electron at rest and hence far from the influence of the nuclei. Due to the Fourier transform, however, no information may be obtained as to the direction of the electron relative to the nuclear frame. All that may be concluded is that the electron is located on an infinitely large sphere, centred on a nucleus. There is

therefore an inverting effect between position and momentum-space. Hence, rather than the distribution of valence electrons in position-space being diffuse and difficult to analyse, in momentum-space the distribution becomes peaked and short ranged. This is very useful as it emphasises the region in the molecule where bonding occurs.

The complimentary nature of the information obtained from the position and momentum distributions suggests that a full understanding of correlation effects requires the analysis to be performed on both spaces. In accordance with this, the following chapter outlines the techniques used to transform the position-space wavefunctions into momentum-space. Our earlier analysis of the correlation effects in H_2 , using a natural orbital approach, and H_3^+ has then been repeated in momentum-space.

CHAPTER II.11

Wavefunctions into Momentum-Space

There are two fundamentally different approaches to evaluating wavefunctions in momentum-space. The first is to formulate the Schrödinger equation directly in terms of the electronic momenta and then solve it, evaluating the wavefunction directly in momentum-space. The Schrödinger equation can be written as

$$(p^2/2m)\Psi(p_1, p_2, \dots, p_N) + [V(p_1, p_2, \dots, p_N) - E]\Psi(p_1, p_2, \dots, p_N) = 0$$

(II.11.1)

in momentum-space. The N-electron momentum-space wavefunction is represented by $\Psi(p_1, p_2, \dots, p_N)$ and $V(p_1, p_2, \dots, p_N)$ is related to the Fourier transform of the position-space potential energy term $V(\underline{r}_1, \underline{r}_2, \dots, \underline{r}_N)$. The Schrödinger equation has therefore been transformed from a differential equation in position-space to an integral equation in momentum-space and, for this reason, evaluation of the momentum-space wavefunction by this method is mathematically complex. Svatholm^(2.xi.1) has developed an iterative method of solving the equation, based upon the Gauss-Hilbert variational principle and the Kellogg theory of iterated functions^(2.xi.2). McWeeny and Coulson were able to obtain approximate wavefunctions for the helium atom^(2.xi.3) and hydrogen molecule^(2.xi.4) using this technique, but with limited success. They concluded that this method was impracticable for larger systems due to the

vast number of iterations required to obtain solutions of sufficient accuracy.

Fortunately, the second approach is much simpler to use and utilises the many highly accurate position-space wavefunctions that already exist. It has consequently enjoyed much more popularity and will also be used in this analysis. Dirac has shown^(2xi.5) that the position and momentum-space wavefunctions are simply Fourier transforms of each other. The one-electron position-space spin-orbital $\phi(\underline{r}, \underline{\sigma})$ can therefore be expressed in terms of its momentum-space equivalent $\phi(\underline{p}, \underline{\sigma})$ as

$$\phi(\underline{r}, \underline{\sigma}) = (2\pi)^{-3/2} \int \phi(\underline{p}, \underline{\sigma}) e^{i\underline{p} \cdot \underline{r}} d\underline{p}. \quad (\text{II.11.2})$$

The integration is understood to be performed only over \underline{p} and hence the spin-functions remain unchanged in either type of space. Obviously equation (II.11.2) can be rearranged as

$$\phi(\underline{p}, \underline{\sigma}) = (2\pi)^{-3/2} \int \phi(\underline{r}, \underline{\sigma}) e^{-i\underline{p} \cdot \underline{r}} d\underline{r} \quad (\text{II.11.3})$$

and can therefore be used to transform the individual spin-orbitals of the position-space wavefunction into momentum-space. It also follows that if the orbital were a function of the positions of two electron the transform would be

$$\phi(\underline{p}_1, \underline{p}_2) = ((2\pi)^{-3/2})^2 \int \phi(\underline{r}_1, \underline{r}_2) \exp(-i(\underline{p}_1 \cdot \underline{r}_1 + \underline{p}_2 \cdot \underline{r}_2)) d\underline{r}_1 d\underline{r}_2. \quad (\text{II.11.4})$$

Perhaps the most attractive features of the transformation method are firstly, the form of the wavefunction is

preserved in momentum-space. That is to say, since the total wavefunction may be transformed into momentum-space by simply transforming the individual basis-functions, the orbitals, configurations and consequently the complete wavefunction are constructed in the same way in each type of space. Secondly, since no approximations have been made, exactly the same amount of energy can be accounted for in each wavefunction. The only problem is that wavefunctions containing explicit reference to the inter-electronic distance cannot be transformed directly.

The same wavefunctions as used in the position-space analysis of the H_2 and H_3^+ molecules will therefore be used to investigate the momentum-space correlation effects.

(II.11.1) The H_2 Molecule

As discussed earlier in this thesis, the natural orbital wavefunction of Davidson and Jones^(2.xi.6) was used to investigate the effects of correlation on the hydrogen molecule as it could describe both the CI and SCF levels of accuracy. By performing a Fourier transform on the position-space representation of the wavefunction, it may be used to investigate momentum-space effects. In position-space the H_2 wavefunction may be written as

$$\Psi(\underline{r}_1, \underline{r}_2) = \sum_{i=1}^{10} \mu_i \begin{cases} \chi_i^*(\underline{r}_1) \chi_i(\underline{r}_2) & \text{if } m = 0 \\ \chi_i^*(\underline{r}_1) \chi_i(\underline{r}_2) + \chi_i(\underline{r}_1) \chi_i^*(\underline{r}_2) & \text{if } m \neq 0 \end{cases} \quad (\text{II.11.5})$$

where

$$\chi_i(\underline{r}) = (2/R)^{3/2} (2\pi)^{-1/2} \sum_{k=1}^{15} c_k \xi^{n_k} \eta^{j_k} (\xi^2 - 1)^{m_i/2} (1 - \eta^2)^{m_i/2} \exp(im_i \phi) \exp(-\alpha \xi). \quad (\text{II.11.6})$$

The constants c_k , n_k , j_k , m_i and α have been given by Davidson and Jones^(2.xi.6). To transform this wavefunction into momentum-space the natural orbitals $\chi_i(\underline{r})$ must be Fourier transformed, the transformed orbitals then being substituted back into equation (II.11.5) to form the complete momentum-space version of the Davidson and Jones wavefunction. A problem arises, however, as the natural orbitals are expressed in confocal ellipsoidal co-ordinates, making it exceedingly difficult to employ an analytical approach to carry out the necessary integrations. A semi-numerical method has therefore been developed and will be demonstrated in the following analysis.

For the confocal ellipsoidal co-ordinate system the incremental volume $d\underline{r}$ is given by^(2.xi.7)

$$d\underline{r} = (R/2)^3 (\xi^2 - \eta^2) d\xi d\eta d\phi \quad (\text{II.11.7})$$

where

$$\begin{aligned} 1 &\leq \xi \leq \infty \\ -1 &\leq \eta \leq 1 \\ 0 &\leq \phi \leq 2\pi. \end{aligned}$$

It is also possible to expand $\underline{p} \cdot \underline{r}$ with respect to nucleus A as the origin to produce

$$\underline{p} \cdot \underline{r} = p r^A (\cos\theta_p^A \cos\theta^A + \sin\theta_p^A \sin\theta^A \cos(\phi_p - \phi)), \quad (\text{II.11.8})$$

the nuclear geometry being illustrated in Figure (II.4.1). It is obvious, however, that $p \cos\theta_p^A$ is simply the component of momentum parallel to the z-axis and $p \sin\theta_p^A$ is the

component of momentum perpendicular to it, hence we may define

$$p' \cos \theta'_p = p_z$$

and (II.11.9)

$$p \sin \theta'_p = p_\rho$$

where z and ρ have their usual cylindrical co-ordinate connotations. By examining the geometry of the molecule it can also be shown that

$$r^A \cos \theta^A = (R/2)(1 + \xi\eta)$$

and (II.11.10)

$$r^A \sin \theta^A = (R/2)[(\xi^2 - 1)(1 - \eta^2)]^{1/2}.$$

Equations (II.11.9) and (II.11.10) can now be substituted into equation (II.11.8) to give

$$\underline{p} \cdot \underline{r} = p_z R(1 + \xi\eta)/2 + p_\rho R[(\xi^2 - 1)(1 - \eta^2)]^{1/2} \cos(\phi_p - \phi)/2. \quad (II.11.11)$$

The momentum-space natural orbital is constructed by substituting equation (II.11.6) into equation (II.11.3) and then introducing equations (II.11.7) and (II.11.11). The integration over the ϕ variable is separable, thus allowing the natural orbital to be written as

$$\chi_i(\underline{p}) = (2\pi)^{-2} (R/2)^{3/2} \int \int \sum_{k=1}^{15} c_k \xi^{nk} \eta^{jk} [(\xi^2 - 1)(1 - \eta^2)]^{mi/2} \exp(-\alpha\xi) (\xi^2 - \eta^2) \exp[-ip_z R(1 + \xi\eta)/2] I_i(\xi\eta) d\xi d\eta \quad (II.11.12)$$

where

$$I_i(\xi\eta) = \int \exp(im_i \phi) \exp\left[-ip_\rho R[(\xi^2 - 1)(1 - \eta^2)]^{1/2} \cos(\phi_p - \phi)/2\right] d\phi. \quad (II.11.13)$$

If the substitution

$$\phi = \phi_p - \pi/2 + \beta \quad (\text{II.11.14})$$

is made to equation (II.11.13) it can be rearranged to give

$$I_i(\xi\eta) = \exp(im_i(\phi_p - \pi/2)) \int_{\beta=0}^{2\pi} \exp\left\{-i(p_\rho R/2)[(\xi^2-1)(1-\eta^2)]^{1/2} \sin\beta + m\beta\right\} d\beta. \quad (\text{II.11.15})$$

This equation, however, can be compared with the generating function of a Bessel function^(2.xi.8)

$$J_n(z) = (1/2\pi) \int \exp(iz\sin\beta - m\beta) d\beta,$$

thus allowing equation (II.11.15) to be written as

$$I_i(\xi\eta) = 2\pi \exp(im_i(\phi_p - \pi/2)) J_m(p_\rho R[(\xi^2-1)(1-\eta^2)]^{1/2}/2). \quad (\text{II.11.16})$$

The ϕ integration being accomplished, equation (II.11.16) may be substituted into equation (II.11.12) to form the remaining ξ and η integrals

$$\chi_i(p) = (2\pi)^{-1} (R/2)^{3/2} \exp(im_i(\phi_p - \pi/2)) \int \int \sum_{k=1}^{15} c_k \xi^{nk} \eta^{jk} [(\xi^2-1)(1-\eta^2)]^{mi/2} \exp(-\alpha\xi)(\xi^2-\eta^2) \exp(-ip_z R(1+\xi\eta)/2) J_m(p_\rho R[(\xi^2-1)(1-\eta^2)]^{1/2}) d\xi d\eta. \quad (\text{II.11.17})$$

The integrals in equation (II.11.17) are not separable and therefore are extremely difficult to evaluate in general. It was therefore decided to employ numerical techniques to solve them. The whole natural orbital was transformed into momentum-space at once rather than individual basis functions (as shown), as it is simpler to integrate numerically one function consisting of the sum of fifteen terms, rather than to perform fifteen individual

integrations.

By a simple rearrangement, the natural orbital $\chi_i(\underline{p})$ becomes

$$\chi_i(\underline{p}) = (2\pi)^{-1}(R/2)^{3/2} \exp(im_i(\phi_p - \pi/2)) \exp(-ip_z R/2) \left(A_i(p_z, p_\rho) - iB_i(p_z, p_\rho) \right), \quad (\text{II.11.18})$$

where

$$A_i(p_z, p_\rho) = \int \int \sum_{k=1}^{15} c_k \xi^{nk} \eta^{jk} [(\xi^2 - 1)(1 - \eta^2)]^{mi/2} \exp(-\alpha\xi)(\xi^2 - \eta^2) J_m(p_\rho R [(\xi^2 - 1)(1 - \eta^2)]^{1/2} / 2) \cos(p_z R \xi \eta / 2) d\xi d\eta \quad (\text{II.11.19})$$

$$B_i(p_z, p_\rho) = \int \int \sum_{k=1}^{15} c_k \xi^{nk} \eta^{jk} [(\xi^2 - 1)(1 - \eta^2)]^{mi/2} \exp(-\alpha\xi)(\xi^2 - \eta^2) J_m(p_\rho R [(\xi^2 - 1)(1 - \eta^2)]^{1/2} / 2) \sin(p_z R \xi \eta / 2) d\xi d\eta. \quad (\text{II.11.20})$$

Unfortunately, since the integrals are functions of the momentum-space co-ordinates p_z and p_ρ , they must be evaluated for each momentum position. Certain simplifications, however, do arise by considering the symmetry of the functions with respect to the integration over the η variable. All of the terms contained within $A_i(p_z, p_\rho)$ and $B_i(p_z, p_\rho)$ are symmetrical about $\eta = 0$ except for $\sin(p_z R \xi \eta / 2)$ contained in $B_i(p_z, p_\rho)$ and the η^{jk} terms for some of the orbitals. Davidson and Jones have chosen the j_k 's to be either all even or all odd for a particular natural orbital. Consequently if the j_k 's are even then $B_i(p_z, p_\rho)$ will be zero and if they are odd, $A_i(p_z, p_\rho)$ will be

zero. Further, since the non-zero functions are symmetrical about $\eta = 0$, the integration limits may be altered to produce

$$A_i(p_z, p_\rho) = 2 \int_{\eta=0}^1 \int \sum_{k=1}^{15} c_k \xi^{nk} \eta^{jk} [(\xi^2-1)(1-\eta^2)]^{mi/2} \exp(-\alpha\xi)(\xi^2-\eta^2) J_m(p_\rho R [(\xi^2-1)(1-\eta^2)]^{1/2}/2) \cos(p_z R \xi \eta / 2) d\xi d\eta \quad (\text{II.11.21})$$

for odd values of j_k and, for even values of j_k ,

$$B_i(p_z, p_\rho) = 2 \int_{\eta=0}^1 \int \sum_{k=1}^{15} c_k \xi^{nk} \eta^{jk} [(\xi^2-1)(1-\eta^2)]^{mi/2} \exp(-\alpha\xi)(\xi^2-\eta^2) J_m(p_\rho R [(\xi^2-1)(1-\eta^2)]^{1/2}/2) \sin(p_z R \xi \eta / 2) d\xi d\eta. \quad (\text{II.11.22})$$

$A_i(p_z p_\rho)$ and $B_i(p_z p_\rho)$ are easily evaluated for each value of p_z and p_ρ required by employing a standard Gaussian double-integration computer library routine. These calculated values for $A_i(p_z p_\rho)$ and $B_i(p_z p_\rho)$ can then be substituted into equation (II.11.18) to evaluate the natural orbitals. The orbitals, applying equation (II.11.5), are subsequently used to compute the magnitude of the total momentum-space wavefunction at the chosen co-ordinates.

It is interesting to point out that single-centred cylindrical co-ordinates have evolved naturally in this analysis from the two-centred confocal ellipsoidal co-ordinates used in position-space. This compares favourably with the recognised cylindrical-symmetry of the momentum-density in bi-polar systems^(2.xi.9).

(II.11.2) The H_3^+ Molecule

As the CI wavefunction of Salmon and Poshusta^(2.xi.10) and the SCF wavefunction of Schwartz and Schaad^(2.xi.11) have been used to study the position-space correlation effects, they will be used again to investigate the equivalent effects in momentum-space. Since both wavefunctions are written in Cartesian co-ordinates they may be transformed into momentum-space by entirely analytical techniques.

As mentioned in Chapter (II.4) the Salmon and Poshusta wavefunction can be expressed in the form

$$\Psi(\underline{r}_1, \underline{r}_2) = \sum_{i=1}^{15} c_i (1 + P_{12}) [\Sigma T] \phi_i(\underline{r}_1, \underline{r}_2), \quad (\text{II.11.23})$$

the Singer polynomial $\phi_i(\underline{r}_1, \underline{r}_2)$ being given by

$$\phi_i(\underline{r}_1, \underline{r}_2) = \exp \left[-a_i (\underline{r}_1 - \underline{S}_{1i})^2 - 2g_i (\underline{r}_1 - \underline{S}_{1i}) \cdot (\underline{r}_2 - \underline{S}_{2i}) - b_i (\underline{r}_2 - \underline{S}_{2i})^2 \right]. \quad (\text{II.11.24})$$

The constants a_i , g_i , b_i and c_i as well as the vectors \underline{S}_{1i} and \underline{S}_{2i} are given by Salmon and Poshusta^(2.xi.10). The permutation operator P_{12} simply interchanges the electron labels and the operator ΣT represents a summation over all of the elements in the C_{3v} symmetry group. Fourier transforms will thus be performed on the Singer polynomials and then equation II.11.23) will be used to construct the momentum-space representation of the Salmon and Poshusta wavefunction.

Any general Singer polynomial may be rearranged as

$$\begin{aligned} \Phi_i(\underline{r}_1, \underline{r}_2) = \exp \left[-a_i \underline{s}_{1i}^2 - 2g_i \underline{s}_{1i} \cdot \underline{s}_{2i} - b_i \underline{s}_{2i}^2 \right] \exp \left[-\underline{r}_1^2 a_i - \underline{r}_2^2 b_i \right. \\ \left. + \underline{r}_1 \cdot (G_i(\underline{p}_1) + i\underline{p}_1) + \underline{r}_2 \cdot (H_i(\underline{p}_2) + i\underline{p}_2) - \underline{r}_1 \cdot \underline{r}_2 2g_i \right] \end{aligned} \quad (\text{II.11.25})$$

where

$$G_i(\underline{p}_1) = 2a_i \underline{s}_{1i} + 2g_i \underline{s}_{2i} - i\underline{p}_1$$

and (II.11.26)

$$H_i(\underline{p}_2) = 2b_i \underline{s}_{2i} + 2g_i \underline{s}_{1i} - i\underline{p}_2.$$

Equation (II.11.25) can now be substituted into the Fourier transform equation (equation (II.11.4)) to express the momentum-space Singer polynomial in the form

$$\begin{aligned} \Phi_i(\underline{p}_1, \underline{p}_2) = (2\pi)^{-3} \exp \left[-a_i \underline{s}_{1i}^2 - 2g_i \underline{s}_{1i} \cdot \underline{s}_{2i} - b_i \underline{s}_{2i}^2 \right] \int \exp \left[-b_i \underline{r}_2^2 \right. \\ \left. + \underline{r}_2 \cdot H_i(\underline{p}_2) \right] E(\underline{r}_2, \underline{p}_1) d\underline{r}_2, \end{aligned} \quad (\text{II.11.27})$$

the function $E(\underline{r}_2)$ being given by

$$E(\underline{r}_2, \underline{p}_1) = \int \exp \left[-a_i \underline{r}_1^2 + \underline{r}_1 \cdot (G_i(\underline{p}_1) - 2g_i \underline{r}_2) \right] d\underline{r}_1.$$

Obviously $E(\underline{r}_2)$ can be separated into three Cartesian-type integrals where

$$d\underline{r} = dx dy dz$$

and

$$\begin{aligned} -\infty &\leq x \leq \infty \\ -\infty &\leq y \leq \infty \\ -\infty &\leq z \leq \infty. \end{aligned}$$

It can be seen that these integrals are of the standard form (2.xi.12)

$$\int \exp(-s^2 x^2 + tx) dx = (\pi/s^2)^{1/2} \exp(t^2/4s^2), \quad (\text{II.11.28})$$

and therefore the \underline{r}_1 integration may be performed immediately to produce $E(\underline{r}_2)$ as

$$E(\underline{r}_2, \underline{p}_1) = (\pi/a_k)^{3/2} \exp\left[(G_i(\underline{p}_1) - 2g_i \underline{r}_2)^2/4a_i\right]. \quad (\text{II.11.29})$$

This expression for $E(\underline{r}_2)$ can now be substituted into equation (II.11.27) and the resulting equation rearranged in quadratic form with respect to \underline{r}_2 to give

$$\begin{aligned} \Phi_i(\underline{p}_1, \underline{p}_2) = (2\pi)^{-3} (\pi/a_k)^{3/2} \exp(-a_i \underline{s}_{1i}^2 - 2g_i \underline{s}_{1i} \cdot \underline{s}_{2i} - b_i \underline{s}_{2i}^2) \\ \int \exp\left[-(b_i - g_i^2/a_i) \underline{r}_2^2 - \underline{r}_2 \cdot G_i(\underline{p}_1) g_i/a_i + (H_i(\underline{p}_2) \right. \\ \left. + G_i(\underline{p}_1)^2/4a_i)\right] d\underline{r}_2. \end{aligned}$$

By utilizing equation (II.11.28) again, the \underline{r}_2 integration may be performed in a similar way to the integration over r_1 . Once this has been performed, after a little manipulation, the Singer polynomial reduces to the surprisingly simple form of

$$\Phi_i(\underline{p}_1, \underline{p}_2) = k_i^{3/2} \exp\left[-a_i k_i \underline{p}_1^2 - b_i k_i \underline{p}_2^2 - i \underline{s}_{2i} \cdot \underline{p}_1 - i \underline{s}_{1i} \cdot \underline{p}_2 + g_i k_i \underline{p}_1 \cdot \underline{p}_2/2\right]. \quad (\text{II.11.30})$$

The constant k_i , which is positive for all values of i , is defined by

$$k_i = 1/4(a_i b_i - g_i^2). \quad (\text{II.11.31})$$

The full Salmon and Poshusta wavefunction in momentum-space is then simply

$$\psi(\underline{p}_1, \underline{p}_2) = \sum_{i=1}^{15} c_i (1 + P_{12}) [\Sigma T] \phi_i(\underline{p}_1, \underline{p}_2). \quad (\text{II.11.32})$$

The Schwartz and Schaad wavefunction is written in position-space as

$$\phi_{\text{SCF}}(\underline{r}_1, \underline{r}_2) = \phi(\underline{r}_1) \phi(\underline{r}_2) \quad (\text{II.11.33})$$

where the molecular orbital $\phi(\underline{r})$ may be expressed as

$$\phi(\underline{r}) = \sum_{i=1}^5 c_i (\phi_i^{\text{A}}(\underline{r}) + \phi_i^{\text{B}}(\underline{r}) + \phi_i^{\text{C}}(\underline{r})). \quad (\text{II.11.34})$$

The orbital $\phi_i^{\text{A}}(\underline{r})$, for example, is then represented by an unnormalised 1s Gaussian orbital with exponent a_i , centred at a distance d_i from nucleus A towards the centre of the molecule, the remaining two orbitals being expressed in a similar way. For convenience, if the centres of these orbitals are located by \underline{s}_j , say, then equation (II.11.34) may be rearranged to give the molecular orbital in the form

$$\phi(\underline{r}) = \sum_{j=1}^{15} c_j \phi_j(\underline{r}) \quad (\text{II.11.35})$$

where the basis orbital is

$$\phi_j(\underline{r}) = \exp[-a_j(\underline{r} - \underline{s}_j)^2]. \quad (\text{II.11.36})$$

By then using equation (II.11.3) the momentum-space representation of the orbital is

$$\phi_j(\underline{p}) = (2\pi)^{-3/2} \int \exp[-a_j(\underline{r} - \underline{s}_j)^2 - i\underline{p} \cdot \underline{r}] d\underline{r}. \quad (\text{II.11.37})$$

This integration is of the same form as the standard integral used previously (II.11.28) and thus equation (II.11.37) becomes

$$\phi_j(\underline{p}) = (2a_j)^{3/2} \exp[-\underline{p}^2/4a_j - i\underline{s}_j \cdot \underline{p}]. \quad (\text{II.11.38})$$

Hence the full Schwartz and Schaad wavefunction in momentum-space is

$$\begin{aligned} \phi_{\text{SCF}}(\underline{p}_1, \underline{p}_2) = \sum_{j=1}^{15} \sum_{k=1}^{15} c_j c_k (4a_j a_k)^{3/2} \exp[-\underline{p}_1^2/4a_j - \underline{p}_2^2/4a_k \\ + i\underline{s}_j \cdot \underline{p}_1 + i\underline{s}_k \cdot \underline{p}_2]. \end{aligned} \quad (\text{II.11.39})$$

CHAPTER II.12

Results for H₂ in Momentum-Space

The Davidson and Jones wavefunction^(2.xii.1) has been transformed into momentum-space semi-numerically and used to generate the results presented in this chapter. The symmetry of the momentum distribution is ellipsoidal, with axial symmetry about the z-axis, and hence cylindrical co-ordinates remain the most logical choice. Thus, since the form of the wavefunction is maintained in momentum-space, the renormalised wavefunction curtailed to embody the first two, three, four and then all ten of the natural configurations may be used to investigate the momentum-space z , ϕ , ρ and second-order correlation effects, respectively. Also, the first natural configuration may still be used to represent the Hartree Fock wavefunction. The abbreviations 1NO, 2NO, 3NO, 4NO and 10NO refer to the number of natural orbitals used in the renormalised wavefunction.

Like the position-space analysis of H₂, the results may be divided into one and two-particle density functions, with the two-particle functions forming the major section. Contours are chosen from the same sets as used in position-space to highlight the geometry of the system, namely:

Hartree Fock Surface Contours

1	0.0001	6	0.02
2	0.0005	7	0.03
3	0.0025	8	0.04
4	0.0075	9	0.10
5	0.01	10	0.15

Δ -Surface Contours

1	-0.0050	15	0.0001
2	-0.0040	16	0.0002
3	-0.0030	17	0.0003
4	-0.0025	18	0.0005
5	-0.0020	19	0.0007
6	-0.0015	20	0.0009
7	-0.0011	21	0.0011
8	-0.0009	22	0.0015
9	-0.0007	23	0.0020
10	-0.0005	24	0.0025
11	-0.0003	25	0.0030
12	-0.0002	26	0.0040
13	-0.0001	27	0.0050
14	0.0000	28	0.0060

The negative contours are also represented by broken curves, the positive contours by full curves and the zero contour by a dotted curve.

In momentum-space it is impossible to locate explicitly the site of a nucleus, however, the following definition may still be employed:

x = position of the fixed electron which is defined with respect to the origin at $p = 0$.

The full width of each of the surfaces represents 8 a.u. of momentum. On the smaller surfaces, 9 millimetres corresponds to 1 a.u. of momentum whereas, on the one-particle density surface (Figure (II.12.1)), 1 a.u. of momentum is represented by 18 millimetres.

(II.12.1) The One-Particle Density Results

Following the position-space study of the one-particle density, the $p_x p_z$ -plane, with $p_y = 0$, is examined in momentum-space. The momentum-space one-particle density inherits the axial symmetry of the position-space function, resulting in contours in perpendicular planes to this forming concentric circles and, as a consequence, would prove uninteresting.

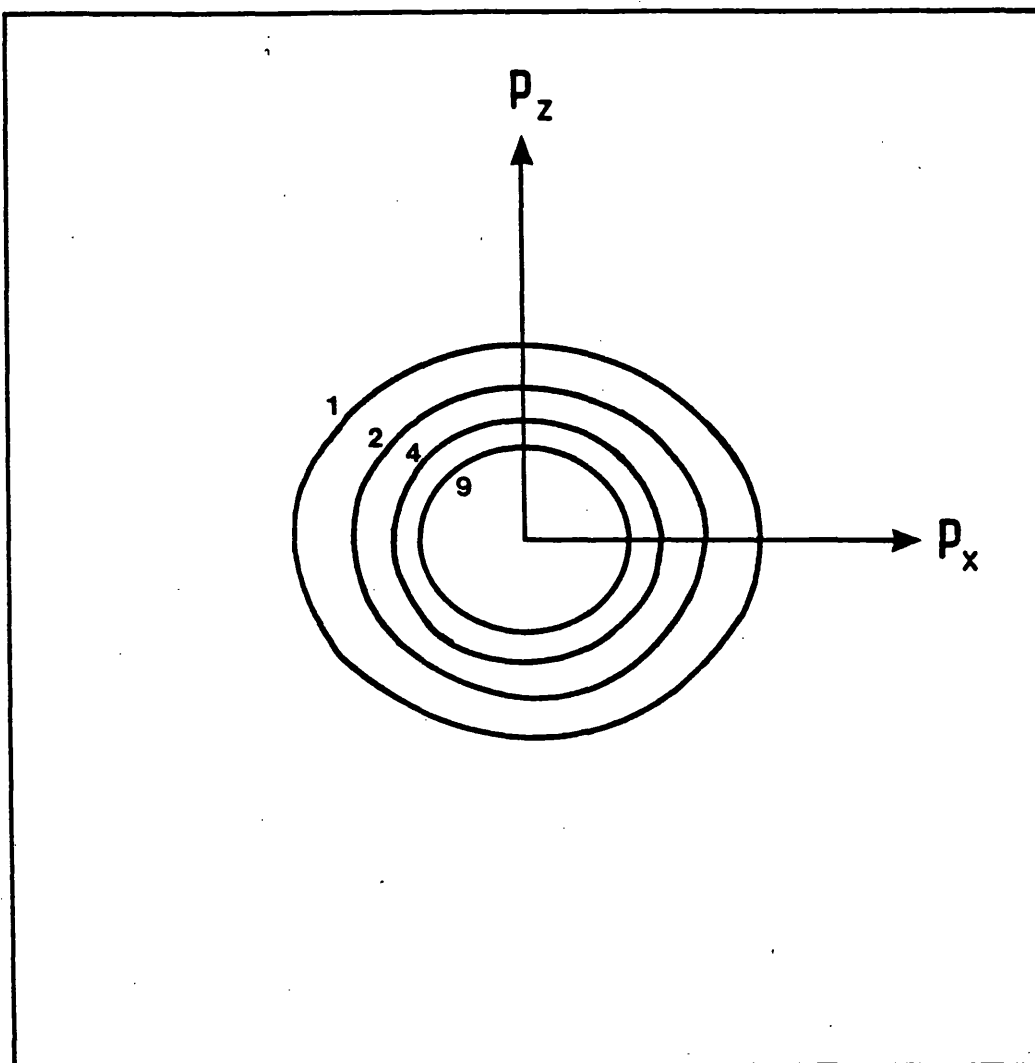
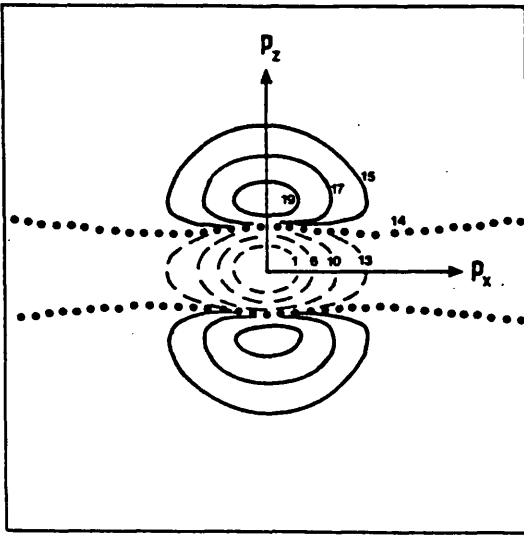
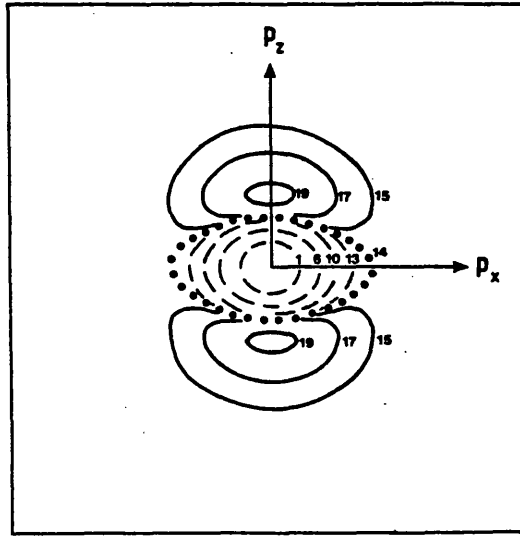


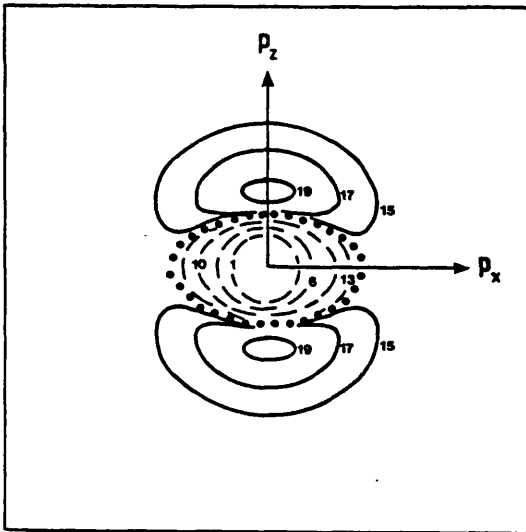
Figure (II.12.1) The H_2 momentum-space HF one-particle density, $\rho(p_1)$, in the $p_x p_z$ -plane with $p_y = 0$.



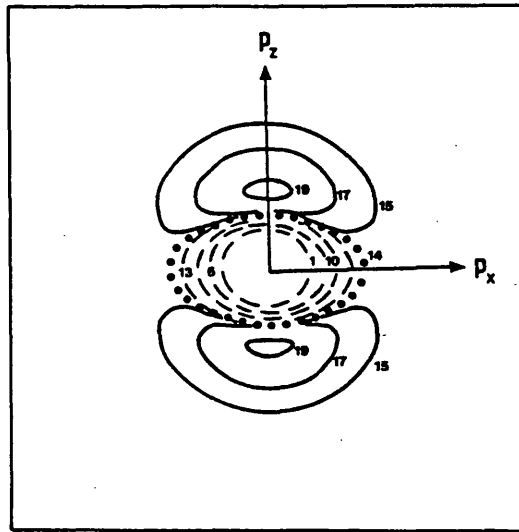
(A) 2NO - 1NO
z - correlation



(B) 3NO - 1NO
(z + ϕ) - correlation



(C) 4NO - 1NO
(z + ϕ + ρ) - correlation



(D) 10NO - 1NO
(z + ϕ + ρ + 2nd order)
- correlation

Figure (II.12.2) The momentum-space Δ -one-particle densities, $\Delta\rho(\mathbf{p}_1)$, in the $p_x p_z$ -plane with $p_y = 0$.

(II.12.2) The Two-Particle Density Results

In momentum-space we cannot locate electron 1 with reference to the nuclear frame, nevertheless, it is important for it to be defined with reference to the momentum distribution of the molecule in some way. It is therefore reasonable to locate electron 1 with respect to the mean momentum of an electron, $\langle p_1 \rangle$.

The first position is chosen to be at $p_1 = 0$. Positions {ii}, {iii}, and {iv} are then defined by electron 1 possessing a momentum given by $p_x = 0.5\langle p_1 \rangle$, $\langle p_1 \rangle$ and $1.5\langle p_1 \rangle$ respectively with p_y and p_z equal to zero. The HF distributions, Δ -surfaces and partial planar Coulomb shifts for these electron positions are presented in Figures (II.12.4-13) for the $p_x p_z$ -plane and in Figures (II.12.14-23) for the $p_x p_y$ -plane with $p_y = 0$. Similarly, positions {v}, {vi} and {vii} are defined by electron 1 having a momentum defined by $p_z = 0.5\langle p_1 \rangle$, $\langle p_1 \rangle$ and $1.5\langle p_1 \rangle$ with p_x and p_y equal to zero. As these positions maintain the axial symmetry of the momentum distribution the $p_x p_y$ -plane results have not been presented, however, the $p_x p_z$ -plane ($p_y = 0$) distributions are displayed in Figures (II.12.24-31). The chosen momentum values of electron 1 are summarised in Figure(II.12.3A). It is also possible to locate electron 1 with a momentum where p_x , p_y and p_z are all non-zero. The physical interpretation of the effects of correlation on such a surface, however, would be difficult to envisage and hence they are not considered.

Successive theoretical calculations have evaluated $\langle p_1 \rangle$ to be 0.929 a.u. (2.xii.2) and 0.92845 a.u. (2.xii.3). This is consistent with the experimentally derived result of 0.93a.u. \pm 0.01a.u. (2.xii.2). Consequently for the purposes of this analysis

$$\langle p_1 \rangle \cong 0.93 \text{ a.u.}$$

In the $p_x p_z$ -plane, ϵ has been defined as the angle subtended between a line parallel to the p_z -axis and the vector p_{12} in an anticlockwise direction (see Figure (II.12.3B)). This means that for the first four values of p_1 , although there is two fold symmetry about the p_x -axis, the angular distribution functions must be generated for the full range of ϵ (ie $0^\circ \leq \epsilon \leq 360^\circ$). Nevertheless, this definition is consistent with previous definitions and it allows all of the angular distribution functions in the $p_x p_z$ -plane to be compared together. In the $p_x p_y$ -plane, ϵ is defined with respect to the p_x -axis as shown by Figure (II.12.3C).

The following results consequently represent a survey of the effect of electron correlation on H_2 in momentum-space:

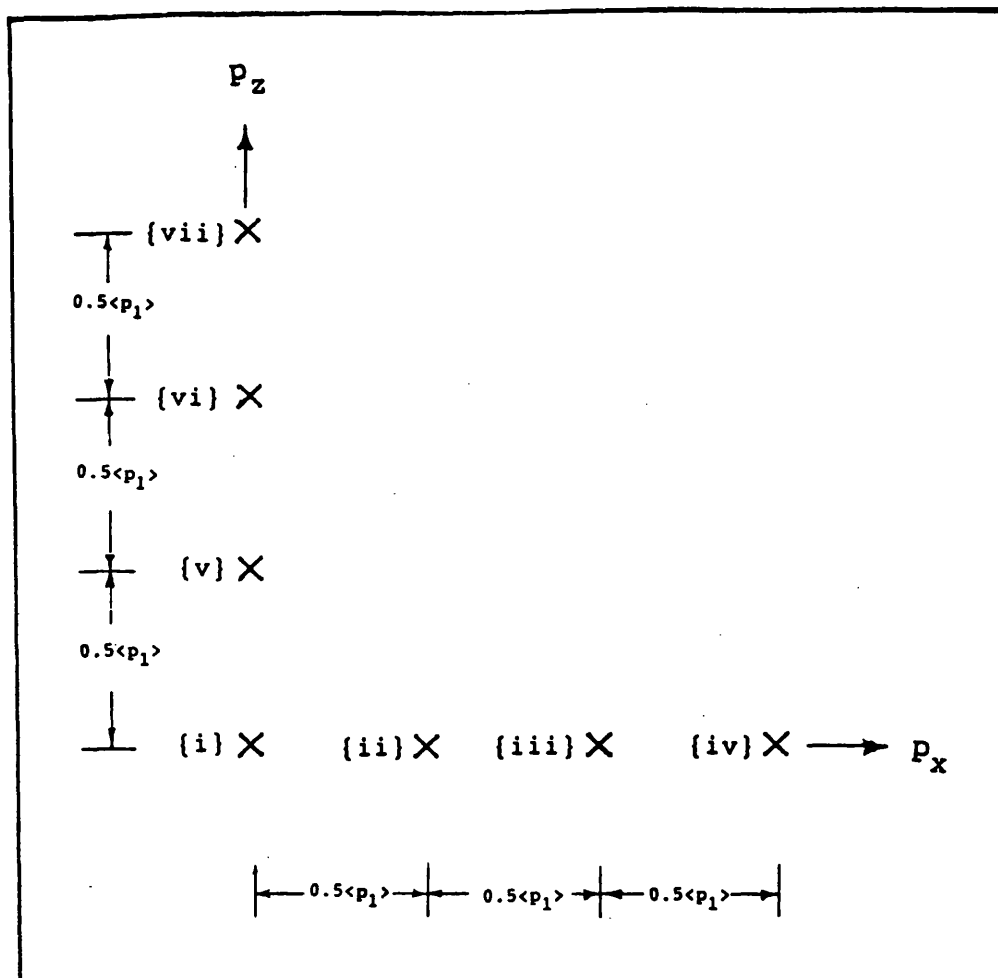


Figure (II.12.3A) The location of the chosen fixed electron positions of the partial planar distribution functions for hydrogen in momentum-space. The expectation value $\langle p_1 \rangle = 0.923$ a.u.

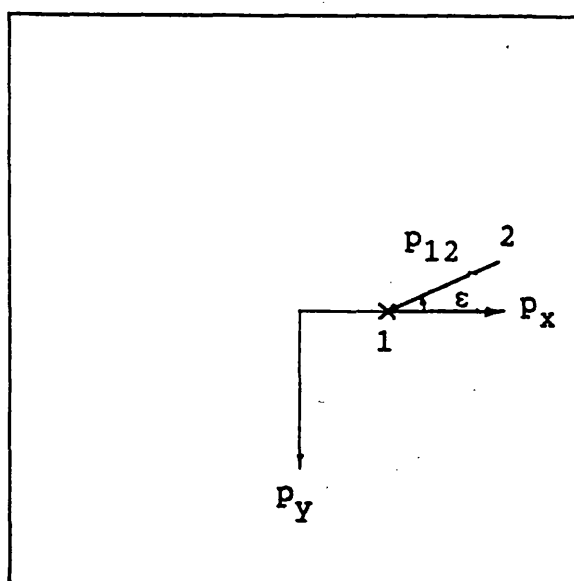
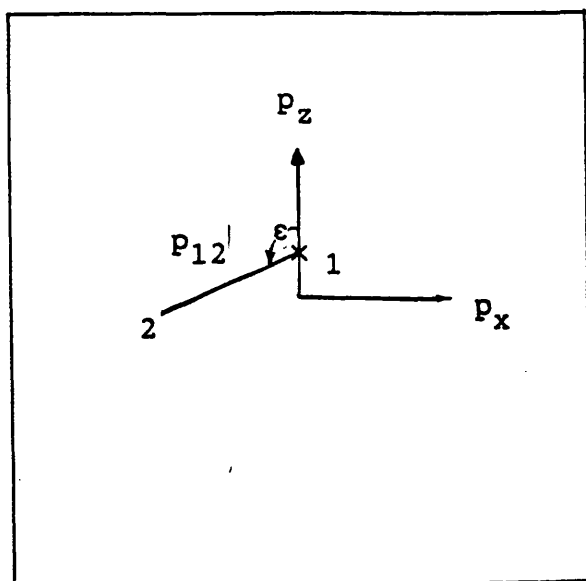
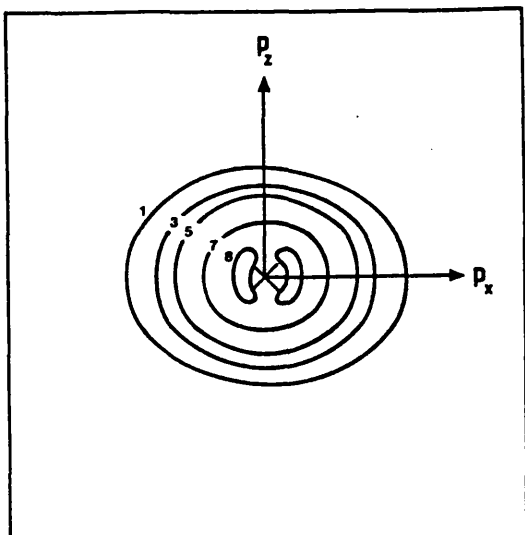
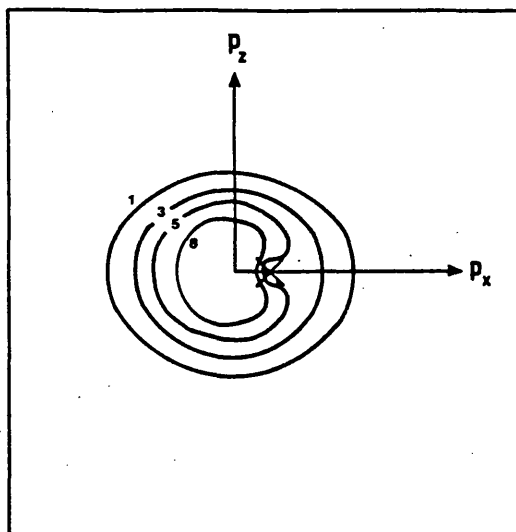


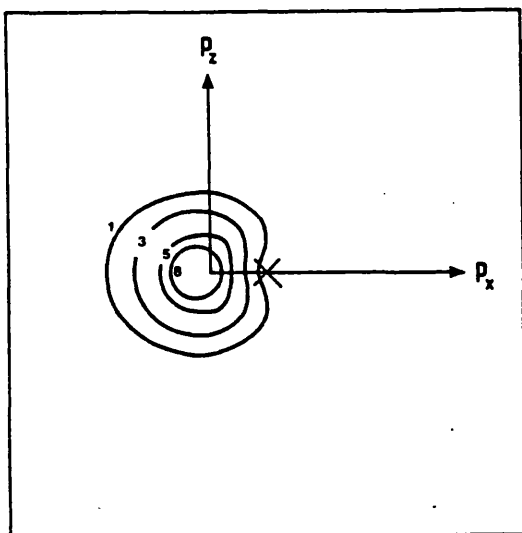
Figure (II.12.3B) & Figure (II.12.3C) The definition of the angle ϵ and the distance p_{12} when analysing correlation effects in (B) the $p_x p_z$ -plane or (C) the $p_x p_y$ -plane.



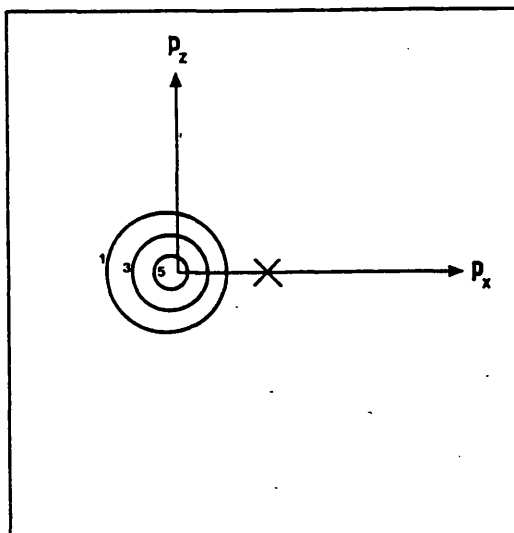
(A) position {i}



(B) position {ii}

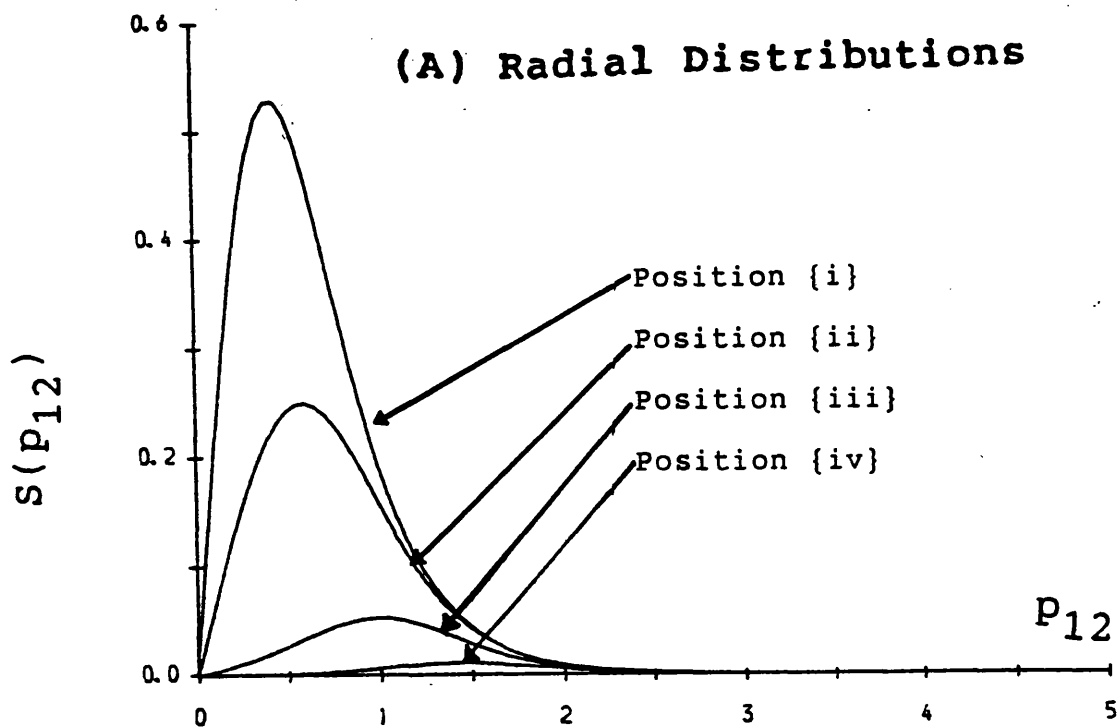


(C) position {iii}



(D) position {iv}

Figure (II.12.4) The momentum-space Hartree Fock $V(p_{12}, p_1)$ distribution functions for positions {i}, {ii}, {iii} and {iv} in the $p_x p_z$ -plane with $p_y = 0$.



(B) Angular Distributions

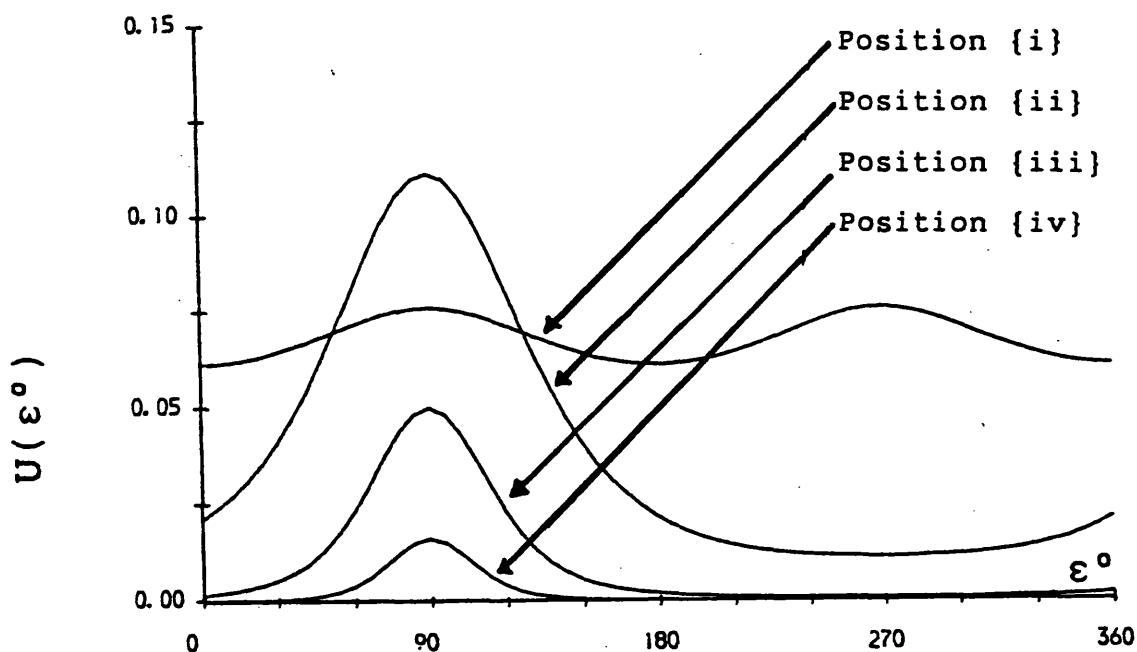
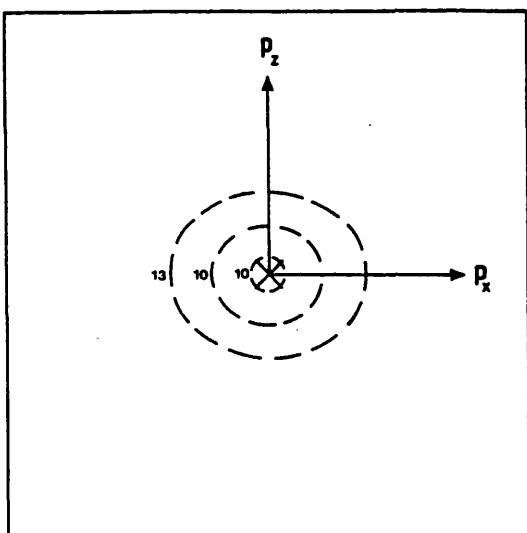
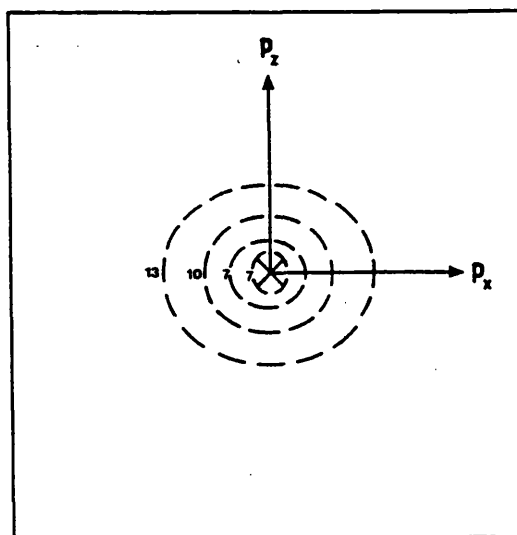


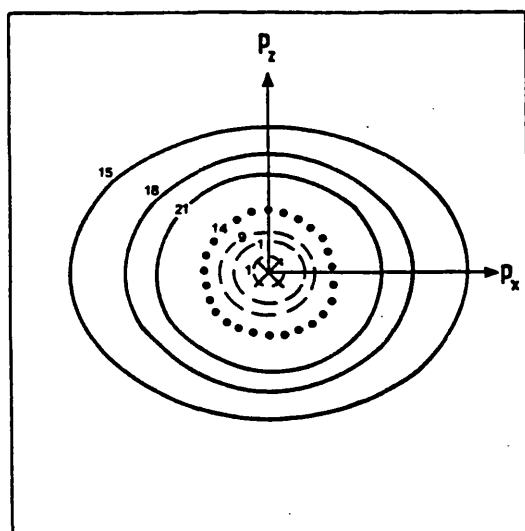
Figure (II.12.5) HF partial planar momentum distribution functions for H_2 , with electron 1 fixed at positions {i}, {ii}, {iii} and {iv} (see Fig.(II.12.3)) and electron 2 moving in the $p_x p_z$ plane, were obtained by appropriate integration of Fig.(II.12.4).



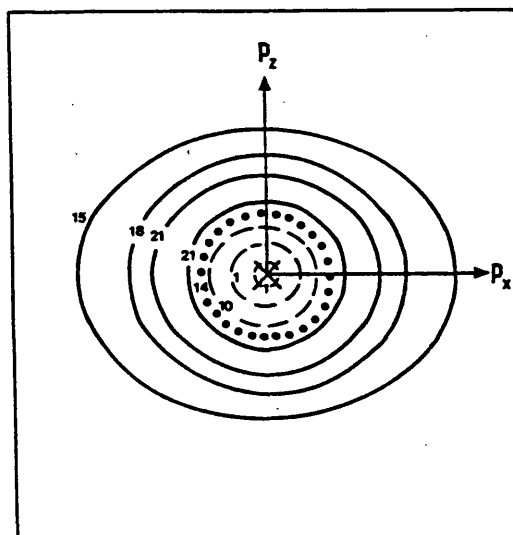
(A) 2NO - 1NO
z - correlation



(B) 3NO - 1NO
(z + φ) - correlation



(C) 4NO - 1NO
(z + φ + ρ) - correlation



(D) 10NO - 1NO
(z + φ + ρ + 2nd order)
- correlation

Figure (II.12.6) The partial planar Δ -surfaces, $\Delta V(p_{12}, p_1)$, for fixed electron position $\{i\}$ (see Figure (II.12.3A) for the definition), with the roving electron located in the $p_x p_z$ -plane with $p_y = 0$.

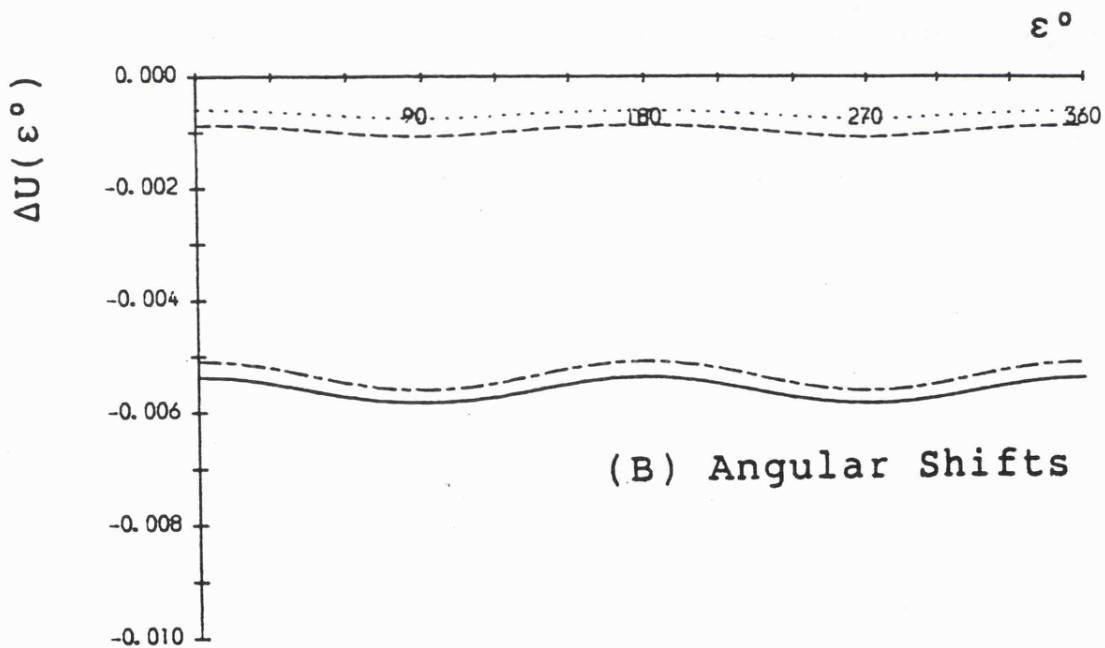
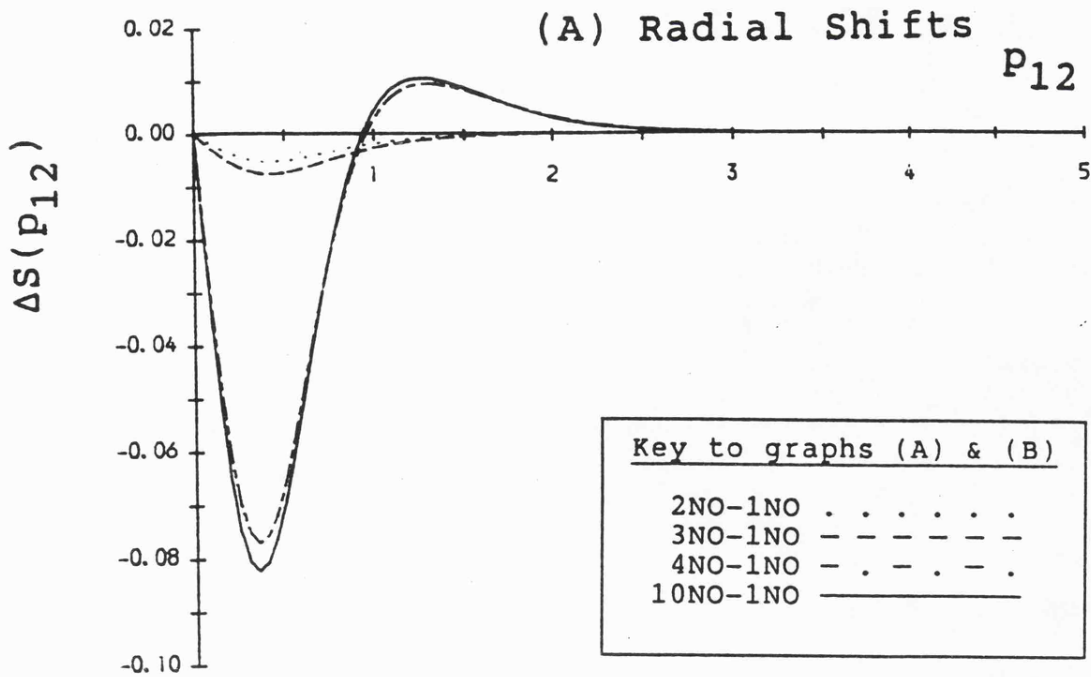
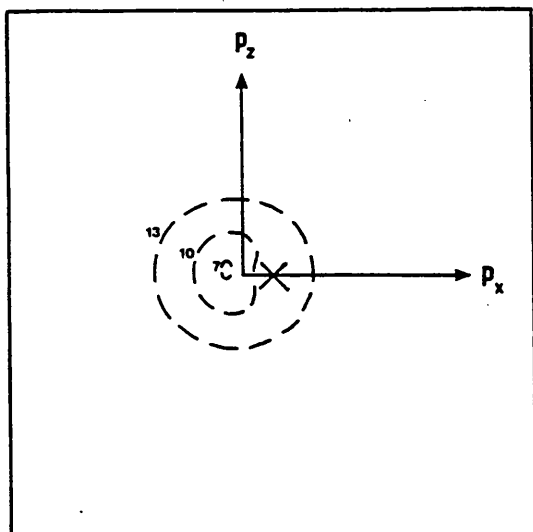
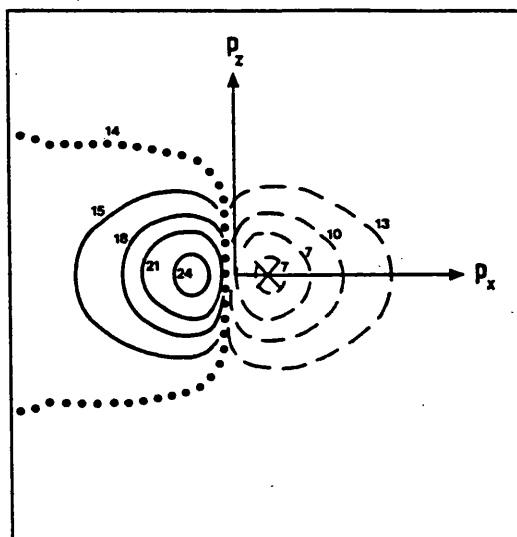


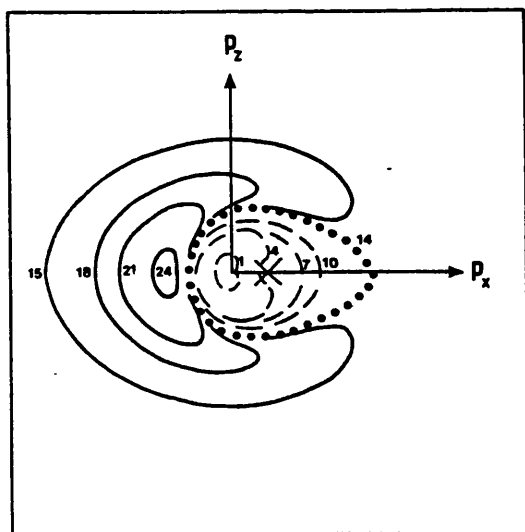
Figure (II.12.7) Partial planar Coulomb shifts for H_2 , with electron 1 fixed at position $\{i\}$ (see Fig.(II.12.3)) and electron 2 moving in the $p_x p_z$ plane, were obtained by appropriate integration of Fig.(II.12.6).



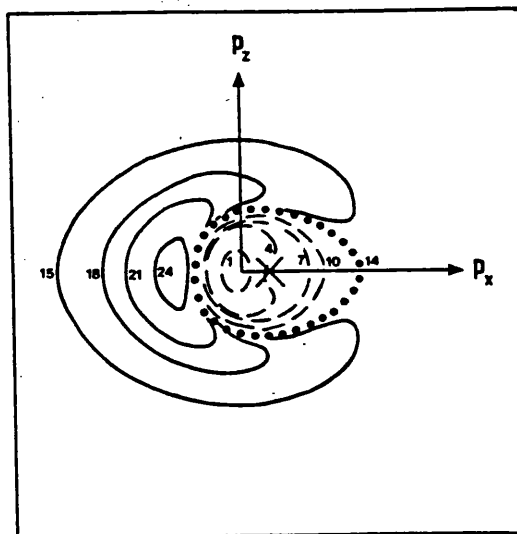
(A) 2NO - 1NO
z - correlation



(B) 3NO - 1NO
(z + φ) - correlation



(C) 4NO - 1NO
(z + φ + ρ) - correlation



(D) 10NO - 1NO
(z + φ + ρ + 2nd order)
- correlation

Figure (II.12.8) The partial planar Δ -surfaces, $\Delta V(p_{12}, p_1)$, for fixed electron position {ii} (see Figure (II.12.3A) for the definition), with the roving electron located in the $p_x p_z$ -plane with $p_y = 0$.

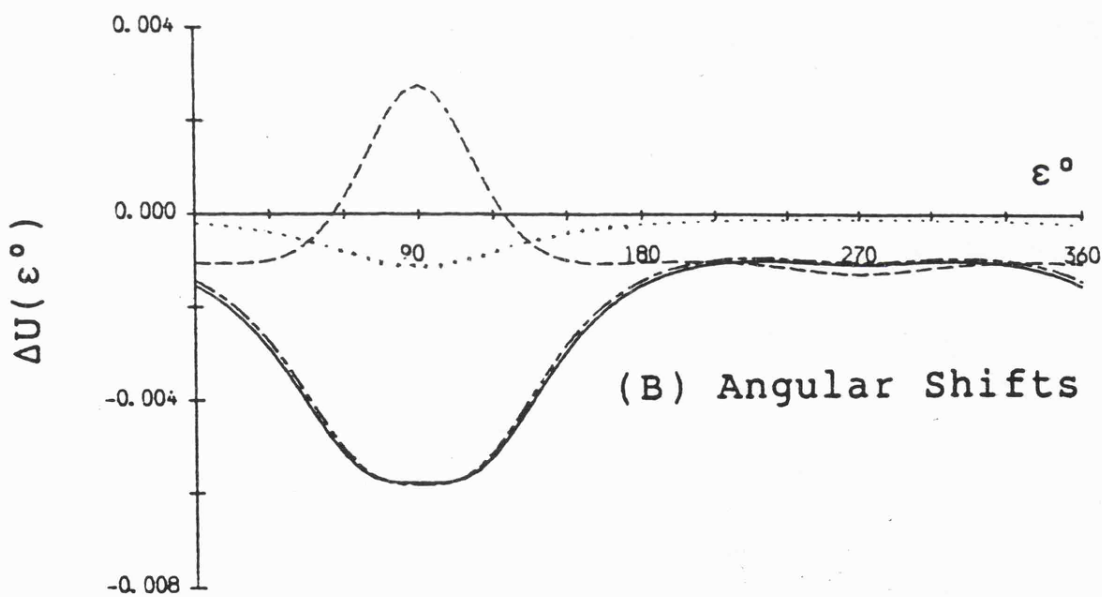
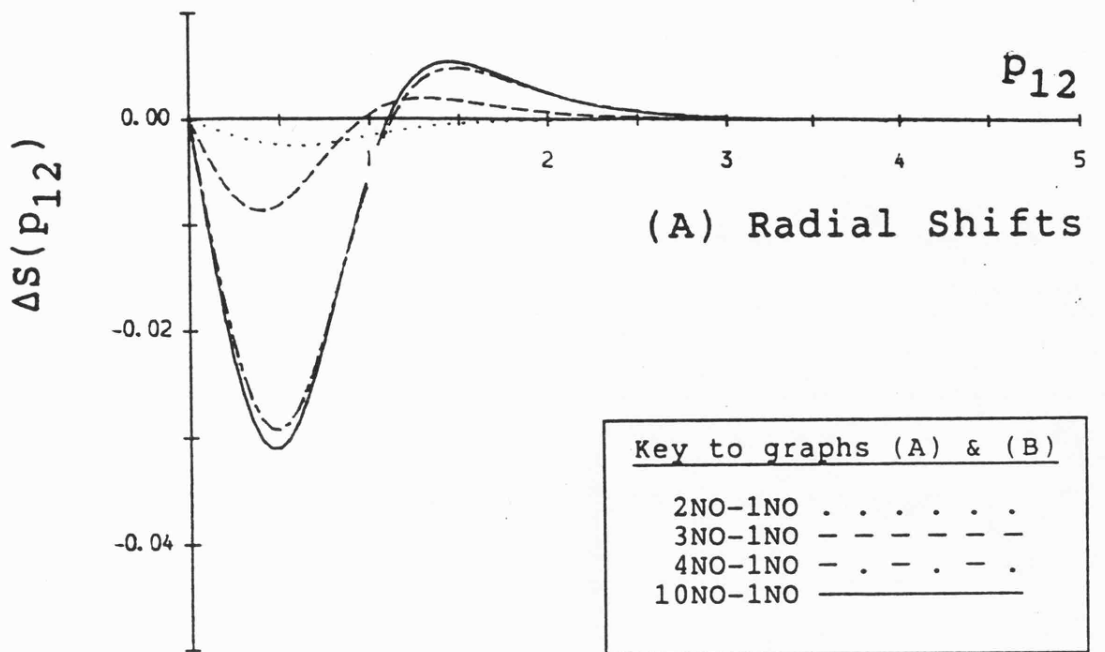
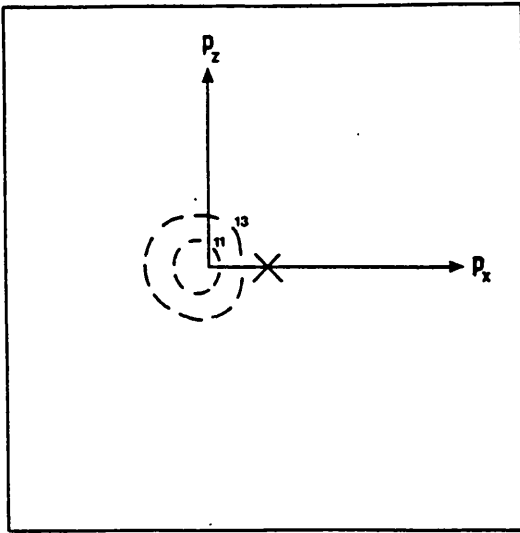
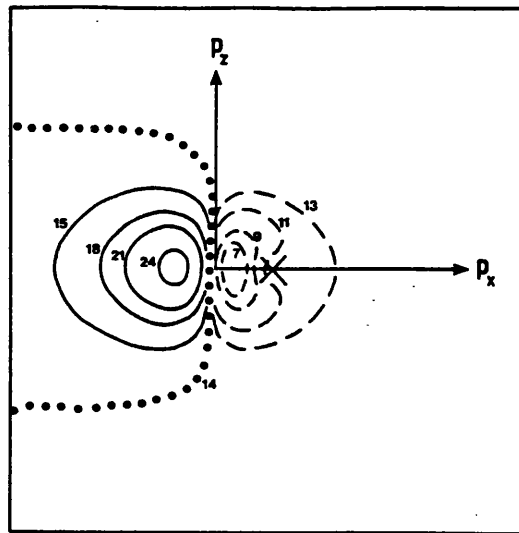


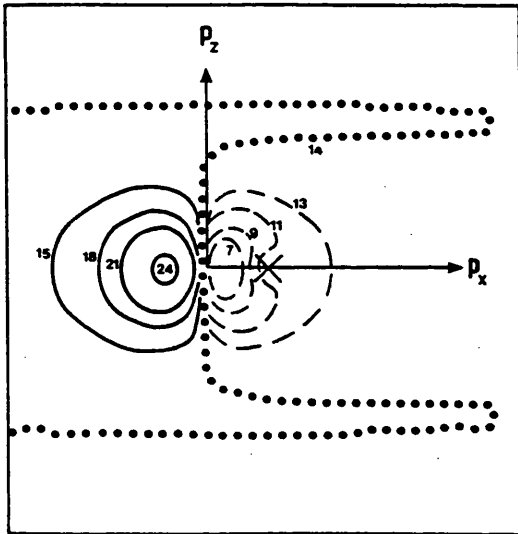
Figure (II.12.9) Partial planar Coulomb shifts for H_2 , with electron 1 fixed at position {ii} (see Fig.(II.12.3)) and electron 2 moving in the $p_x p_z$ plane, were obtained by appropriate integration of Fig.(II.12.8).



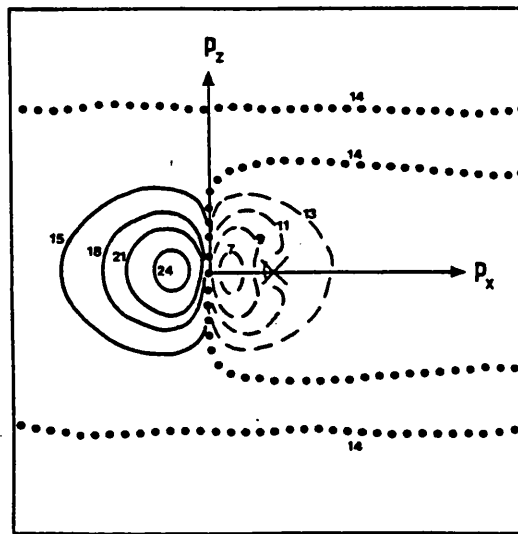
(A) 2NO - 1NO
z - correlation



(B) 3NO - 1NO
(z + φ) - correlation

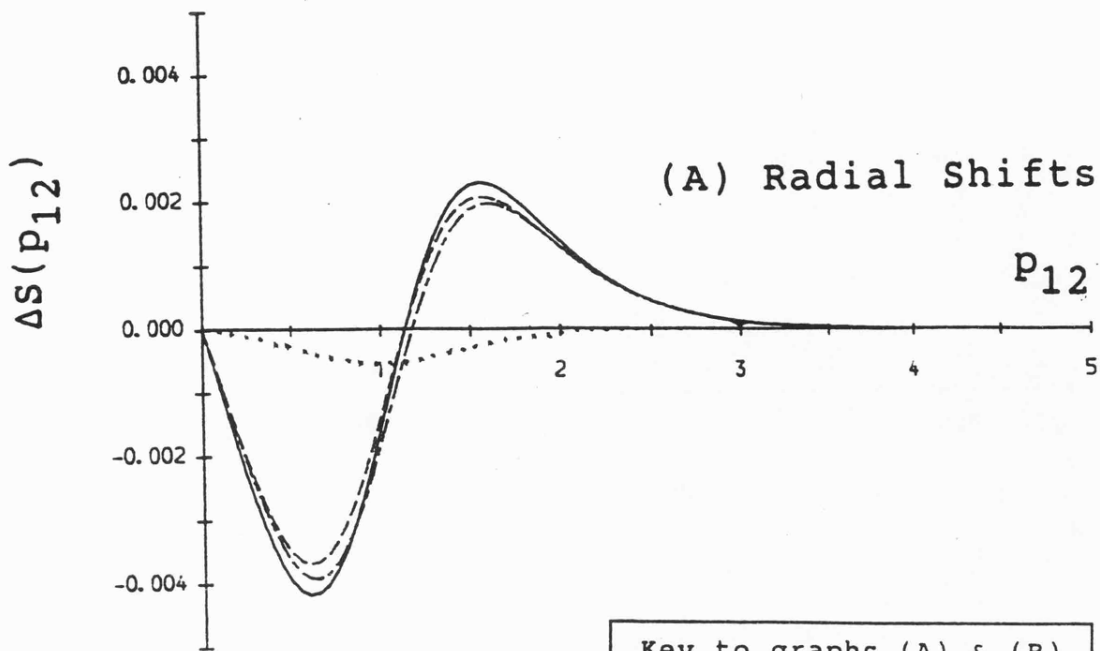


(C) 4NO - 1NO
(z + φ + ρ) - correlation



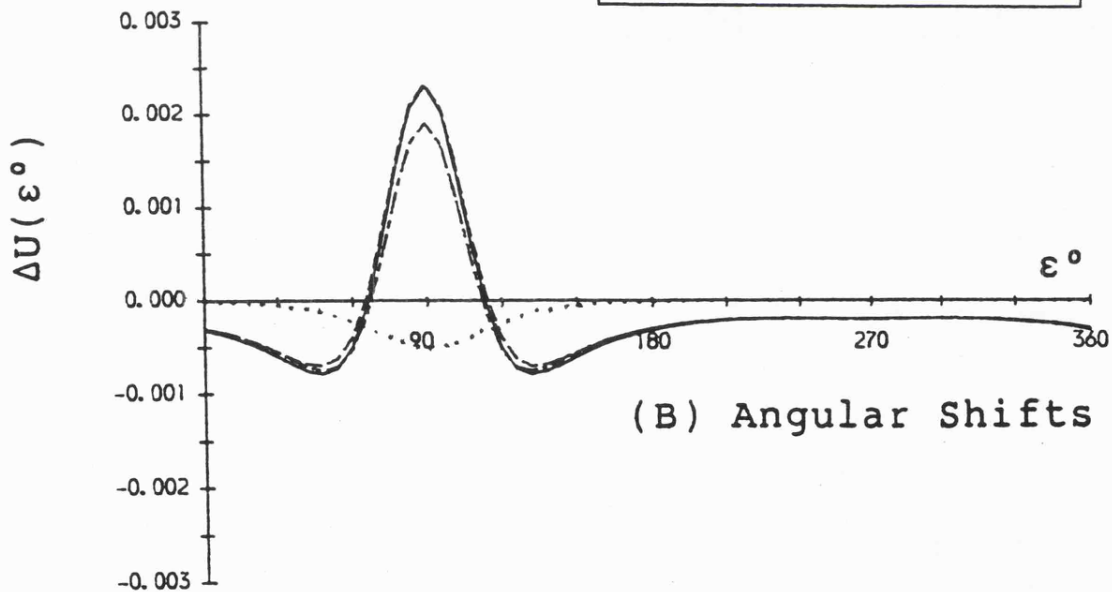
(D) 10NO - 1NO
(z + φ + ρ + 2nd order)
- correlation

Figure (II.12.10) The partial planar Δ -surfaces, $\Delta V(p_{12}, p_1)$, for fixed electron position {iii} (see Figure (II.12.3A) for the definition), with the roving electron located in the $p_x p_z$ -plane with $p_y = 0$.



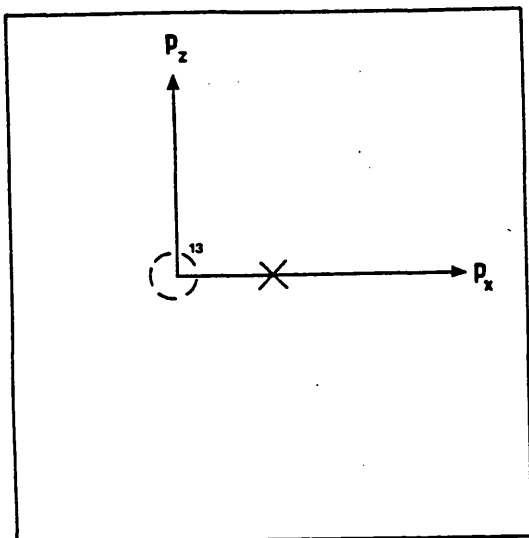
Key to graphs (A) & (B)

2NO-1NO
3NO-1NO	-----
4NO-1NO	- . - . - .
10NO-1NO	—————

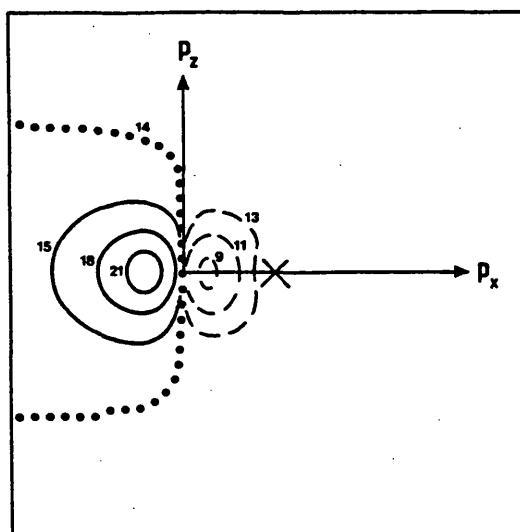


(B) Angular Shifts

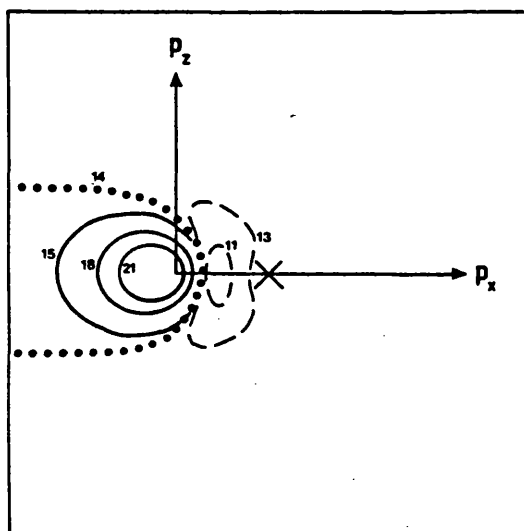
Figure (II.12.11) Partial planar Coulomb shifts for H_2 , with electron 1 fixed at position {iii} (see Fig.(II.12.3)) and electron 2 moving in the $p_x p_z$ plane, were obtained by appropriate integration of Fig.(II.12.10).



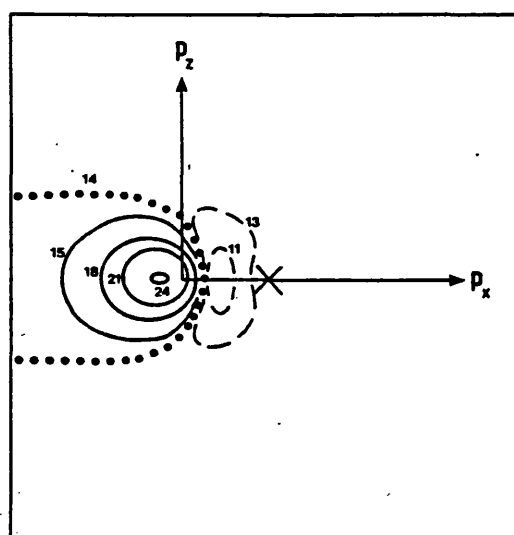
(A) 2NO - 1NO
z - correlation



(B) 3NO - 1NO
(z + φ) - correlation

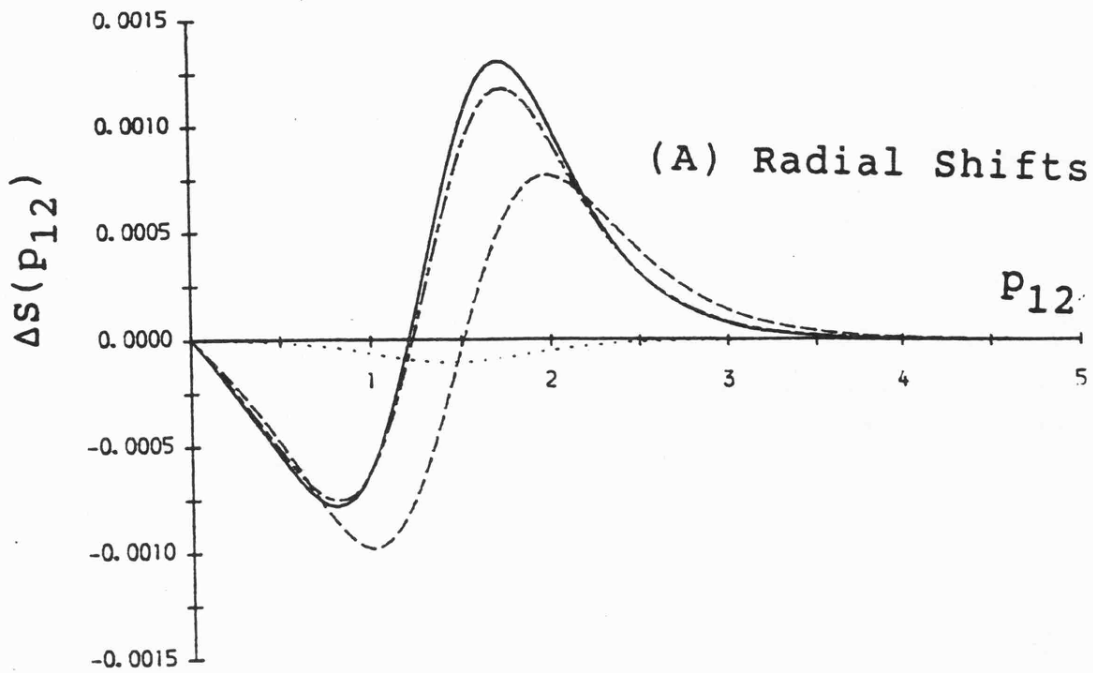


(C) 4NO - 1NO
(z + φ + ρ) - correlation



(D) 10NO - 1NO
(z + φ + ρ + 2nd order)
- correlation

Figure (II.12.12) The partial planar Δ -surfaces, $\Delta V(p_{12}, p_1)$, for fixed electron position {iv} (see Figure (II.12.3A) for the definition), with the roving electron located in the $p_x p_z$ -plane with $p_y = 0$.



Key to graphs (A) & (B)

2NO-1NO
3NO-1NO	- - - - -
4NO-1NO	- . - . - .
10NO-1NO	_____

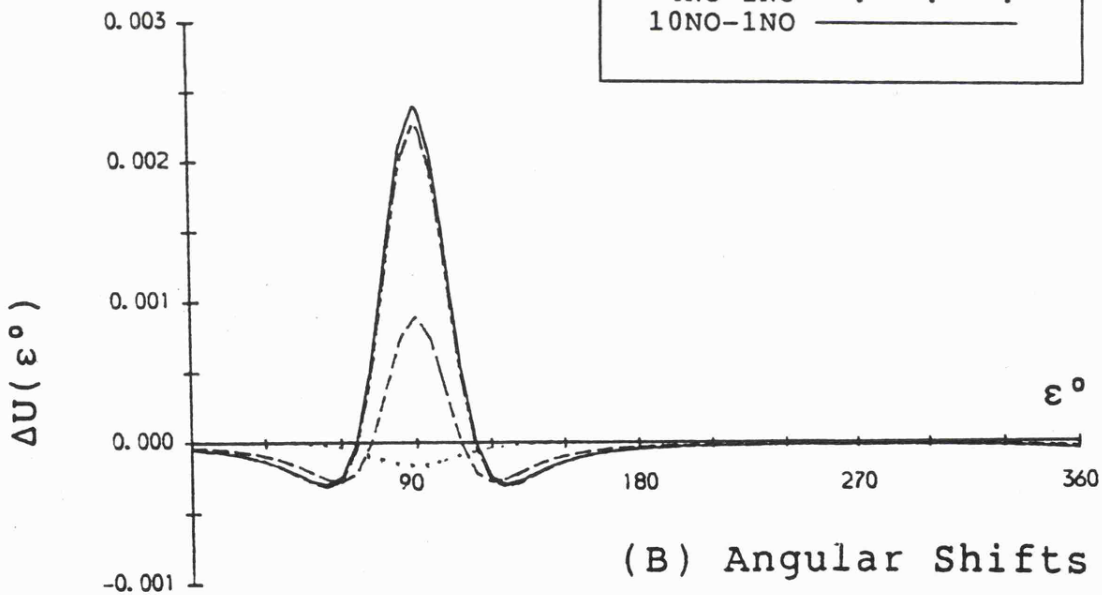
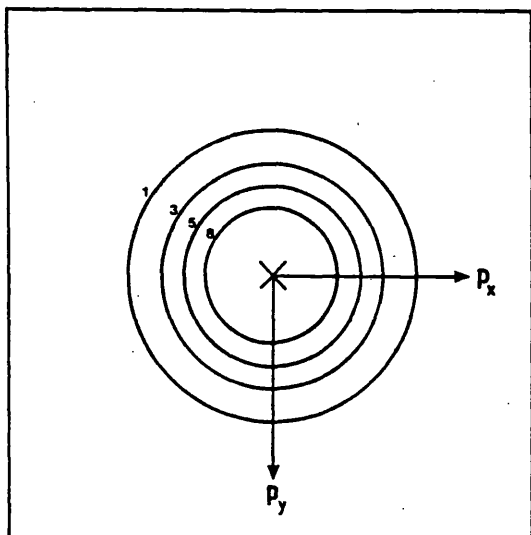
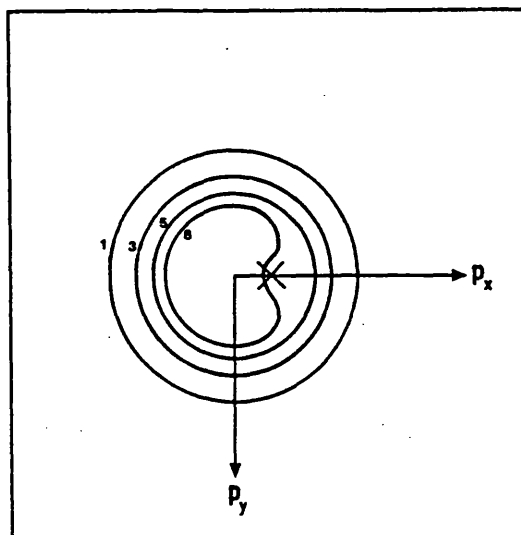


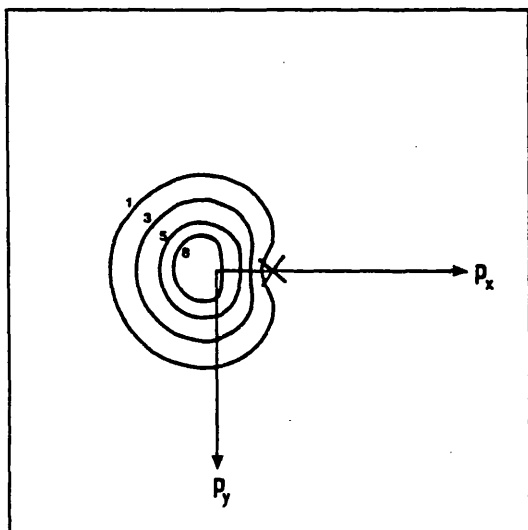
Figure (II.12.13) Partial planar Coulomb shifts for H_2 , with electron 1 fixed at position {iv} (see Fig.(II.12.3)) and electron 2 moving in the $p_x p_z$ plane, were obtained by appropriate integration of Fig.(II.12.12).



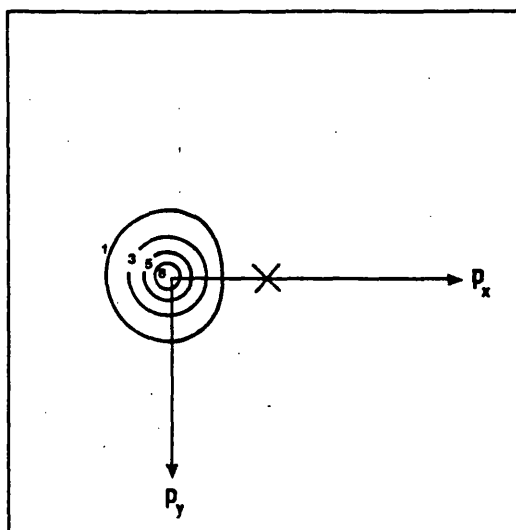
(A) position {i}



(B) position {ii}



(C) position {iii}



(D) position {iv}

Figure (II.12.14) The momentum-space Hartree Fock $V(p_{12}, p_1)$ distribution functions for positions {i}, {ii}, {iii} and {iv} in the $p_x p_y$ -plane with $p_z = 0$.

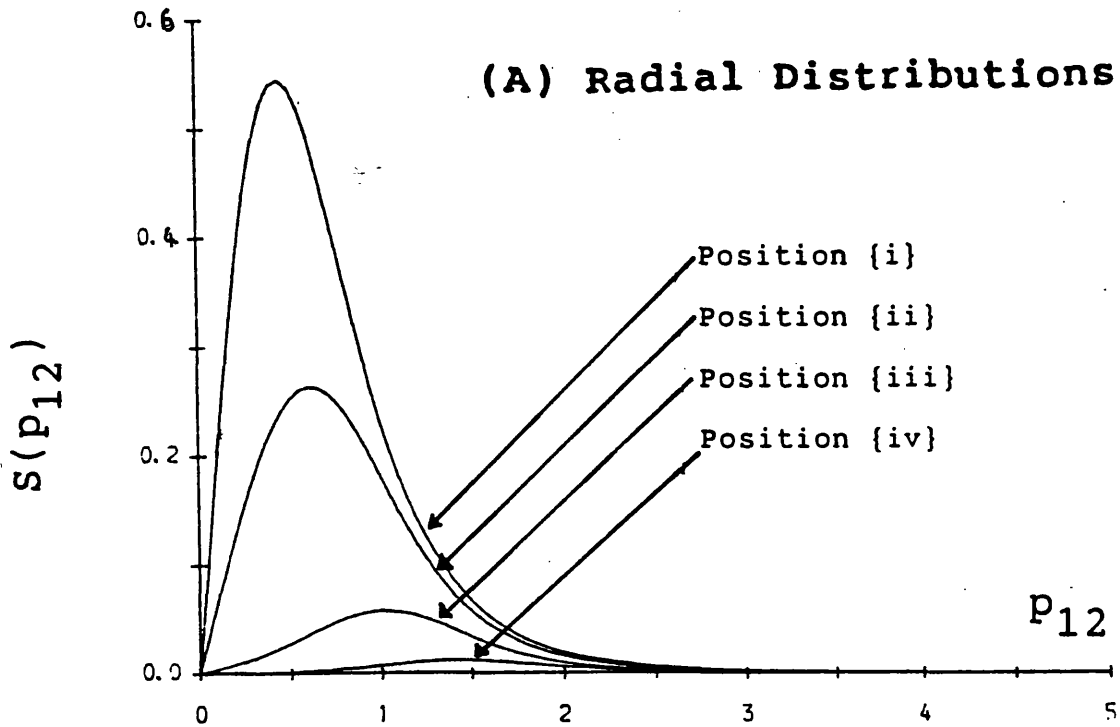
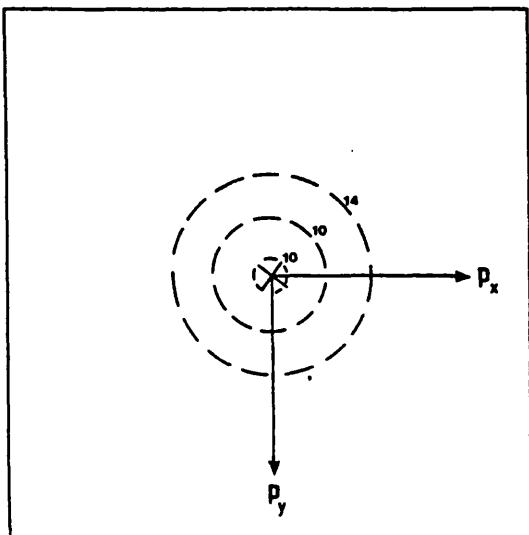
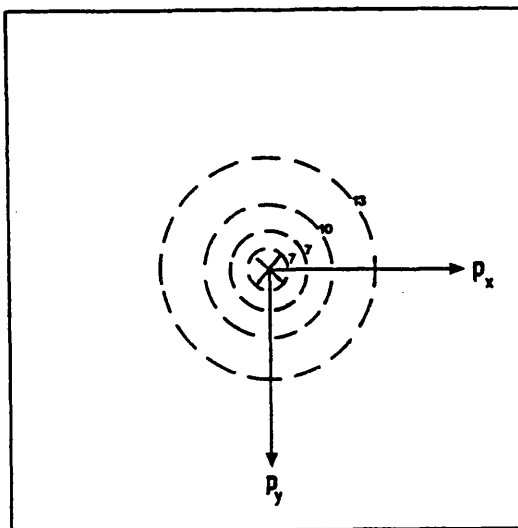


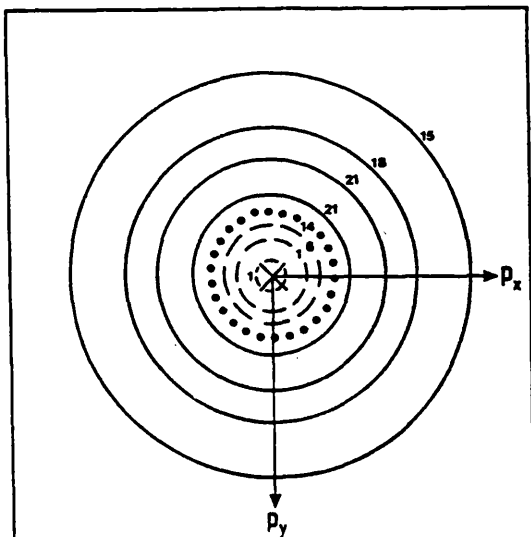
Figure (II.12.15) HF partial planar momentum distribution functions for H_2 , with electron 1 fixed at positions {i}, {ii}, {iii} and {iv} (see Fig.(II.12.3)) and electron 2 moving in the $p_x p_y$ plane, were obtained by appropriate integration of Fig.(II.12.14).



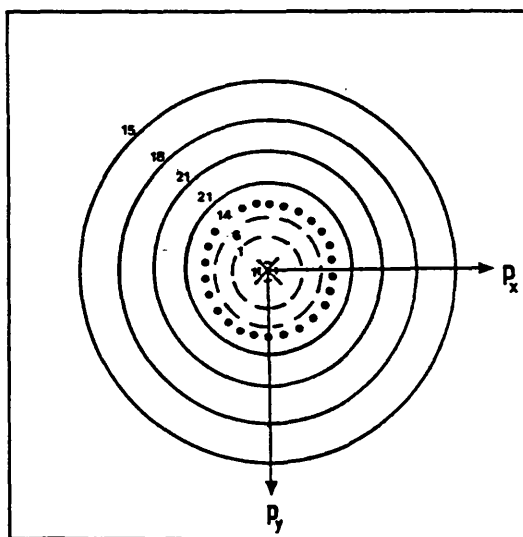
(A) 2NO - 1NO
z - correlation



(B) 3NO - 1NO
(z + φ) - correlation



(C) 4NO - 1NO
(z + φ + ρ) - correlation



(D) 10NO - 1NO
(z + φ + ρ + 2nd order)
- correlation

Figure (II.12.16) The partial planar Δ -surfaces, $\Delta V(p_{12}, p_1)$, for fixed electron position $\{i\}$ (see Figure (II.12.3A) for the definition), with the roving electron located in the $p_x p_y$ -plane with $p_z = 0$.

(A) Radial Shifts

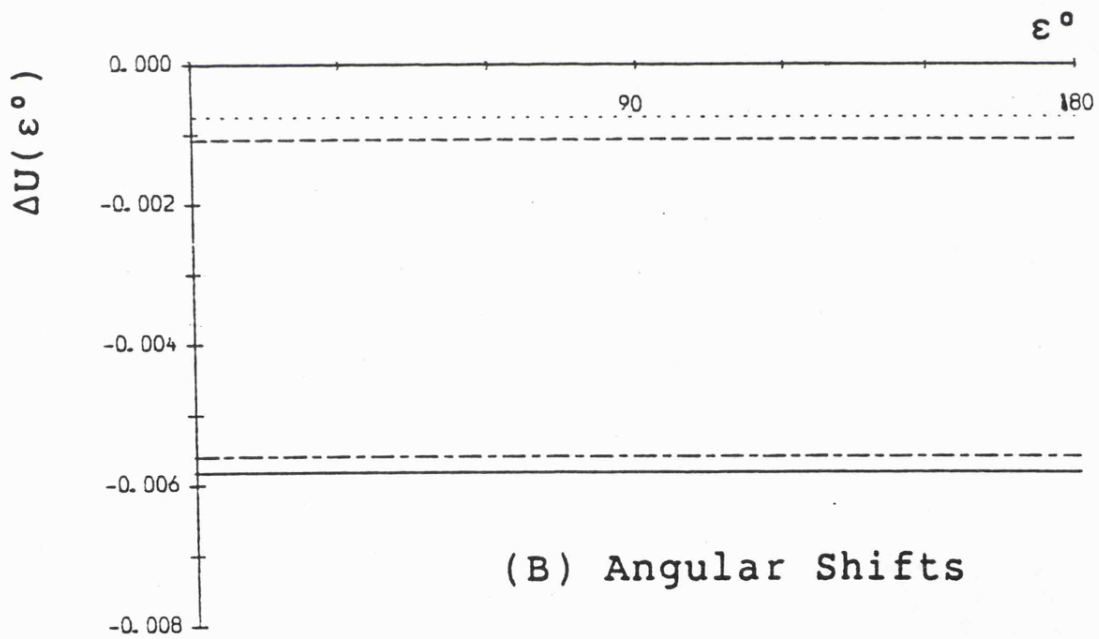
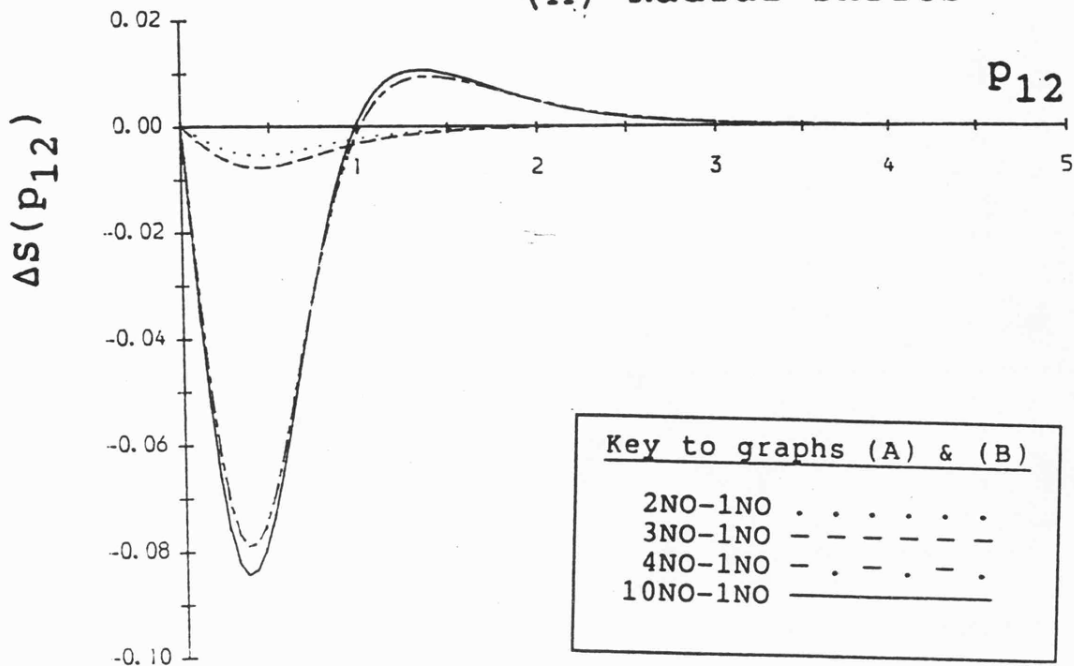
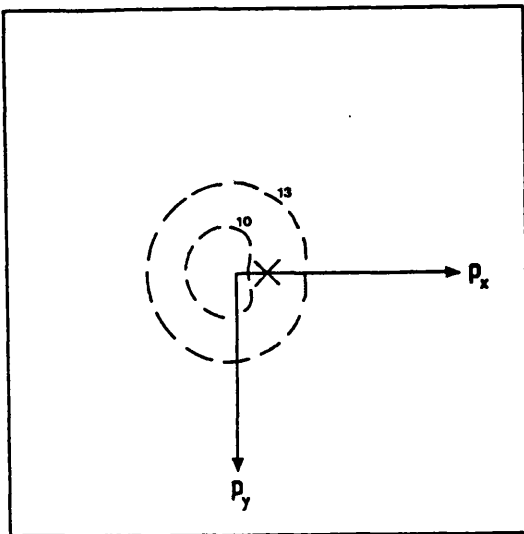
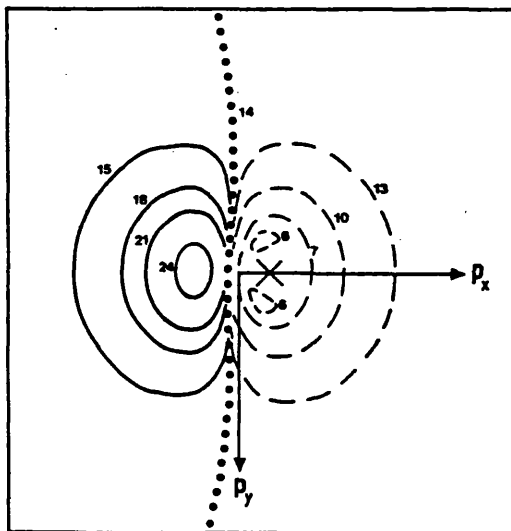


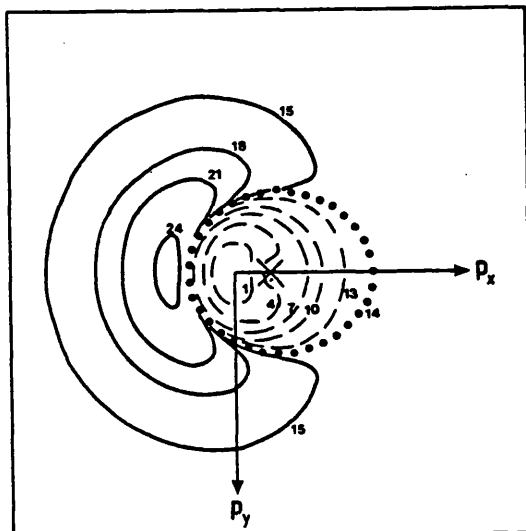
Figure (II.12.17) Partial planar Coulomb shifts for H_2 , with electron 1 fixed at position $\{i\}$ (see Fig.(II.12.3)) and electron 2 moving in the $p_x p_y$ plane, were obtained by appropriate integration of Fig.(II.12.16).



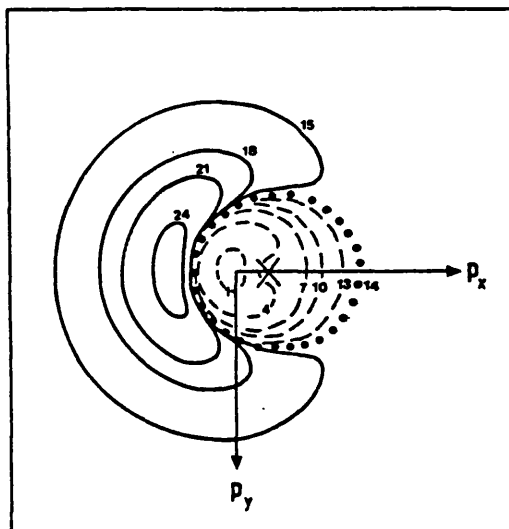
(A) 2NO - 1NO
z - correlation



(B) 3NO - 1NO
(z + φ) - correlation



(C) 4NO - 1NO
(z + φ + ρ) - correlation



(D) 10NO - 1NO
(z + φ + ρ + 2nd order)
- correlation

Figure (II.12.18) The partial planar Δ -surfaces, $\Delta V(p_2, p_1)$, for fixed electron position {ii} (see Figure (II.12.3A) for the definition), with the roving electron located in the $p_x p_y$ -plane with $p_z = 0$.

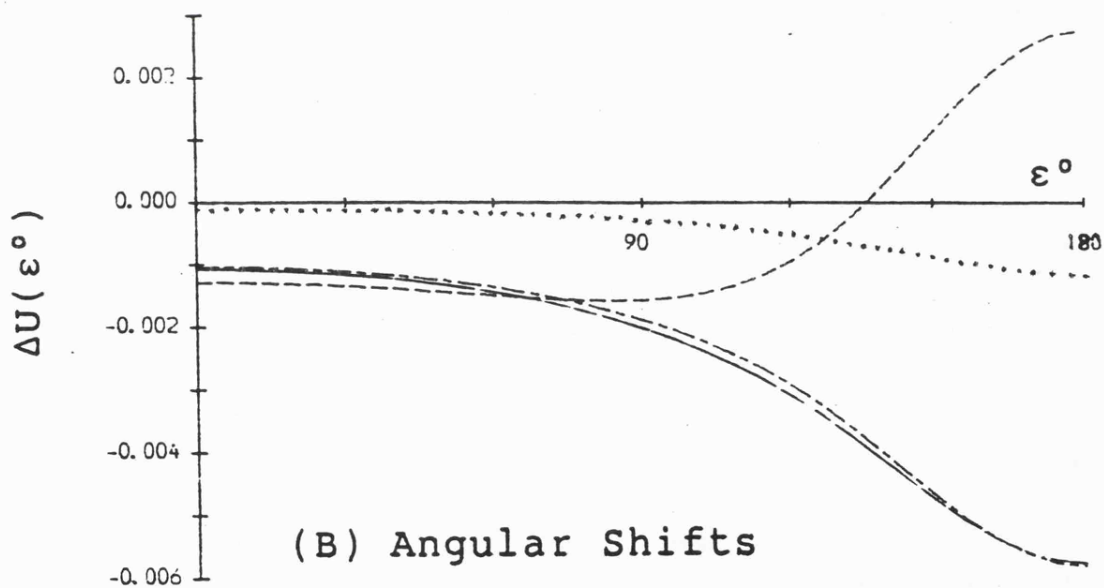
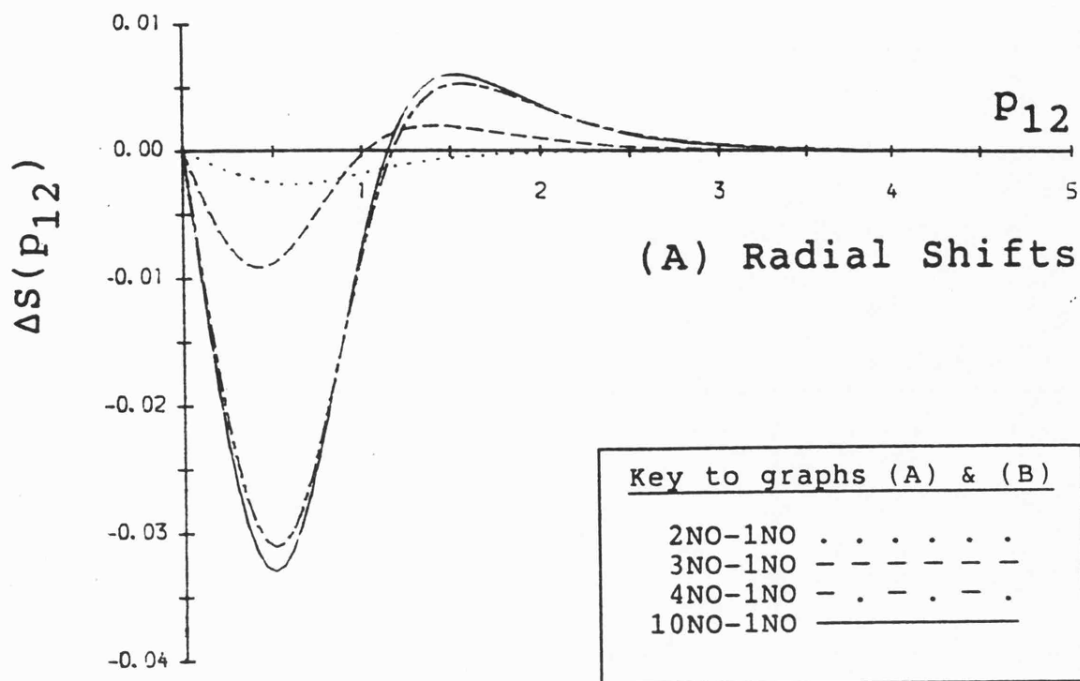
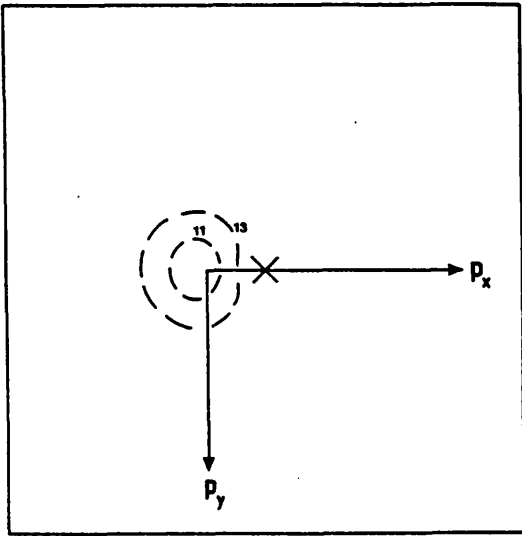
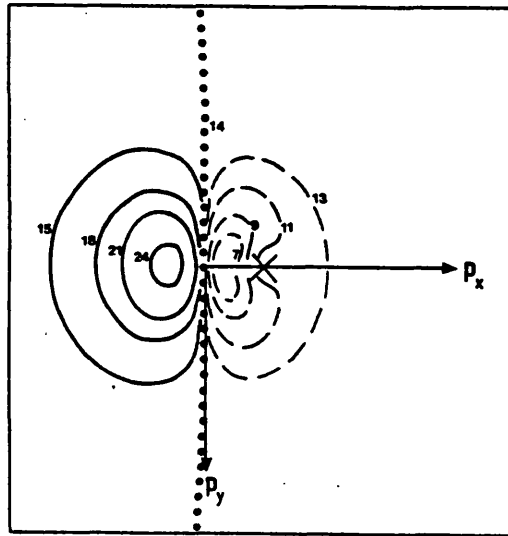


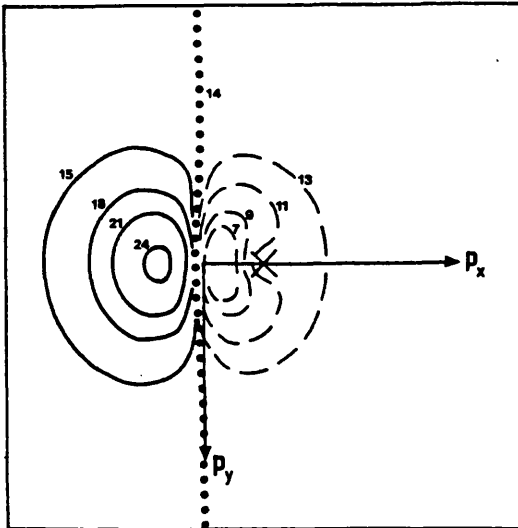
Figure (II.12.19) Partial planar Coulomb shifts for H_2 , with electron 1 fixed at position {ii} (see Fig.(II.12.3)) and electron 2 moving in the $p_x p_y$ plane, were obtained by appropriate integration of Fig.(II.12.18).



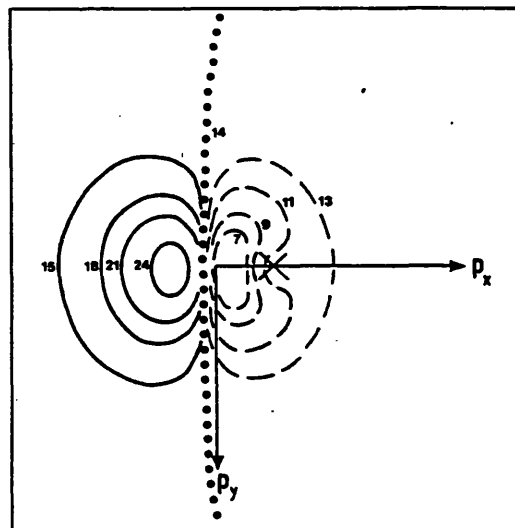
(A) 2NO - 1NO
z - correlation



(B) 3NO - 1NO
(z + φ) - correlation



(C) 4NO - 1NO
(z + φ + ρ) - correlation



(D) 10NO - 1NO
(z + φ + ρ + 2nd order)
- correlation

Figure (II.12.20) The partial planar Δ -surfaces, $\Delta V(p_{12}, p_1)$, for fixed electron position {iii} (see Figure (II.12.3A) for the definition), with the roving electron located in the $p_x p_y$ -plane with $p_z = 0$.

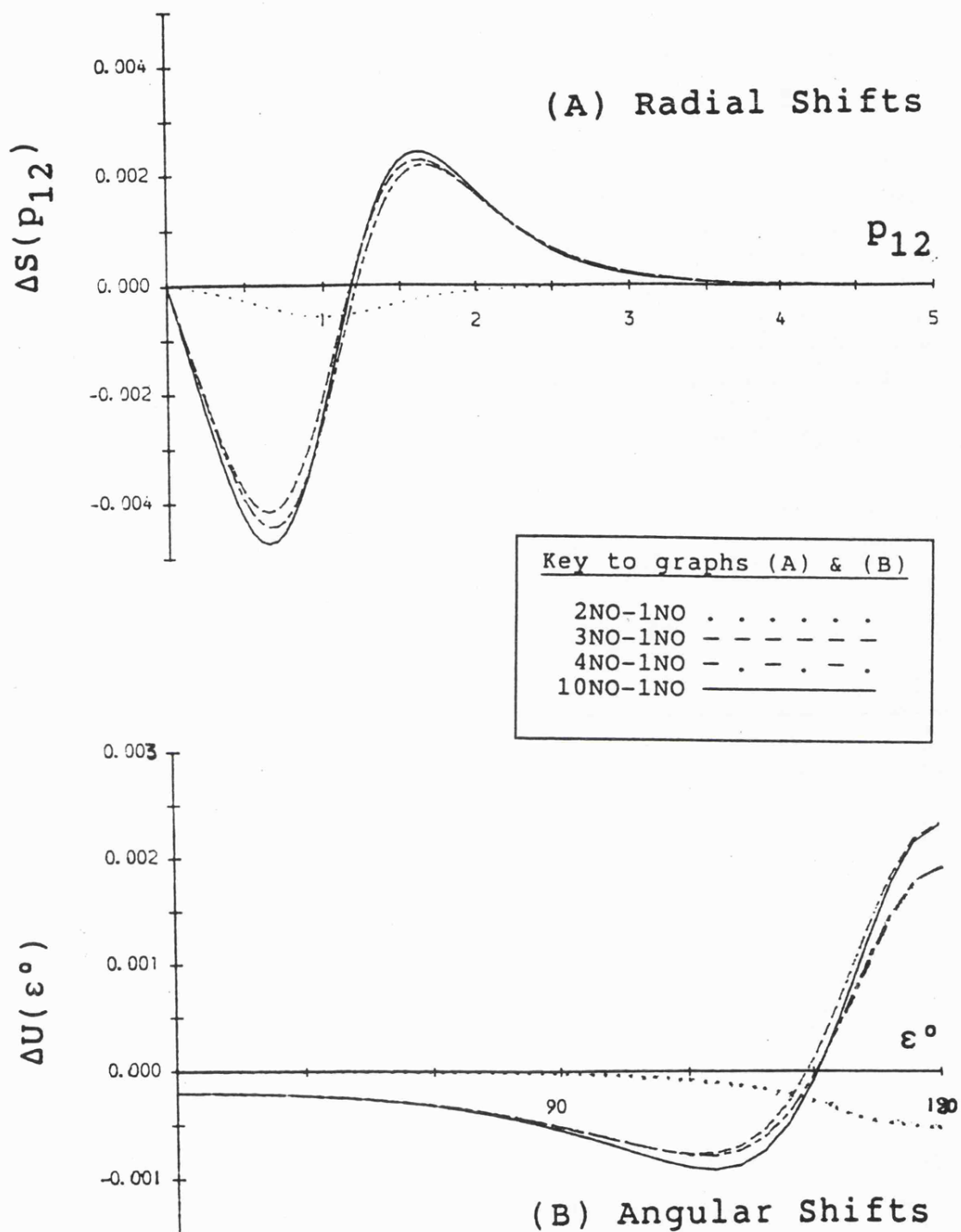
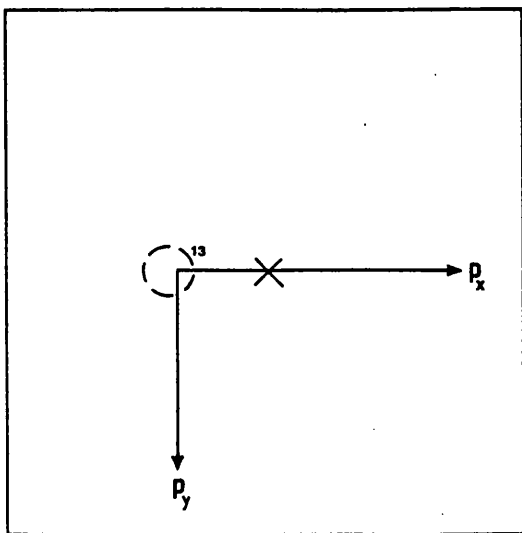
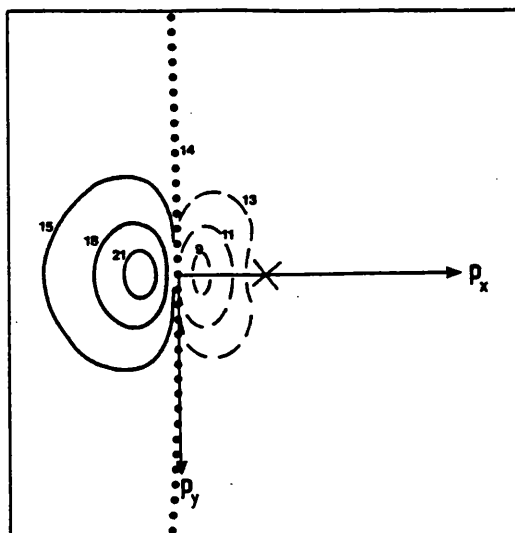


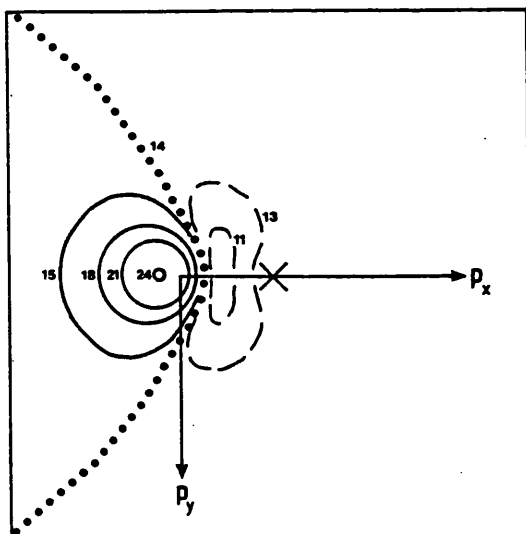
Figure (II.12.21) Partial planar Coulomb shifts for H_2 , with electron 1 fixed at position {iii} (see Fig.(II.12.3)) and electron 2 moving in the $p_x p_y$ plane, were obtained by appropriate integration of Fig.(II.12.20).



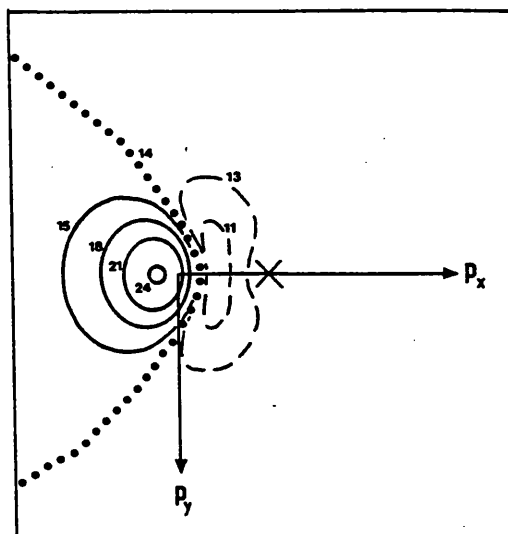
(A) 2NO - 1NO
z - correlation



(B) 3NO - 1NO
(z + φ) - correlation



(C) 4NO - 1NO
(z + φ + ρ) - correlation



(D) 10NO - 1NO
(z + φ + ρ + 2nd order)
- correlation

Figure (II.12.22) The partial planar Δ -surfaces, $\Delta V(p_{12}, p_1)$, for fixed electron position {iv} (see Figure (II.12.3A) for the definition), with the roving electron located in the $p_x p_y$ -plane with $p_z = 0$.

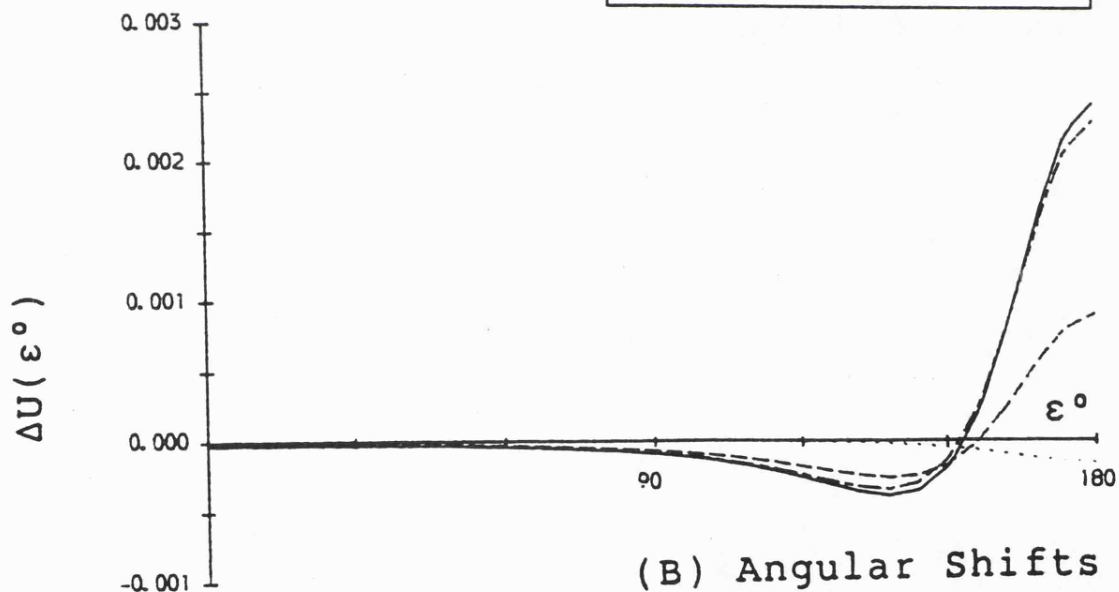
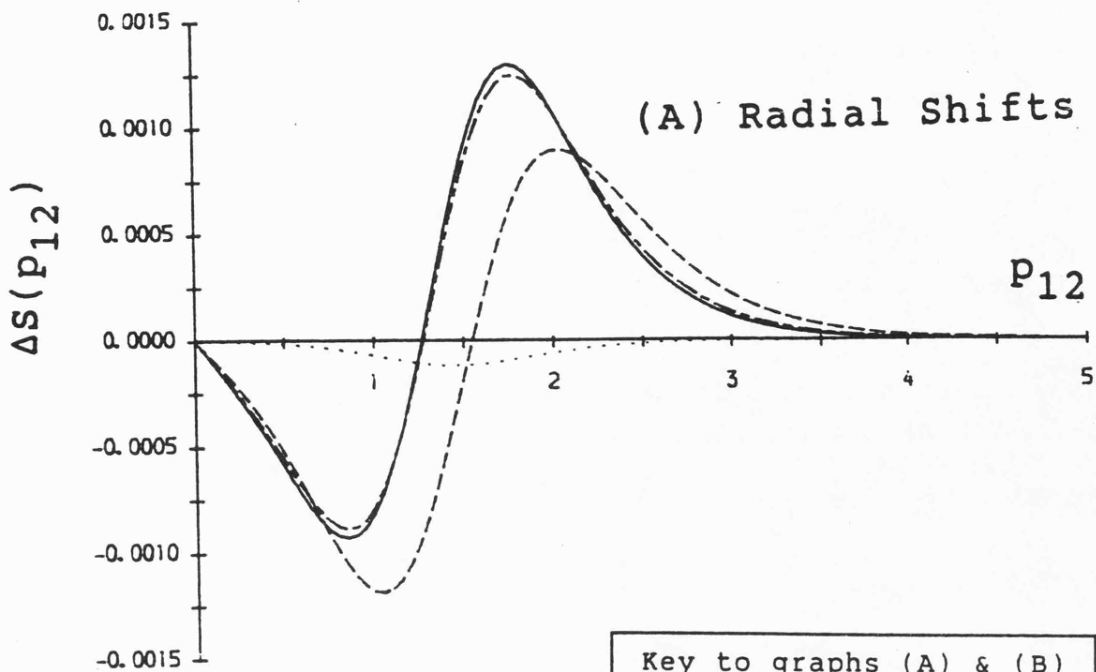
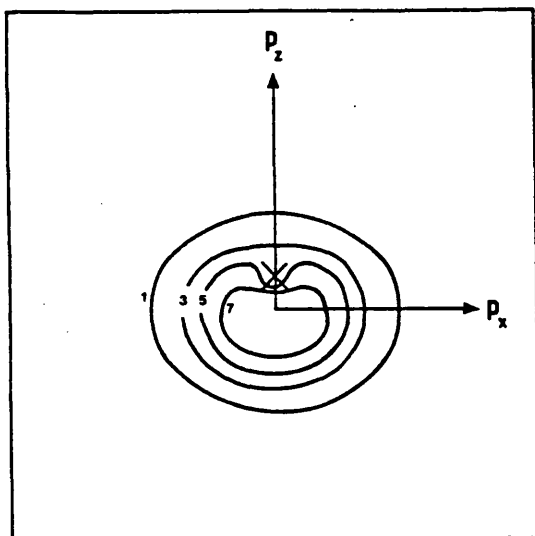
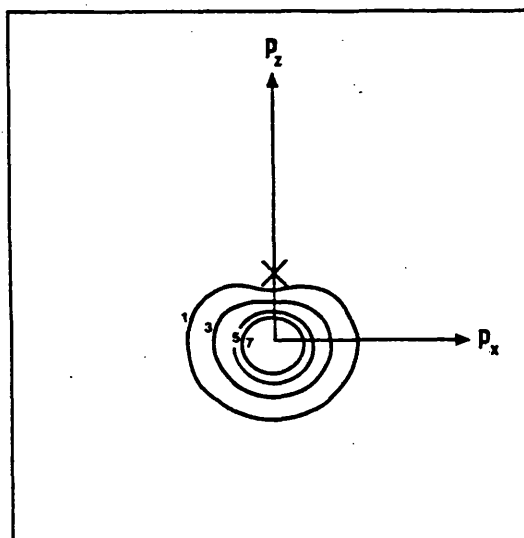


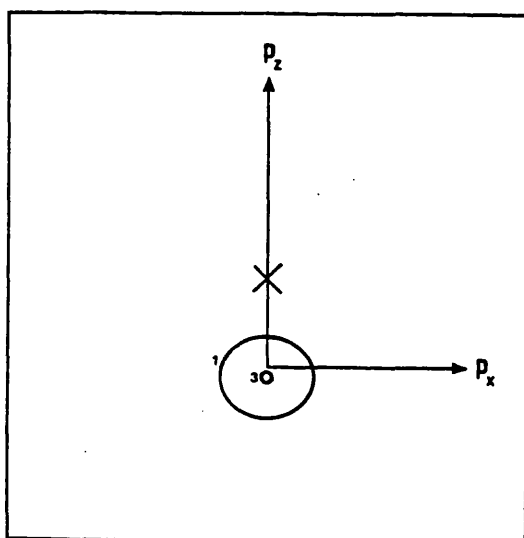
Figure (II.12.23) Partial planar Coulomb shifts for H_2 , with electron 1 fixed at position {iv} (see Fig.(II.12.3)) and electron 2 moving in the $p_x p_y$ plane, were obtained by appropriate integration of Fig.(II.12.22).



(A) position {v}



(B) position {vi}



(C) position {vii}

Figure (II.12.24) The momentum-space Hartree Fock $V(p_{12}, p_1)$ distribution functions for positions {v}, {vi} and {vii} in the $p_x p_z$ -plane with $p_y = 0$.

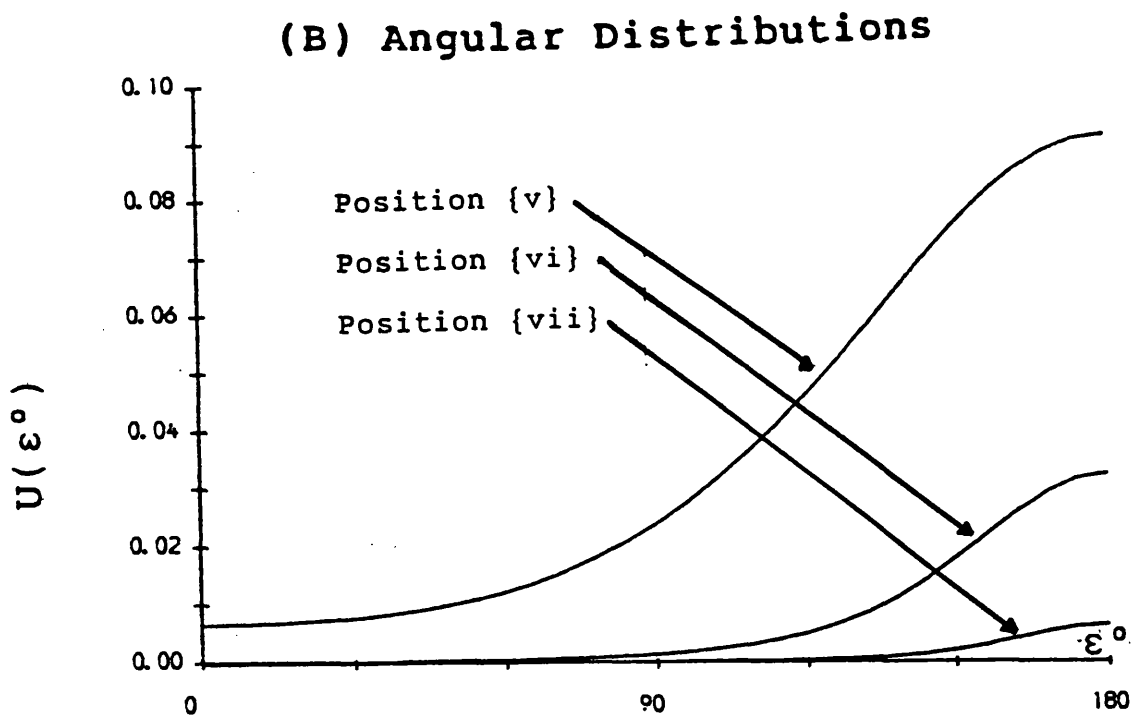
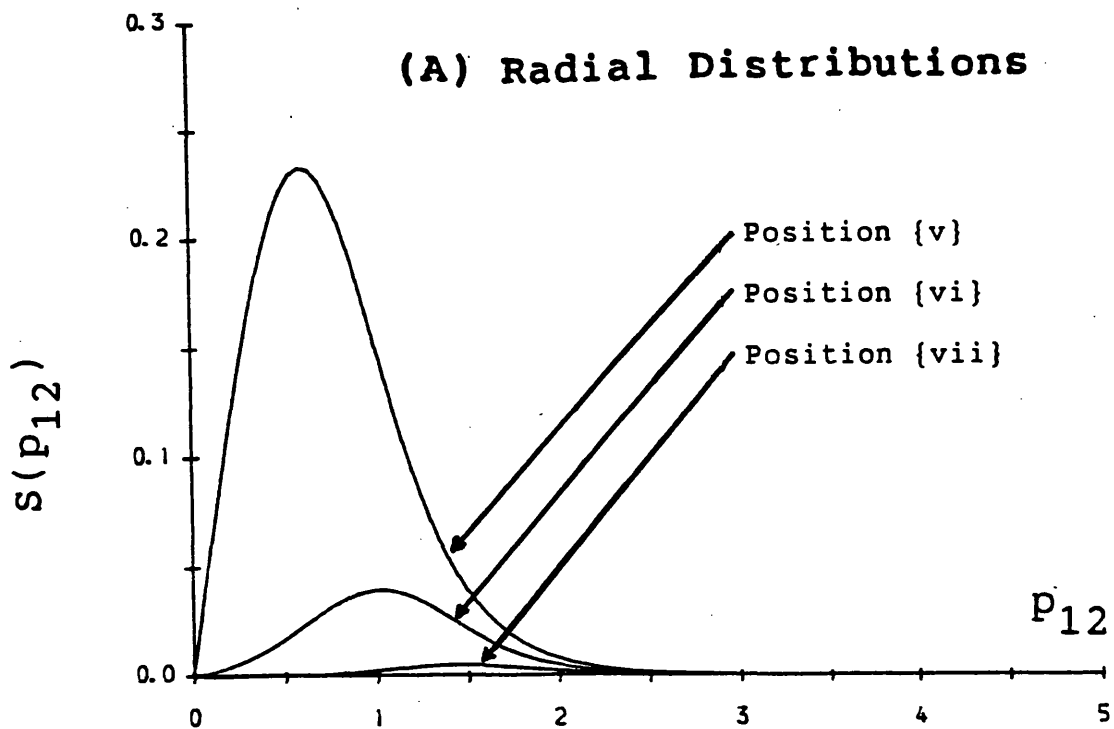
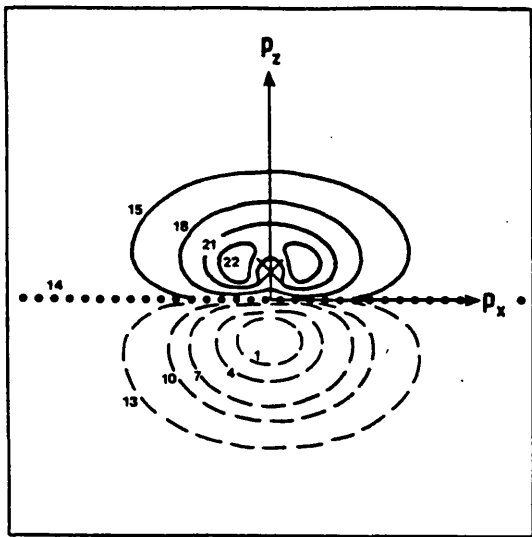
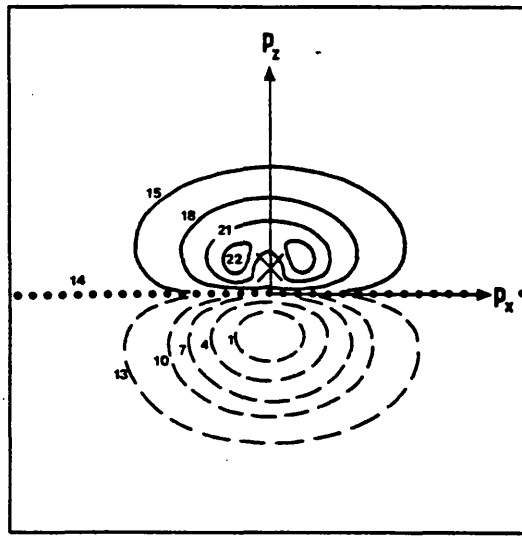


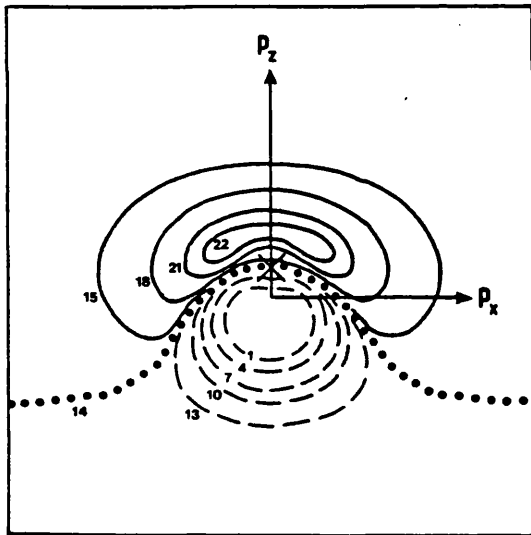
Figure (II.12.25) HF partial planar momentum distribution functions for H_2 , with electron 1 fixed at positions {v}, {vi} and {vii} (see Fig.(II.12.3)) and electron 2 moving in the $p_x p_z$ plane, were obtained by appropriate integration of Fig.(II.12.24).



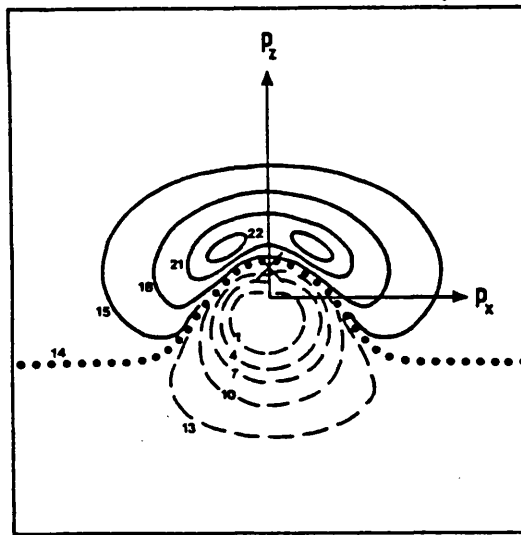
(A) 2NO - 1NO
z - correlation



(B) 3NO - 1NO
(z + φ) - correlation



(C) 4NO - 1NO
(z + φ + ρ) - correlation



(D) 10NO - 1NO
(z + φ + ρ + 2nd order)
- correlation

Figure (II.12.26) The partial planar Δ -surfaces, $\Delta V(p_{12}, p_1)$, for fixed electron position $\{v\}$ (see Figure (II.12.3A) for the definition), with the roving electron located in the $p_x p_z$ -plane with $p_y = 0$.

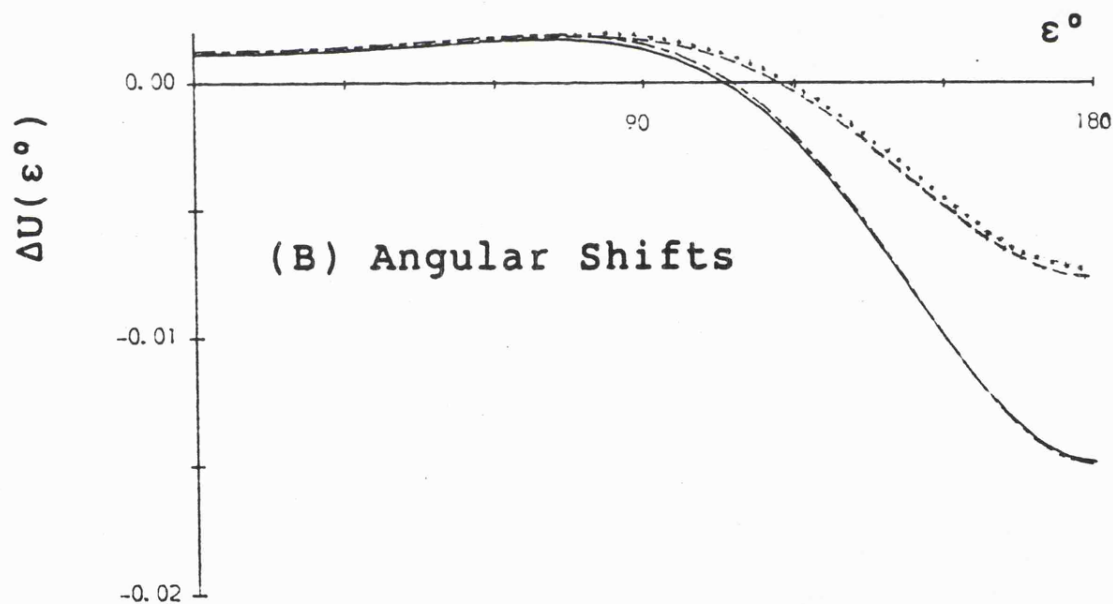
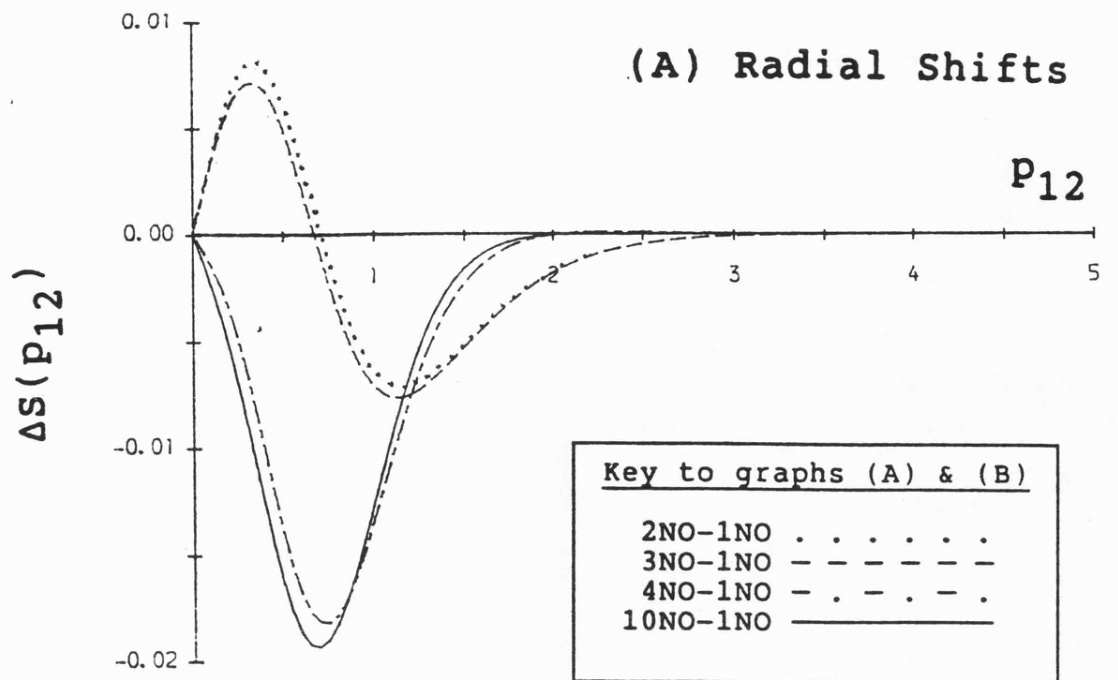
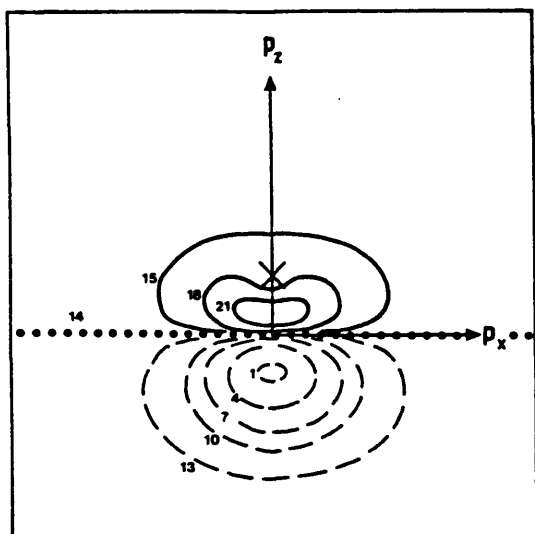
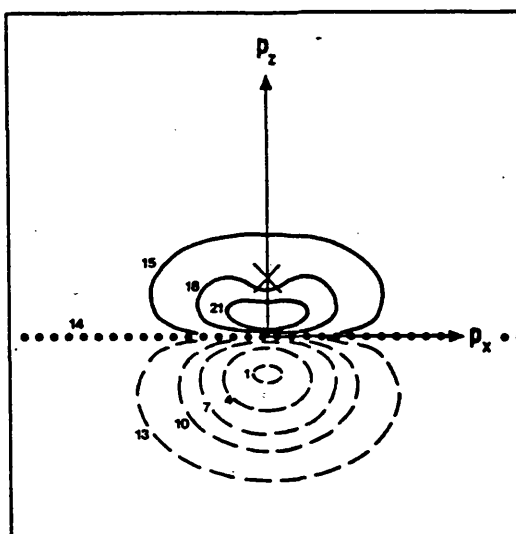


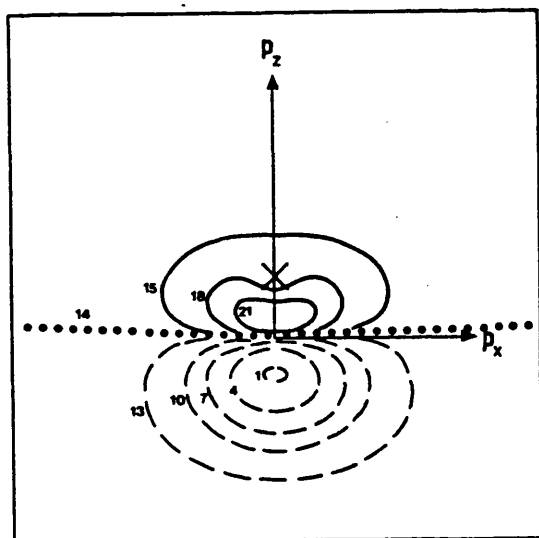
Figure (II.12.27) Partial planar Coulomb shifts for H_2 , with electron 1 fixed at position $\{v\}$ (see Fig.(II.12.3)) and electron 2 moving in the $p_x p_z$ plane, were obtained by appropriate integration of Fig.(II.12.26).



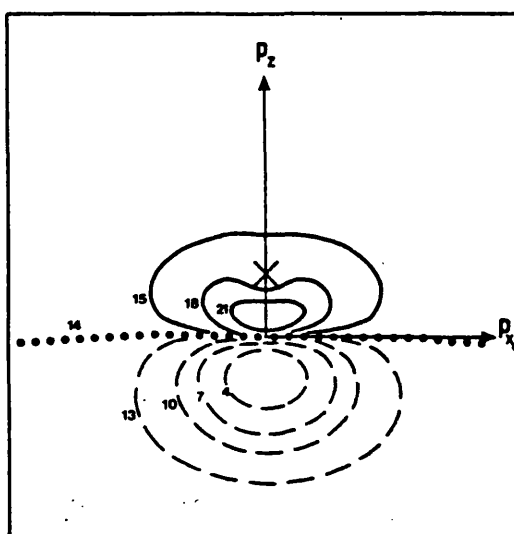
(A) 2NO - 1NO
z - correlation



(B) 3NO - 1NO
(z + φ) - correlation



(C) 4NO - 1NO
(z + φ + ρ) - correlation



(D) 10NO - 1NO
(z + φ + ρ + 2nd order)
- correlation

Figure (II.12.28) The partial planar Δ -surfaces, $\Delta V(p_{12}, \dot{p}_1)$, for fixed electron position $\{vi\}$ (see Figure (II.12.3A) for the definition), with the roving electron located in the $p_x p_z$ -plane with $p_y = 0$.

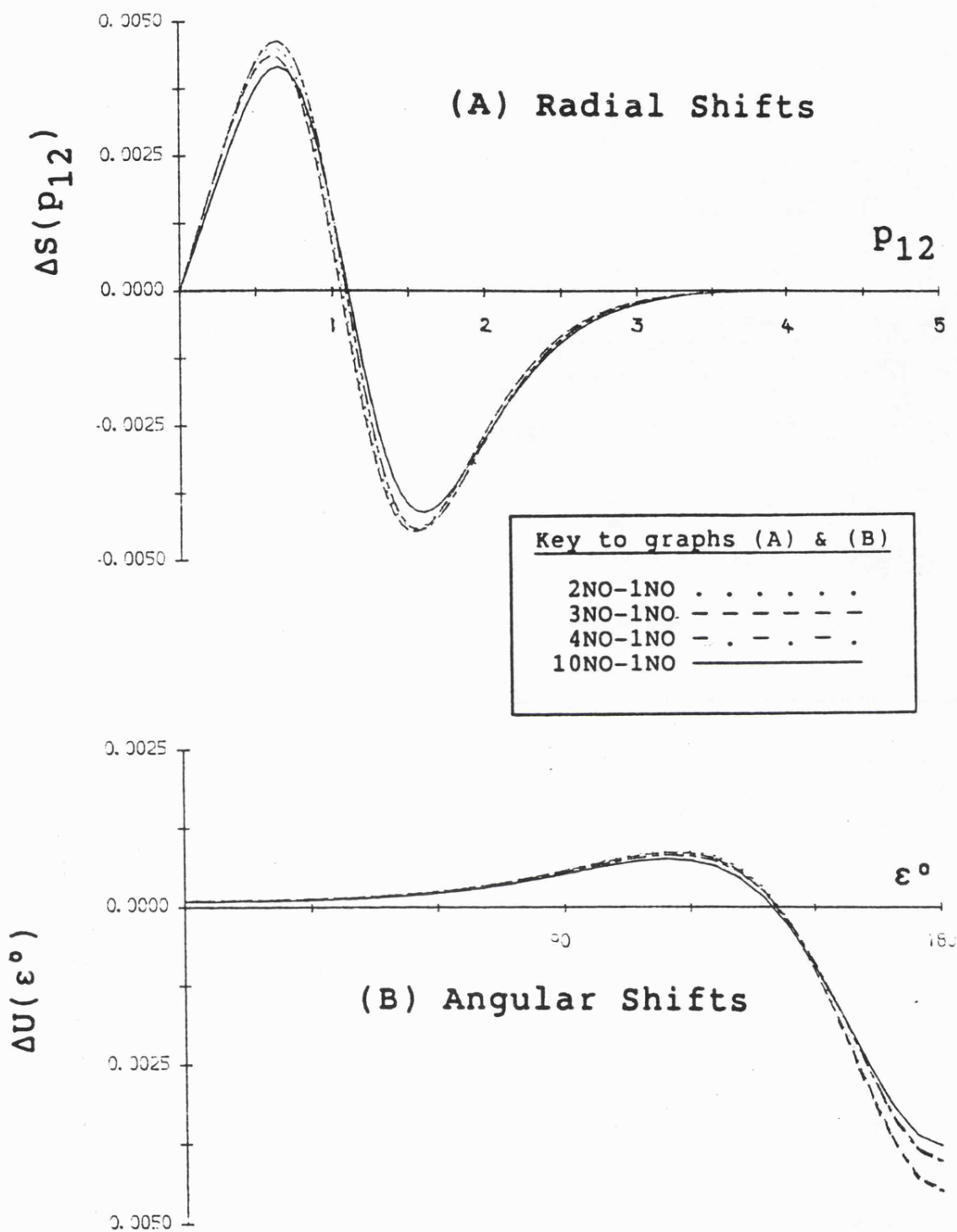
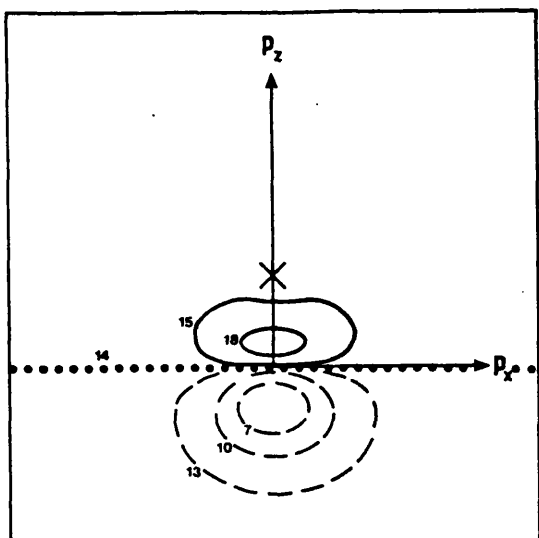
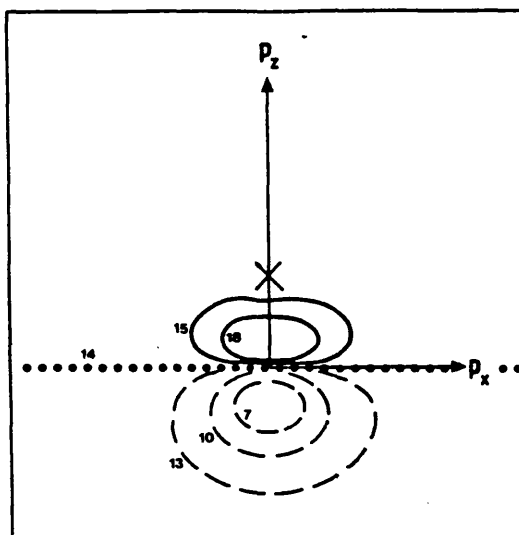


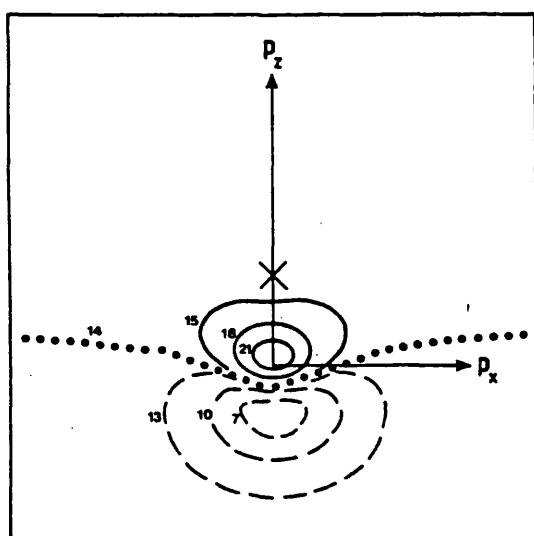
Figure (II.12.29) Partial planar Coulomb shifts for H_2 , with electron 1 fixed at position {vi} (see Fig.(II.12.3)) and electron 2 moving in the $p_x p_z$ plane, were obtained by appropriate integration of Fig.(II.12.28).



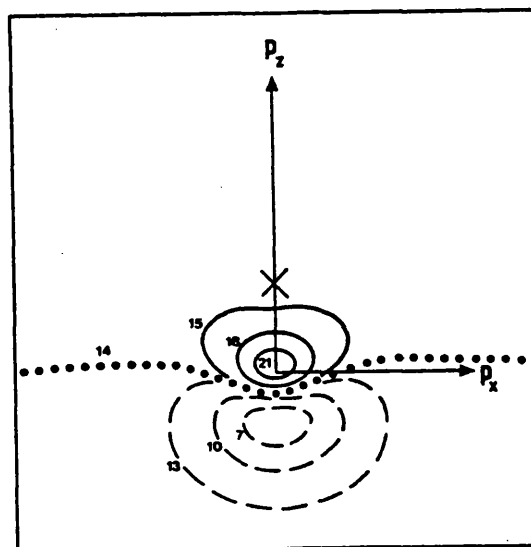
(A) 2NO - 1NO
z - correlation



(B) 3NO - 1NO
(z + φ) - correlation



(C) 4NO - 1NO
(z + φ + ρ) - correlation



(D) 10NO - 1NO
(z + φ + ρ + 2nd order)
- correlation

Figure (II.12.30) The partial planar Δ -surfaces, $\Delta V(p_{12}, p_1)$, for fixed electron position (vii) (see Figure (II.12.3A) for the definition), with the roving electron located in the $p_x p_z$ -plane with $p_y = 0$.

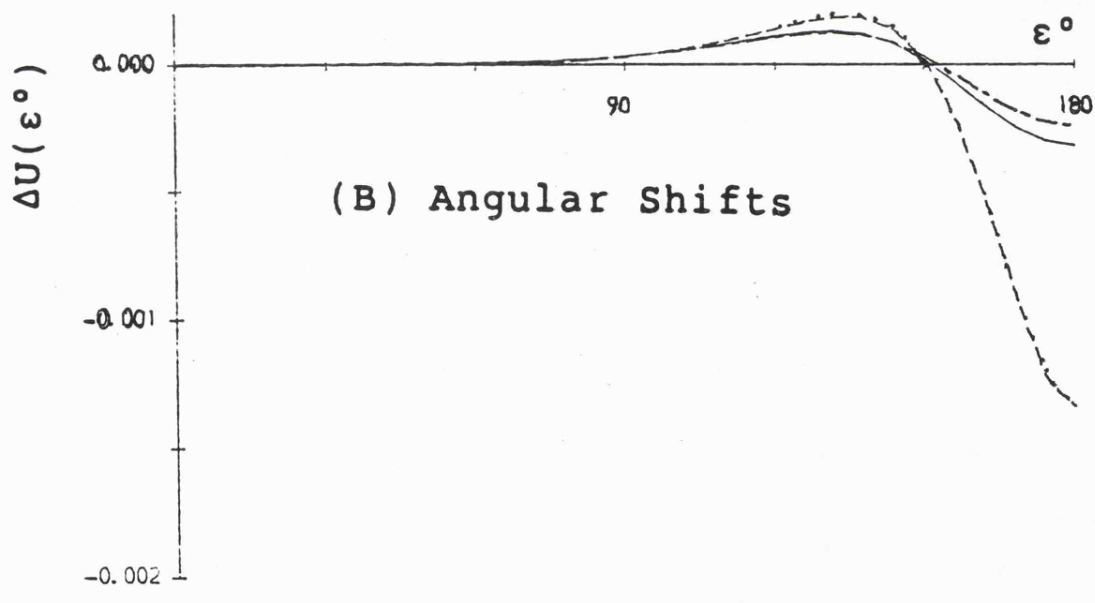
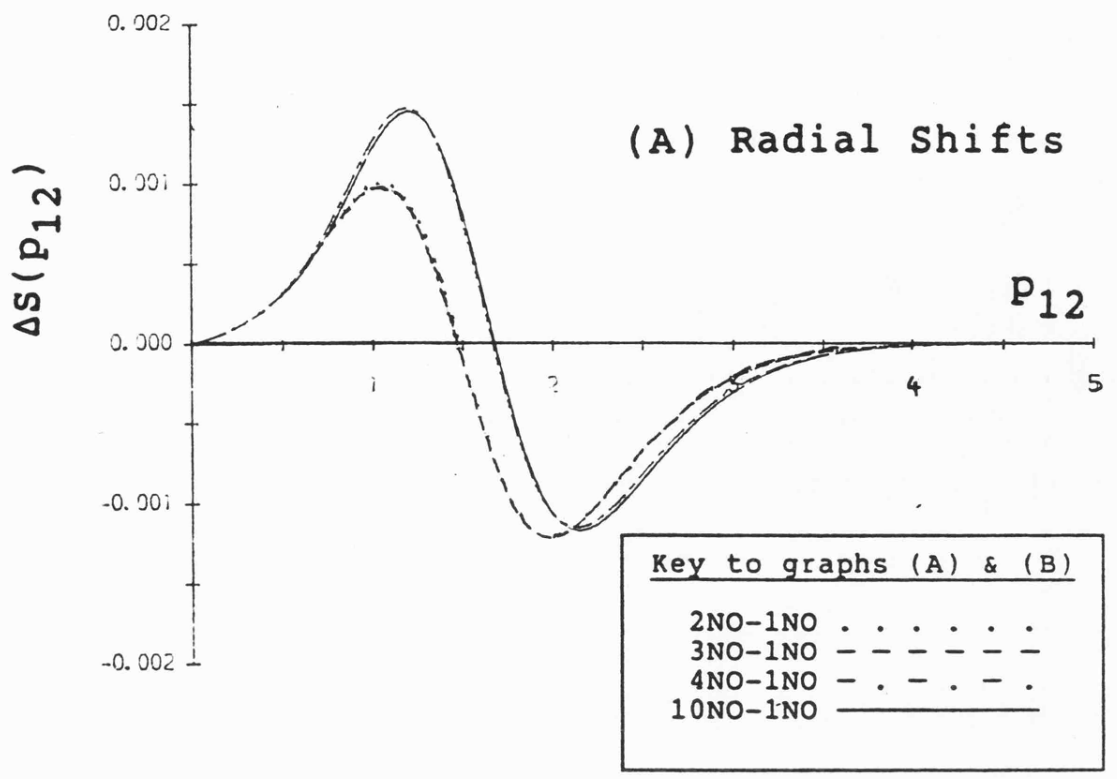


Figure (II.12.31) Partial planar Coulomb shifts for H_2 , with electron 1 fixed at position {vii} (see Fig.(II.12.3)) and electron 2 moving in the $p_x p_z$ plane, were obtained by appropriate integration of Fig.(II.12.30).

CHAPTER II.13

Discussion of H₂ Results in Momentum-Space

The first general observation to make when considering all of the momentum-space electron distributions displayed in Chapter (II.12) is that they are single-centred in nature and possess an 'ellipsoidal-type' symmetry that is aligned to be perpendicular to the bond. Thus, as noted by Coulson^(2.xiii.1), the presence of the bond decreases the mean component of the velocity along the bond axis but increases it in perpendicular directions.

(II.13.1) The Momentum-Space One-Particle Density Analysis

In order to obtain a theoretical model of the electron momentum distribution in the H₂ molecule, the uncorrelated one-particle density in the xz-plane is presented in Figure (II.12.1). It inherits the axial symmetry of the position-space distribution but contains a maximum at the origin. For small values of momentum, the electron is far from the molecule and hence only experiences what is effectively a single nuclear force; the contours are consequently almost circular in form. Higher momentum is then associated with the electron coming nearer to the nuclear frame where it is employed in bonding, where the contours develop into a characteristic ellipse-shape which

is accentuated as the momentum is increased.

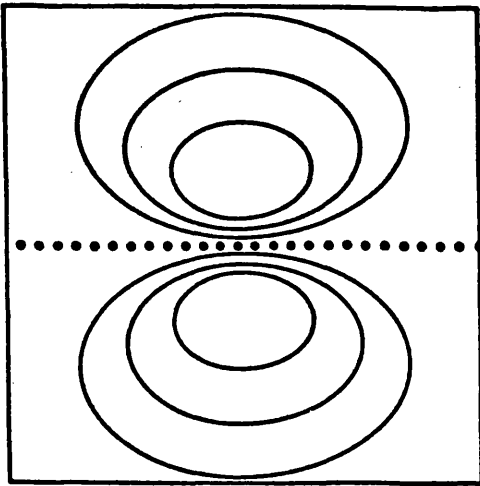
By considering the Δ -surfaces, shown in Figure (II.12.2), we see that they have a complex structure and their range is comparable with the range of the HF one-particle density itself. It has already been pointed out that an advantage of transforming a wavefunction into momentum-space using the Fourier transform technique is that the form of the function is preserved and only the natural orbitals need to be transformed. Consequently, the Δ -one-particle density has the same mathematical form as the position-space Δ -one-particle density and may be written as

$$\Delta\rho_M(\mathbf{p}_1) = \sum_{i=2}^M A_M \mu_i^2 \chi_i^*(\mathbf{p}_1) \chi_i(\mathbf{p}_1) - (A_1 - A_M) \mu_1^2 \chi_1^*(\mathbf{p}_1) \chi_1(\mathbf{p}_1). \quad (\text{II.13.1})$$

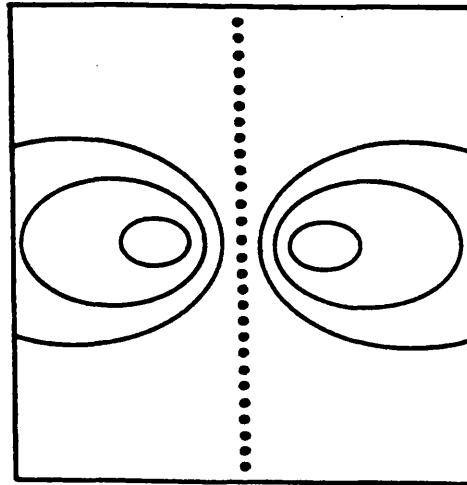
The momentum-space natural orbital $\chi_i(\mathbf{p}_1)$ is defined in equation (II.11.18), from which it is easily seen that the product $\chi_i^*(\mathbf{p}_1) \chi_i(\mathbf{p}_1)$ is real. The renormalisation constant A_M is given by

$$A_M = 1 / \sum_{i=1}^M \mu_i^2. \quad (\text{II.13.2})$$

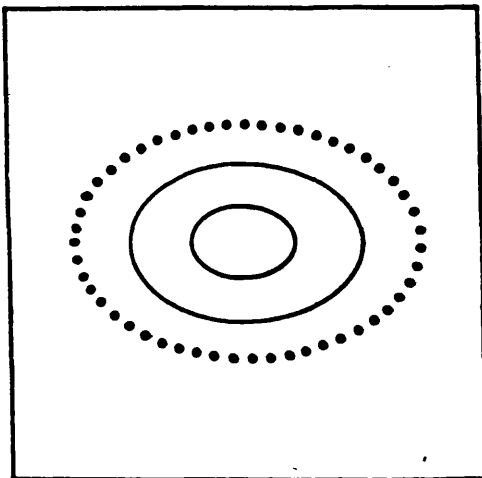
Due to the mathematical similarities between the position and momentum-space analysis, the occupation numbers are identical and are given in equations (II.6.5), (II.6.6), (II.6.7) and (II.6.8), and hence are not repeated here. It is necessary, however, to remind ourselves that electron



(A) $\chi_2^*(p_1)\chi_2(p_1)$



(B) $\chi_3^*(p_1)\chi_3(p_1)$



(C) $\chi_4^*(p)\chi_4(p)$

Figure (II.13.1) Sketches of the $\chi_i^*(p_1)\chi_i(p_1)$ probability surfaces for $2 \leq i \leq 4$ where $\chi_i(p)$ has been defined in equation (II.11.18). The surfaces are viewed in the xz -plane and are aligned in the z -direction.

correlation is introduced into the one-particle density by the transfer of probability from the HF description of the molecule into the correlating orbitals (see Chapter (II.6.1) for further details). In addition, since the occupation numbers are virtually independent of the number of configurations employed in the generation of the surfaces, the different correlation types can be examined separately.

The probability surfaces, defined by $\chi_i^*(\underline{p}_1)\chi_i(\underline{p}_1)$, differ from the equivalent position-space surfaces and should be discussed before considering the Δ -one-particle density surfaces further. The $\chi_1^*(\underline{p}_1)\chi_1(\underline{p}_1)$ surface represents the HF one-particle-density and is given in Figure (II.12.1).

Figure (II.13.1A) shows that there is a nodal plane in the $\chi_2^*(\underline{p}_1)\chi_2(\underline{p}_1)$ probability surface when $p_z = 0$ and maxima occur at approximately ± 1 a.u. from the origin on the p_z -axis. The probability decreases rapidly from these maxima in the p_z -direction but in the p_x and p_y directions the reduction is much less steep. The p_z -axis on the ϕ -correlating surface, $\chi_3^*(\underline{p}_1)\chi_3(\underline{p}_1)$, represents a node and a torus shape of maximum probability, centred on the p_z -axis may be observed. Furthermore, the decay from this maximum is again faster in the p_z -direction than in either the p_x or p_y direction. The ρ -correlating surface $\chi_4^*(\underline{p}_1)\chi_4(\underline{p}_1)$, on the other hand, contains an ellipsoidal shaped zero contour with a maximum of probability at the origin.

It must be noted that the magnitudes of the shifts in

probability due to correlation $\Delta\rho(\underline{p}_1)$ is generally greater than in the position-space results even though both distributions possess the same occupation numbers and the orbitals are normalised. This is due to the fact that, since the position-space orbitals are two-centred, the probability is spread over a greater area than the momentum-space orbitals and hence a similar percentage redistribution in probability will yield a larger effect. We note also that, as a result of the requirement for $\Delta\rho_M(\underline{p}_1)$ to be equal to $\Delta\rho_M(-\underline{p}_1)$ to enable the total averaged momentum of the system to remain zero, the Δ -surfaces all possess ~~four~~^{two}-fold symmetry.

Z-correlation only is introduced in Figure (II.12.2A). This has the effect of reducing the probability of locating electron 1 with a low momentum but increasing it when $p_z = \pm 1.0$ a.u. and the zero contours have a slight tendency to bend towards the positive regions of the surface. The surface may be generated by mentally subtracting Figure (II.12.1) from the z-correlating surface (Figure (II.13.1A)). We see, therefore, it is the effect of the $\chi_1^*(\underline{p}_1)\chi_1(\underline{p}_1)$ HF surface that is responsible for the minimum at the origin. Although this surface is not an exact representation of the momentum distribution in the equivalent position-space surface, Figure (II.5.2A), certain comparisons may still be made. For example, Figure (II.12.2A) can be interpreted as reducing the probability of locating electron 1 in a region of low momentum, ie far from the influence of the nuclei, yet increasing the probability

of discovering it with higher values of momentum, especially in the z-direction. This compares favourably with Figure (II.5.2A) in position-space where the probability of locating electron 1 is reduced far from the nucleus and in the mid bond position but increased just behind the nuclei, i.e. in regions of high momentum.

The effect of ϕ -correlation, as well as z-correlation, is included in Figure (II.12.2B). As the occupation numbers vary only slightly, the shape of Figure (II.12.2B) may be generated by adding Figure (II.13.1B) to Figure (II.12.2A) and then subtracting additional HF probability to compensate. It is therefore the effect of the third natural orbital that causes the zero contours in Figure (II.12.2B) to form into an ellipse-type shape. The area covered by the positive region is thus increased yet, due to the effect of the HF orbitals, the height of the maximum is decreased and the depth of the minimum increased.

Surprisingly, we see that ρ -correlation, which is introduced in Figure (II.12.2C), has the opposite effect to z and ϕ -correlation as the magnitude of the minimum is decreased. The maximum at the centre of the $\chi_4^*(\underline{p}_1)\chi_4(\underline{p}_1)$ probability surface must therefore be greater than the maximum associated with the HF probability distribution. Contrary to the effect of the other correlation-types ρ -correlation therefore has the effect of increasing the probability of discovering the electron with a small momentum and hence, in position-space, far from the influence of the nuclear forces. This agrees with the

position-space surface where the maxima associated with each of the nuclei are reduced slightly.

The remaining six natural orbitals have very little effect on the Δ -one-particle density as demonstrated by Figure (II.12.2D); this diagram nevertheless represents the most accurate view of the effect of electron correlation on the momentum-space one-particle density. The gross effect of correlation is seen to decrease the probability of locating the electron with low momentum and to increase it with a higher momentum in the p_z -direction. Thus, $\Delta\rho(p_1)$ offsets, in part, the general increase of momentum in the $p_x p_y$ -plane that is associated with bond formation. This effect has also been observed in HeH^+ by Banyard and Reed^(2.xiii.2). The overall increase in momentum, however, must be responsible for introducing additional stability to the H_2 system. As argued in Chapter (II.6.1), an increased momentum corresponds to a larger electronic kinetic energy and, if the virial theorem^(2.xiii.3), is to hold, the potential energy will lower by twice as much, and hence lower the total energy. This has been reiterated by Epstein and Tanner^(2.xiii.4) but with particular reference to momentum distributions. They were also able to conclude that correlation has the effect of increasing the values of $\langle p^n \rangle$ for $n > 0$ and decreasing them for $n < 0$.

When equation (II.10.1) is considered, it can be seen that the improvement in the Compton profile due to the effect of electron correlation is

$$\Delta J(q) = \frac{1}{2} \int_{p=q}^{\infty} [\Delta I(p)/p] dp \quad (\text{II.13.3})$$

where

$$\Delta I(p) = \int_{\theta=0}^{\pi} \int_{\phi=0}^{2\pi} \Delta \rho(\underline{p}) p^2 \sin\theta d\theta d\phi. \quad (\text{II.13.4})$$

This provides a relationship between the Δ -one-particle density and the improvement to the Compton profile from which certain observations can be drawn. As $\Delta I(p)$ is essentially the angular average of $\Delta \rho(\underline{p})$, it will have a similar form as the Δ -one-particle density. It may then be argued that, for large values of q , $\Delta J(q)$ will be positive and for small values of q $\Delta J(q)$ will be negative; the most negative value, of course, being found at $q = 0$. Consequently, electron correlation has the effect of reducing the magnitude of the Compton profile of H_2 for small values of q but increasing it, and therefore its range, at larger values of q . It is known that when $q = 0$, this corresponds to scattering from the outer electrons whereas, as q increases, electrons closer to the nucleus are responsible. The change in the shape of $J(q)$ due to electron correlation is therefore simply a further reflection of the fact that charge is moved closer to the nuclei. The effect of correlation on the H_2 profile was first noted by Brown and Smith^(2.xiii.5) and was employed to reduce the discrimination between theory and the experimental results of Eisenberger^(2.xiii.6). It was not until the vibrational and rotational effects were also included^(2.xiii.7), however, that the accuracy of the experimental results could

be finally confirmed.

(II.13.2) The Momentum-Space Two-Particle Density Analysis

[A] Investigation of the momentum-space functions

The mathematical form of the momentum-space Δ -partial planar distribution surface $\Delta V(p_{12}, p_1)$ is similar to the position-space surface. We see from equation (II.11.18), however, that the momentum-space natural orbitals are, in general, complex even in the $p_x p_z$ -plane. Consequently, $\Delta V(p_{12}, p_1)$ for the Davidson and Jones wavefunction curtailed to M natural configurations, must be written very precisely as

$$\begin{aligned} \Delta V(p_{12}, p_1) = & \sum_{i,j=1}^M A_M \mu_i \mu_j p_{12} [i]^*(p_1, p_2) [j](p_1, p_2) \\ & - A_1 \mu_1 \mu_1 p_{12} [1]^*(p_1, p_2) [1](p_1, p_2), \end{aligned} \quad (\text{II.13.5})$$

where the notation $[i](p_1, p_2)$ represents the i^{th} momentum-space natural configuration and A_M is the renormalisation constant (see equation (II.13.2)). Equation (II.13.5) may then be rearranged to be

$$\Delta V(p_{12}, p_1) = \sum_{i>j=1}^M a_{ij} p_{12} \left(\begin{aligned} & [i]^*(p_1, p_2) [j](p_1, p_2) \\ & + [i](p_1, p_2) [j]^*(p_1, p_2) \end{aligned} \right)$$

$$+ \sum_{i=1}^M a_{ii} p_{12} [i]^*(p_1, p_2) [i](p_1, p_2) \quad (\text{II.13.6})$$

where the renormalised occupation numbers a_{ij} are given in Tables (II.6.1), (II.6.2) and (II.6.3) for $M = 2, 3$ and 4 respectively. For the magnetic quantum numbers, m_i and m_j , both equal to zero, the product of the natural configurations may be written as

$$[i]^*(p_1, p_2) [j](p_1, p_2) = \chi_i^*(p_1) \chi_j^*(p_1) \chi_i(p_2) \chi_j(p_2) \quad (\text{II.13.7})$$

but a linear combination of such functions must be used for non-zero values of m_i or m_j .

The first term of equation (II.13.6) is in the form of a function added to its complex conjugate and hence must be equal to twice the real part of $[i]^*(p_1, p_2) [j](p_1, p_2)$. The remaining two terms may also be shown to be real, hence making $\Delta V(p_{12}, p_1)$ itself real in momentum-space. We must now investigate the mathematical form of the Δ -surface paying particular attention to the contributions from the main correlating terms.

From equation (II.11.18), the momentum-space natural orbital is in the form

$$\chi_i(p) = (2\pi)^{-1} (R/2)^{3/2} \exp(im_i(\phi_p - \pi/2)) \exp(-ip_z R/2) [A_i(p_z, p_\rho) - iB_i(p_z, p_\rho)] \quad (\text{II.13.8})$$

where

$$A_i(p_z, p_\rho) = 2 \int_{\eta=0}^1 \int_{\xi=1}^{\infty} \sum_{k=1}^{15} c_k \xi^{nk} \eta^{jk} [(\xi^2-1)(1-\eta^2)]^{m_i/2} \exp(-\alpha\xi) \\ (\xi^2-\eta^2) J_m(p_\rho R [(\xi^2-1)(1-\eta^2)]^{1/2}/2) \\ \cos(p_z R \xi \eta / 2) d\xi d\eta \quad (\text{II.13.9})$$

and

$$B_i(p_z, p_\rho) = 2 \int_{\eta=0}^1 \int_{\xi=1}^{\infty} \sum_{k=1}^{15} c_k \xi^{nk} \eta^{jk} [(\xi^2-1)(1-\eta^2)]^{m_i/2} \exp(-\alpha\xi) \\ (\xi^2-\eta^2) J_m(p_\rho R [(\xi^2-1)(1-\eta^2)]^{1/2}/2) \\ \sin(p_z R \xi \eta / 2) d\xi d\eta. \quad (\text{II.13.10})$$

It is also understood that if the j_k 's, the powers of η in $A_i(p_z, p_\rho)$ and $B_i(p_z, p_\rho)$, are even values for a particular choice of 'i' then $B_i(p_z, p_\rho)$ will be zero and $A_i(p_z, p_\rho)$ will be zero for a natural orbital with odd j_k values. All of the contributions to the $\Delta V(p_{12}, p_1)$ surface must therefore originate from combinations of $A_i(p_z, p_\rho)$ and $B_i(p_z, p_\rho)$ functions. They are very similar in form and, in fact, only differ by either a $\cos(p_z R \xi \eta / 2)$ or $\sin(p_z R \xi \eta / 2)$ term. This has the effect of causing $A_i(p_z, p_\rho)$ to be at its maximum value when $p_z = 0$, whereas $B_i(p_z, p_\rho)$ will contain a nodal plane at this location. Thus, $A_i(p_z, p_\rho)$ possesses σ_g symmetry about the x-axis whereas $B_i(p_z, p_\rho)$ possesses σ_u symmetry. If $m_i = 0$, both $A_i(p_z, p_\rho)$ and $B_i(p_z, p_\rho)$ will have their maximum values at $p_\rho = 0$, but for $m_i = 1$ or 2 , due to the Bessel function, they will be both zero along the p_z -axis. Thus, although at first sight these functions appear to be extremely complex, they are of surprisingly

simple form.

The a_{12} occupation number has the largest magnitude and it is therefore the term

$$a_{12}P_{12}([1]^*(p_1, p_2)[2](p_1, p_2) + [1](p_1, p_2)[2]^*(p_1, p_2))$$

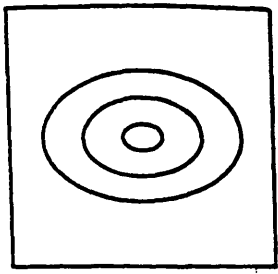
that is responsible for the introduction of z-correlation.

By substituting the natural orbitals into this term we obtain

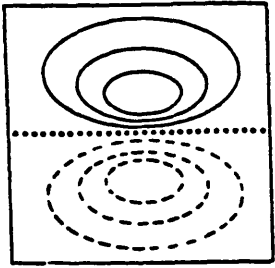
$$\begin{aligned} a_{12}P_{12}([1]^*(p_1, p_2)[2](p_1, p_2) + [1](p_1, p_2)[2]^*(p_1, p_2)) \\ = -2a_{12}P_{12}^k A_1(p_1)B_2(p_1) A_1(p_2)B_2(p_2) \quad (\text{II.13.11}) \end{aligned}$$

where k is simply the normalisation constant of the momentum-space natural orbitals. In a similar way to the position-space analysis, it is useful to sketch the form of the one-particle probability surfaces, in this case defined by $A_1(p)B_2(p)$. From these surfaces, both the importance of the type of correlation due to the location of electron 1 with momentum p_1 as well as the structure of the actual redistribution of electron 2 due to correlation may be observed.

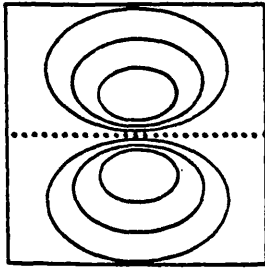
We see, from Figure (II.13.2), that the $A_1(p)B_2(p)$ surface bears a striking resemblance to the equivalent position-space surface except, of course, that the nuclear sites may not be located and a negative sign occurs. This is expected as the momentum-space natural orbital should be of the same type of symmetry as the position-space orbital. Indeed, it has been shown that the angular distributions of the orbitals remain unchanged in either type of space^(2.xiii.9).



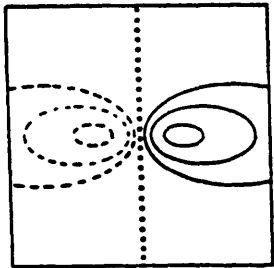
$A_1(p)A_1(p)$



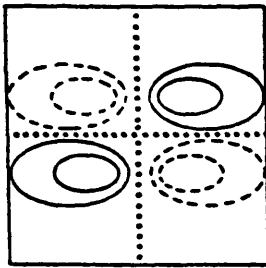
$A_1(p)B_2(p)$



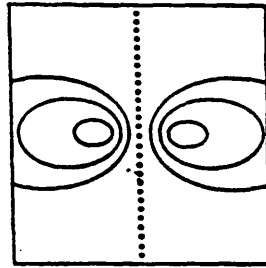
$B_2(p)B_2(p)$



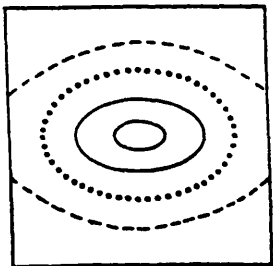
$A_1(p)A_3(p)$



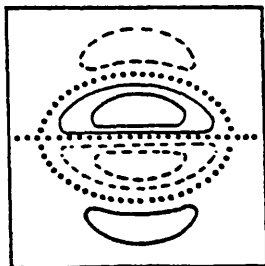
$B_2(p)A_3(p)$



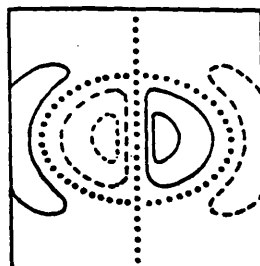
$A_3(p)A_3(p)$



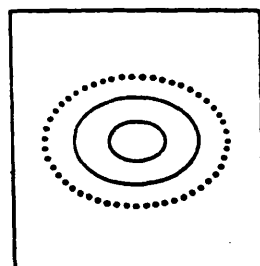
$A_1(p)A_4(p)$



$B_2(p)A_4(p)$



$A_3(p)A_4(p)$



$A_4(p)A_4(p)$

Figure (II.13.2) Sketches of the real parts of the $X_i^*(p)X_j(p)$ probability surfaces for $1 \leq i, j \leq 4$ using the definition of $X_i(p)$, and hence A_i and B_i , found in equation (II.13.8). The surfaces are viewed in the $p_x p_z$ -plane and are aligned in the p_z -direction.

If the fixed electron is located on the positive side of the $A_1(\underline{p})B_2(\underline{p})$ surface the probability of also locating the roving electron on this side will increase as the negative sign of a_{12} will cancel with the negative in equation (II.13.11). Also, the probability of locating the roving electron on the the other side will decrease. A similar argument may also be used when the fixed electron is located on the negative side of the surface and similar results are obtained. Thus, in momentum-space, z-correlation has the effect of increasing the probability of discovering both electrons with momenta in the same p_z -direction and decreasing the probability of locating them with momenta in opposite directions. This type of correlation is directly analogous to the angular-based correlation effect in atomic work. The greatest changes occur at $p_z = \langle p_1 \rangle$ and $-\langle p_1 \rangle$ with p_x and $p_y = 0$. Interestingly, we note that z-correlation can have no effect in momentum-space when $p_z = 0$, i.e. when either or both of the electrons are travelling in directions perpendicular to the bond axis.

The effect of the other two terms associated with z-correlation is firstly, from the $i = 1, j = 1$ term, to reduce the magnitude over the whole surface very slightly, causing the zero contour to bend towards the region of positive probability. The $i = 2, j = 2$ term then makes the entire surface more positive.

The term

$$a_{13}p_{12}([1]^*(p_1, p_2)[3](p_1, p_2) + [1](p_1, p_2)[3]^*(p_1, p_2)),$$

which is responsible for introducing the main ϕ -correlation effect, is more complex than the other terms as $m_3 = 1$. By substituting, in the $p_x p_z$ -plane, we have

$$\begin{aligned} a_{13}r_{12}([1]^*(p_1, p_2)[3](p_1, p_2) + [1](p_1, p_2)[3]^*(p_1, p_2)) \\ = 2a_{13}r_{12}^k A_1(p_1)A_3(p_1) A_1(p_2)A_3(p_2) \cos(\phi_p(1) - \phi_p(2)). \end{aligned}$$

(II.13.12)

Thus, if $\phi_p(1)$ is defined to be zero, the probability surface $A_1(p)A_3(p)\cos\phi_p$ is of interest. It is consequently the angular dependency that is responsible for the nodal plane at $\phi_p(2) = \pi/2$ and the negative region when $\phi_p(2) = \pi$. Therefore, when the sign of a_{13} is included in the calculation, ϕ -correlation has the effect of reducing the probability of locating both electrons with momenta in the same ϕ_p -direction but increasing the probability of locating them with momenta in opposite directions. It can be seen that ϕ -correlation can have no effect when either of the electrons is travelling solely in the p_z -direction. The remaining terms that are introduced with ϕ -correlation have also been sketched but have very little effect on the probability distribution of the surface. The HF renormalisation term, that is the $A_1(p)A_1(p)$ surface is again responsible for the slight bending of the zero contour to the region of positive probability. This type of correlation has no direct analogy in atomic calculations as it represents the distribution in directions perpendicular to the bond axis.

It is the term

$$a_{14}p_{12} ([1]^*(p_1, p_2)[4](p_1, p_2) + [1](p_1, p_2)[4]^*(p_1, p_2))$$

that is responsible for introducing the major ρ -correlation effect. It is possible to show that

$$\begin{aligned} a_{14}p_{12}([1]^*(p_1, p_2)[4](p_1, p_2) + [1](p_1, p_2)[4]^*(p_1, p_2)) \\ = 2a_{12}p_{12}^k A_1(p_1)A_4(p_1) A_1(p_2)A_4(p_2) \quad (\text{II.13.13}) \end{aligned}$$

which is real. It is the choice of coefficients c_k , defined in equation (II.13.4), in the summation of the fourth natural orbital that causes the $A_1(p)A_4(p)$ surface to possess a negative region for large momentum and also the zero contour to be of ellipsoidal form (see Figure (II.13.2)). It therefore follows that if the fixed electron is located within the positive region of the surface is with a relatively small momentum, the probability of locating the roving electron with a high momentum, i.e. in the negative region of the $A_1(p)A_4(p)$ surface, will increase. When the electron 1 possesses a high momentum, however, the probability of locating electron 2 with a small momentum will increase. The effect of ρ -correlation in momentum-space is therefore to increase the difference between the magnitudes of the momenta of the electrons, irrespective of any direction. Also, if the fixed electron is located within the positive region of the $A_1(p)A_4(p)$ surface, the zero contour encloses the region of positive probability of $\Delta V(p_{12}, p_1)$, whereas the negative region is enclosed if the fixed electron was located with a high momentum.

We can summarise the above observations by noting that in momentum-space, relative to the Hartree Fock model, z-correlation has the effect of increasing the probability of locating both electrons in the same p_z -direction and ϕ -correlation increases the probability of locating the electrons in opposite p_x -directions. Depending upon the location of one of the electrons, ρ -correlation can then either act to increase or decrease the momentum of the other electron. Using this information, we are now in a position to analyse the actual $\Delta V(p_{12}, p_1)$ surfaces and the partial planar Coulomb shifts in terms of the relative composition of z, ϕ and ρ -correlation. We have defined the momentum of the test electron to be in the p_x -direction (perpendicular to the bond) and the in the p_z -direction (parallel to the bond).

[B] Increasing momentum of test electron in the p_x -direction

The $V(p_{12}, p_1)$ surfaces corresponding to positions {i}, {ii}, {iii} and {iv} (see Figure (II.12.3A) for the definitions) are displayed in Figure (II.12.4) for the $p_x p_z$ -plane and Figure (II.12.14) for the $p_x p_y$ -plane. Like the one-particle density functions^(2.xiii.1), we can see that the component of momentum in the p_z -direction, that is parallel to the bond direction, is reduced. In directions perpendicular to the bond, however, the distributions are almost radially symmetric. The radial and angular distributions (Figures (II.12.5) and (II.12.15)) illustrate graphically the relatively large magnitude of the momentum-distributions as compared to the position-space distributions. We may also observe, however, that the

distributions are more short ranged in momentum-space and they decay rapidly as the momentum of electron 1 is increased.

Electron 1 is defined to possess no momentum in location {i}. This is an extremely interesting position as it corresponds to an electron that is far from the influence of the nuclei and hence may be thought of, in position-space, as lying on an infinitely large sphere, centred at a nucleus. This is equivalent to the H_2 molecule being ionized and therefore electron correlation has the effect of modifying the momentum distribution of electron 2 to resemble the distribution that would be observed in H_2^+ at this bond length. From Figures (II.12.6A) and (II.12.16A) we see that the only effect of z-correlation is seen in the renormalisation of the HF wavefunction. Similarly, from Figures (II.12.6B) and (II.12.16B) it can be seen that ϕ -correlation also has only an effect due to the renormalisation as one would predict from the previous discussion. The introduction of ρ -correlation, however, has a dramatic effect upon the Δ -surface as shown in Figures (II.12.6C) and (II.12.16C). The probability of locating the roving electron with a high momentum is increased and the probability of a low momentum is decreased in both planes. The $p_x p_z$ -plane exhibits a characteristic ellipse-type symmetry, whereas the $p_x p_y$ -plane is axially symmetric. Nevertheless, the global feature is that the mean momentum of the roving electron is increased in all planes which, in position-space, corresponds to the charge being drawn closer to the nuclei from all directions. It is pleasing to note

that the importance of ρ -correlation at small momentum values of electron 1 has already been predicted from the position-space analysis (see Figure (II.6.3D)). The effect of the remaining six natural orbitals in momentum-space, which introduce a second-order correlation effect, is small as it is virtually indistinguishable from the surface that has been generated by employing only the first four configurations. The relative importance of ρ -correlation is again emphasised by the partial planar Coulomb shifts, Figures (II.12.7) and (II.12.17). Also, the axial symmetry of the $p_x p_y$ -plane is illustrated by the $\Delta U(\epsilon)$ curves being horizontal lines.

Since location {ii} is fixed on the p_x -axis, in this instance with $p_x = 0.5\langle p_1 \rangle$, we see from Figures (II.12.8A) and (II.12.18A) that z -correlation has no effect again. However, as first observed by Banyard and Reed for He (2.xiii.8), the effect of angular correlation increases with an increase in the value of p_1 . From Figures (II.12.8B) and (II.12.18B) we note that the probability of discovering the roving electron in the vicinity of the fixed electron is reduced but an increase in probability is observed in the $-p_x$ direction. The zero contour bends slightly towards the region of positive probability in the usual manner in the $p_x p_y$ -plane but, in the $p_x p_z$ -plane, a dramatic bending of the zero contour is observed for large values of p_z . This is due to the fact that the decay in probability in the p_z -direction is rapid and hence the magnitudes of both the correlated and HF $V(p_{12}, p_1)$ surfaces will become extremely small relatively quickly. Only a slight perturbation to

$\Delta V(p_{12}, p_1)$ will consequently be required to alter the sign of the surface. In this case, it is due to the negative contribution associated with the renormalisation of the wavefunction. The introduction of ρ -correlation only reduces the magnitude of the maximum very slightly, though, a large enclosed area of negative probability is introduced, centred at $p_2 = 0$. This leads us to conclude that ρ -correlation is responsible for increasing the momentum of electron 2 and hence electron 1 must still be located within the positive region of the $A_1(p)A_4(p)$ surface.

The angular shifts for this location are particularly interesting (Figures (II.12.9B) and (II.12.19B)) in that it would appear that ϕ and ρ -correlation act in opposition to each other. In particular, we note that ϕ -correlation increases the probability of locating the roving electron in a direction towards $p_2 = 0$ ($\epsilon = 90^\circ$ for the $p_x p_z$ -plane but $\epsilon = 180^\circ$ for the $p_x p_y$ -plane). By introducing ρ -correlation, though, a drastic reduction in probability along this direction may be observed. If the associated Δ -surfaces are subsequently examined, however, it may be seen that ρ -correlation reduces the probability in the area around the origin which completely overwhelms the maximum behind the origin that is due to ϕ -correlation. The angularly averaged effect of ϕ and ρ -correlation in this case is to act in opposition to each other but the radial shifts show that the mean p_{12} distance is increased with the inclusion of different correlation-types.

The effect of z and ϕ -correlation in position {iii} is

very similar to position {ii} (see Figures (II.12.10A&B) and (II.12.20A&B)) although, in this case, the effect of ρ -correlation is very much reduced. In both the $p_x p_z$ and $p_x p_y$ -planes a minimum is observed, centred at the origin, indicating that this fixed electron position is still within the positive region of the $A_1(p)A_4(p)$ surface. Nevertheless,

the curvature of the zero contour in the $p_x p_y$ -plane is very slight which suggests that the effect of ρ -correlation is relatively minor. In the $p_x p_z$ -plane, the zero contour bends rapidly towards the negative region of the surface as would be expected but then turns swiftly back towards the positive region. This is again a consequence of the fact that the probability is very small in this region and the fixed electron is very close to the boundary between the positive and negative regions of $A_1(p)A_4(p)$. The ρ -correlation characteristics are then slightly emphasised by the introduction of the second-order configurations as shown in Figures (II.12.10D) and (II.12.20D). The relative importance of ϕ -correlation may be seen in the partial planar Coulomb shifts shown in Figures (II.12.11) and (II.12.21). We see that almost all of the correlation is due to the introduction of the third natural configuration and consequently to ϕ -correlation.

The distributions observed in position {iv} are very small, nevertheless, some interesting characteristics emerge. Z-correlation still has no effect although, from Figures (II.12.12B) and (II.12.22B), the usual ϕ -correlation characteristics are apparent. Figures (II.12.12C) and (II.12.22C) show that, contrary to the previous fixed

electron locations, ρ -correlation now has the effect of increasing the magnitude of $\Delta V(p_{12}, p_1)$ at the origin and is responsible for enhancing the bending of the zero contour more towards the region of positive probability.

[C] Increasing momentum of test electron in p_z -direction

The HF $V(p_{12}, p_1)$ surfaces for locations {v}, {vi} and {vii} are presented in Figure (II.12.24) for the $p_x p_z$ -plane but, since these momentum values maintain the axial symmetry of the system, the $p_x p_y$ -plane surfaces are radially symmetric and consequently have not been shown. The associated HF $S(p_{12})$ and $U(\epsilon)$ curves are displayed in Figure (II.12.25) and again the rapid decay in magnitude of the distributions as the momentum of electron 1 is increased is particularly evident. Also, due to the symmetry of the positions (i.e. $U(\epsilon) = U(180-\epsilon)$), only half of the range of the $U(\epsilon)$ curves has been presented.

As predicted, z -correlation has a marked effect in position {v} (see Figure(II.12.26A)). We see that the probability of locating electron 2 with a momentum in the same p_z -direction as electron 1 is increased with the probability of locating them in opposite directions being decreased. The curvature of the zero contour is very small indeed, indicating that the HF renormalisation effect is negligible when compared to the total z -correlation contribution. From Figure (II.12.26B) we see that ϕ -correlation now has no effect on this fixed electron location. However, due to the slight increase in the curvature of the zero contour and the small decrease in

probability over the entire surface, the contribution of the HF natural configuration may be observed. Probability is removed from the region around the origin with the introduction of ρ -correlation as demonstrated in Figure (II.12.26C) and the zero contour bends initially to encompass the negative probability region. This suggests that the fixed electron position is within the positive region of the $A_1(\underline{p})A_4(\underline{p})$ surface. The subsequent addition of the second-order correlation effects then only introduce a very small perturbation to this distribution.

It can be seen from the $\Delta S(p_{12})$ curves (Figure (II.12.27A)) that z correlation works to decrease the inter-electronic momentum p_{12} and then ρ -correlation has the effect of increasing p_{12} . A completely different picture may be obtained from the angular shifts where both z and ρ -correlation decrease the probability of locating the roving electron along a line towards the origin.

The two maxima that were observed in the previous location have formed into one when z -correlation is introduced at location {vi} and very little difference is seen when ϕ -correlation is included in the $V(p_{12}, p_1)$ surface (Figure (II.12.29B)). From Figure (II.12.29C), however, we see that ρ -correlation also has almost no effect, suggesting that this fixed electron position lies virtually on the border between the positive and negative regions of the $A_1(\underline{p})A_4(\underline{p})$ surface. As we would hope to find, the $\Delta S(p_{12})$ and $\Delta(\epsilon)$ curves demonstrate that z -correlation has the effect of decreasing the p_{12} separation but ϕ and

ρ -correlation contribute very little to the total curves.

Standard z and ϕ -correlation characteristics may be observed in position {vii} (Figure (II.12.30)) but as this location is within the negative region of $A_1(p)A_4(p)$, a marked increase in probability is observed at the origin and the zero contour is bent towards the positive region of the surface. These effects are reflected in the associated shifts in Figure (II.12.31).

[D] Comparison with HeH^+

This newly acquired information may be employed to understand further the shape of certain other Coulomb shift functions. As an example of this, we have presented the partial Coulomb shift $\Delta g(p_{12}, p_1, \theta_1)$ evaluated by Banyard and Reed^(2.xiii.2) in the study of the effect of electron correlation on the HeH^+ molecular-ion in Figure (II.13.3). The $\Delta g(p_{12}, p_1, \theta_1)$ function simply represents the change in probability of locating electron 2 with a momentum different from that of electron 1 by an amount p_{12} , irrespective of direction, and electron 1 possessing a momentum defined by p_1 and θ_1 . It is therefore related to our $\Delta V(p_{12}, p_1)$ functions and certain comparisons may be made.

Banyard and Reed have defined θ_1 to be the angle subtended between p_1 and the bond axis, consequently in Figure (II.13.3A), when $\theta_1 = 0^\circ$, this describes the redistribution in probability when electron 1 is travelling parallel to the bond. It can now be seen that the first shallow minimum at small values of p_1 is due to

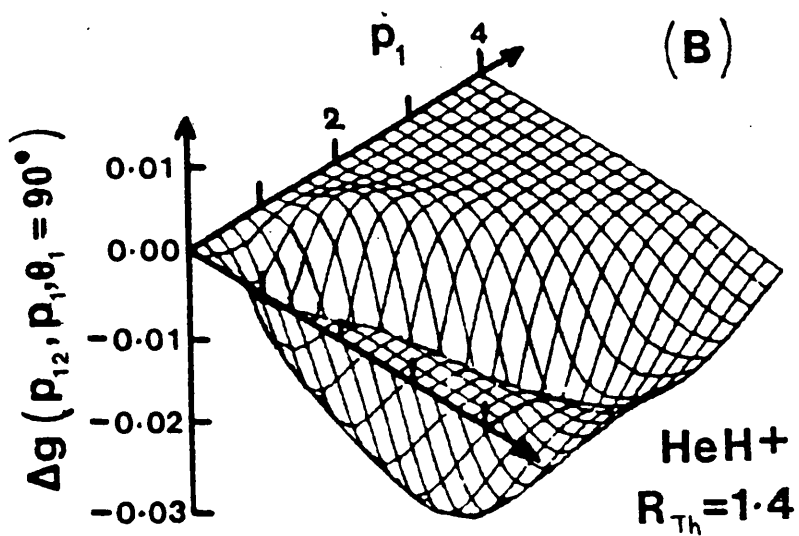
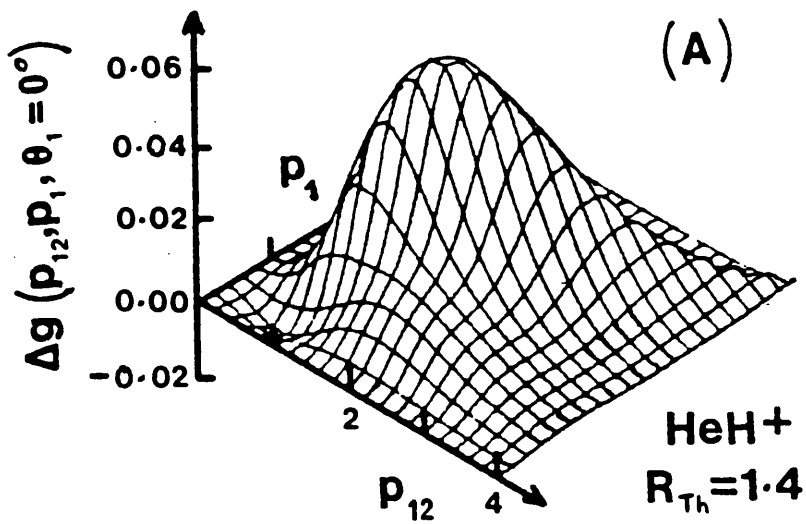


Figure (II.13.3) The partial Coulomb shifts $\Delta g(p_{12}, p_1, \theta_1)$ evaluated by Banyard and Reed for HeH⁺ at the near equilibrium bond length of 1.4 a.u. with (A) $\theta_1 = 0^\circ$ and (B) $\theta_1 = 90^\circ$.

ρ -correlation acting to remove electron probability from the vicinity of $p_2 = 0$. At larger values of p_1 , a huge maximum is observed which we may attribute to the dominant effect of z -correlation. Far from the origin the z -correlation effect is augmented by ρ -correlation that is now acting to increase the probability at $p_2 = 0$.

A completely different picture is obtained when $\theta_1 = 90^\circ$ and electron 1 is moving perpendicular to the bond. Again, for small values of p_1 , a minimum is obtained due to the effect of ρ -correlation but, as expected, z -correlation now has no effect. Instead a deep minimum may be observed due to the combined effect of ϕ and ρ -correlation both acting to increase the p_{12} separation.

CHAPTER II.14

Results for H_3^+ in Momentum-Space

Using the formulae derived in Chapter (II.11), the momentum-space versions of the Salmon and Poshusta^(2.xiv.1) and Schwartz and Schaad^(2.xiv.2) wavefunctions have been used to generate the results displayed in this chapter.

The same sets of contours that were used in the H_2 analysis (see Chapter (II.12) for values) have been employed in these surfaces. The negative contours are represented as usual by broken curves, the positive contours by full curves and the zero contour by a dotted curve. In addition, where applicable, the notation

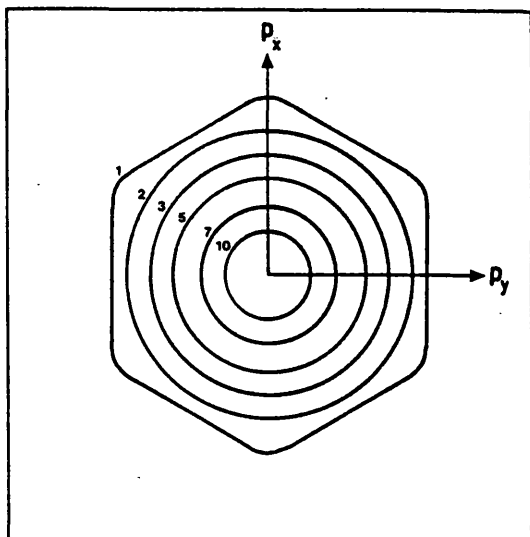
x = location of electron 1 which possesses a momentum of

\underline{p}_1

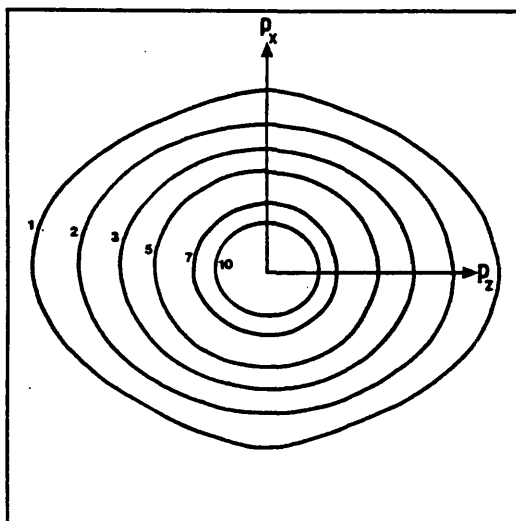
is employed. The full width of all of the surfaces corresponds to 8 a.u. and consequently 1 a.u. of momentum is represented by 9 millimetres.

(II.14.1) The One-Particle Density Results

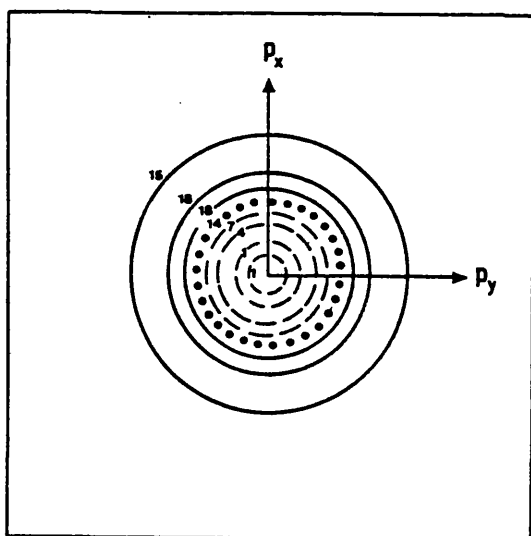
Like in the position-space analysis of H_3^+ , the HF momentum-space one-particle density distribution $\rho(\underline{p}_1)$ and the difference due to the effect of correlation $\Delta\rho(\underline{p}_1)$ have been evaluated in both the $p_x p_y$ -plane (parallel to the plane of the molecule) and the $p_x p_z$ -plane (perpendicular to the molecule).



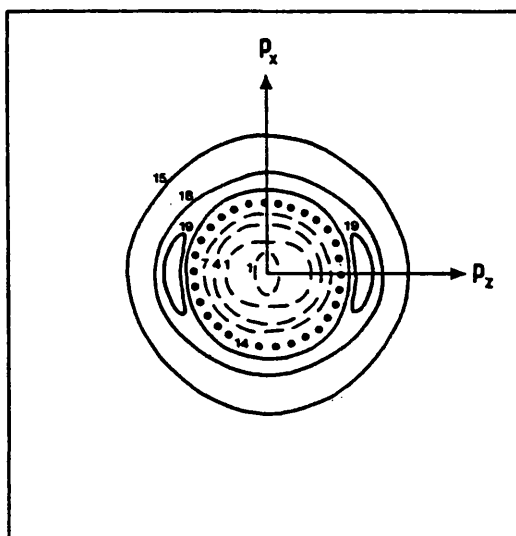
(A) $\rho(p_1)$
 $p_x p_y$ -plane ($p_z = 0$)



(B) $\rho(p_1)$
 $p_x p_z$ -plane ($p_y = 0$)



(C) $\Delta\rho(p_1)$
 $p_x p_y$ -plane ($p_z = 0$)



(D) $\Delta\rho(p_1)$
 $p_x p_z$ -plane ($p_y = 0$)

Figure (II.14.1) The one-particle density $\Delta\rho(p_1)$ and Δ -one-particle density $\Delta\rho(p_1)$ for H_3^+ in the $p_x p_y$ -plane (with $p_z = 0$) and the $p_x p_z$ -plane (with $p_y = 0$).

(II.14.2) the Two-Particle Density Results

The same format that was employed in the position-space analysis of H_3^+ has been used in the presentation of these results. In other words, we have evaluated $V(p_{12}, p_1)$ at the HF level and $\Delta V(p_{12}, p_1)$ for the $p_x p_y$ -plane and usually the $p_x p_z$ -plane with the associated partial planar Coulomb Shifts for each location of electron 1.

The chosen values of momentum assigned to electron 1 have been defined in Figure (II.14.2A). The first location was chosen such that electron 1 possesses no momentum and obviously this represents a system where the electron is far from the influence of the nuclei. The next three locations, {b}, {c} and {d}, are concerned with increasing the momentum of electron 1 in the p_x -direction; in a direction that is perpendicular to one bond and at sixty degrees to the other two. The remaining locations, {e} and {f}, are then defined by electron 1 possessing a momentum purely in a direction that is perpendicular to the plane of the molecule. Only the plane that is parallel to the plane of the molecule (ie the $p_x p_y$ -plane ($z \neq 0$)) has been considered for these two positions.

As defined in Figures (II.14.2B&C), ϵ is defined as the angle subtended between a vector that is parallel to the p_x -axis and the vector p_{12} in an anticlockwise direction.

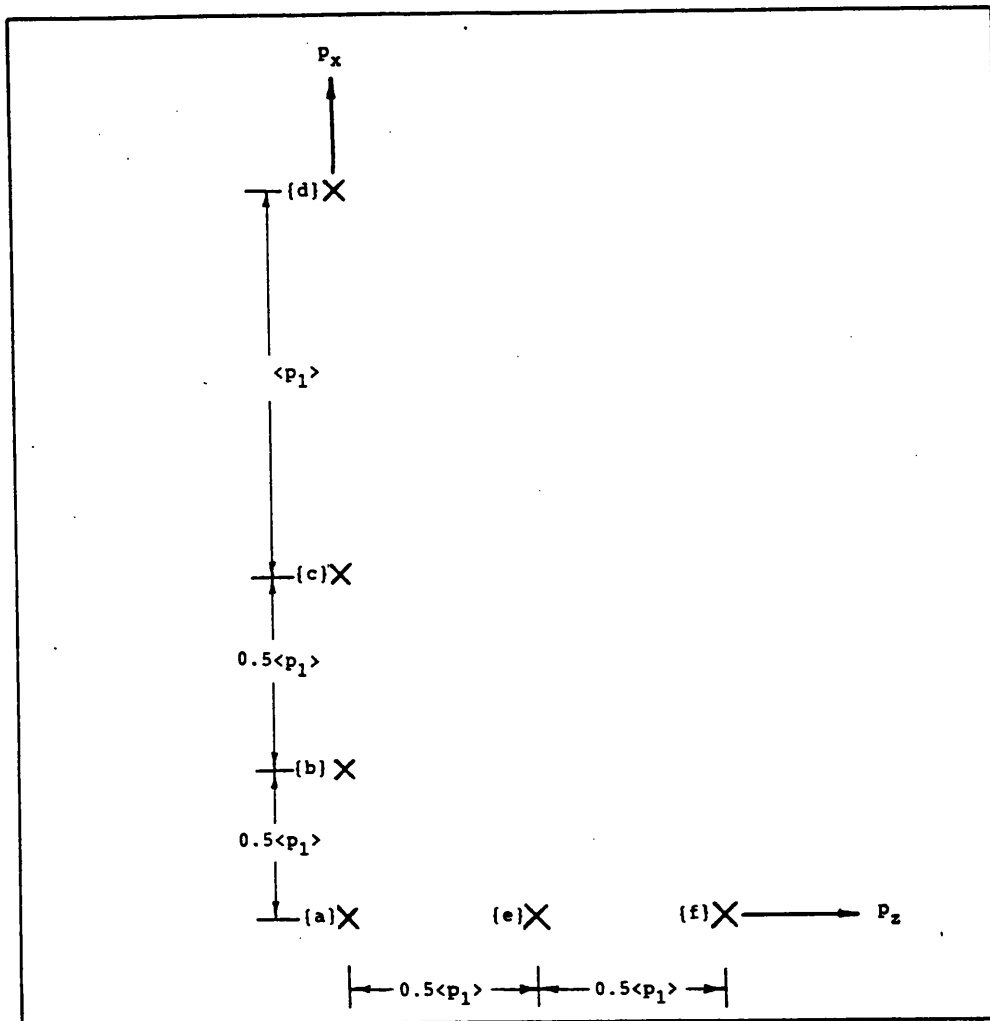


Figure (II.14.2A) The chosen momentum values of electron 1 employed in the partial planar distribution functions for H_3^+ in momentum-space. The expectation value $\langle p_1 \rangle = 0.97$ a.u.

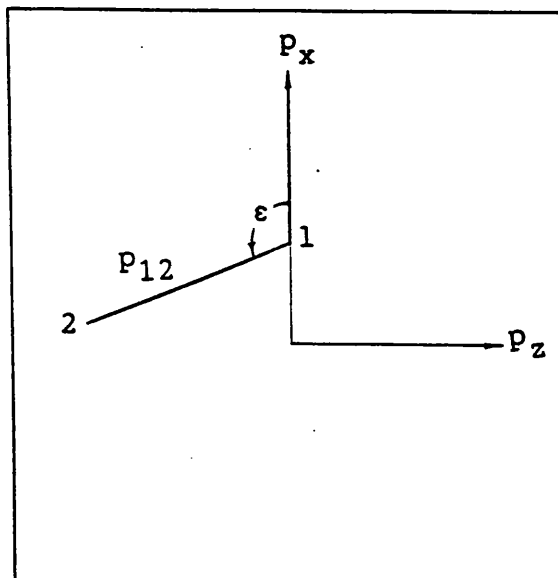
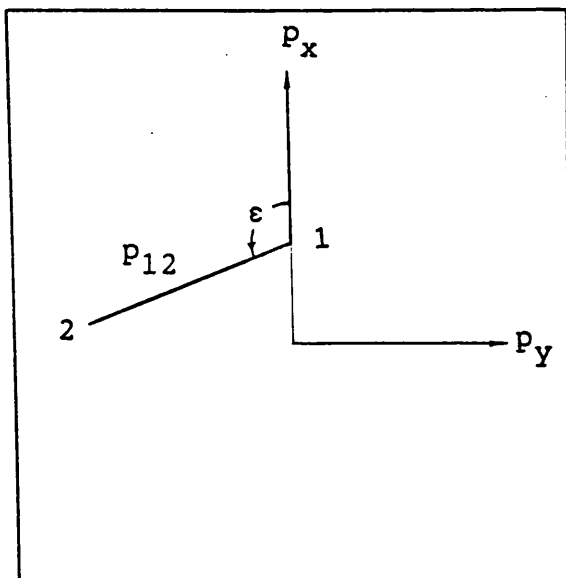
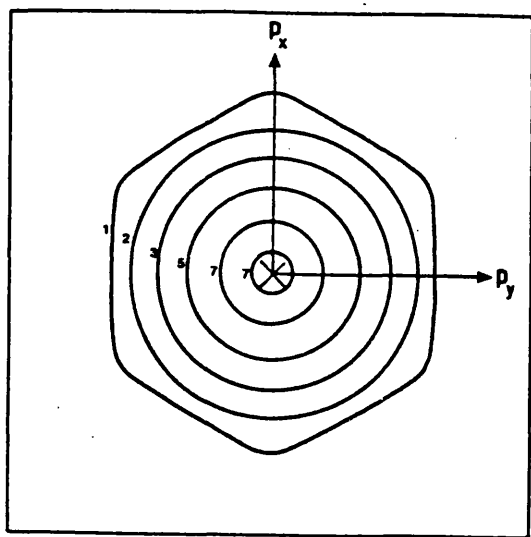
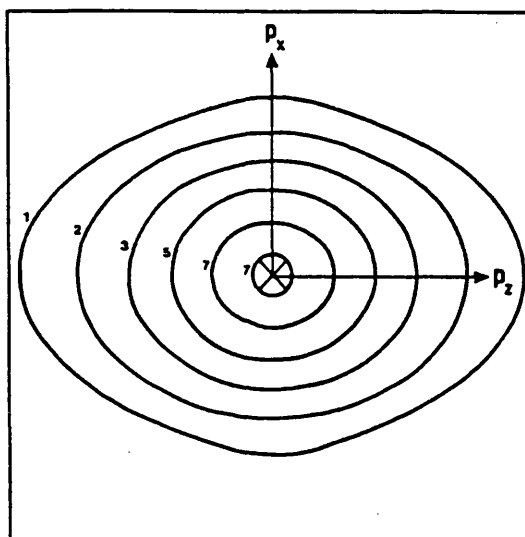


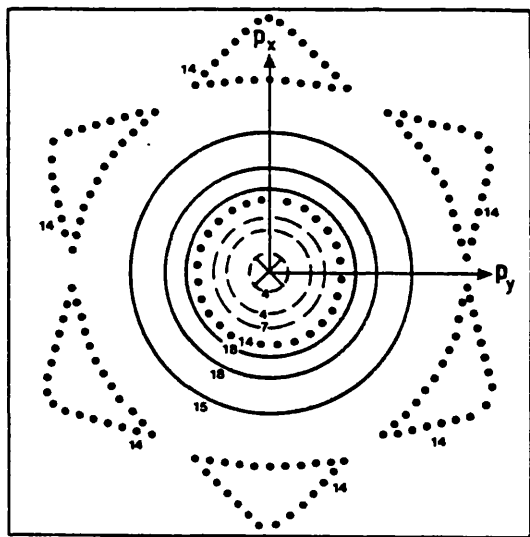
Figure (II.14.2B) & Figure (II.14.3C) The definition of the angle ϵ and the distance p_{12} when analysing correlation effects in (B) the $p_x p_y$ -plane and (C) the $p_x p_z$ -plane.



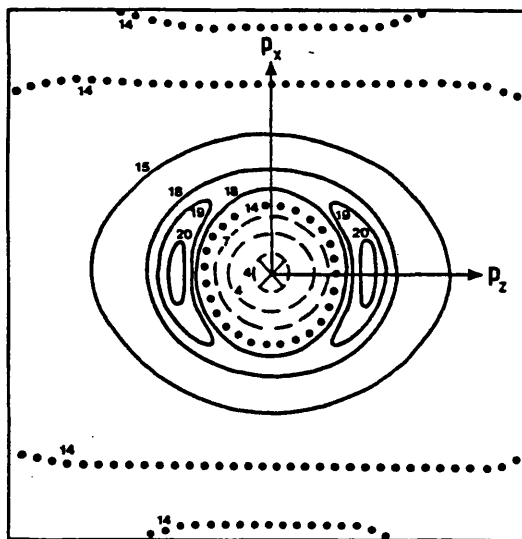
(A) $V(p_{12}, p_1)$
 $p_x p_y$ -plane ($p_z = 0$)



(B) $V(p_{12}, p_1)$
 $p_x p_z$ -plane ($p_y = 0$)



(C) $\Delta V(p_{12}, p_1)$
 $p_x p_y$ -plane ($p_z = 0$)



(D) $\Delta V(p_{12}, p_1)$
 $p_x p_z$ -plane ($p_y = 0$)

Figure (II.14.3) The Hartree Fock $V(p_{12}, p_1)$ surfaces and the $\Delta V(p_{12}, p_1)$ surfaces for electron location {a} (see Figure (II.14.2A) for the definition).

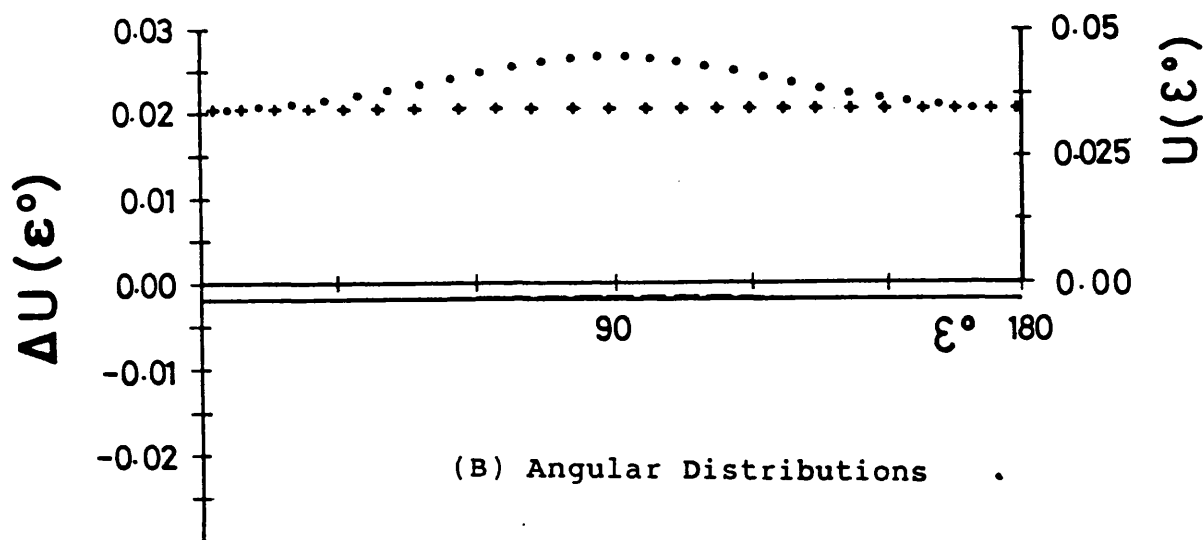
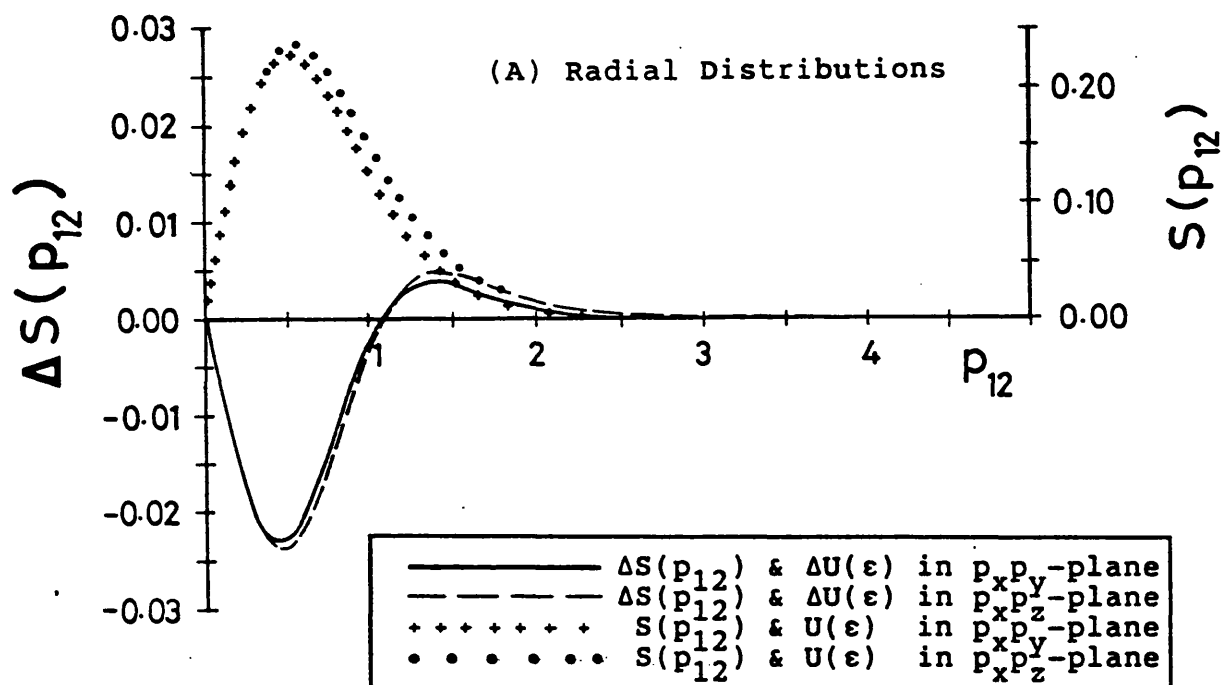
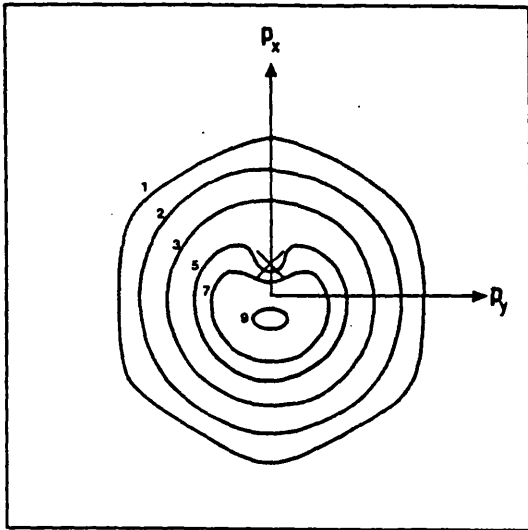
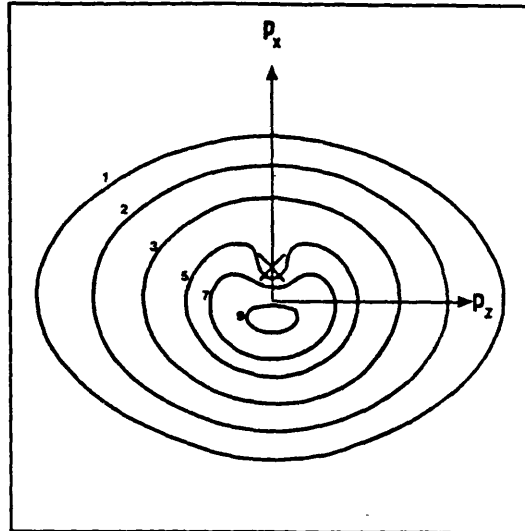


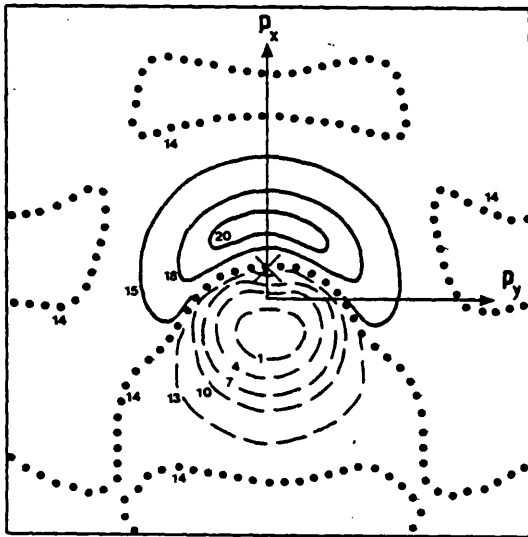
Figure (II.14.4) Partial planar Coulomb shifts and distribution functions for H_3^+ with electron 1 at location {a} (see Figure (II.14.2A) for definition) and electron 2 moving in either the $p_x p_y$ -plane or the $p_x p_z$ -plane.



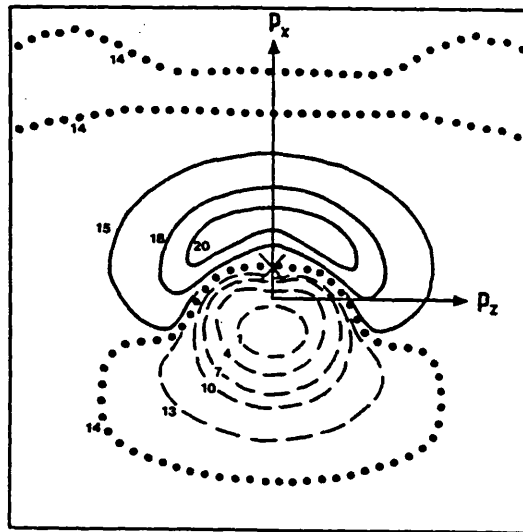
(A) $V(p_{12}, p_1)$
 $p_x p_y$ -plane ($p_z = 0$)



(B) $V(p_{12}, p_1)$
 $p_x p_z$ -plane ($p_y = 0$)



(C) $\Delta V(p_{12}, p_1)$
 $p_x p_y$ -plane ($p_z = 0$)



(D) $\Delta V(p_{12}, p_1)$
 $p_x p_z$ -plane ($p_y = 0$)

Figure (II.14.5) The Hartree Fock $V(p_{12}, p_1)$ surfaces and the $\Delta V(p_{12}, p_1)$ surfaces for electron location {b} (see Figure (II.14.2A) for the definition).

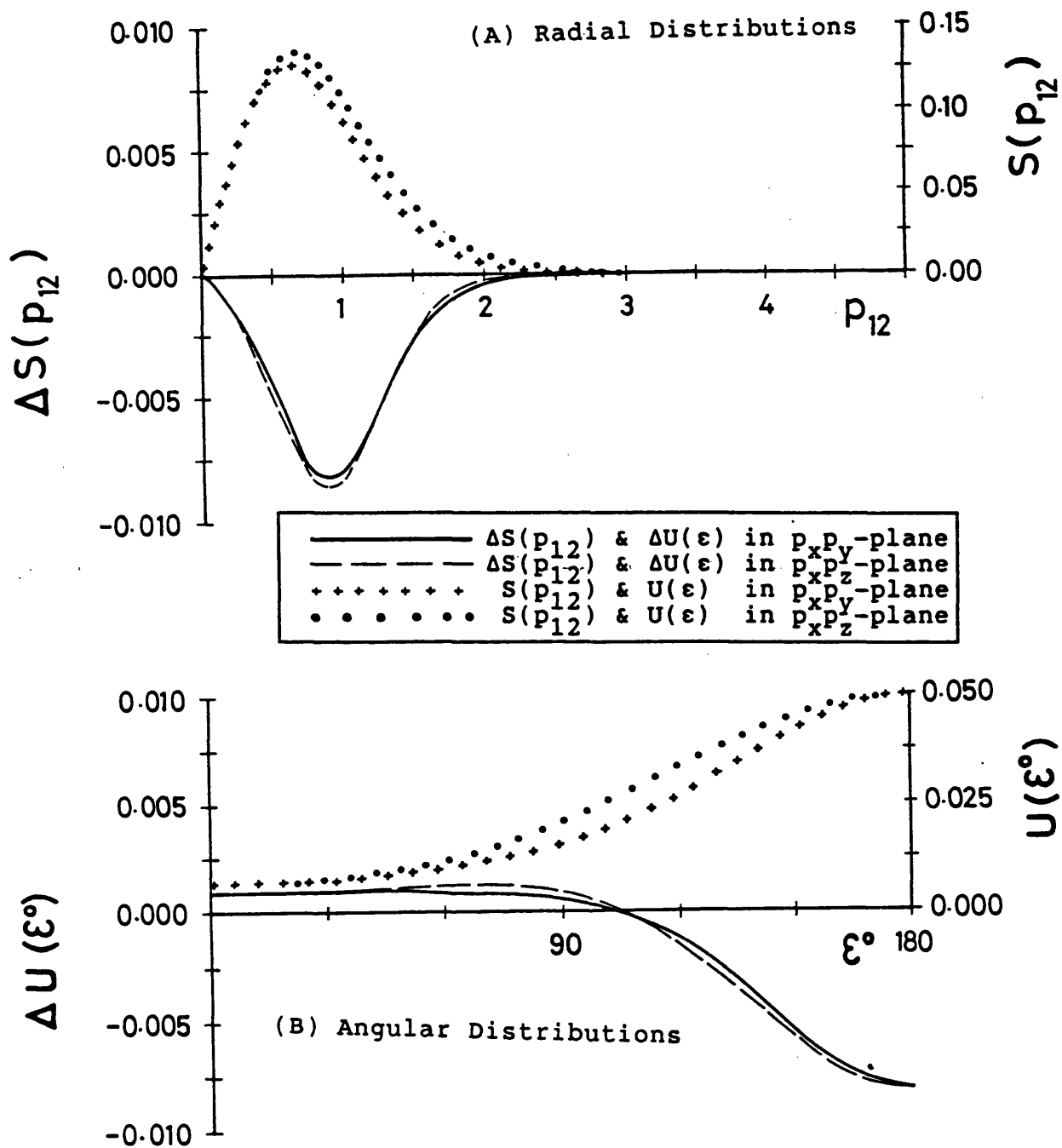
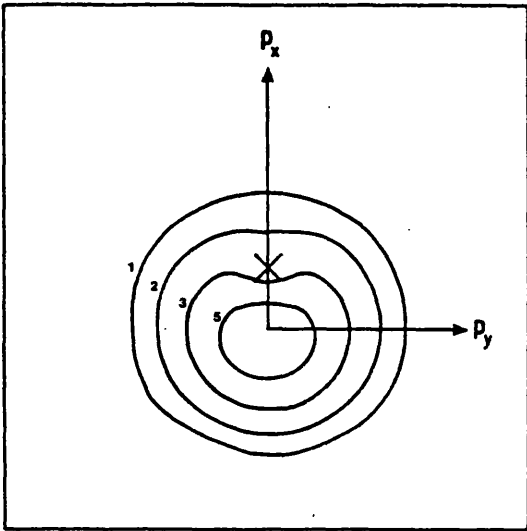
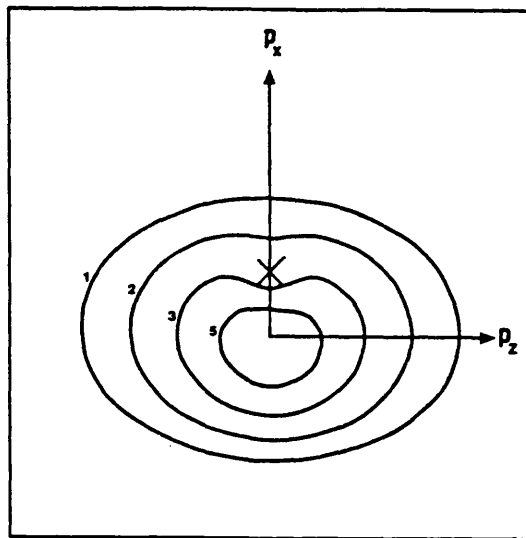


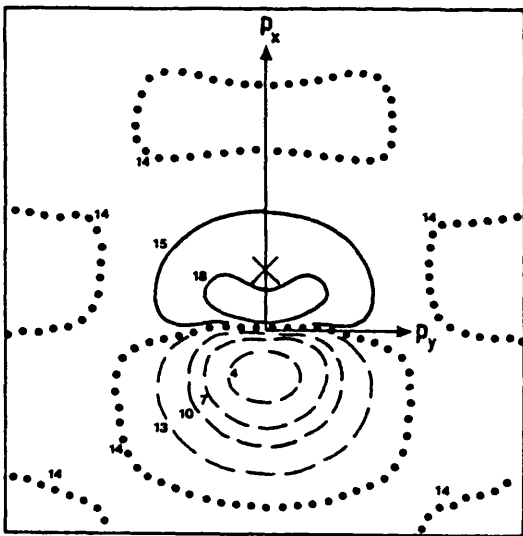
Figure (II.14.6) Partial planar Coulomb shifts and distribution functions for H_3^+ with electron 1 at location {b} (see Figure (II.14.2A) for definition) and electron 2 moving in either the $p_x p_y$ -plane or the $p_x p_z$ -plane.



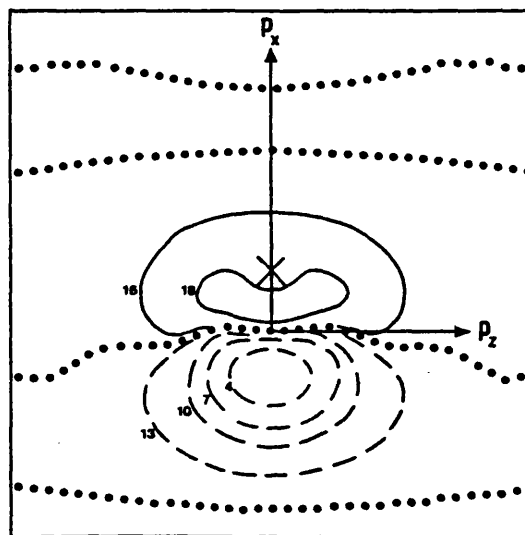
(A) $V(p_{12}, p_1)$
 $p_x p_y$ -plane ($p_z = 0$)



(B) $V(p_{12}, p_1)$
 $p_x p_z$ -plane ($p_y = 0$)



(C) $\Delta V(p_{12}, p_1)$
 $p_x p_y$ -plane ($p_z = 0$)



(D) $\Delta V(p_{12}, p_1)$
 $p_x p_z$ -plane ($p_y = 0$)

Figure (II.14.7) The Hartree Fock $V(p_{12}, p_1)$ surfaces and the $\Delta V(p_{12}, p_1)$ surfaces for electron location {c} (see Figure (II.14.2A) for the definition).

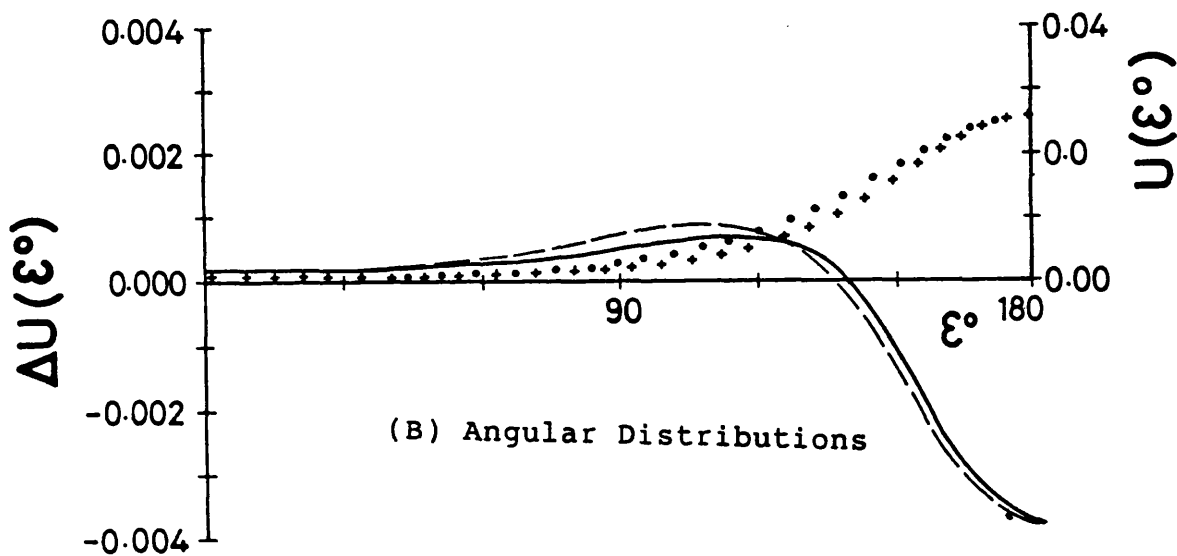
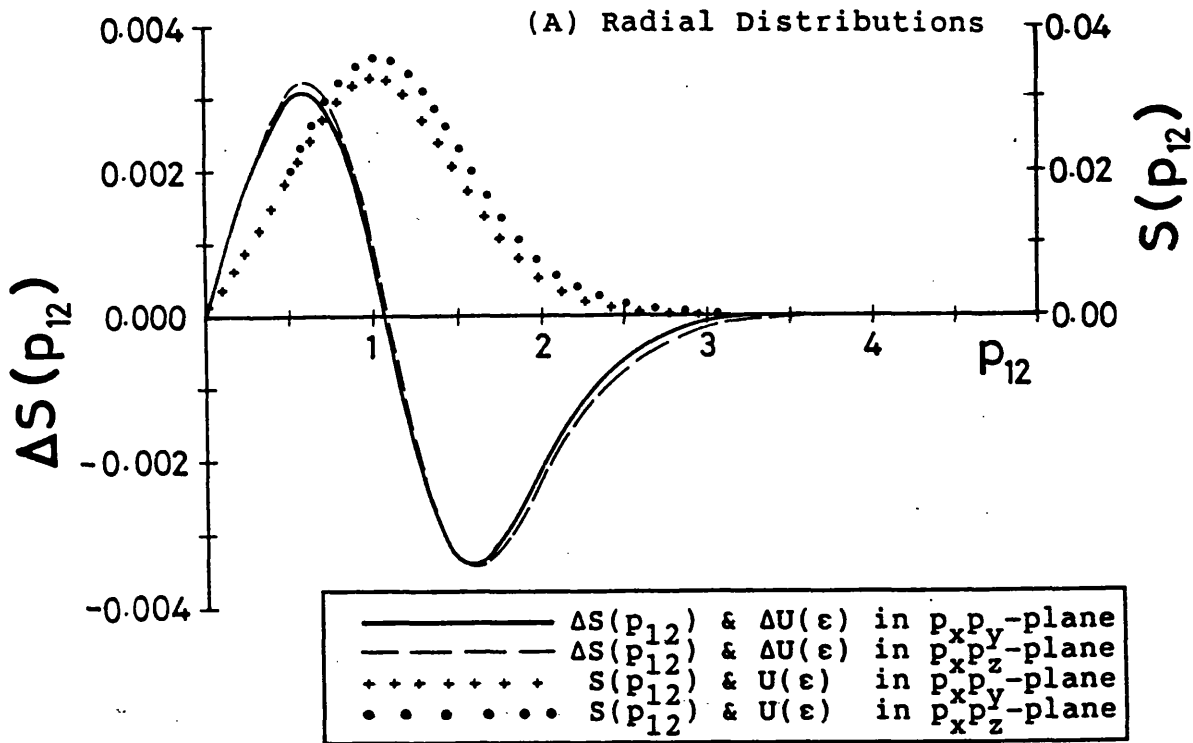
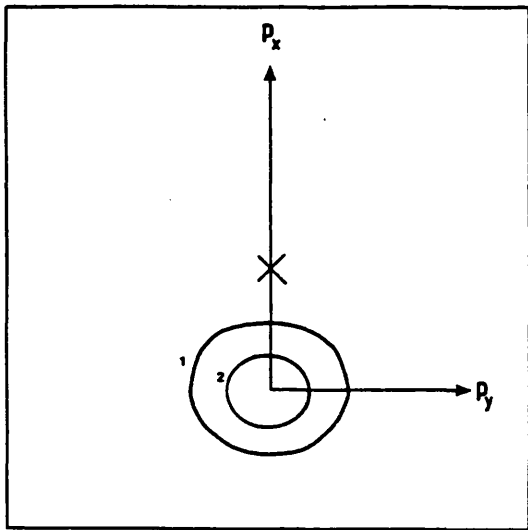
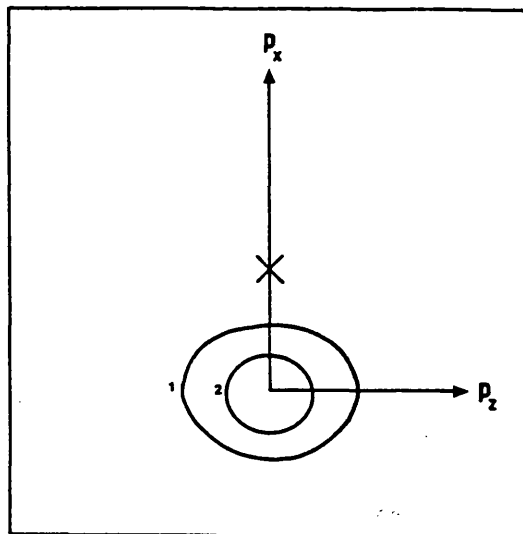


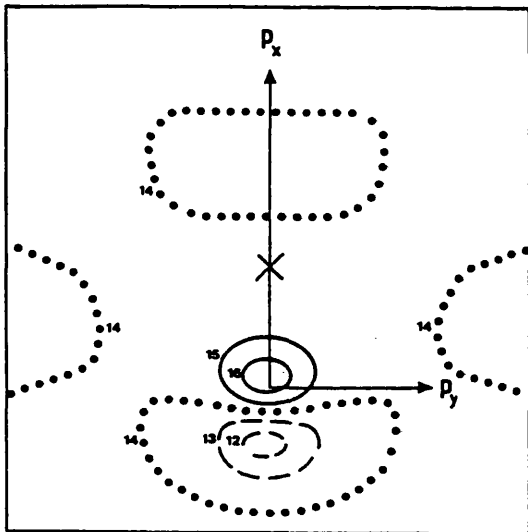
Figure (II.14.8) Partial planar Coulomb shifts and distribution functions for H_3^+ with electron 1 at location {c} (see Figure (II.14.2A) for definition) and electron 2 moving in either the $p_x p_y$ -plane or the $p_x p_z$ -plane.



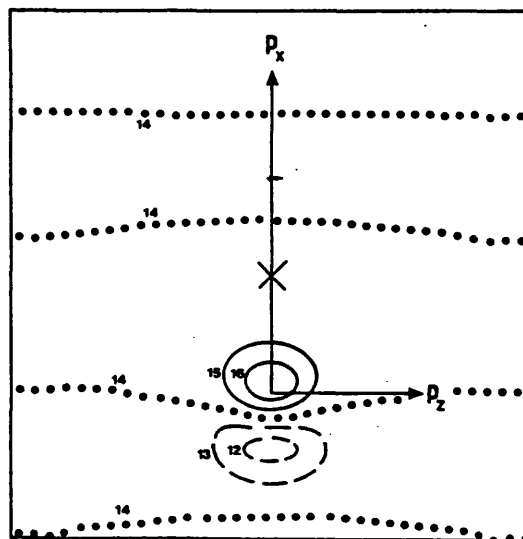
(A) $V(p_{12}, p_1)$
 $p_x p_y$ -plane ($p_z = 0$)



(B) $V(p_{12}, p_1)$
 $p_x p_z$ -plane ($p_y = 0$)



(C) $\Delta V(p_{12}, p_1)$
 $p_x p_y$ -plane ($p_z = 0$)



(D) $\Delta V(p_{12}, p_1)$
 $p_x p_z$ -plane ($p_y = 0$)

Figure (II.14.9) The Hartree Fock $V(p_{12}, p_1)$ surfaces and the $\Delta V(p_{12}, p_1)$ surfaces for electron location {d} (see Figure (II.14.2A) for the definition).

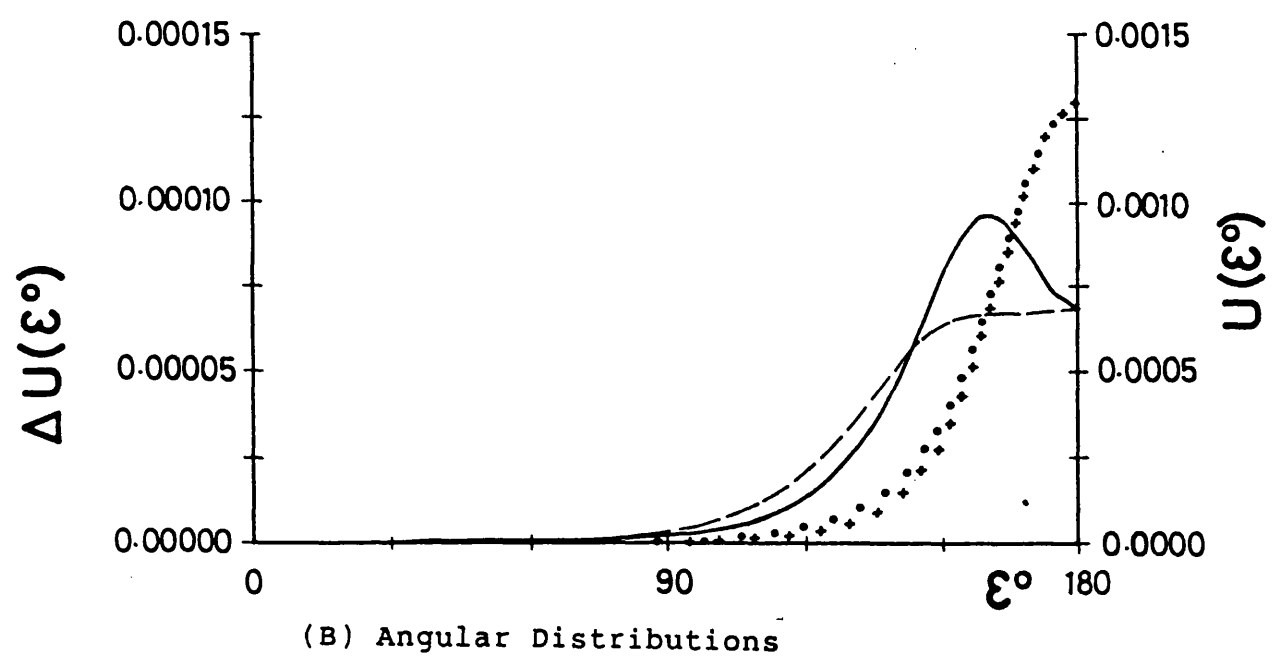
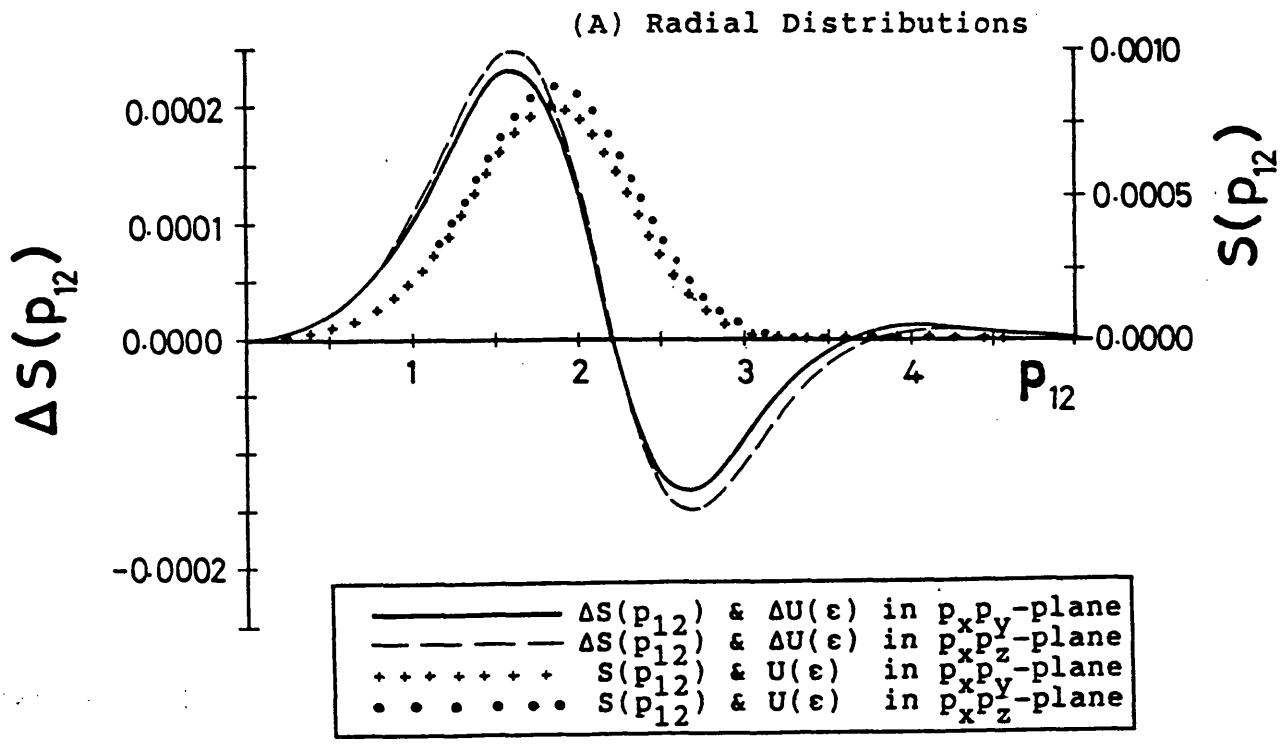
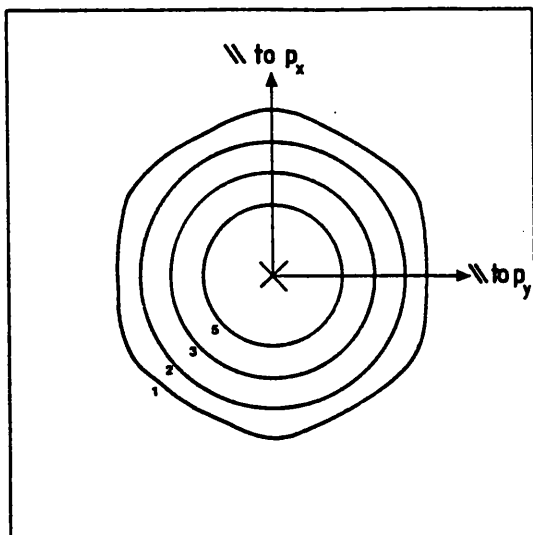
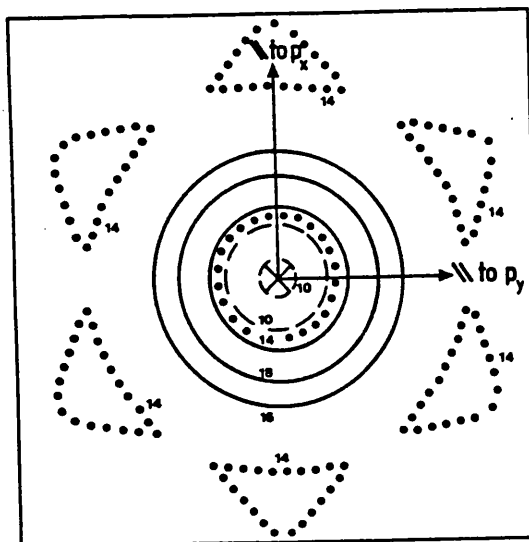


Figure (II.14.10) Partial planar Coulomb shifts and distribution functions for H_3^+ with electron 1 at location {d} (see Figure (II.14.2A) for definition) and electron 2 moving in either the $p_x p_y$ -plane or the $p_x p_z$ -plane.

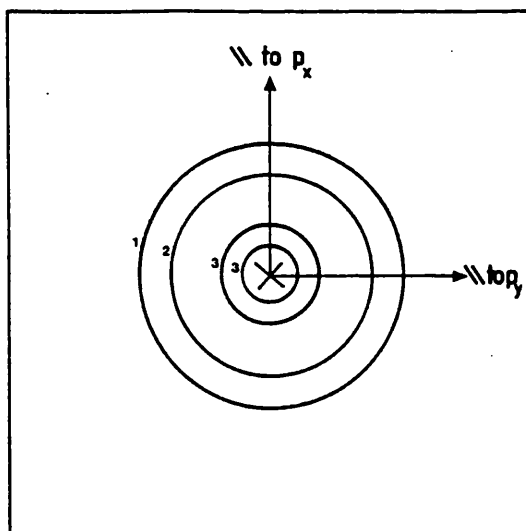


(A) $V(p_{12}, p_1)$
 $p_x p_y$ -plane ($p_z = 0.5 \langle p_1 \rangle$)

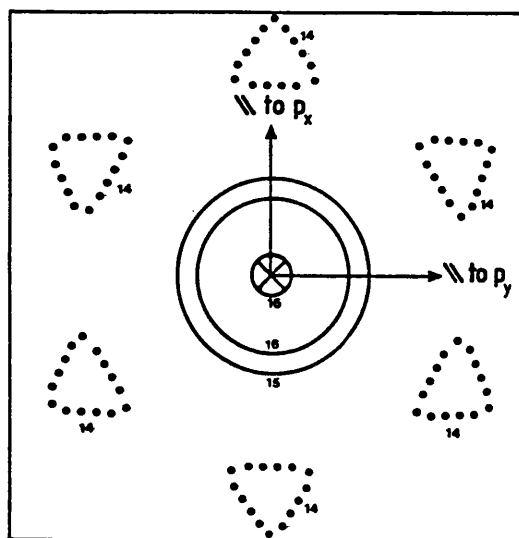


(B) $\Delta V(p_{12}, p_1)$
 $p_x p_y$ -plane ($p_z = 0.5 \langle p_1 \rangle$)

Figure (II.14.11) The Hartree Fock $V(p_{12}, p_1)$ surface and the $\Delta V(p_{12}, p_1)$ surface for electron location {e} (see Figure (II.14.2A) for the definition).



(A) $V(p_{12}, p_1)$
 $p_x p_y$ -plane ($p_z = \langle p_1 \rangle$)



(B) $\Delta V(p_{12}, p_1)$
 $p_x p_y$ -plane ($p_z = \langle p_1 \rangle$)

Figure (II.14.12) The Hartree Fock $V(p_{12}, p_1)$ surface and the $\Delta V(p_{12}, p_1)$ surface for electron location {f} (see Figure (II.14.2A) for the definition).

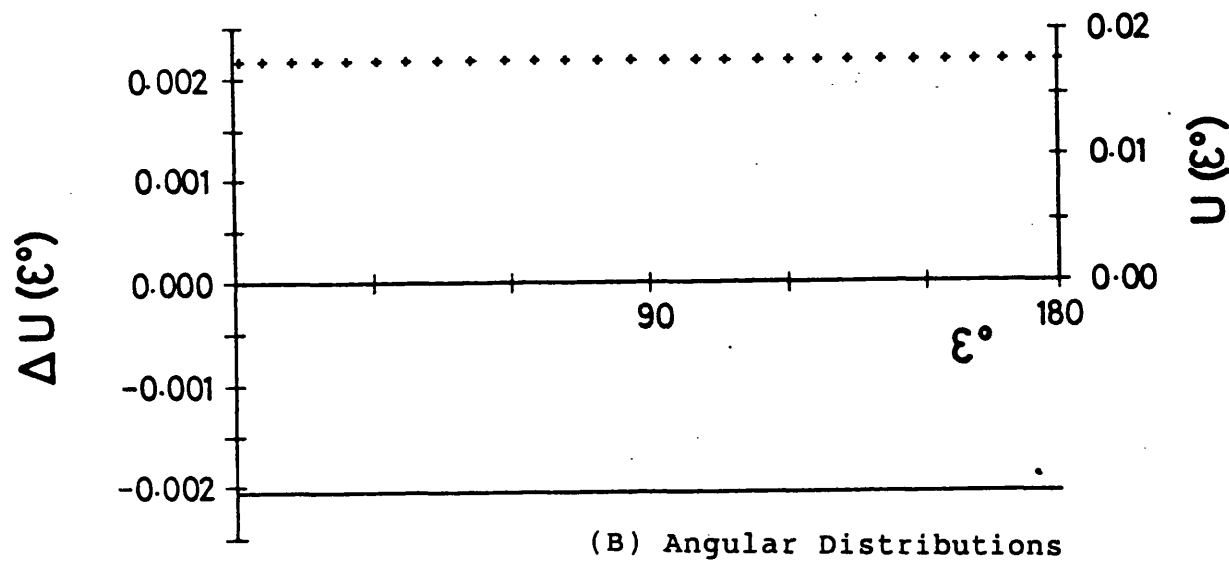
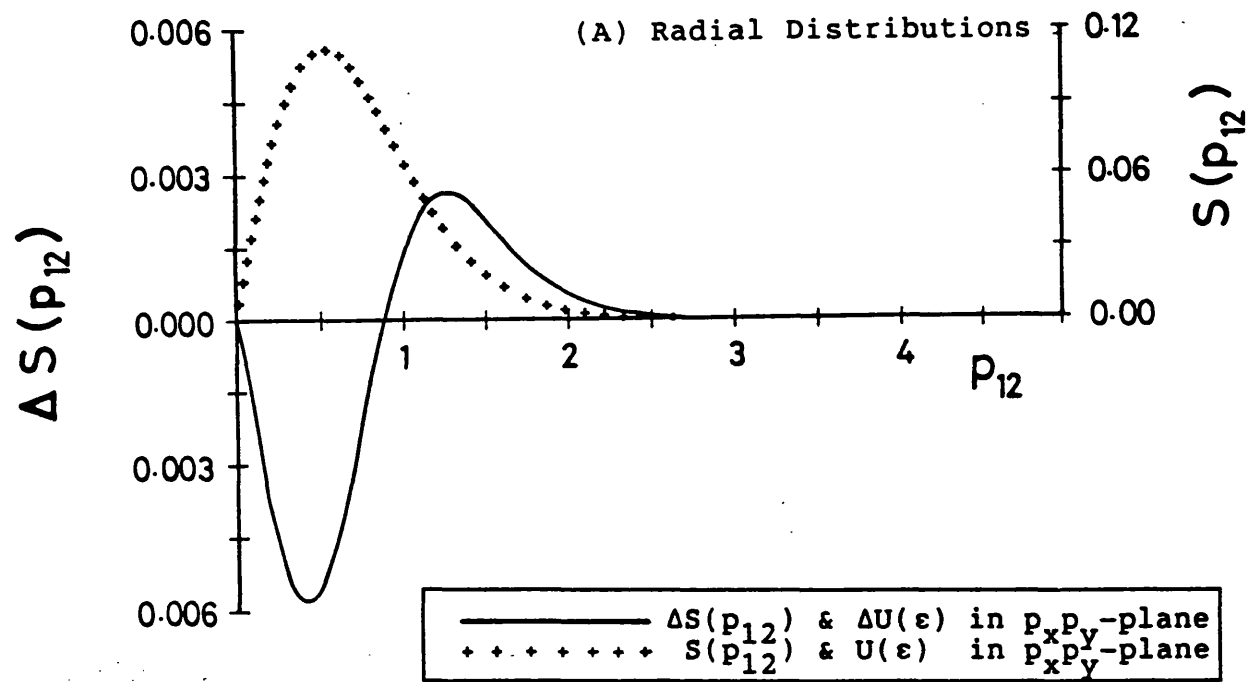


Figure (II.14.13) Partial planar Coulomb shifts and distribution functions for H_3^+ with electron 1 at location {e} (see Figure (II.14.2A) for definition) and electron 2 moving in the $p_x p_y$ -plane.

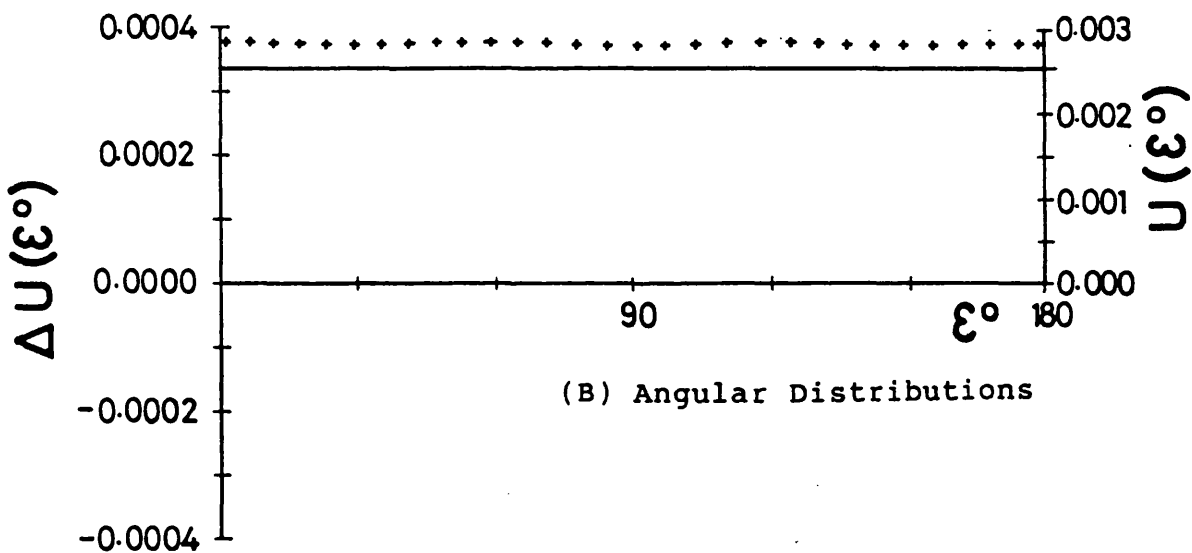
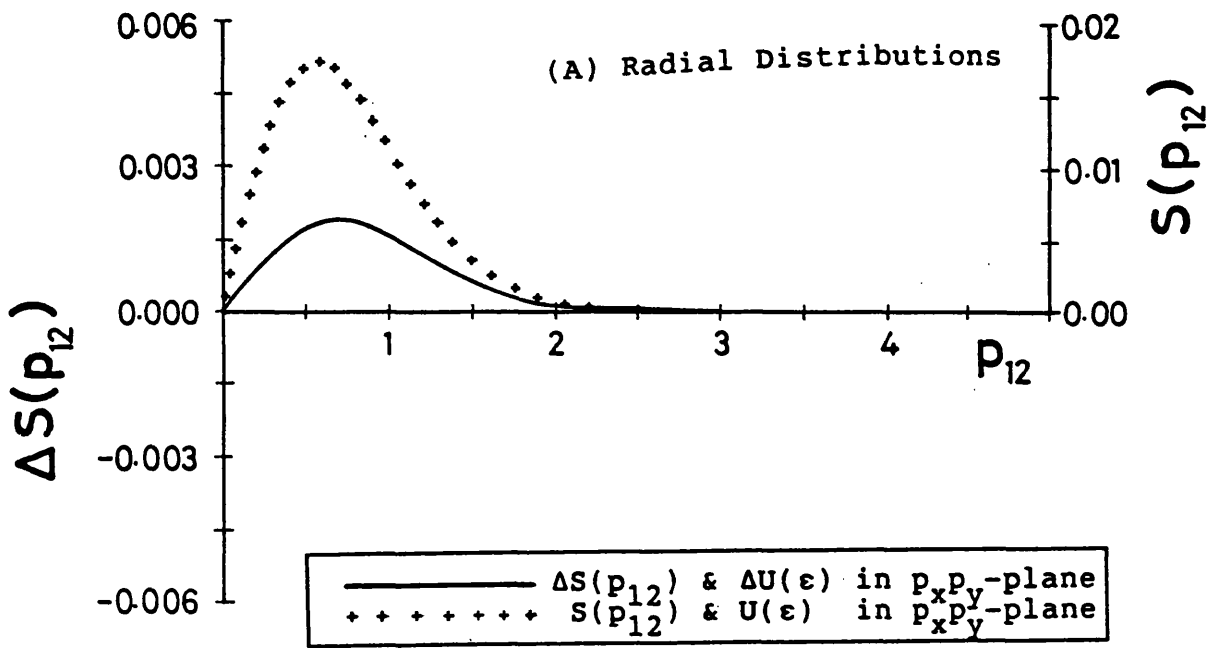


Figure (II.14.14) Partial planar Coulomb shifts and distribution functions for H_3^+ with electron 1 at location {f} (see Figure (II.14.2A) for definition) and electron 2 moving in the $p_x p_y$ -plane.

CHAPTER II.15

Discussion of H_3^+ Results in Momentum-Space

The momentum-space arrangements of the Salmon and Poshusta CI wavefunction^(2.xv.1) and the Schwartz and Schaad HF wavefunction^(2.xv.2) have been used to generate the results in this section. Before proceeding with the discussion of the results we shall first investigate the forms of the chosen wavefunctions.

When comparing the Salmon and Poshusta wavefunction in momentum-space (Equation (II.11.30)) with that of Schwartz and Schaad (Equation (II.11.39)), the only difference in format between them is the presence of the term $\exp(g_i k_i p_1 \cdot p_2 / 2)$ in the Salmon and Poshusta wavefunction. This term therefore is responsible for introducing correlation into the H_3^+ molecule. It may be re-expressed as $\exp(g_i k_i p_1 p_2 \cos \gamma)$, where γ is the angle subtended between the two electronic momentum vectors. Since this term is multiplied by a positive coefficient, when formed into a density it has the property of increasing the probability of locating the electrons with a small inter-electronic angle γ and decreasing the probability of locating them with a large inter-electronic angle. Consequently, the term is responsible for increasing the probability of locating both electrons travelling in the same direction and decreasing the probability of locating them travelling in opposite directions. It therefore introduces mainly an angular

correlation effect which is responsible for reducing the mean inter-electronic momentum. Interestingly, this term is derived from the expression $\exp(-2g_i \underline{r}_1 \cdot \underline{r}_2)$ in the position-space Singer polynomial (see Equation (II.4.5) for further details). By expressing this term in the same way as before, we may see that it is also responsible for introducing angular correlation. Due to the negative sign in the exponent, the term has the opposite effect to that previously observed in momentum-space and favours locating the electrons with a large inter-electronic angle. The probability of discovering the electrons on opposite sides of the molecule is therefore enhanced and the probability of finding them on the same side is reduced. This demonstrates mathematically how angular correlation in position-space has the effect of increasing the mean inter-electronic distance whereas, in momentum-space, it has the opposite effect and reduces the inter-electronic momentum.

Recently, Regier and Thakkar have transformed floating Gaussian orbital based CI wavefunctions for H^- , He and Li^+ into momentum-space^(2.xv.3,4). These wavefunctions are of the same form as the Salmon and Poshusta wavefunction except that the terms $\exp(-i\underline{S}_{2i} \cdot \underline{p}_1)$ and $\exp(-i\underline{S}_{1i} \cdot \underline{p}_2)$, containing the expansion centres, do not occur in them. Since these terms are totally imaginary, they lead to a cosine distribution function rather than an exponential decay in the two-particle electronic density and thus have equal effect for all values of \underline{p}_1 and \underline{p}_2 and are periodic. This function is therefore responsible for describing the molecular nature of the system.

(II.15.1) The Momentum-Space One-Particle Density Analysis

From Figure (II.14.1A), we see that the momentum-space one-particle density $\rho(\underline{p}_1)$ in the $p_x p_y$ -plane possesses symmetry such that $\rho(\underline{p}_1) = \rho(-\underline{p}_1)$. It also inherits the three-fold symmetry of the position-space representation of the molecule, making the total distribution six-fold symmetric. Another, more informative, way of accounting for the shape of the distribution is to envisage the H_3^+ molecule as the conglomeration of three H_2 molecule-type systems located at 120° to each other. From the work performed on H_2 (2.xv.5), however, we know that the momentum of the electrons is increased in directions perpendicular to the bond. Hence, the two 'corners' that are located on the p_x -axis of Figure (II.14.1A), for example, are due to the distribution of electrons associated with the 'bond' formed between the two nuclei that are located off the p_x -axis. In a similar way, the remaining maxima may be seen to be a result of the remaining two 'bonds'. It should be remembered, however, that, although we have discussed three distinct 'bonds', they cannot be thought of as conventionally occupied σ -bonds due to the electron deficient nature of H_3^+ .

The effect of electron correlation on the one-particle density $\Delta\rho(\underline{p}_1)$ is shown in Figures (II.14.1C) and (II.14.1D). They demonstrate that correlation in momentum-space is responsible for a general increase in the electronic momentum. Surprisingly, only at extremely high momentum values can the six-fold symmetry that was observed

in $\rho(\mathbf{p}_1)$ in the $p_x p_y$ -plane be seen and at all other momentum values the $\Delta\rho(\mathbf{p}_1)$ surface is almost radially symmetric. In the perpendicular plane to this, the $p_x p_z$ -plane, we observe an increase of momentum in the p_z -direction from small p_z values to form maxima at $p_z \approx \pm 1.5$ a.u.. In position-space we have seen that, due to the limitations of the HF wavefunction, correlation has the effect of compressing the electronic charge cloud above and below the plane of the molecule (see Chapter (II.8)). It is known, however, that as the density of a charge cloud increases, the kinetic energy and therefore the momentum of the electrons also increases due to the larger electron-electron repulsive forces. This increase in momentum is then observed on the $\Delta\rho(\mathbf{p}_1)$ surface in the $p_x p_z$ -plane.

(II.15.2) The Momentum-Space Two-Particle Density Analysis

The first location of electron 1, location {a}, is when it possesses no momentum and is far from the influence of the nuclei. A result of this is that the six-fold symmetry of the HF distribution in the $p_x p_y$ -plane is preserved. In addition, the HF $V(\mathbf{p}_{12}, \mathbf{p}_1)$ distributions in the $p_x p_y$ -plane (Figure (II.14.3A)) and the $p_x p_z$ -plane (Figure (II.14.3B)) bear a striking resemblance in form to the one-particle density functions in the same planes (Figures (II.14.1A) and (II.14.1B)).

From Figure (II.14.3C) we see that the effect of electron correlation in the $p_x p_y$ -plane is almost radially

symmetric over nearly all of the surface. However, at high momentum values six small minima may be observed. By comparing this diagram with Figure (II.14.3A) we note that correlation has the effect of reducing the probability of locating electron 2 with a momentum perpendicular to the 'bonds' which, from the H_2 analysis, may be attributed to ' ϕ -correlation'. By examining the Δ -surface in the $p_x p_z$ -plane (Figure (II.14.3D)) it may be seen that the zero contours that were associated with the six minima in the $p_x p_y$ -plane form almost parallel lines. This indicates that the effect of ϕ -correlation on them is almost independent of the momentum of electron 2 in the p_z -direction.

The next three locations of electron 1 are concerned with gradually increasing the momentum of the electron in the p_x -direction. This means that the velocity of electron 1 is increased perpendicularly to one of our partially occupied ' σ -type bonds' and at thirty degrees to the other two.

In location {b} electron 1 possesses a momentum of $0.5\langle p_1 \rangle$ in the p_x -direction and, from Figures (II.14.5A) and (II.14.5B), we see that the HF $V(p_{12}, p_1)$ surfaces are similar in form to the last location except that the six-fold symmetry in the $p_x p_y$ -plane is less well defined. The effect of electron correlation is different from that seen previously as demonstrated in Figure (II.14.5C) and (II.14.5D). It is found that, in both planes, the probability of discovering electron 2 with a very low momentum is reduced but the probability of discovering it

with a momentum in the same direction as electron 1 is increased. This is due to the effect of electron correlation redistributing electronic probability in directions parallel to the 'bonds' (defined as z-correlation in the analysis performed on H_2 due to the alignment of the bond). The shapes of the six minima have also been altered slightly. The minimum on the positive side of the p_x -axis, which is due to 'bonding' perpendicular to the p_x -axis, has been expanded in area and depth whereas the two off-axis minima remain almost at the same position with respect to the origin of the co-ordinate system although their shapes have been altered. The minima on the negative side of the p_x -axis may still be located but are less well defined.

The deep minimum at low momentum can be seen still to dominate the Coulomb shifts (Figure (II.14.6~~3~~)). Indeed, we see that the minimum is so large that the radial shifts remain negative over virtually their entire range and also the minimum at $\epsilon \approx 180^\circ$ dominates the angular shift. This suggests that at this momentum value of electron 1, radial correlation is still the most important correlation effect.

The momentum of electron 1 is increased to $\langle p_1 \rangle$ in the p_x -direction to define location {c}. We see from Figure (II.14.7A) that the distribution is almost radially symmetric in the $p_x p_y$ -plane although the distribution in the $p_x p_z$ -plane possesses elliptical geometry. The large minimum that was observed in the previous Δ -surfaces has been moved to more negative values (Figures (II.14.7C) and (II.14.7D)) and the maximum of the surface now lies on the other side of

electron 1. The shallow minima that are observed at high momentum, however, remain almost at the same location in space and their shapes vary only slightly.

Due to the close proximity of the maximum point of the surface to electron 1 in location {c}, the radial shift becomes first positive then negative (Figure (II.14.5A)). This emphasises the relative increase in importance of correlation parallel to the 'bonds'. Thus, for example, configurations that are constructed from $2p_{\sigma}$ orbitals based on the nucleus and pointing towards the centre of the molecule will now have the greatest effect in lowering the energy.

Electron 1 was given a momentum of $2\langle p_1 \rangle$ a.u. in location {d}. We see that the HF $V(p_{12}, p_1)$ surfaces, shown in Figures (II.14.6A) and (II.14.6B), are almost identical and the magnitudes of the distributions are very small. From the Δ -surfaces we see that the probability of locating electron 2 at $p_2 = 0$ is now increased. From this we note that radial correlation is now acting to decrease the momentum of electron 2. The small outer minima are slightly larger than before but they remain at the same position in space. These observations suggest that this correlation effect (ϕ -correlation) is largely independent of the momentum of electron 1.

In the remaining two locations we investigate the effect of increasing the momentum of electron 1 in the p_z -direction with p_x reduced to zero. For reasons of brevity, surfaces

parallel to the $p_x p_y$ -plane only have been presented for these two locations.

Electron 1 has been assigned a momentum of $0.5 \langle p_1 \rangle$ in the p_z -direction in location {e} and the surfaces are given in Figure (II.14.10). The HF $V(p_{12}, p_1)$ surface for location {e} is very similar to that of location {a}. This is demonstrated by the fact that the radial distribution $S(p_{12})$ in location {e} is only a factor of two less than in location {a} whereas the depth of the minimum in $\Delta S(p_{12})$ is a factor of five less.

With location {f}, we see from Figure (II.14.11A) that the HF $V(p_{12}, p_1)$ distribution is almost radially symmetric, however, the six minima may still be seen on the Δ -surface although their size is now diminished. The minimum near to the origin on the last surface has now developed into a maximum in this location. The importance of the maximum is illustrated by the partial planar Coulomb shifts (Figure (II.14.13)) as they are both positive over their entire range. Again this maximum may be attributed to a more precise description of the electronic probability distribution in the regions above and below the plane of the molecule in position-space.

To summarise, from this brief survey there seems to be three 'distinct bonding regions' in H_3^+ . The observed correlation effects in the $p_x p_y$ -plane were almost consistent with the effect that would be observed from three H_2

molecule-type 'bonds' located at sixty degrees to each other. From the position-space analysis we have seen that they are actually bent towards the centre of the molecule but, of course, they cannot be thought of as conventional fully occupied σ -bonds due to the electron deficient nature of H_3^+ . Thus, considerable new insight has been gained into the bonding arrangement of the molecule.

CHAPTER II.16

Summary of Momentum-Space Analysis

The Davidson and Jones^(2.xvi.1), Salmon and Poshusta^(2.xvi.2) and Schwartz and Schaad^(2.xvi.3) wave-functions were transformed into momentum-space by employing the Fourier transform technique^(2.xvi.4) and the effects of correlation on the electron momentum distributions in the H_2 and H_3^+ molecules were investigated. For the case of H_2 , correlation effects were again studied in terms of motions parallel to the bond (z-correlation), axially around the bond (ϕ -correlation) and perpendicular to the bond (ρ -correlation). This allowed us to compare the effect of each type of correlation in momentum-space with its equivalent position-space version.

(II.16.1) The One-Particle Density

The HF one-particle momentum density $\rho(p_1)$ and the difference in it due to the effects of electron correlation $\Delta\rho(p_1)$ were evaluated in surfaces for the electron travelling parallel to the plane of the molecule and, for the H_3^+ molecule only, perpendicular to the molecule.

For both molecules a greater momentum was observed perpendicular to each bond than parallel to them; this was consistent with the early theoretical work performed by

Coulson^(2.xvi.5). It was therefore possible to associate certain areas of the one-particle density surfaces with momentum distributions of specific bonds. For example, the one-particle momentum density for the electron travelling parallel to the plane of the H_3^+ molecule was found to be six-fold symmetric. This was explained by realising that it was the combined effect of three elliptically-shaped densities distributions arranged perpendicular to each of the σ -type bonds (obviously, due to the electron deficient nature of H_3^+ , conventional fully occupied σ -bonding does not occur between any given pair of nuclei).

For H_2 , the overall effect of electron correlation on the one-particle density surface was to reduce the probability of discovering electron 1 with a small momentum and to increase the probability of locating it with a momentum parallel to the bond. For the case of H_3^+ , however, the Δ -surface ($\Delta\rho(\underline{p}_1)$) was found to be almost radially symmetric when the electron was travelling parallel to the molecule although, in the perpendicular plane, a redistribution from low to high momentum in the p_z -direction could be seen. This was attributed to a better description of the electronic probability distribution above and below the plane of the molecule.

The Compton profile of an atom or molecule, $J(q)$, was shown to be related to the radial momentum distribution^(2.xvi.6). The angularly integrated Δ -surface thus gave a measure of the improvement in the Compton profile due to correlation effects. Consequently, for low

values of q , $J(q)$ is reduced since $\Delta\rho(p_1)$ is negative but, for higher values, it is increased. This was shown to be consistent with previous calculations performed upon other systems^(2.xvi.7,8)

(II.16.2) The Two-Particle Density

The momentum-space HF partial planar distribution surfaces $V(p_{12}, p_1)$ and the Δ -partial planar distribution surfaces $\Delta V(p_{12}, p_1)$ were used to study the effect of electron correlation on the H_2 and H_3^+ molecules.

The form of $\Delta V(p_{12}, p_1)$, for H_2 , was analysed in terms of its composition of z , ϕ and ρ -correlation. It was observed that in momentum-space, with respect to the HF model, z -correlation has the effect of reducing the mean inter-electronic momentum whereas it is increased by ϕ and ρ -correlation. This was found to be contrary to the effect of correlation in position-space where all correlation types were seen to be responsible for increasing the inter-electronic separation. These observations represent the molecular analogue of the atomic work performed by Banyard and Reed^(2.xvi.9,10). They reported that, relative to the HF model, both radial and angular-based correlation acted to increase the average inter-electronic separation in position-space, but in momentum-space they discovered that the effects acted in opposition to each other. We have therefore observed that z -correlation acts in a similar way to angular correlation in atoms and, as would perhaps be

expected, ρ -correlation behaves in the same fashion as radial correlation. In addition, ϕ -correlation in molecules, which has no counterpart in single-centred systems, has been seen to act in the same way as radial correlation

The form of the Salmon and Poshusta wavefunction for H_3^+ was more complicated to analyse than the Davidson and Jones wavefunction for H_2 , nevertheless certain comparisons between the position and momentum-space forms of it were made. For example, it was seen that correlation in position-space has the effect of increasing the angle subtended between the position vectors of the electrons whereas, in momentum-space, the angle subtended between the momentum-space vectors is reduced.

For each chosen momentum of electron 1, the $\Delta V(p_{12}, p_1)$ surfaces for H_2 were analysed in terms of the relative contributions from the three major correlation-types. When the test electron was located with a very small momentum, ie far from the influence of the nuclei in position-space, ρ -correlation dominated the $\Delta V(p_{12}, p_1)$ surface. The ϕ component of correlation became dominant as the momentum of the test electron was increased perpendicularly to the molecular bond and it was noticed that z-correlation had no effect when either of the electrons were travelling solely in this direction. Once the test electron acquired a momentum parallel to the molecule bond, however, z-correlation was seen to be responsible for increasing the probability of locating both electrons with momenta parallel to the molecular bond in the same direction. These

observations were then employed to shed new light on the partial Coulomb shift surfaces $\Delta g(p_{12}, p_1, \theta_1)$ evaluated by Banyard and Reed^(2.xvi.10) for the HeH^+ molecular-ion.

Electron correlation was found to be responsible for reducing the probability of locating the electrons perpendicular to each σ -type 'bond' in the H_3^+ molecule, and was attributable to ϕ -correlation. This effect was investigated as the momentum of electron 1 was increased perpendicularly to one of the bonding regions and was found to be almost independent of the momentum of the test electron. By increasing the momentum of electron 1 perpendicular to the plane of the molecule correlation effects in the p_z -direction were seen.

The study of the momentum-space correlation effects in molecules using partial planar techniques has been seen to be extremely useful and gives complementary information to that obtained from position-space investigations. In particular, the effect of bonding is highlighted in momentum-space and it is also interesting to note that, as for atomic systems, the different components of correlation act in opposition to each other in momentum-space. Future studies into the effect of electron correlation on larger molecular structures should therefore take the form of tandem investigations in position and momentum-space.

APPENDICES

APPENDIX I

Atomic Units

Atomic units (a.u) have been used throughout this thesis and must therefore be defined.

- Mass:** 1 a.u. of mass is defined as the rest mass of an electron, namely, $m_e = 9.10953 \times 10^{-31} \text{kg}$.
- Length:** 1 a.u. of length is defined as the radius of the first Bohr orbit of atomic hydrogen, ie $0.52918 \times 10^{-10} \text{m}$.
- Time:** 1 a.u. of time is the time required for an electron to travel 1 a.u. of length in the first Bohr orbital of atomic hydrogen, $2.42354 \times 10^{-17} \text{s}$.
- Momentum:** 1.a.u. of momentum is equal to the instantaneous momentum of an electron in the first Bohr orbit of atomic hydrogen, $0.19926 \times 10^{-23} \text{Ns}$.
- Energy:** 1.a.u. of energy is defined as twice the ionization potential of the hydrogen atom, being 27.210eV or $4.35956 \times 10^{-18} \text{J}$.

For a more complete discussion on atomic units see F.L.Pilar, 'Elementary Quantum Chemistry', McGraw-Hill Book Company: New York (1968) page 175.

APPENDIX II

The Hartree Fock Technique

It is well known that the Schrödinger equation cannot be solved exactly for more than one electron due to the electron-electron interaction term in the Hamiltonian. The N-electron Schrödinger equation is usually written as

$$H_{\text{exact}}\Psi(\underline{x}_1, \underline{x}_2, \dots, \underline{x}_N) = E_{\text{exact}}\Psi(\underline{x}_1, \underline{x}_2, \dots, \underline{x}_N) \quad (\text{A2.1})$$

where the exact Coulombic Hamiltonian, for atoms, is defined by

$$H_{\text{exact}} = \sum_{i=1}^N (-\nabla_i^2/2 - Z/r_i) + \sum_{i>j=1}^N r_{ij}^{-1} \quad (\text{A2.2})$$

or

$$H_{\text{exact}} = \sum_{i=1}^N h^{\circ}(r_i) + \sum_{i>j=1}^N r_{ij}^{-1}, \quad (\text{A2.3})$$

$h^{\circ}(r_i)$ being the bare nucleus Hamiltonian. The exact space-spin wavefunction is represented by $\Psi(\underline{x}_1, \underline{x}_2, \dots, \underline{x}_N)$. If the electron-electron repulsion term $\sum_{i>j=1}^N r_{ij}^{-1}$ were replaced by the sum of N, one-electron potentials, and the wavefunction were written as the product of one-electron space-spin functions the N-electron Schrödinger equation could then be rearranged as N one-electron Schrödinger equations and hence, easily solved^(ii.1). These substitutions are known as the Self-Consistent Field (SCF) approximation, the most accurate and highly energy optimised SCF wavefunction being termed the Hartree Fock wavefunction. The Hamiltonian is therefore approximated to

$$H_{\text{SCF}} = \sum_{i=1}^N h^{\circ}(r_i) + \sum_{i=1}^N V_i(\underline{x}_i), \quad (\text{A2.4})$$

where $V_i(\underline{x}_i)$ is the repulsive field experienced by the i^{th} electron, described by the i^{th} spin-orbital, due to the presence of the remaining $N-1$ electrons. By convention the subscripts refer to spin-orbital labels whereas the bracketed numbers refer to electron labels.

Only antisymmetric energy states are observed for Fermions, hence the wavefunction, as well as being split into one-electron space-spin orbitals must also be antisymmetric with respect to the interchange of electrons, as the Hamiltonian is symmetric. Consequently, it follows that the SCF wavefunction can be written as

$$\Phi_{\text{SCF}}(\underline{x}_1, \underline{x}_2, \dots, \underline{x}_N) = \hat{A}(\phi_1(\underline{x}_1), \phi_2(\underline{x}_2), \dots, \phi_N(\underline{x}_N)). \quad (\text{A2.5})$$

The ϕ 's represent the one-electron spin-orbitals and \hat{A} is the antisymmetrizing operator. If the orbitals were constructed to be orthonormal to each other then a convenient way of expressing the wavefunction would be in determinantal form, ie

$$\Phi_{\text{SCF}}(\underline{x}_1, \underline{x}_2, \dots, \underline{x}_N) = (N!)^{-1/2} \det \left\{ \phi_1(\underline{x}_1), \phi_2(\underline{x}_2), \dots, \phi_N(\underline{x}_N) \right\}. \quad (\text{A2.6})$$

The constant $(N!)^{-1/2}$ simply ensures that the wavefunction has been normalised to unity. The spin-orbitals contain optimising parameters that can be varied to produce the wavefunction that yields the lowest possible energy. An expression for the SCF energy must therefore be formulated and a method developed to find the conditions that are

necessary to energy optimise it.

In general the energy associated with an unnormalised SCF wavefunction is defined as

$$E_{\text{SCF}} = \int \phi_{\text{SCF}}^* H_{\text{exact}} \phi_{\text{SCF}} d\underline{x}_1 d\underline{x}_2 \dots d\underline{x}_N / \int \phi_{\text{SCF}}^* \phi_{\text{SCF}} d\underline{x}_1 d\underline{x}_2 \dots d\underline{x}_N. \quad (\text{A2.7})$$

By rearranging and substituting for H_{exact} using equation (A2.3), equation (A2.7) can then be expressed as

$$E_{\text{SCF}} \int \phi_{\text{SCF}}^* \phi_{\text{SCF}} d\underline{x}_1 d\underline{x}_2 \dots d\underline{x}_N = \int \phi_{\text{SCF}}^* \sum_{i=1}^N h^o(r_i) \phi_{\text{SCF}} d\underline{x}_1 d\underline{x}_2 \dots d\underline{x}_N + \int \phi_{\text{SCF}}^* \sum_{i>j=1}^N r_{ij}^{-1} \phi_{\text{SCF}} d\underline{x}_1 d\underline{x}_2 \dots d\underline{x}_N. \quad (\text{A2.8})$$

Clearly this equation is simply a statement of the conservation of energy for atomic systems. By making the definitions

$$\rho(\underline{x}'_i \underline{x}_j) = \sum_{\alpha=1}^N \phi_{\alpha}^*(\underline{x}_i) \phi_{\alpha}(\underline{x}_j) \quad (\text{A2.9})$$

and thus

$$\rho(\underline{x}'_1, \underline{x}'_2, \dots, \underline{x}'_N | \underline{x}_1, \underline{x}_2, \dots, \underline{x}_N) = \det \left\{ \rho(\underline{x}'_1 \underline{x}_1), \rho(\underline{x}'_2 \underline{x}_2), \dots, \rho(\underline{x}'_N \underline{x}_N) \right\}, \quad (\text{A2.10})$$

the dashes indicating that if the functions are acted upon by an operator it is only the unprimed co-ordinates that are affected, equation (A2.8) becomes

$$E_{\text{SCF}} \int \rho(\underline{x}'_1, \underline{x}'_2, \dots, \underline{x}'_N | \underline{x}_1, \underline{x}_2, \dots, \underline{x}_N) d\underline{x}_1 d\underline{x}_2 \dots d\underline{x}_N = \sum_{i=1}^N \int h^o(r_i) \rho(\underline{x}'_1, \underline{x}'_2, \dots, \underline{x}'_N | \underline{x}_1, \underline{x}_2, \dots, \underline{x}_N) d\underline{x}_1 d\underline{x}_2 \dots d\underline{x}_N$$

$$+ \sum_{i>j=1}^N r_{ij}^{-1} \rho(\underline{x}'_1, \underline{x}'_2, \dots, \underline{x}'_N | \underline{x}_1, \underline{x}_2, \dots, \underline{x}_N) d\underline{x}_1 d\underline{x}_2 \dots d\underline{x}_N. \quad (\text{A2.11})$$

The three terms of equation (A2.11) will now be investigated separately to determine a more convenient expression for E_{SCF} . Firstly, it can easily be shown that

$$E_{\text{SCF}} \int \rho(\underline{x}'_1, \underline{x}'_2, \dots, \underline{x}'_N | \underline{x}_1, \underline{x}_2, \dots, \underline{x}_N) d\underline{x}_1 d\underline{x}_2 \dots d\underline{x}_N = N! E_{\text{SCF}}. \quad (\text{A2.12})$$

As the operator in the second term of equation (A2.11) is only a function of the position of the i^{th} electron, the remaining integrations can be performed immediately, resulting in

$$\begin{aligned} \sum_{i=1}^N \int h^{\circ}(r_i) \rho(\underline{x}'_1, \underline{x}'_2, \dots, \underline{x}'_N | \underline{x}_1, \underline{x}_2, \dots, \underline{x}_N) d\underline{x}_1 d\underline{x}_2 \dots d\underline{x}_N \\ = (N-1)! \sum_{i=1}^N \int h^{\circ}(r_i) \rho(\underline{x}'_i | \underline{x}_i) d\underline{x}_i \end{aligned}$$

or, by using equation (A2.9), it can be written in full as

$$\begin{aligned} \sum_{i=1}^N \int h^{\circ}(r_i) \rho(\underline{x}'_1, \underline{x}'_2, \dots, \underline{x}'_N | \underline{x}_1, \underline{x}_2, \dots, \underline{x}_N) d\underline{x}_1 d\underline{x}_2 \dots d\underline{x}_N \\ = (N-1)! \sum_{i=1}^N \sum_{\alpha=1}^N \int \phi_{\alpha}^*(\underline{x}_i) h^{\circ}(r_i) \phi_{\alpha}(\underline{x}_i) d\underline{x}_i. \quad (\text{A2.13}) \end{aligned}$$

The summation over the electron labels \underline{x}_i does not have any effect on the integration and therefore it gives rise to N identical terms,

$$\begin{aligned} \sum_{i=1}^N \int h^{\circ}(r_i) \rho(\underline{x}'_1, \underline{x}'_2, \dots, \underline{x}'_N | \underline{x}_1, \underline{x}_2, \dots, \underline{x}_N) d\underline{x}_1 d\underline{x}_2 \dots d\underline{x}_N \\ = N(N-1)! \sum_{\alpha=1}^N \int \phi_{\alpha}^*(\underline{x}_i) h^{\circ}(r_i) \phi_{\alpha}(\underline{x}_i) d\underline{x}_i. \quad (\text{A2.14}) \end{aligned}$$

The integrations in the third term of equation (A2.11)

can be carried out except over the positions of the i^{th} and j^{th} electrons to give

$$\begin{aligned} & \sum_{i>j=1}^N \int r_{ij}^{-1} \rho(\underline{x}'_1, \underline{x}'_2, \dots, \underline{x}'_N | \underline{x}_1, \underline{x}_2, \dots, \underline{x}_N) d\underline{x}_1 d\underline{x}_2 \dots d\underline{x}_N \\ &= (N-2)! \sum_{i>j=1}^N \int r_{ij}^{-1} \det \left\{ \rho(\underline{x}'_i \underline{x}_i), \rho(\underline{x}'_j \underline{x}_j) \right\} d\underline{x}_i d\underline{x}_j. \quad (\text{A2.15}) \end{aligned}$$

By expanding the determinant in equation (A2.15) and realising that the summations over the i^{th} and j^{th} electron labels do not have any effect upon the integrations, thus producing $N(N-1)/2$ identical terms, it can be written as

$$\begin{aligned} & \sum_{i>j=1}^N \int r_{ij}^{-1} \rho(\underline{x}'_1, \underline{x}'_2, \dots, \underline{x}'_N | \underline{x}_1, \underline{x}_2, \dots, \underline{x}_N) d\underline{x}_1 d\underline{x}_2 \dots d\underline{x}_N \\ &= (N(N-1)/2)(N-2)! \sum_{\alpha=1}^N \sum_{\beta=1}^N \int \left(\phi_{\alpha}^*(\underline{x}_i) \phi_{\beta}^*(\underline{x}_j) r_{ij}^{-1} (\phi_{\alpha}(\underline{x}_i) \phi_{\beta}(\underline{x}_j) \right. \\ & \quad \left. - \phi_{\beta}(\underline{x}_i) \phi_{\alpha}(\underline{x}_j)) d\underline{x}_i d\underline{x}_j. \quad (\text{A2.16}) \end{aligned}$$

An expression for the SCF energy can now be obtained^(ii.2) by substituting equations (A2.12), (A2.14) and (A2.16) into equation (A2.11) and dividing throughout by a factor of $N!$ to give

$$\begin{aligned} E_{\text{SCF}} &= \sum_{\alpha=1}^N \int \phi_{\alpha}^*(\underline{x}_i) h^0(r_i) \phi_{\alpha}(\underline{x}_i) d\underline{x}_i + 1/2 \sum_{\alpha=1}^N \sum_{\beta=1}^N \int \left(\phi_{\alpha}^*(\underline{x}_i) \phi_{\beta}^*(\underline{x}_j) \right. \\ & \quad \left. r_{ij}^{-1} (\phi_{\alpha}(\underline{x}_i) \phi_{\beta}(\underline{x}_j) - \phi_{\beta}(\underline{x}_i) \phi_{\alpha}(\underline{x}_j)) d\underline{x}_i d\underline{x}_j \quad (\text{A2.17}) \end{aligned}$$

which can be rearranged in the form

$$\begin{aligned} E_{\text{SCF}} &= \sum_{\alpha=1}^N \int \phi_{\alpha}^*(\underline{x}_i) h^0(r_i) \phi_{\alpha}(\underline{x}_i) d\underline{x}_i + \sum_{\alpha>\beta=1}^N \int \left(\phi_{\alpha}^*(\underline{x}_i) \phi_{\beta}^*(\underline{x}_j) r_{ij}^{-1} \right. \\ & \quad \left. (\phi_{\alpha}(\underline{x}_i) \phi_{\beta}(\underline{x}_j) - \phi_{\beta}(\underline{x}_i) \phi_{\alpha}(\underline{x}_j)) d\underline{x}_i d\underline{x}_j. \quad (\text{A2.18}) \end{aligned}$$

These two equations represent expressions for the SCF energy. The conditions to ensure that the E_{SCF} has been

energy optimised, maintaining the subsidiary conditions that the spin-orbitals should remain normalised to unity and orthogonal to each other, must now be established.

By exploiting the method of undetermined multipliers^(ii.3) we obtain

$$\delta \left[E_{\text{SCF}} + \sum_{\alpha=1}^N \lambda_{\alpha\alpha} \int \phi_{\alpha}^*(\underline{x}_i) \phi_{\alpha}(\underline{x}_i) d\underline{x}_i + \sum_{\alpha>\beta=1}^N \left(\lambda_{\alpha\beta} \int \phi_{\alpha}^*(\underline{x}_i) \phi_{\beta}(\underline{x}_i) d\underline{x}_i + \lambda_{\beta\alpha} \int \phi_{\beta}^*(\underline{x}_i) \phi_{\alpha}(\underline{x}_i) d\underline{x}_i \right) \right] = 0, \quad (\text{A2.19})$$

where the λ 's are the undetermined multipliers and have been chosen so that $\lambda_{\alpha\beta} = \lambda_{\beta\alpha}$. The first term in the equation ensures optimum SCF energy, the second, normalisation and the last terms, orthogonality. For E_{SCF} to be at its minimum value each spin-orbital must be optimised and thus, from equation (A2.18), δE_{SCF} is given by

$$\begin{aligned} \delta E_{\text{SCF}} = & \int \delta \phi_{\alpha}^*(\underline{x}_i) h^{\circ}(r_i) \phi_{\alpha}(\underline{x}_i) d\underline{x}_i + \int \phi_{\alpha}^*(\underline{x}_i) h^{\circ}(r_i) \delta \phi_{\alpha}(\underline{x}_i) d\underline{x}_i \\ & + \sum_{\beta=1}^N \int \delta \phi_{\alpha}^*(\underline{x}_i) \phi_{\beta}^*(\underline{x}_j) r_{ij}^{-1} (\phi_{\alpha}(\underline{x}_i) \phi_{\beta}(\underline{x}_j) - \phi_{\beta}(\underline{x}_i) \phi_{\alpha}(\underline{x}_j)) d\underline{x}_i d\underline{x}_j \\ & + \sum_{\beta=1}^N \int \phi_{\alpha}^*(\underline{x}_i) \phi_{\beta}^*(\underline{x}_j) r_{ij}^{-1} (\delta \phi_{\alpha}(\underline{x}_i) \phi_{\beta}(\underline{x}_j) - \phi_{\beta}(\underline{x}_i) \delta \phi_{\alpha}(\underline{x}_j)) d\underline{x}_i d\underline{x}_j \end{aligned} \quad (\text{A2.20})$$

then a simple rearrangement produces

$$\begin{aligned} \delta E_{\text{SCF}} = & \int \delta \phi_{\alpha}^*(\underline{x}_i) \left[h^{\circ}(r_i) \phi_{\alpha}(\underline{x}_i) \right. \\ & \left. + \sum_{\beta=1}^N \int \phi_{\beta}^*(\underline{x}_j) r_{ij}^{-1} (\phi_{\alpha}(\underline{x}_i) \phi_{\beta}(\underline{x}_j) - \phi_{\beta}(\underline{x}_i) \phi_{\alpha}(\underline{x}_j)) d\underline{x}_j \right] d\underline{x}_i \\ & + (\text{complex conjugate of the above}). \end{aligned} \quad (\text{A2.21})$$

The expression is now substituted into equation (A2.19) and rearranged as

$$\int \delta \phi_{\alpha}^*(\underline{x}_i) \left[h^{\circ}(r_i) \phi_{\alpha}(\underline{x}_i) + \sum_{\beta=1}^N \int \phi_{\beta}^*(\underline{x}_j) r_{ij}^{-1} (\phi_{\alpha}(\underline{x}_i) \phi_{\beta}(\underline{x}_j) - \phi_{\beta}(\underline{x}_i) \phi_{\alpha}(\underline{x}_j)) d\underline{x}_j + \sum_{\alpha=1}^N \lambda_{\alpha\alpha} \phi_{\alpha}(\underline{x}_i) + \sum_{\alpha>\beta=1}^N \lambda_{\alpha\beta} \phi_{\beta}(\underline{x}_i) \right] d\underline{x}_i + (\text{complex conjugate of this expression}) = 0. \quad (\text{A2.22})$$

This equation is in the form of a function added to its complex conjugate being equal to zero. The solution can therefore be chosen so that the function, and therefore its conjugate, are each zero. Further, the remaining equation can be expressed in the form

$$\int \delta \phi_{\alpha}^*(\underline{x}_i) f_{\alpha}(\underline{x}_i, \underline{x}_j) = 0,$$

and for this to be true in general, the solution is that $f_{\alpha}(\underline{x}_i, \underline{x}_j) = 0$. This can be written in full as

$$h^{\circ}(r_i) \phi_{\alpha}(\underline{x}_i) + \sum_{\beta=1}^N \int \phi_{\beta}^*(\underline{x}_j) r_{ij}^{-1} (\phi_{\alpha}(\underline{x}_i) \phi_{\beta}(\underline{x}_j) - \phi_{\beta}(\underline{x}_i) \phi_{\alpha}(\underline{x}_j)) d\underline{x}_j + \sum_{\alpha=1}^N \lambda_{\alpha\alpha} \phi_{\alpha}(\underline{x}_i) + \sum_{\alpha>\beta=1}^N \lambda_{\alpha\beta} \phi_{\beta}(\underline{x}_i) = 0. \quad (\text{A2.23})$$

By combining the λ 's and converting the matrix containing them into diagonal form^(ii.4), it follows that

$$\begin{aligned}
& h^0(r_i) \phi_\alpha(\underline{x}_i) + \phi_\alpha(\underline{x}_i) \sum_{\beta=1}^N \int \phi_\beta^*(\underline{x}_j) r_{ij}^{-1} \phi_\beta(\underline{x}_j) d\underline{x}_j \\
& - \sum_{\beta=1}^N \int \phi_\beta(\underline{x}_j) \phi_\beta^*(\underline{x}_j) r_{ij}^{-1} \phi_\alpha(\underline{x}_j) d\underline{x}_j = -\epsilon_\alpha \phi_\alpha(\underline{x}_i)
\end{aligned} \tag{A2.24}$$

where the energy required to ionize the electron in the α^{th} spin-orbital is given by $-\epsilon_\alpha$. By defining the HF integral operator $R_{\alpha\beta}(\underline{x}_i)$ such that

$$R_{\alpha\beta}(\underline{x}_i) \phi_\alpha(\underline{x}_i) = \phi_\beta(\underline{x}_i) \int \phi_\beta^*(\underline{x}_j) r_{ij}^{-1} \phi_\alpha(\underline{x}_j) d\underline{x}_j \tag{A2.25}$$

Equation (A2.24) may be rearranged in the form

$$\left[h^0(r_i) + V_\alpha(\underline{x}_i) \right] \phi_\alpha(\underline{x}_i) = -\epsilon_\alpha \phi_\alpha(\underline{x}_i) \tag{A2.26}$$

where

$$V_\alpha(\underline{x}_i) = \sum_{\beta=1}^N \left(\int \phi_\beta^*(\underline{x}_j) r_{ij}^{-1} \phi_\beta(\underline{x}_j) d\underline{x}_j - R_{\alpha\beta}(\underline{x}_i) \right). \tag{A2.27}$$

(The potential experienced between two electrons (electron 1 in spin-orbital α and electron 2 in spin-orbital β , say) may be written as

$$\begin{aligned}
v_{\alpha\beta}(\underline{x}_1, \underline{x}_2) &= \int \phi_\beta^*(\underline{x}_2) \overbrace{r_{12}^{-1}} \phi_\beta(\underline{x}_2) d\underline{x}_2 + \int \phi_\alpha^*(\underline{x}_1) \overbrace{r_{12}^{-1}} \phi_\alpha(\underline{x}_1) d\underline{x}_1 \\
&\quad - R_{\alpha\beta}(\underline{x}_1) \quad - R_{\beta\alpha}(\underline{x}_2)
\end{aligned} \tag{A2.28}$$

which is the potential experienced by electron 1 due to the averaged effect of electron 2 added to the potential experienced by electron 2 due to the averaged effect of electron 1.)

Equation (A2.26) may now be seen to be in the form of a one-electron Schrödinger equation where $V_{\alpha}(\underline{x}_i)$ represents the potential experienced by electron 'i' due to the averaged effect of the other electrons. Unfortunately, the operator $R_{\alpha\beta}(\underline{x}_i)$ may not be evaluated at a given point ^{easily} in space due to the complexity of the mathematics. Nevertheless, the spin-orbitals, and hence the total SCF wavefunction, may be optimised using equation (A2.25). Firstly^(ii.5), an arbitrary set of spin-orbitals is chosen (the choice, of course, being guided by any previous knowledge of approximate atomic wavefunctions). The spin-orbitals are used, in conjunction with equation (A2.25), to obtain an improved version of $\phi_{\alpha}(\underline{x}_i)$. This process is repeated for the other orbitals, exploiting the best available spin-orbitals to calculate the potentials, to evaluate a better optimised set of orbitals. The entire procedure is repeated until it has been judged that the forms of the spin-orbitals have converged, at which point the set of simultaneous equations has been solved. By substituting these energy-optimised spin-orbitals into the SCF wavefunction (equation (A2.6)), the optimal energy for that choice of basis set can be obtained. With a suitable choice of spin-orbitals extremely accurate SCF wavefunctions have been evaluated^(ii.6-9) and may subsequently be used as excellent approximations to the ideal Hartree Fock wavefunction.

References

- (ii.1) see for example, D.R.Hartree, 'The Calculation of Atomic Structures', Wiley and Sons (1955)
- (ii.2) N.F.Mott and I.N.Sneddon, 'Wave Mechanics and its Applications', Wiley and Sons (1955), page 135
- (ii.3) J.C.Slater, 'Quantum Theory of Atomic Structure Vol I', McGraw-Hill Book Co. (1960), page 113
- (ii.4) J.C.Slater, 'Quantum Theory of Atomic Structure Vol II', McGraw-Hill Book Co. (1960), page 8
- (ii.5) H.Eyring, J.Walter and G.E.Kimball, 'Quantum Chemistry', Oxford Uni. Press (1936), page 165
- (ii.6) B.D.Joshi, J.Chem.Phys. 44 3627 (1966)
- (ii.7) M.E.Schwartz and L.J.Schaad, J.Chem.Phys. 46 4112 (1967)
- (ii.8) E.R.Davidson, J.Chem.Phys. 42 4199 (1965)
- (ii.9) R.F.Curl, Jr. and C.A.Coulson, Proc.Phys.Soc 85 647 (1965).

APPENDIX III

The General Theory of Natural Spin-Orbitals

Any normalised configuration interaction (CI) wavefunction, describing an N-electron system, may be represented by a linear combination of Slater determinants. By increasing the number of determinants employed in the series, the total energy associated with the wavefunction will become nearer to the experimentally derived value. The rate of convergence to this value, however, cannot be predicted, consequently the importance of each determinant in the expansion and the number of determinants required to give any desired accuracy is difficult to ascertain. Much interest has therefore been focused on a method to evaluate the wavefunction with the most rapidly energy convergent series possible. Löwdin has shown^(iii.1) that this occurs when the spin-orbitals contained within the determinants diagonalise the first-order reduced density matrix. This particular choice of spin-orbitals defines the natural spin-orbital (NSO) set as it may be specified uniquely for each system.

Before investigating the method used to arrange a wavefunction in natural orbital form it proves necessary to introduce some fundamental mathematical formulae.

(A3.1) Mathematical Formulae

As discussed earlier an N-electron CI wavefunction may be written as

$$\Psi(\underline{x}_1, \underline{x}_2, \dots, \underline{x}_N) = \sum_i c_i \Phi_i(\underline{x}_1, \underline{x}_2, \dots, \underline{x}_N) \quad (\text{A3.1})$$

where the c_i 's are linear coefficients and the Slater determinants $\Phi_i(\underline{x}_1, \underline{x}_2, \dots, \underline{x}_N)$ are defined by

$$\Phi_i(\underline{x}_1, \underline{x}_2, \underline{x}_3, \dots, \underline{x}_N) = (N!)^{-1/2} \det \left\{ \phi_a^i(\underline{x}_1), \phi_b^i(\underline{x}_2), \dots, \phi_n^i(\underline{x}_N) \right\}. \quad (\text{A3.2})$$

The factor $(N!)^{-1/2}$ simply ensures that the determinant is itself normalised to unity and the co-ordinate \underline{x}_1 , for example, represents both the space and spin co-ordinates of the first electron. The elements ϕ^i in the i^{th} determinant are spin-orbitals (either molecular or atomic) taken from an extended basis set. Although an individual determinant does not necessarily possess the symmetry of the full system they are grouped together to form 'configurations' which do have this symmetry. The angular momentum and spin properties are thus preserved only in the entirety of expansion (A3.1).

Consider two of the Slater determinants from the wavefunction, Φ_k and Φ_l say, where obviously

$$\Phi_k = (N!)^{-1/2} \det \left\{ \phi_a^k(\underline{x}_1), \phi_b^k(\underline{x}_2), \dots, \phi_n^k(\underline{x}_N) \right\}$$

and

$$\Phi_l = (N!)^{-1/2} \det \left\{ \phi_a^l(\underline{x}_1), \phi_b^l(\underline{x}_2), \dots, \phi_n^l(\underline{x}_N) \right\}. \quad (\text{A3.3})$$

Overlap integrals may be defined between the spin-orbitals in these determinants as, in general, they are non-orthogonal, ie

$$d_{ab}^{kl} = \int \phi_a^{k*}(\underline{x}_1) \phi_b^l(\underline{x}_1) d\underline{x}_1. \quad (\text{A3.4})$$

The integral between the two Slater determinants defined in equation (A3.3) may be shown to be $N!$ times the integral of the product of the diagonal term Φ_k and the determinant in Φ_1 , or expressed mathematically

$$\begin{aligned} \int \Phi_k^* \Phi_1 d\underline{x}_1 d\underline{x}_2 \dots d\underline{x}_N &= (N!)(N!)^{-1} \int \phi_a^{k*}(\underline{x}_1) \phi_b^{k*}(\underline{x}_2) \dots \phi_n^{k*}(\underline{x}_N) \\ &\quad \det \left\{ \phi_a^l(\underline{x}_1), \phi_b^l(\underline{x}_2), \dots, \phi_n^l(\underline{x}_N) \right\} d\underline{x}_1 d\underline{x}_2 \dots d\underline{x}_N \\ &= D^{kl}. \end{aligned} \quad (\text{A3.5})$$

D^{kl} can then be simply defined by

$$D^{kl} = \det \left\{ d_{aa}^{kl}, d_{bb}^{kl}, \dots, d_{nn}^{kl} \right\}. \quad (\text{A3.6})$$

Both Φ_k and Φ_1 may be expanded about the first rows of their determinants producing

$$\Phi_k = (N!)^{-1/2} \sum_{\alpha}^{(k)} \phi_{\alpha}^k(\underline{x}_1) \det^k(1|\alpha)$$

and (A3.7)

$$\Phi_1 = (N!)^{-1/2} \sum_{\beta}^{(k)} \phi_{\beta}^1(\underline{x}_1) \det^1(1|\beta)$$

The notation $\sum_{\alpha}^{(k)}$ emphasises that the summation takes place

only over the spin orbitals that are contained in the k^{th} determinant. The $(N-1)^{\text{th}}$ order cofactors of Φ_k and Φ_1 are defined by $\det^k(1|\alpha)$ and $\det^1(1|\beta)$ respectively and the 1 indicates that the first row has been removed from the complete determinant whereas the α (or β) indicates that the α^{th} (or β^{th}) column has been erased.

In a similar way to that in which equation (A3.5) was derived it may also be shown that

$$\int \det^k(1|\alpha) \det^l(1|\beta) \, d\underline{x}_2 \dots d\underline{x}_N = (N-1)! D^{kl}(\alpha|\beta) \quad (\text{A3.8})$$

where $D^{kl}(\alpha|\beta)$ is a $(N-1)^{\text{th}}$ order cofactor of D^{kl} . The expression relates the cofactors of the determinants Φ_k and Φ_1 to those of the determinant D^{kl} , containing the non-orthogonality integrals.

(A3.2) The Derivation of the First-order Reduced Density Matrix

The first-order reduced density matrix $\gamma(\underline{x}'_1|\underline{x}_1)$ for the system represented by the normalised CI wavefunction $\Psi(\underline{x}_1, \underline{x}_2, \dots, \underline{x}_N)$ can be expressed as

$$\gamma(\underline{x}'_1|\underline{x}_1) = N \int \Psi^*(\underline{x}'_1, \underline{x}'_2, \dots, \underline{x}'_N) \Psi(\underline{x}_1, \underline{x}_2, \dots, \underline{x}_N) \, d\underline{x}_2 \, d\underline{x}_3 \dots d\underline{x}_N. \quad (\text{A3.9})$$

The prime on the \underline{x}_1 co-ordinate indicates that when evaluating the expectation value of an operator, \underline{x}'_1 is put equal to \underline{x}_1 after the operation has been performed and consequently the operator only acts upon the unprimed co-ordinates.

By substituting the expression for the wavefunction (equation (A3.1)) into equation (A3.9) it yields

$$\gamma(\underline{x}'_1|\underline{x}_1) = N \int \sum_k c_k \Phi_k^* \sum_l c_l \Phi_l \, d\underline{x}_2 \, d\underline{x}_3 \dots d\underline{x}_N.$$

If equation (A3.7) is now employed, the determinants Φ_k and Φ_1 may be expanded about their first rows to give

$$\gamma(\underline{x}'_1 | \underline{x}_1) = N(N!)^{-1} \int \sum_k c_k \sum_{\alpha}^{(k)} \phi_{\alpha}^{k*}(\underline{x}_1) \det^k(1|\alpha) \sum_1 c_1 \sum_{\beta}^{(1)} \phi_{\beta}^1(\underline{x}_1) \det^1(1|\beta) d\underline{x}_2 d\underline{x}_3 \dots d\underline{x}_N. \quad (\text{A3.10})$$

The double summation $\sum_k \sum_{\alpha}^{(k)}$ infers, firstly sum over all of the spin-orbitals contained in the k^{th} determinant and then sum over all possible determinants. This can be clearly rearranged as $\sum_{\alpha} \sum_k^{(\alpha)}$, meaning sum over the determinants that contain a member from the α^{th} spin-orbital set and then sum over all possible spin-orbitals α . By rearranging the summations in this way equation (A3.10) can be expressed,

$$\gamma(\underline{x}'_1 | \underline{x}_1) = N(N!)^{-1} \int \sum_{\alpha} \phi_{\alpha}^*(\underline{x}_1) \sum_k^{(\alpha)} c_k \det^k(1|\alpha) \sum_{\beta} \phi_{\beta}(\underline{x}_1) \sum_1^{(\beta)} c_1 \det^1(1|\beta) d\underline{x}_2 d\underline{x}_3 \dots d\underline{x}_N.$$

The integrations are then seen to be in the form of equation (A3.8) and thus produce

$$\gamma(\underline{x}'_1 | \underline{x}_1) = N(N!)^{-1} (N-1)! \sum_{\alpha, \beta} \phi_{\alpha}^*(\underline{x}'_1) \phi_{\beta}(\underline{x}_1) \sum_k^{(\alpha)} \sum_1^{(\beta)} c_k D^{k1}(\alpha|\beta) c_1.$$

By a simple rearrangement the first-order reduced density matrix may then be written as

$$\gamma(\underline{x}'_1 | \underline{x}_1) = \sum_{\alpha, \beta} \phi_{\alpha}^*(\underline{x}'_1) \gamma(\alpha|\beta) \phi_{\beta}(\underline{x}_1). \quad (\text{A3.11})$$

where $\gamma(\alpha|\beta)$ is defined by

$$\gamma(\alpha|\beta) = \sum_k^{(\alpha)} \sum_1^{(\beta)} c_k D^{k1}(\alpha|\beta) c_1. \quad (\text{A3.12})$$

The first-order reduced density matrix can thus be calculated from (A3.11). It is, however, a tedious task to compute as $(N-1)^{\text{th}}$ order co-factors of determinants

containing overlap integrals must be evaluated.

(A3.3) Natural Spin-orbitals for an N-electron System

A natural spin-orbital (NSO) may be expressed as a linear combination of the original spin-orbitals, ie

$$\chi_k = \sum_I \phi_I A_{Ik} \quad (\text{A3.13})$$

or in matrix notation

$$\underline{\chi} = \underline{\phi} \underline{A}. \quad (\text{A3.14})$$

A row-vector of the NSOs is given by $\underline{\chi}$, $\underline{\phi}$ represents a row-vector of the original spin-orbitals and \underline{A} is a transformation matrix. The NSO's are defined to be orthonormal and also, as mentioned earlier, must diagonalise the reduced density matrix^(iii.1). These two stipulations may be expressed mathematically:

(A3.3.I) Orthonormality

This condition can be written in matrix form as

$$\langle \underline{\chi}^\uparrow | \underline{\chi} \rangle = \underline{I} \quad (\text{A3.15})$$

where the notation $^\uparrow$ represents the transpose of the matrix.

By substituting equation (A3.14) into (A3.15) we obtain

$$\langle \underline{A}^\uparrow \underline{\phi}^\uparrow \underline{\phi} \underline{A} \rangle = \underline{I}. \quad (\text{A3.16})$$

As matrix \underline{A} is constructed solely of numbers it may be removed from the integration to give

$$\underline{A}^\uparrow \underline{\Delta} \underline{A} = \underline{I} \quad (\text{A3.17})$$

where

$$\underline{\Delta} = \langle \underline{\phi}^\uparrow \underline{\phi} \rangle$$

and obviously $\underline{\Delta}$ is the overlap matrix between the original

basis spin-orbitals. It can also be seen that if these spin-orbitals were orthonormal then $\underline{\Delta} = \underline{I}$, reducing equation (A3.17) to $\underline{A}^\dagger \underline{A} = \underline{I}$ and thus defining \underline{A} to be any unitary matrix^(iii.2).

(A3.3.II) Diagonalisation of the first-order reduced density matrix

From equation (A3.11) the first-order reduced density matrix can be written as

$$\gamma(\underline{x}'_1 | \underline{x}_1) = \underline{\phi} \underline{\gamma} \underline{\phi}^\dagger. \quad (\text{A3.18})$$

Equation (A3.14) is again employed to substitute for $\underline{\phi}$, resulting in

$$\gamma(\underline{x}'_1 | \underline{x}_1) = \underline{X} \underline{A}^{-1} \underline{\gamma} (\underline{A}^{-1})^\dagger \underline{X}^\dagger$$

and by defining a new matrix \underline{n} as

$$\underline{n} = \underline{A}^{-1} \underline{\gamma} (\underline{A}^{-1})^\dagger \quad (\text{A3.19})$$

the density matrix can be written,

$$\gamma(\underline{x}'_1 | \underline{x}_1) = \underline{X} \underline{n} \underline{X}^\dagger. \quad (\text{A3.20})$$

It can now be seen that $\gamma(\underline{x}'_1 | \underline{x}_1)$ will be in diagonal form if the matrix \underline{n} is also diagonal. Further, by integrating equation (A3.20) over electron 1 we obtain

$$N = \sum_k n_k. \quad (\text{A3.21})$$

This infers that the sum of the elements in the diagonal matrix \underline{n} is equal to the number of electrons in the system. Because of this, the elements of \underline{n} are known as the 'occupation numbers' of the NSO's.

To summarise, the two mathematical conditions to be satisfied simultaneously when selecting NSOs are

$$\underline{A}^\dagger \underline{\Delta} \underline{A} = \underline{I} \quad (\text{A3.22}) \quad \text{for orthonormality and}$$

$$\underline{A}^{-1} \underline{\gamma} (\underline{A}^{-1})^\dagger = \underline{n} \quad (\text{A3.23}) \quad \text{where } \underline{n} \text{ is diagonal,}$$

ensures the density matrix is diagonal.

(A3.4) A Simplification for the Case of two Electrons ^(iii.3)

It is well known that for a singlet two-electron wavefunction the spin-function can be factorized out of the Slater determinants giving

$${}^1\Psi(\underline{x}_1, \underline{x}_2) = \sum_{k,l} C_{kl} \phi_k^*(\underline{r}_1) \phi_l(\underline{r}_2) (2)^{-1/2} \left(\alpha(\underline{1})\beta(\underline{2}) - \beta(\underline{1})\alpha(\underline{2}) \right), \quad (\text{A3.24})$$

or in matrix notation omitting the spin-functions

$${}^1\Psi(\underline{r}_1, \underline{r}_2) = \underline{\phi} \underline{C} \underline{\phi}^\dagger. \quad (\text{A3.25})$$

Here \underline{r} represents purely the space co-ordinates of the electron, consequently $\underline{\phi}$ is a row vector of space-orbitals and \underline{C} is a matrix containing the coefficients of the original wavefunction. By substituting for $\underline{\phi}$ in equation (A3.25) using only the spatial component of equation (A3.14) we obtain

$${}^1\Psi(\underline{r}_1, \underline{r}_2) = \underline{X} \underline{A}^{-1} \underline{C} (\underline{A}^{-1})^\dagger \underline{X}^\dagger. \quad (\text{A3.26})$$

The wavefunction may therefore be written in the form

$${}^1\Psi(\underline{r}_1, \underline{r}_2) = \underline{X} \underline{C} \underline{X}^\dagger \text{ where } \underline{C} = \underline{A}^{-1} \underline{C} (\underline{A}^{-1})^\dagger \quad (\text{A3.27})$$

By simple manipulation the first-order reduced density matrix is then simply

$$\gamma(\underline{x}'_1 | \underline{x}_1) = \underline{X} \underline{C}^2 \underline{X}^\dagger.$$

This matrix will subsequently be in diagonal form if \underline{c} is also diagonal. It is therefore possible to solve equation (A3.27) instead of equation (A3.19) for the two-electron system, thus alleviating the problem of computing the $\underline{\gamma}$ matrix. Further, by comparing equation (A3.26) with equation (A3.20) it can be shown that

$$\underline{n} = \underline{c}^2 \quad (\text{A3.28})$$

and thus for a particular element of \underline{n} ,

$$n_k = c_k^2.$$

The simplification for the two-electron system is purely a consequence of the fact that the wavefunction can be written in quadratic form.

(A3.5) Solving the Equations

The simultaneous equations to be solved for the N-electron case are

$$\underline{A}^\uparrow \underline{\Delta} \underline{A} = \underline{I} \quad (\text{A3.29})$$

with

$$\underline{A}^\uparrow \underline{\gamma} (\underline{A}^{-1})^\uparrow = \underline{n} \quad (\text{A3.30})$$

and for the two-electron case

$$\underline{A}^\uparrow \underline{\Delta} \underline{A} = \underline{I} \quad (\text{A3.31})$$

with

$$\underline{A}^{-1} \underline{C} (\underline{A}^{-1})^\uparrow = \underline{c}. \quad (\text{A3.32})$$

Once $\underline{\gamma}$ or \underline{C} have been evaluated the N-electron equations can be solved in exactly the same way as the two-electron equations. This analysis will therefore restrict itself to solving equation (A3.29) with equation (A3.30) on the understanding that, by simply substituting \underline{C} for $\underline{\gamma}$, the other two equations may be solved.

Firstly a unitary transformation is performed on the overlap matrix $\underline{\Delta}$ to obtain

$$\underline{U}^\dagger \underline{\Delta} \underline{U} = \underline{T}. \quad (\text{A3.33})$$

Here \underline{U} is a unitary matrix whose columns represent the eigenvectors of $\underline{\Delta}$ and \underline{T} is a diagonal matrix containing the eigenvalues of $\underline{\Delta}$. If the elements of a matrix \underline{W} are defined such that

$$W_{ij} = U_{ij} / (T_{jj})^{1/2}.$$

This forces out the identity matrix from equation (A3.33) giving

$$\underline{W}^\dagger \underline{\Delta} \underline{W} = \underline{I}. \quad (\text{A3.34})$$

Comparing equations (A3.29) with (A3.34) it would appear that \underline{W} and \underline{A} are identical. This is not the case, however, as, in general, \underline{A} is given by the product of \underline{W} and some other transformation matrix \underline{X} , ie

$$\underline{A} = \underline{W} \underline{X}. \quad (\text{A3.35})$$

By substituting equation (A3.35) into (A3.29) the nature of \underline{X} may be discovered, thus

$$\underline{X}^\dagger \underline{W}^\dagger \underline{\Delta} \underline{W} \underline{X} = \underline{I}.$$

By comparing this equation with equation (A3.34) it immediately reduces to

$$\underline{X}^\dagger \underline{X} = \underline{I}.$$

So, to satisfy equation (A3.29), \underline{X} may be any unitary matrix. To solve equation (A3.30), equation (A3.35) is substituted into it to become

$$\underline{X}^{-1} \underline{W}^{-1} \underline{Y} (\underline{W}^{-1})^\dagger (\underline{X}^{-1})^\dagger = \underline{n}.$$

By defining $\underline{W}^{-1} \underline{Y} (\underline{W}^{-1})^\dagger = \underline{M}$ and using the fact that \underline{X} is unitary this equation may be rearranged as

$$\underline{X}^\dagger \underline{M} \underline{X} = \underline{n}. \quad (\text{A3.36})$$

If a unitary transformation is thus performed on the known

matrix \underline{M} , the eigenvalues obtained fill the diagonal matrix of occupation numbers \underline{n} . In addition, the columns of \underline{X} are constructed from the eigenvectors of \underline{M} . As \underline{W} and \underline{X} are now known \underline{A} can be evaluated using equation (A3.35). The natural spin-orbitals can then be constructed by employing equation (A3.14).

(A3.6) A Solved Example

The simple two-electron CI wavefunction of Stuart and Matsen^(iii.4) will be used to highlight the principles of transforming a wavefunction into natural spin-orbital form (see also ref(iii.5)). The wavefunction is formed from the linear combination of three normalised configurations and is given by

$$\Psi(\underline{x}_1, \underline{x}_2) = (2)^{-1/2} \left(c_1 \{1s1s\} + c_2 \{1s2s\} + c_3 \{2s2s\} \right) \quad (\text{A3.37})$$

where

$$c_1 = 0.23586511,$$

$$c_2 = 0.37591055,$$

$$c_3 = 0.17935024$$

and $\int 1s(\underline{r})2s(\underline{r})d\underline{r} = S = 0.71103715.$

Equation (A3.37) can be written in full as

$$\Psi(\underline{x}_1, \underline{x}_2) = (2)^{-1/2} \left(c_1 \begin{vmatrix} 1s(\underline{1})\alpha(\underline{1}), & 1s(\underline{1})\beta(\underline{1}) \\ 1s(\underline{2})\alpha(\underline{2}), & 1s(\underline{2})\beta(\underline{2}) \end{vmatrix} \right. \\ \left. + c_2 \begin{vmatrix} 1s(\underline{1})\alpha(\underline{1}), & 2s(\underline{1})\beta(\underline{1}) \\ 1s(\underline{2})\alpha(\underline{2}), & 2s(\underline{2})\beta(\underline{2}) \end{vmatrix} + c_3 \begin{vmatrix} 2s(\underline{1})\alpha(\underline{1}), & 1s(\underline{1})\beta(\underline{1}) \\ 2s(\underline{2})\alpha(\underline{2}), & 1s(\underline{2})\beta(\underline{2}) \end{vmatrix} \right)$$

$$+ c_3 \left| \begin{array}{cc} 2s(\underline{1})\alpha(\underline{1}), & 2s(\underline{1})\beta(\underline{1}) \\ 2s(\underline{2})\alpha(\underline{2}), & 2s(\underline{2})\beta(\underline{2}) \end{array} \right| \right]. \quad (\text{A3.38})$$

After factorizing out the spin component of the wavefunction, the space-function becomes

$$\Psi(\underline{r}_1, \underline{r}_2) = c_1 1s(\underline{1})1s(\underline{2}) + c_2 1s(\underline{1})2s(\underline{2}) + c_3 2s(\underline{1})1s(\underline{2}) + c_3 2s(\underline{1})2s(\underline{2}). \quad (\text{A3.39})$$

As can be seen, there are four distinct spin-orbitals but, as they are made up from two doubly filled spatial orbitals, only two natural orbitals need be considered.

The first-order reduced density matrix is easily evaluated from equation (A3.39) as

$$\begin{aligned} \gamma(\underline{x}'_1 | \underline{x}_1) = & 1s(\underline{1})1s(\underline{1})[c_1^2 + c_2^2 + 2c_1c_2S] \\ & + 1s(\underline{1})2s(\underline{1})[c_1c_2 + c_1c_3S + c_2^2S + c_2c_3] \\ & + 2s(\underline{1})1s(\underline{1})[c_3c_2 + c_2^2S + c_3c_1S + c_2c_1] \\ & + 2s(\underline{1})2s(\underline{1})[c_2^2 + c_3^2 + 2c_2c_3S]. \end{aligned}$$

$\gamma(\underline{x}'_1 | \underline{x}_1)$ is then written in the form

$$\gamma(\underline{x}'_1 | \underline{x}_1) = \underline{\phi} \underline{\gamma} \underline{\phi}^\dagger$$

where $\underline{\gamma}$ is defined as

$$\underline{\gamma} = \begin{pmatrix} c_1^2 + c_2^2 + 2Sc_1c_2, & c_1c_2 + Sc_1c_3 + Sc_2^2 + c_2c_3 \\ c_1c_2 + Sc_1c_3 + Sc_2^2 + c_2c_3, & c_2^2 + c_3^2 + 2Sc_2c_3 \end{pmatrix}.$$

The matrices $\underline{\gamma}$, \underline{C} and $\underline{\Delta}$ are therefore

$$\underline{\gamma} = \begin{pmatrix} 0.32302814, & 0.28663820 \\ 0.28663820, & 0.26935098 \end{pmatrix}, \quad \underline{C} = \begin{pmatrix} 0.23586511, & 0.37591055 \\ 0.37591055, & 0.17935024 \end{pmatrix}$$

$$\text{and } \underline{\Delta} = \begin{pmatrix} 1.0 & 0.71103715 \\ 0.71103715, & 1.0 \end{pmatrix}.$$

Many different methods exist for solving the equations and for more complicated examples standard computer library

subroutines should be employed. However, for this particularly simple example the following analytical technique provides insight into the method.

Equation (A3.33) states

$$\underline{U}^\dagger \underline{\Delta} \underline{U} = \underline{T}$$

and thus this expression is left multiplied by \underline{U} we obtain

$$\underline{\Delta} \underline{U} = \underline{U} \underline{T}. \quad (\text{A3.40})$$

The columns of the unitary matrix \underline{U} has columns representing the eigenvectors of $\underline{\Delta}$ and \underline{T} is a diagonal matrix containing the eigenvalues of $\underline{\Delta}$. \underline{U} and \underline{T} can therefore be defined as

$$\underline{U} = \left(\left[\begin{array}{c} \underline{U}_1 \\ \end{array} \right], \left[\begin{array}{c} \underline{U}_2 \\ \end{array} \right] \right) \text{ and } \underline{T} = \left(\begin{array}{cc} \lambda_1 & 0 \\ 0 & \lambda_2 \end{array} \right).$$

By substituting these forms of \underline{U} and \underline{T} into equation (A3.40) two equations are formed, namely

$$\underline{\Delta} \underline{U}_1 = \underline{U}_1 \lambda_1 \underline{I}$$

and

$$\underline{\Delta} \underline{U}_2 = \underline{U}_2 \lambda_2 \underline{I}$$

but for non-trivial solutions

$$\det(\underline{\Delta} - \lambda_1 \underline{I}) = 0 \quad (\text{A3.41})$$

and

$$\det(\underline{\Delta} - \lambda_2 \underline{I}) = 0. \quad (\text{A3.42})$$

Firstly, by solving equation (A3.41),

$$\left| \begin{array}{cc} 1-\lambda_1 & 0.71103715 \\ 0.71103715 & 1-\lambda_1 \end{array} \right| = 0$$

the solutions $\lambda_1 = 1.71103715$ or $\lambda_1 = 0.28896285$ are obtained. By solving equation (A3.42) in the same way we obtain $\lambda_2 = 0.28896285$ or $\lambda_2 = 1.71103715$. These results

imply that λ_1 and λ_2 can be placed in \underline{T} in any order as this simply specifies the arrangement of \underline{U}_1 and \underline{U}_2 in \underline{U} . \underline{T} may therefore be defined to be

$$\underline{T} = \begin{pmatrix} 1.71103715, & 0.0 \\ 0.0, & 0.28896285 \end{pmatrix}.$$

To evaluate \underline{U} equation (A3.40) can be written,

$$(\underline{\Delta} - \lambda_1 \underline{I}) \underline{U}_1 = 0 \quad (\text{A3.43})$$

and

$$(\underline{\Delta} - \lambda_2 \underline{I}) \underline{U}_2 = 0. \quad (\text{A3.44})$$

If \underline{U}_1 and \underline{U}_2 are expressed as

$$\underline{U}_1 = \begin{pmatrix} u_{a1} \\ u_{b1} \end{pmatrix} \quad \text{and} \quad \underline{U}_2 = \begin{pmatrix} u_{a2} \\ u_{b2} \end{pmatrix}$$

then equation (A3.43) becomes

$$\begin{pmatrix} -0.71103715, & 0.71103715 \\ 0.71103715, & 0.71103715 \end{pmatrix} \begin{pmatrix} u_{a1} \\ u_{b1} \end{pmatrix} = 0.$$

The solution is obviously $u_{a1} = u_{b1}$ and for \underline{U}_1 to be normalised it must be of the form

$$\underline{U}_1 = \begin{pmatrix} 0.70710678 \\ 0.70710678 \end{pmatrix}.$$

Solving equation (A3.44) in the same manner results in the solution $u_{a2} = -u_{b2}$ to give

$$\underline{U}_2 = \begin{pmatrix} 0.70710678 \\ -0.70710678 \end{pmatrix}$$

and therefore the matrix \underline{U} is constructed as

$$\underline{U} = \begin{pmatrix} 0.70710678, & 0.70710678 \\ 0.70710678, & -0.70710678 \end{pmatrix}.$$

By definition $W_{ij} = U_{ij} (T_{jj})^{-1/2}$, thus

$$\underline{W} = \begin{pmatrix} 0.54057416, & 1.31541865 \\ 0.54057416, & -1.31541865 \end{pmatrix}$$

and by simple matrix algebra

$$\underline{W}^{-1} = \begin{pmatrix} 0.92494247, & 0.92494247 \\ 0.38010714, & -0.38010714 \end{pmatrix}.$$

At this point the method for the two-electron and N-electron cases differ slightly, for the purposes of completeness in this example, however, both will be shown concurrently.

$$\text{For the N-electron case } \underline{M}_\gamma = \underline{W}^{-1} \underline{\gamma} (\underline{W}^{-1})^\dagger \quad (\text{A3.45})$$

$$\text{whereas for two-electrons } \underline{M}_C = \underline{W}^{-1} \underline{c} (\underline{W}^{-1})^\dagger. \quad (\text{A3.46})$$

By simple manipulation we therefore have

$$\underline{M}_\gamma = \begin{pmatrix} 0.99723995, & 0.01887167 \\ 0.01887167, & 0.00275999 \end{pmatrix}$$

and

$$\underline{M}_C = \begin{pmatrix} 0.99842136, & 0.01986934 \\ 0.01986934, & -0.04863328 \end{pmatrix}.$$

Then by performing unitary transforms on these matrices, defined by equation (A3.36), we obtain \underline{x}_γ , \underline{x}_C , \underline{n} and \underline{c} as

$$\underline{x}_\gamma = \begin{pmatrix} 0.99982013, & 0.01896618 \\ 0.01896618, & -0.99982013 \end{pmatrix},$$

$$\underline{x}_C = \begin{pmatrix} 0.99982014, & 0.01896616 \\ 0.01896616, & -0.99982014 \end{pmatrix},$$

$$\underline{n} = \begin{pmatrix} 0.99759792, & 0.0 \\ 0.0, & 0.00240200 \end{pmatrix},$$

$$\underline{c} = \begin{pmatrix} 0.99879827, & 0.0 \\ 0.0, & -0.04901019 \end{pmatrix}$$

then

$$\underline{c}^2 = \begin{pmatrix} 0.99759799, & 0.0 \\ 0.0, & 0.00240200 \end{pmatrix}.$$

It can be seen that \underline{x}_γ is equal to \underline{x}_C and \underline{c}^2 is equal to \underline{n} , showing that the two methods are equivalent. The sum of the occupation numbers is 1 and not 2 as a factor of two was

omitted from the first-order reduced density matrix.

Using equation (A3.35), the matrix \underline{A} can be evaluated as

$$\underline{A} = \begin{pmatrix} 0.56542539, -1.30492941 \\ 0.51552846, 1.32543467 \end{pmatrix}.$$

This allows the two natural orbitals to be written as

$$\chi(1s) = 0.56542539\phi(1s) + 0.51552846\phi(2s) \quad (\text{A3.47})$$

and

$$\chi(2s) = -1.30492941\phi(1s) + 1.32543467\phi(2s). \quad (\text{A3.48})$$

The full Stuart and Matsen^(iii.4) CI wavefunction can thus be expressed as

$$\Psi(\underline{x}_1, \underline{x}_2) = (2)^{-1/2} \left(\begin{array}{l} 0.99879827 \begin{vmatrix} 1s(1)\alpha(1), 1s(1)\beta(1) \\ 1s(2)\alpha(2), 1s(2)\beta(2) \end{vmatrix} \\ -0.04901019 \begin{vmatrix} 2s(1)\alpha(1), 2s(1)\beta(1) \\ 2s(2)\alpha(2), 2s(2)\beta(2) \end{vmatrix} \end{array} \right)$$

where the orbital labels refer to the natural-spin orbitals evaluated.

(A3.7) References

- (iii.1) P.O.Löwdin, Adv.in Phys. 5 151 (1956)
- (iii.2) P.O.Löwdin, Phys.Rev. 97 1474 (1955)
- (iii.3) P.O.Löwdin and H.Shull, Phys.Rev. 101 1730 (1956)
- (iii.4) J.D.Stuart and F.A.Matsen, J.Chem.Phys. 41 1646 (1964)
- (iii.5) C.C.Baker, 'Correlation effects and electron densities in some two-electron systems', University of Leicester (1969), page184

REFERENCES

- (1.a) E.Schrödinger, Ann.der Physik 79 361, 489, 734 (1926)
- (1.b) E.Schrödinger, Ann.der Physik 81 109 (1926)
- (1.c) E.Schrödinger, Phys.Rev. 28 1049 (1926)
- (2) M.Born and J.R.Oppenheimer, Ann.der Physik. 84 457 (1927)
- (3) D.R.Hartree, Proc.Cam.Phil.Soc. 24 89, 111 (1928)
- (4) J.C.Slater, Phys.Rev. 32 339 (1928)
- (5) J.A.Gaunt, Proc.Cam.Phil.Soc. 24 328 (1928)
- (6) W.Pauli, Jr., Z.Physik 43 601 (1927)
- (7) J.C.Slater, Phys.Rev. 34 1293 (1929)
- (8) C.E.Eckart, Phys.Rev. 36 878 (1930)
- (9) R.F.Curl, Jr. and C.A.Coulson, Proc.Phys.Soc. 85 647 (1965)
- (10) B.D.Joshi, J.Chem.Phys. 44 3627 (1966)
- (11) M.E.Schwartz and L.J.Schaad, J.Chem.Phys. 46 4112 (1967)
- (12) V.Fock, Z.Physik 61 126 (1930)
- (13) P.O.Löwdin, Adv.Chem.Phys. 2 207 (1959)
- (14) for example, O.Sinanoglu, J.Chem.Phys. 36 706 (1962)
- (15) E.A.Hylleraas, Z.Physik 48 469 (1928)
- (16) E.A.Hylleraas, Z.Physik 54 347 (1929)
- (17) H.M.James and A.S.Coolidge, J.Chem.Phys. 1 825 (1933)
- (18) H.A.S.Eriksson, Z.Physik 109 762 (1938)
- (19) S.Chandrasekhar and G.Herzberg, Phys.Rev. 98 1050 (1955)
- (20) C.L.Perkeris, Phys.Rev. 112 1649 (1958)
- (21) W.Kolos and C.C.J.Roothaan, Rev.Mod.Phys. 32 205 (1960)
- (22) P.Wang, J.Chem.Phys. 47 2229 (1967)

- (23) I.C.Hayes and A.J.Stone, Molec.Phys. 53 69 (1984)
- (24) S.C.Leasure and G.G.Balint-Kurti, Phys.Rev.A 31 2107 (1985)
- (25) D.L.Cooper, J.Gerratt and M.Raimondi, Faraday Symp.Chem.Soc. 19 149 (1984)
- (26) J.H.van Lenthe and G.G.Balint-Kurti, J.Chem. Phys. 78 569 (1983)
- (27) J.A.Pople, J.S.Binkley and R.Seager, Int.J.Quant. Chem.Symp. 10 1 (1976)
- (28) V.R.Saunders and J.H.van Lenthe, Molec.Phys. 48 923 (1983)
- (29) S.M.Colwell, Molec.Phys. 51 1217 (1984)
- (30) D.R.Beck and C.A.Nicolaidis, Chem.Phys.Lett. 59 525 (1978)
- (31) R.Jauregui and C.F.Bunge, J.Chem.Phys. 71 11 (1979)
- (32) C.F.Bender and E.R.Davidson, J.Chem.Phys. 49 4222 (1968)
- (33) N.C.Handy, J.Phys.Chem. 88 4852 (1984)
- (34) C.A.Coulson and A.H.Neilson, Proc.Phys.Soc. 78 831 (1961)

References Part I

Chapter (I.1)

- (1.i.1) K.E.Banyard, J.Chem.Ed. 47 668 (1970)
- (1.i.2) C.A.Coulson and A.H.Neilson, Proc.Phys.Soc. 78 831 (1961)
- (1.i.3) O.Sinanoglu, Phys.Rev. 122 493 (1961)
- (1.i.4) O.Sinanoglu, J.Chem.Phys. 36 706 (1962)
- (1.i.5) O.Sinanoglu, J.Chem.Phys. 33 1212 (1960)
- (1.i.6) O.Sinanoglu, Proc.Roy.Soc. (Lond.) A260 379 (1961)
- (1.i.7) O.Sinanoglu, Rev.Mod.Phys. 35 517 (1963)
- (1.i.8) O.Sinanoglu and D.F.Tuan, J.Chem.Phys. 38 1740 (1963)
- (1.i.9) O.Sinanoglu, 'Adv.Chem.Phys. Vol VI', Wiley (1964), page 315
- (1.i.10) A.J.Duben and J.P.Lowe, J.Chem.Phys. 55 4270 (1971)
- (1.i.11) G.K.Taylor and K.E.Banyard, Phys Rev.A 8 1157 (1973)

Chapter (I.2)

- (1.ii.1) H.Eyring, J.Walter and G.E.Kimball, 'Quantum Chemistry' Wiley (1954), page 369
- (1.ii.2) E.Clementi and C.Roetti, Atomic Data and Nuclear Data Tables 14 177 (1974)
- (1.ii.3) P.K.Youngman and K.E.Banyard, J.Phys.B 20 3313 (1987)
- (1.ii.4) K.E.Banyard and P.K.Youngman, J.Phys.B 20 5585 (1987)
- (1.ii.5) K.E.Banyard and M.M.Mashat, J.Chem.Phys. 67 1405 (1977)
- (1.ii.6) K.E.Banyard and K.H.Al-Bayati, J.Phys.B 20 465 (1987)
- (1.ii.7) K.E.Banyard and C.C.Baker, J.Chem.Phys. 51 2680 (1969)
- (1.ii.8) C.C.Baker and K.E.Banyard, Phys.Rev. 188 57 (1969)

- (1.ii.9) K.E.Banyard, M.Dixon and A.D.Tait, Phys.Rev.A 4 2199 (1971)
- (1.ii.10) O.Sinanoglu, J.Chem.Phys. 36 706 (1962)
- (1.ii.11) O.Sinanoglu and D.F.Tuan, J.Chem.Phys. 38 1740 (1963)

Chapter (I.3)

- (1.iii.1) For example, N.C.Handy, Molec.Phys. 26 169 (1973)
- (1.iii.2) G.K.Taylor and K.E.Banyard, Phys.Rev.A 8 (1973)
- (1.iii.3) R.J.Mobbs and K.E.Banyard, J.Chem.Phys. 78 6106 (1983)
- (1.iii.4) K.E.Banyard and K.H.Al-Bayati, J.Phys.B 19 2211 (1986)
- (1.iii.5) P.K.Youngman and K.E.Banyard, J.Phys.B 20 3313 (1987)
- (1.iii.6) K.E.Banyard and G.K.Taylor, Phys.Rev.A 10 1972 (1974)

References Part II

Chapter (II.1)

- (2.i.1) For example, E.R.Davidson, 'Reduced Density Matrices in Quantum Chemistry', Academic Press New York (1976)
- (2.i.2) For example, O.Sinanoglu, J.Chem.Phys. 36 706 (1962)
- (2.i.3) K.E.Banyard and M.M.Mashat, J.Chem.Phys. 67 1405 (1977)
- (2.i.4) K.E.Banyard and R.J.Mobbs, J.Chem.Phys. 75 3433 (1981)
- (2.i.5) K.E.Banyard and K.H.Al-Bayati, J.Phys.B 19 2211 (1986)
- (2.i.6) C.A.Coulson and A.H.Neilson, Proc.Phys.Soc. 78 831 (1961)
- (2.i.7) T.L.Gilbert, Rev.Mod.Phys. 35 491 (1963)
- (2.i.8) H.Tatewaki and K Tanaka, J.Chem.Phys. 60 601 (1974)
- (2.i.9) R.F.Curl, Jr. and C.A.Coulson, Proc.Phys.Soc. 85 647 (1965)
- (2.i.10) E.M.Peiscoto, C.R.Bunge and R.A.Bonham, Phys.Rev 181 322 (1969)
- (2.i.11) K.E.Banyard and C.C.Baker, Phys.Rev 188 57 (1969)
- (2.i.12) R.Benesch and V.H.Smith, Jr., J.Chem.Phys. 55 482 (1971)
- (2.i.13) N.Moiseyev, J.Katriel and R.J.Boyd, Theoret. Chim.Acta. 45 61 (1977)
- (2.i.14) K.E.Banyard and C.E.Reed, J.Phys.B 14 411 (1981)
- (2.i.15) R.J.Boyd and C.A.Coulson, J.Phys.B 6 782 (1973)
- (2.i.16) K.E.Banyard and P.K.Youngman, J.Phys.B 15 853 (1982)
- (2.i.17) K.H.Al-Bayati and K.E.Banyard, J.Phys.B 20 465 (1987)
- (2.i.18) K.E.Banyard and C.E.Reed, J.Phys.B 14 411 (1981)
- (2.i.19) B.S.Sharma and A.J.Thakkar, J.Phys.B 17 3405 (1984)
- (2.i.20) K.E.Banyard and D.J.Ellis, Mol.Phys. 24 1291

- (1972)
- (2.i.21) J.P.Tatum, Int.J.Quant.Chem. 10 967 (1976)
- (2.i.22) N.Moiseyev and P.R.Certain, Chem.Phys.Lett. 55 451 (1978)
- (2.i.23) R.J.Boyd and M.C.Yee, J.Chem.Phys. 77 3578 (1982)
- (2.i.24) J.Lennard-Jones and J.A.Pople, Phil.Mag. 43 581 (1952)
- (2.i.25) P.Rehmus, M.E.Kellman and R.S.Berry, Chem.Phys. 31 239 (1978)
- (2.i.26) P.Rehmus and R.S.Berry, Chem.Phys. 38 257 (1979)
- (2.i.27.a) R.E.Brown and V.H.Smith,Jr., Phys.Rev.A 5 140 (1971)
- (2.i.27.b) B.Jeziorski and K.Szalewicz, Phys.Rev.A 19 2360 (1977)
- (2.i.27.c) J.W.Lui and V.H.Smith,Jr., Mol.Phys. 35 145 (1978)
- (2.i.27.d) A.J.Thakkar, A.N.Tripathi and V.H.Smith,Jr., Phys.Rev.A 29 1108 (1984)
- (2.i.28) K.E.Banyard and C.E.Reed, J.Phys.B 11 2957 (1978)
- (2.i.29) C.E.Reed and K.E.Banyard, J.Phys.B 13 1519 (1980)
- (2.i.30) R.J.Mobbs and K.E.Banyard, J.Chem.Phys. 78 6106 (1983)
- (2.i.31) P.K.Youngman and K.E.Banyard, J.Phys.B 20 3313 (1987)
- (2.i.32) A.S.Eddington, 'Fundamental Theory', Cambridge University Press (1946), page 19
- (2.i.33) A.J.Coleman, Int. J.Quant.Chem. 1 457 (1967)
- (2.i.34) A.J.Thakkar and N.J.Moore, Int.J.Quant.Chem. Symp. 15 393 (1981)
- (2.i.35) W.A.Lester and M.Krauss, J.Chem.Phys. 44 207 (1966)
- (2.i.36) L.Salmon and R.D.Poshusta, J.Chem.Phys. 59 7 (1973)
- (2.i.37) A.J.Thakkar and V.H.Smith,Jr., J.Chem.Phys. 67 1191 (1977)
- (2.i.38) A.J.Thakkar, A.N.Tripathi and V.H.Smith,Jr.,

Int.J.Quant.Chem. 16 167 (1984)

- (2.i.39) A.J.Thakkar, 'Density Matrices and Density Functionals', D.Reidel Publishing Co. (1984), page 553
- (2.i.40) A.J.Duben and J.P.Lowe, J.Chem.Phys. 55 4270 (1971)
- (2.i.41) G.Doggett, Mol.Phys. 34 1739 (1977)
- (2.i.42) G.Doggett, Mol.Phys. 38 853 (1979)

Chapter (II.2)

- (2.ii.1) K.E.Banyard and C.E.Reed, J.Phys.B 11 2957 (1978)
- (2.ii.2) R.J.Boyd and C.A.Coulson, J.Phys.B 6 782 (1973)
- (2.ii.3) K.E.Banyard and P.K.Youngman, J.Phys.B 15 853 (1982)
- (2.ii.4) R.J.Mobbs and K.E.Banyard, J.Chem.Phys. 78 6106 (1983)
- (2.ii.5) K.E.Banyard and K.H.Al-Bayati, J.Phys.B 19 2211 (1986)
- (2.ii.6) K.E.Banyard and M.M.Mashat, J.Chem.Phys. 67 1405 (1977)
- (2.ii.7) O.Sinanoglu and D.Tuan, Ann.Rev.Phys.Chem. R15 251 (1964)

Chapter (II.3)

- (2.iii.1) W.Heitler and F.London, Z.Physik. 44 455 (1927)
- (2.iii.2) H.M.James and A.S.Coolidge, J.Chem.Phys. 1 825 (1933)
- (2.iii.3) A.L.Hughes and M.M.Mann, Phys.Rev. 53 50 (1937)
- (2.iii.4) B.Hicks, Phys.Rev. 52 436 (1937)
- (2.iii.5) P.Eisenberger, Phys.Rev.A 2 1678 (1970)
- (2.iii.6) H.F.Wellenstein and R.A.Bonham, Phys.Rev.A 7 1568 (1973)
- (2.iii.7) R.C.Ulsh, H.F.Wellenstein and R.A.Bonham, J.Chem.Phys. 60 103 (1974)
- (2.iii.8) J.S.Lee, J.Chem.Phys. 66 4906 (1977)

- (2.iii.9) B.Jeziorski and K.Szalewicz, Phys.Rev.A 19 2360 (1982)
- (2.iii.10) J.J.Thomson, Lond.Edinb.Dubl.Phil.Mag. 24 209 (1912)
- (2.iii.11) F.Petty and T.F.Moran, Chem.Phys.Lett. 5 64 (1970)
- (2.iii.12) M.F.Payne and A.C.Riverie J.Phys.D 5 69 (1972)
- (2.iii.13) J.C.Ford et al, Phys.Rev.A 5 1705 (1972)
- (2.iii.14) M.J.Gaillard et al, Phys.Rev.A 17 1797 (1978)
- (2.iii.15) R.E.Christoffersen, J.Chem.Phys. 41 960 (1964)
- (2.iii.16) T.Oka, Phys.Rev.Lett. 45 531 (1980)
- (2.iii.17) J.T-Shy, J.W.Farley, W.E.Lamb and W.H.Wing, Phys.Rev.Lett. 45 (1980)
- (2.iii.18) I.N.Kozin, O.L.Polyansky and N.F.Zobov, J.Mol.Spect. 128 126 (1988)
- (2.iii.19) S.Saito et al, J.Chem.Phys. 82 45 (1985)
- (2.iii.20) B.Peart and K.T.Dolder, J.Phys.B 7 1567 (1974)
- (2.iii.21) D.Lupu and R.V.Bacur, J.Phys.Chem.Solids, 38 387 (1977)
- (2.iii.22) P.Thaddeus, Phil.Tran.R.Soc. A 303 469 (1981)
- (2.iii.23) T.Oka, Phil.Trans.R.Soc A 303 543 (1981)
- (2.iii.24) A.J.Duben and J.P.Lowe, J.Chem.Phys. 55 4276 (1971)
- (2.iii.25) W.A.Lester Jr. and M.Krauss, J.Chem.Phys. 44 1 (1966)

Chapter (II.4)

- (2.iv.1) W.Kolos and L.Wolniewicz, J.Chem.Phys. 49 404 (1968)
- (2.iv.2) J.V.Longstaff and K.Singer, Proc.R.Soc.Lond. A258 421 (1960)
- (2.iv.3) N.C.Handy, Molec.Phys. 26 169 (1973)
- (2.iv.4) M.E.Schwartz and L.J.Schaad, J.Chem.Phys. 46 412 (1966)
- (2.iv.5) B.Jeriorski and K.Szalewicz, Phys.Rev.A 19 2360 (1979)
- (2.iv.6) E.F.Hayes, J.Chem.Phys. 46 4004 (1967)

- (2.iv.7) W.Kolos and C.C.J.Roothaan, Rev.Mod.Phys. 32 205 (1960)
- (2.iv.8) E.R.Davidson, J.Chem.Phys. 37 577 (1962)
- (2.iv.9) E.R.Davidson and L.L.Jones, J.Chem.Phys. 37 1918 (1962)
- (2.iv.10) P.O.Löwdin, Phys.Rev. 97 1474 (1955)
- (2.iv.11) P.O.Löwdin, Adv. in Phys. 5 150 (1956)
- (2.iv.12) E.R.Davidson, Adv.in Quant.Chem. 6 235 (1972)
- (2.iv.13) O.K.Sinanoglu, J.Chem.Phys. 36 706 (1962)
- (2.iv.14) C.E.Reed and K.E.Banyard, J.Phy.B 13 1519 (1980)
- (2.iv.15) K.E.Banyard and C.C.Baker, J.Chem.Phys. 51 2680 (1969)
- (2.iv.16) R.F.Borkman, J.Chem.Phys. 53 3153 (1970)
- (2.iv.17) W.A.Lester,Jr. and M.Krauss, J.Chem.Phys. 44 207 (1966)
- (2.iv.18) J.P.Considine and E.F.Hayes, J.Chem.Phys. 46 1119 (1967)
- (2.iv.19) K.Kawaoka and R.F.Borkman, J.Chem.Phys. 55 4637 (1971)
- (2.iv.20) R.E.Christoffersen, J.Chem.Phys. 41 960 (1964)
- (2.iv.21) A.J.Duben and J.P.Lowe, J.Chem.Phys. 55 4270(1971)
- (2.iv.22) H.Conroy, J.Chem.Phys. 47 912 (1967)
- (2.iv.23) C.E.Dykstra and W.C.Swope, J.Chem.Phys. 70 1 (1979)
- (2.iv.24) A.Preiskorn and W.Woznicki, Chem.Phys.Lett. 86 369 (1982) and Molec.Phys. 52 1291 (1984)
- (2.iv.25) B.D.Joshi, J.Chem.Phys. 44 3627 (1966)
- (2.iv.26) L.Salmon and R.D.Poshusta, J.Chem.Phys. 59 7 (1973)
- (2.iv.27) M.E.Schwartz and L.J.Schaad, J.Chem.Phys. 47 5327 (1967)
- (2.iv.28) K.Singer, Proc.R.Soc.London. A258 412 (1960)
- (2.iv.29) M.Frisch, 'Gaussian 82 User Manual-version H', Carnegie-Mellon University (1986)

Chapter (II.5)

- (2.v.1) E.R.Davidson and L.L.Jones, J.Chem.Phys. 37 1918 (1962)
- (2.v.2) W.Kolos and C.C.J.Roothaan, Rev.Mod.Phys. 32 205 (1960)

Chapter (II.6)

- (2.vi.1) E.R.Davidson and L.L.Jones, J.Chem.Phys. 37 1918 (1962)
- (2.vi.2) K.E.Banyard and C.C.Baker, Int.J.Quant.Chem. 4 431 (1970)
- (2.vi.3) M.R.Hayns, PhD Thesis, 'The Quantum Mechanical Study of HeH⁺ and LiH', University of Leicester (1969)
- (2.vi.4) F.Grimaldi, Adv.Chem.Phys. 14 341 (1969)
- (2.vi.5) F.Grimaldi, J.Chem.Phys. 43 59 (1965)
- (2.vi.6) E.M.Layton, Jr. and K.Ruedenberg, J.Phys.Chem. 68 1654 (1964)
- (2.vi.7) C.Edmiston and K.Ruedenberg, J.Phys.Chem. 68 1628 (1964)
- (2.vi.8) W.Kauzmann, 'Quantum Chemistry', Academic Press (1957), page 230
- (2.vi.9) H.Shull, J.Chem.Phys. 30 1405 (1959)
- (2.vi.10) K.E.Banyard and G.J.Seddon, J.Chem.Phys. 58 1132 (1971)
- (2.vi.11) K.E.Banyard and D.J.Ellis, Mol.Phys. 24 1291 (1972)

Chapter (II.7)

- (2.vii.1) L.Salmon and R.D.Poshusta, J.Chem.Phys. 59 7 (1973)
- (2.vii.2) M.E.Schwartz and L.J.Schaad, J.Chem.Phys. 47 5327 (1967)

Chapter (II.8)

- (2.viii.1) R.E.Christoffersen, J.Chem.Phys. 41 960 (1964)
- (2.viii.2) A.J.Duben and J.P.Lowe, J.Chem.Phys. 55 4276 (1971)
- (2.viii.3) K.E.Banyard and C.E.Reed, J.Phys.B 14 411 (1981)
- (2.viii.4) F.Grimaldi, Adv.Chem.Phys. 14 341 (1969)

- (2.viii.5) F.Grimaldi, J.Chem.Phys. 43 59 (1965)
- (2.viii.6) R.E.Christoffersen, PhD Thesis, 'A CI study of the Ground State of the H_3^+ Molecule', Indiana University (1963)

Chapter (II.9)

- (2.ix.1) P.O.Löwdin, Phys.Rev. 97 1474 (1955)
- (2.ix.2) W.Kolos and C.C.J.Roothaan, Rev.Mod.Phys. 32 205 (1960)
- (2.ix.3) E.R.Davidson and L.L.Jones, J.Chem.Phys. 37 1918 (1962)
- (2.ix.4) For example, C.C.Baker and K.E.Banyard, Phys.Rev. 188 57 (1967)
- (2.ix.5) F.Grimaldi, Adv.Chem.Phys. 14 341 (1969) and also J.Chem.Phys. 43 59 (1965)
- (2.ix.6) K.E.Banyard and C.E.Reed, J.Phys.B 14 411 (1981)

Chapter (II.10)

- (2.x.1) P.A.M.Dirac, 'The Principles of Quantum Mechanics', Oxford University Press (1935)
- (2.x.2) A.S.Eve, Phil.Mag. 8 669 (1904)
- (2.x.3) W.H.Bragg, Phil.Mag. 14 429 (1907)
- (2.x.4) J.A.Gray, Phil.Mag. 26 611 (1913)
- (2.x.5) R.H.Stuewer and M.J.Cooper, 'Compton Scattering', Ed. B.G.Williams, McGraw-hill Book Co. (1977)
- (2.x.6) P.Eisenberger, Phys.Rev.A 2 1678 (1970)
- (2.x.7) R.E.Brown and V.H.Smith,Jr., Phys.Rev.A 5 140 (1972)
- (2.x.8) B.Jeziorski and K.Szalewicz, Phys.Rev.A 19 2360 (1979)
- (2.x.9) K.E.Banyard and C.E.Reed, J.Phys.B 11 2957 (1978)

Chapter (II.11)

- (2.xi.1) N.Swartholm, PhD Thesis, 'The Binding Energies of the Lightest Atomic Nucleii', Lund University
- (2.xi.2) See for example, I.N.Sneddon, 'Fourier Transforms', Mc-Graw-Hill (1951), page 384

- (2.xi.3) R.McWeeny and C.A.Coulson, Proc.Phys.Soc.Lond. 62A 509 (1949)
- (2.xi.4) R.McWeeny, Proc.Phys.Soc.London. 62A 519 (1949)
- (2.xi.5) P.A.M.Dirac, 'Principles of Quantum Mechanics', Oxford University Press (1935), page 103
- (2.xi.6) E.R.Davidson and L.L.Jones, J.Chem.Phys. 37 1918 (1962)
- (2.xi.7) B.H.Bransden and C.J.Joachain, 'Physics of atoms and molecules', Longman Group (1983) page 645
- (2.xi.8) I.S.GradshTEyn and I.M.Ryzhik, 'Tables of Integrals, Series and Products', Academic Press (1980), page 952, equation 8.411.1
- (2.xi.9) C.A.Coulson, Proc.Cam.Phil.Soc. 37 55 (1941)
- (2.xi.10) L.Salmon and R.D.Poshusta, J.Chem.Phys. 59 7 (1973)
- (2.xi.11) M.E.Schwartz and L.J.Schaad, J.Chem.Phys. 47 5327 (1967)
- (2.xi.12) I.S.GradshTEyn and I.M.Ryzhik, 'Tables of Integrals, Series and Products', Academic Press (1980), page 307, equation 3.323.2

Chapter (II.12)

- (2.xii.1) E.R.Davidson and L.L.Jones, J.Chem.Phys. 37 1918 (1962)
- (2.xii.2) J.S.Lee, J.Chem.Phys. 66 4907 (1977)
- (2.xii.3) B.Jeziorski, Phys.Rev.A 19 2360 (1979)

Chapter (II.13)

- (2.xiii.1) C.A.Coulson, Proc.Cam.Phil.Soc. 37 55 (1941)
- (2.xiii.2) K.E.Banyard and C.E.Reed, J.Phys.B 13 1519 (1980)
- (2.xiii.3) W.Kauzmann, 'Quantum Chemistry', Academic Press (1957), page 230
- (2.xiii.4) I.R.Epstein and A.C.Tanner, 'Compton Scattering', Ed. B.G.Williams, McGraw-Hill Book Co. (1977)

- (2.xiii.5) R.E.Brown and V.H.Smith,Jr., Phys.Rev.A 5 140
(1972)
- (2.xiii.6) P.Eisenberger, Phys.Rev.A 2 1678 (1970)
- (2.xiii.7) V.H.Smith,Jr. et al, J.Chem.Phys. 67 3676 (1977)
- (2.xiii.8) K.E.Banyard and C.E.Reed, J.Phys.B 11 2957
(1978)
- (2.xiii.9) C.E.Reed, PhD Thesis, 'Properties of Electron
Momentum Distributions', University of Leicester
(1980)

Chapter (II.14)

- (2.xiv.1) L.Salmon and R.D.Poshusta, J.Chem.Phys. 59 7
(1973)
- (2.xiv.2) M.E.Schwartz and L.J.Schaad, J.Chem.Phys. 47
5327 (1967)

Chapter (II.15)

- (2.xv.1) L.Salmon and R.D.Poshusta, J.Chem.Phys. 59 7
(1973)
- (2.xv.2) M.E.Schwartz and L.J.Schaad, J.Chem.Phys. 47
5327 (1967)
- (2.xv.3) P.E.Regier and A.J.Thakkar, Phys.Rev.A 30 30
(1984)
- (2.xv.4) P.E.Regier and A.J.Thakkar, J.Phys.B 18 3061
(1985)
- (2.xv.5) C.A.Coulson, Proc.Cam.Phil.Soc. 37 55 (1941)

Chapter (II.16)

- (2.xvi.1) E.R.Davidson and L.L.Jones, J.Chem.Phys. 37 1918
(1962)
- (2.xvi.2) L.Salmon and R.D.Poshusta, J.Chem.Phys. 59 7
(1973)
- (2.xvi.3) M.E.Schwartz and L.J.Schaad, J.Chem.Phys. 47
5327 (1967)
- (2.xvi.4) P.A.M.Dirac, 'Principles of Quantum Mechanics',
Oxford University Press (1935), page 103
- (2.xvi.5) C.A.Coulson, Proc.Cam.Phil.Soc. 37 55 (1941)
- (2.xvi.6) J.W.M.DuMond and H.A.Kirkpatrick, Phys.Rev. 52
419 (1937)

- (2.xvi.7) R.E.Brown and V.H.Smith,Jr., Phys.Rev.A 5 140
(1972)
- (2.xvi.8) B.Jeziorski and K.Szalewicz, Phys.Rev.A 19 2360
(1979)
- (2.xvi.9) K.E.Banyard and C.E.Reed, J.Phys.B 11 2957
(1978)
- (2.xvi.10) K.E.Banyard and C.E.Reed, J.Phys.B 13 1519
(1980)